AD

USAAVLABS TECHNICAL REPORT 67-9D

IN-FLIGHT MEASUREMENT OF ROTOR BLADE AIRLOADS, BENDING MOMENTS, AND MOTIONS, TOGETHER WITH ROTOR SHAFT LOADS AND FUSELAGE VIBRATION, ON A TANDEM ROTOR HELICOPTER

VOLUME IV

SUMMARY AND EVALUATION OF RESULTS

By

Richard R. Pruyn

November 1967

U. S. ARMY AVIATION MATERIEL LABORATORIES
FORT EUSTIS, VIRGINIA

CONTRACT DA 44-177-AMC-124(T)
VERTOL DIVISION
THE BOEING COMPANY
MORTON, PENNSYLVANIA

285

DISCLAIMERS

The findings in this report are not to be construed as an official Department of the Army position unless so designated by other authorized documents.

When Government drawings, specifications, or other data are used for any purpose other than in connection with a definitely related Government procurement operation, the United States Government thereby incurs no responsibility nor any obligation whatsoever; and the fact that the Government may have formulated, furnished, or in any way supplied the said drawings, specifications, or other data is not to be regarded by implication or otherwise as in any manner licensing the holder or any other person or corporation, or conveying any rights or permission to manufacture, use, or sell any patented invention that may in any way be related thereto.

DISPOSITION INSTRUCTIONS

Destroy this report when no longer needed. Do not return it to originator.

DEPARTMENT OF THE ARMY
U. S. ARMY AVIATION MATERIEL LABORATORIES
FORT EUSTIS, VIRGINIA 23604

This report has been reviewed by the U. S. Army Aviation Materiel Laboratories and is considered to be technically sound. The work was performed under Contract DA-44-177-AMC-124(T) for the purpose of measuring the dynamic air pressures on the blades of a tandem rotor helicopter and the resulting blade and shaft stresses and fuselage vibrations during flight. The report is published for the dissemination and application of information and the stimulation of ideas.

Task 1F125901A14604
Contract DA 44-177-AMC-124(T)
USAAVLABS Technical Report 67-9D
November 1967

IN-FLIGHT MEASUREMENT OF ROTOR BLADE AIRLOADS, BENDING MOMENTS, AND MOTIONS, TOGETHER WITH ROTOR SHAFT LOADS AND FUSELAGE VIBRATION, ON A TANDEM ROTOR HELICOPTER

VOLUME IV

SUMMARY AND EVALUATION OF RESULTS

D8-0382-4

by

Richard R. Pruyn

Prepared by

VERTOL DIVISION
THE BOEING COMPANY
Morton, Pennsylvania

for

U.S. ARMY AVIATION MATERIEL LABORATORIES
FORT EUSTIS, VIRGINIA

SUMMARY

A program for the in-flight measurement of rotor blade airloads, blade bending, and the resulting control and rotor shaft loads and fuselage vibration response has been conducted on a CH-47A tandem rotor helicopter. The accomplishments of this project are documented in a multivolume report. A review and critique of the highlights of the flight test results, and a brief comparison of the results with theoretical predictions and with other rotor airloads data, are presented in this volume. Due to the large variety and great volume of data obtained, it is acknowledged that this effort has been of limited depth, and that considerably more value can be obtained from further analysis. However, some of each type of data are presented and illustrated, with the main objective of establishing a starting place for subsequent analysis.

The airload measurements obtained in this program are similar to the measurements obtained in other airloads programs. A significant exception is that single lifting-rotor helicopter data differ from the forward rotor data of a tandem. Apparently, the aft rotor produces an upwash which gives an increase in the airloads on the inboard region of the forward rotor. This effect results in an airload distribution that is similar to that which would be obtained with an increased blade twist of the forward rotor. For most longitudinal cyclic trim settings, the oscillations of the airloads of both tandem rotors tend to be similar to those of a single rotor, with intrarotor tip vortex intersections causing the predominant disturbances. Longitudinal cyclic trim settings can be obtained experimentally with the tandem helicopter which cause large airload pressure oscillations due to the intersection of forward rotor blade vortexes by the aft rotor blades. These pressure oscillations occur rapidly and do not appear to increase blade stresses, rotor shaft loads, or airframe vibration.

FOREWORD

This report consists of a review and evaluation of the data obtained in a program conducted under Contract DA 44-177-AMC-124(T) for the measurement of dynamic airloads on a tandem rotor helicopter. Discussion of data comparisons which show consistency and accuracy of the data and some theoretical comparisons are presented. It is noted that this effort considerably exceeds the general requirements of this contract, which are to:

> "Instrument a government-furnished CH-47A helicopter to observe and record for two (2) basic flight conditions the following in-flight data:
>
> a. Rotor blade differential pressure
> b. Rotor blade strain and motion
> c. Control strain and motion
> d. Rotor hub and shaft loads
> e. Fuselage vibration response
>
> Prepare and submit a draft final report in triplicate in accordance with USATRECOM regulation 715-10. Graphical presentation of the performance data, together with sections including structural and flight test data, shall be included."

These requirements have been exceeded in that additional data were acquired; these data have received preliminary analysis and evaluation, and are ready for subsequent detailed analysis.

In this volume, brief descriptions are given of instrumentation, data system, and flight testing aspects of this project with the supporting details reported in the other volumes of this report. These volumes are as follows:

Volume	I,	Instrumentation and In-Flight Recording System
Volume	II,	Calibrations and Instrumented Component Testing
Volume	III,	Data Processing and Analysis System

The findings of this project are also discussed in references 17 and 19, and tabular data summaries, references 4 and 20, are

available. Flight testing details are reported in reference 25. An extension to this program to obtain data under extreme operating conditions produced additional tabular data which are included in reference 4, and a fifth volume of this report, as follows:

Volume V, Investigation of Blade Stall Conditions

This project was conducted under the technical cognizance of William T. Alexander, Jr., of the Aeromechanics Division of USAAVLABS. The author of this report is Richard R. Pruyn, who also served as the Boeing-Vertol Project Engineer. Other Vertol Division personnel who contributed significantly to the success of this project are:

Project Group	Data Systems
W. J. Grant	J. W. Obbard
A. Meyer	G. Eliason
W. Koroljow	
E. Haren	
J. Fries	

Flight Test

Instrumentation	Operations	Pilot
R. Golub	T. Danford	E. Nelson
W. McLachlan	R. Reber	
H. Fairchild		

The consultation and assistance of F. D. Harris and J. Liiva of the Vertol Aerodynamics Staff are also gratefully acknowledged.

CONTENTS

CONTENTS

ILLUSTRATIONS

ILLUSTRATIONS

ILLUSTRATIONS

ILLUSTRATIONS

ILLUSTRATIONS

ILLUSTRATIONS

ILLUSTRATIONS

ILLUSTRATIONS

ILLUSTRATIONS

ILLUSTRATIONS

ILLUSTRATIONS

TABLES

TABLES

TABLES

SYMBOLS

a	lag damper moment arm length, inches
A_K	Fourier coefficient of Kth harmonic cosine term in positive series of sine and cosine terms (see equation (2))
b	number of blades per rotor
B_K	Fourier coefficient of Kth harmonic sine term in positive series of sine and cosine terms (see equation (2))
c	rotor blade chord, inches
$\bar{c}$	mean aerodynamic chord, equal to blade chord for rectangular planform rotor blades, inches or feet
cg	center of gravity
C_{do}	average rotor profile drag coefficient
C_n	normal force coefficient obtained from two-dimensional airfoil data
$\overline{C_n}$	azimuthal average value of normal force coefficients obtained from two-dimensional airfoil data
C_{NP}	normal force coefficient calculated from pressure measurements using theoretical local resultant velocity
$\overline{C_{NP}}$	azimuthal average of normal force coefficients obtained from pressure measurements
C_P	rotor power coefficient
C_{PP}	rotor parasite power coefficient
C_{TW}	thrust coefficient based on run gross weight - for mid-cg, $C_{TW} = RGW/2\rho\pi R^2 (\Omega R)^2$

SYMBOLS

e_β	flapping hinge offset, inches
e_ζ	lag hinge offset, inches
f	rotor hub torque offset, inches (see Figure 4), or helicopter equivalent parasite drag area, square feet
g	the acceleration of gravity, 32.2 feet per second per second
IGE	in ground effect, defined for this project as an altitude with a wheel-to-ground clearance of approximately 10 feet
K	harmonic number based on rotor rotational frequency - K = 0 for azimuthal average terms
K_i	induced power factor resulting from nonuniform downwash
K_1, K_2	constants of an exponential function used to smooth the values of p(x) - values determined for given test point and radius by least-squares fit of p(x) measurements
$\left\|\ell_K\right\|$	Kth harmonic airload ratio, Kth harmonic resultant of lift per unit span divided by the ratio of the run gross weight to the blade tip radius
LF	lift force produced by airloads on the fuselage, pounds
LS	lift per unit span, integration of chordwise pressure distribution at particular radius and azimuth position, pounds per inch
$\left\|\frac{LS_K}{c}\right\|$	Kth harmonic resultant of lift per unit span per unit chord at a given radius, pounds per square inch
M(.85,270)	Mach number at 85-percent radius of the retreating blade at 270 degrees azimuth

SYMBOLS

M(1.0,90)	Mach number at the tip of the advancing rotor blade at 90 degrees azimuth
M(1.0,270)	Mach number at the tip of the retreating rotor blade at 270 degrees azimuth
MF_{325}	pitching moment produced by airloads on the fuselage, aerodynamic center assumed to be at station 325, foot-pounds
n	upper limit value of K considered in Fourier analysis of data, commonly 12 for this project
OAT	outside air temperature, °C
OGE	out of ground effect, defined for this project as an altitude greater than 200 feet from the ground
p(x)	azimuthal average airload pressure at a given radius and at chordwise location x, pounds per square inch differential
P	blade pitch control arm length, inches
PM	pitching moment per unit span determined by integrating airload moments about a particular chord reference position
q	dynamic pressure, pounds per square foot
r	distance from the center of rotation to a particular blade station, inches
R	rotor blade tip radius, inches
RC	root cutout, radius to beginning of airfoil section of blade with blade at zero lag, inches
RGW	run gross weight, pounds
RHDL	region of high dynamic loads
R_K	resultant amplitude of Kth harmonic in a positive series of sine terms (see equation (3))

SYMBOLS

$\lvert S_{A1} \rvert$	longitudinal first harmonic shaft shear to rotor lift ratio; for mid-cg as tested, rotor lift was assumed to be one-half of the run gross weight
t	time, seconds
TAS	true airspeed, knots
TOGW	takeoff gross weight of helicopter, pounds
TPN	test point number
U	resultant velocity in the plane of the chord at a particular blade station and azimuth divided by ΩR
V	resultant velocity, feet per second
x	distance measured parallel to centerline of airframe or chordwise distance on blade from leading edge, inches
y	distance from centerline of airframe measured in plane of the waterlines, inches
Y	any arbitrary parameter used for illustrative purposes only
z	distance measured in direction perpendicular to fuselage waterlines, inches
α	local angle of attack, degrees
α_s	angle of inclination of rotor shaft (used for comparative wind tunnel data only), positive when inclined toward the drag vector, degrees
$\approx\alpha(1.0,270)$	approximate angle of attack of the retreating blade tip as calculated assuming uniform downwash and rigid blades
β_{A1C}	longitudinal first harmonic blade flapping amplitude with respect to the control axis, degrees

SYMBOLS

ΔP	differential pressure (lower surface - upper surface) measured at a particular span, chordwise position, and azimuth angle (instantaneous), pounds per square inch differential
$\lvert \Delta P_K \rvert$	Kth harmonic resultant of local blade pressure at a given radius and chordwise location, pounds per square inch differential
ζ	blade lag angle, degrees
θ_{B1}	longitudinal cyclic blade pitch (longitudinal cyclic trim control on tandem helicopter), degrees
μ'	rotor advance ratio, calibrated true airspeed of helicopter divided by the rotational tip speed of the rotors
ρ	mass density of air, slugs per cubic foot
σ	rotor solidity, $\sigma = b\bar{c}/\pi R$
ϕ_K	phase angle of Kth harmonic term in a positive series of sine terms (see equation (3))
ψ	rotor azimuth angle, measured in direction of rotation from position over the centerline of the helicopter when blade tip is pointing aft
$\omega n\zeta$	natural frequency of lag motion of rotor blades, cycles per second
Ω	rotor rotational speed, radians per second
1/rev.,3/rev.,etc.	one per revolution, three per revolution, etc.

SYMBOLS

Note: A consistent symbol definition has been used in this report to designate the flight which was the source of the data. The symbols used are as follows:

Symbol	Flight Number
◊	384
◺	386
⏢	389
◇	390
△	391
◊	393
◺	394
◇	395
○	397
□	398

INTRODUCTION

The evolution of the helicopter has reached a point at which there will be greatly increased competition for the next generation models. This competition will be intensified by the fact that there do not appear to be any significant new increases available in speed or any other measure of the performance of the helicopter. Exploration of the maximum reasonable speed envelope of the helicopter by flight research vehicles has not uncovered any new findings which would indicate that the predicted performance limitations of the rotor can be efficiently broached. However, it seems likely that the helicopter, with its excellent hovering and low-speed maneuvering capability, will not be replaced but will only be supplemented by VTOL vehicles which are capable of greater speeds. Therefore, the competitive feature of the next generation of helicopter models will be that of extreme efficiency. Weight compromises presently made to achieve acceptable vibration levels are significant in present helicopters, and therefore efficiency can be improved by reducing vibratory loads. Structural efficiency achieved by proper tuning of the aerodynamic-dynamic system to reduce dynamic loads also appears to be relatively unexploited. While some attempts in these directions have been made, a much finer resolution of the aerodynamic excitations on the rotor is required. A key to this understanding has been made available by the measurement of rotor airloads.

While obvious to the rotor aeroelastician, it should be pointed out that rotor blade sections routinely experience larger variations in operating conditions with every revolution than the sections of most airplane wings ever experience. It would require a near-sonic acrobatic airplane which could fly backward to duplicate all the normal operating conditions of rotor blade sections. Of particular importance for the rotor is the large rate of change of conditions which occurs, since all these variations happen each revolution. The analogous situation in the airplane occurs in a rapid pullup. This maneuver has been known to produce considerably larger lift than would be expected from quasi-static airfoil data, due to the time-dependence of aerodynamics at high angles of attack. As shown in reference 5, the primary parameter of this phenomenon is $\left(\frac{\bar{c}}{V}\right)\frac{d\alpha}{dt}$, and time-dependence becomes significant when this parameter has a value in excess of 0.003. Rotor blade sections for typical level-flight cruising conditions (120 to 140 knots) routinely experience changes in angle of attack of 10 to 12 degrees, or considerably higher if disturbed by a tip vortex. If it is

conservatively assumed that this angle-of-attack variation is sinusoidal and that the advance ratio of the rotor is 0.3, the angle-of-attack rate parameter for the retreating tip of a blade wit' aspect ratio of 15 is 0.02. This value is nearly one order of magnitude larger than the boundary value, so it should not be surprising to find that time-dependence is a very significant parameter in rotor aerodynamics, even for first harmonic loadings.

The rotor airloads measurement research efforts sponsored by USAAVLABS and others have included in-flight measurements on various contemporary helicopter configurations. This project is the most ambitious of these programs, with simultaneous measurements of airloads, blade dynamics, control loads, and airframe response being made on both rotors of a tandem configuration. This effort is related to the previous dynamic airloads tests as shown in Table I. These programs have stimulated rotor research and have contributed a fund of knowledge that is now being actively utilized to improve helicopter efficiency.

The related experience of the contractor in performing this type of research is illustrated in Figure 1. This program has drawn on two previous rotor airloads and rotor shaft loads programs. This experience significantly benefited this program, particularly in the development of instrumentation, calibration, and data reduction techniques. These previous programs also showed the need for an automatic digital data system. The analysis of the results of this program under USAAVLABS contract is to be performed by Cornell Aeronautical Laboratories; however, Boeing-Vertol will also be performing various analyses. As shown in Figure 1, these efforts will include consideration of acoustics, vibration, loads and stress, rotor dynamics, and aerodynamics. These data will also be used for correlation with the oscillating airfoil test data which will be obtained under USAAVLABS Contract DA 44-177-AMC-438(T). This effort is expected to provide increased understanding of the time-dependent aspects of rotor aerodynamics, to show how well these effects can be measured in wind tunnel testing, and to indicate the types of airfoil sections which should be used to take maximum benefit from these effects.

The test helicopter used for this program was an experimental flight test version of the CH-47A. As illustrated in Figure 2, this vehicle was externally identical to a standard CH-47A, except for instrumentation; however, it should be noted that through years of flight testing, numerous detail changes had

TABLE I

RELATIONSHIPS BETWEEN PRESENT TESTS AND EXISTING ROTOR AIRLOADS DATA

ROTOR GEOMETRY						
		SINGLE ROTOR			TANDEM ROTOR	
BLADES PER ROTOR		2	3	4	2	3
SMALL MODELS (ROTOR DIAMETER <8 FEET)						
HUB CONFIG.	TEETERING	-	-	-	-	-
	FULLY ARTICULATED	Meyer and Falabella (16)	-	-	-	-
LARGE MODELS (ROTOR DIAMETER ≥8 FEET)						
HUB CONFIG.	TEETERING	Rabbott (21,24) Mayo(15)	-	-	Huston(14)	-
	FULLY ARTICULATED	-	Ham(10)	X	-	Ham(9)
FULL SCALE (WIND TUNNEL OR FLIGHT TEST)						
HUB CONFIG.	TEETERING	Burpo (2,3)	X	-	-	-
	FULLY ARTICULATED	-	X	Scheiman (27) Rabbott (22)	-	Present Tests Gabel (8)

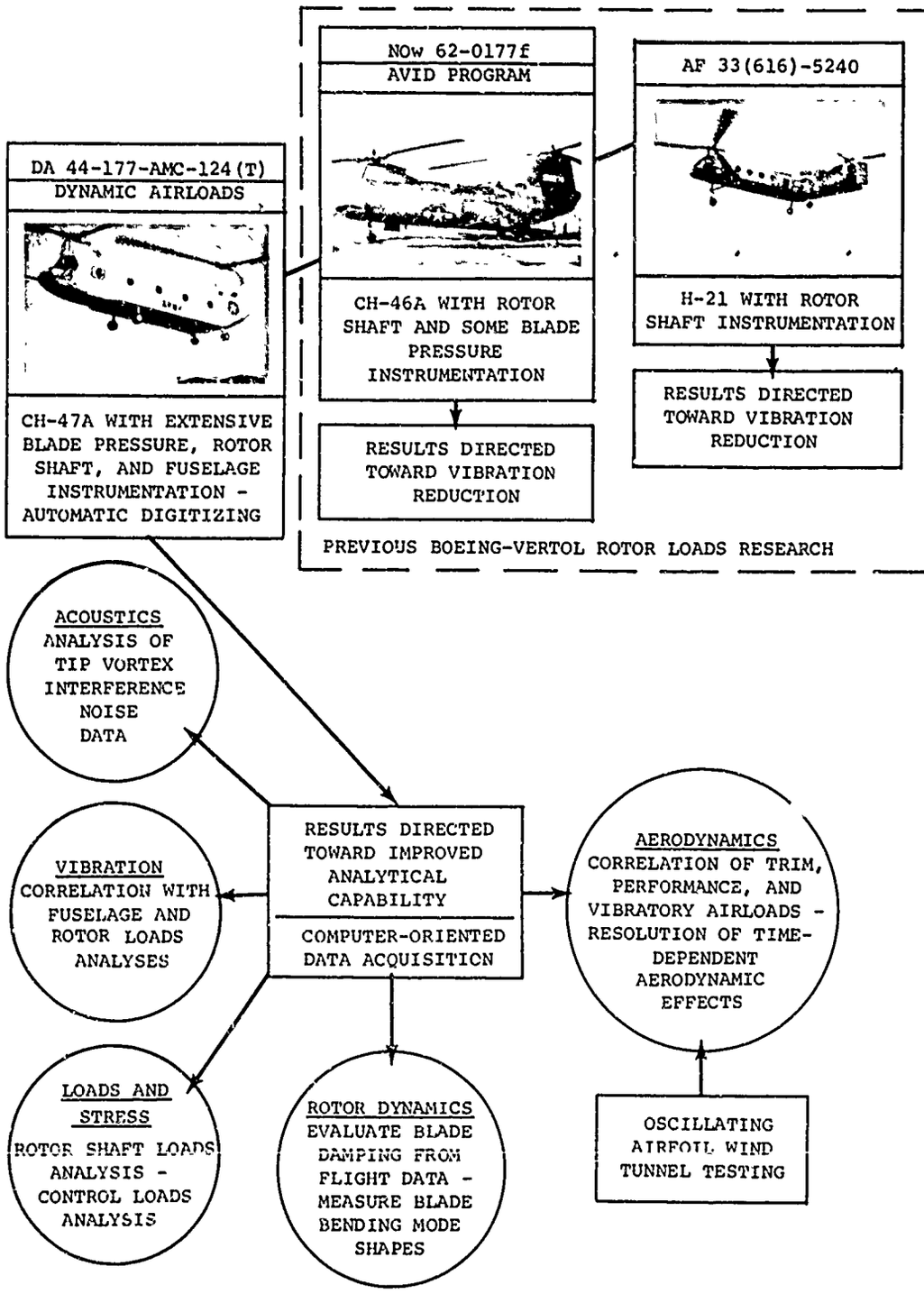

Figure 1. Relation of Program to Experience and Planned Future Efforts of Contractor.

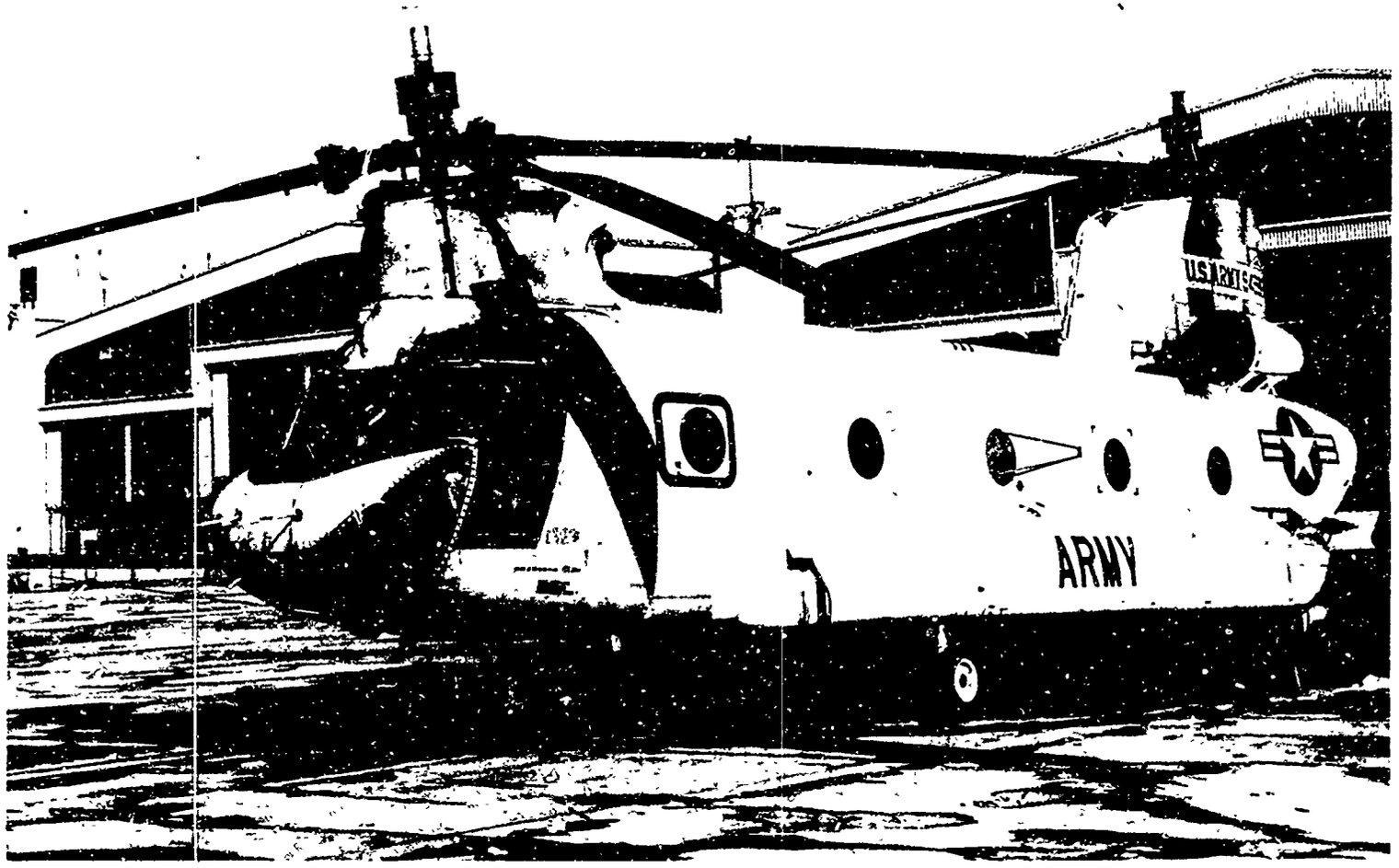

Figure 2. External Configuration of Test Aircraft.

been incorporated. For example, the rotor control system was an experimental model of the control system used in the last production version of the CH-47A. An experimental version of the isolated cargo floor was also incorporated. The remainder of the aircraft was predominantly the initial production model CH-47A(YHC-1B). The differences are significant and should be considered before any conclusions are drawn from the data of this program and applied to the production CH-47A. However, these differences are not believed to reduce the value of these data, since this program was a research program aimed at analytical capability improvement, and any product improvement which is achieved should come from the analysis.

The approach followed in this report, whenever possible, was to present all available data to illustrate the accuracy and scatter. Subsequent data analyses should utilize the presentations of this report to select values which minimize experimental variations. It is believed that this approach tends to make the test data appear somewhat inconsistent; however, this result should put the analyst on his guard so that he is selective. Present methods are not adequate to insure that some spurious data are not included in the voluminous output of this program.

DESCRIPTION OF TEST ITEM

The general arrangement of the test helicopter is shown in Figure 3. This aircraft has tandem rotors which are mounted with a large overlap and a small vertical separation. The only modifications to the test aircraft for this program were to provide the required instrumentation. The rotor blades, rotor shafts, rotor controls, and the airframe were instrumented. These components are discussed in detail in the other volumes of this report, and this section of the report will therefore be limited to the aspects of those components which apparently have influenced the results.

ROTOR BLADES

This testing utilized modified CH-47A rotor blades with one blade of each rotor modified to provide the required instrumentation and with the two mating blades of each rotor modified to provide additional tip balance weights. The pertinent rotor blade geometry and physical characteristics are given in Table II.

TABLE II

PRINCIPAL DIMENSIONS AND PHYSICAL CHARACTERISTICS OF TEST ROTORS

Number of blades per rotor	3
Rotor blade radius, inches	354.62
Cutout radius, inches	68.5
Flap hinge offset, inches	8.0
Lag hinge offset, inches	29.5
Weight per blade (approximate), pounds	268.0
Construction - metal spar, fiber glass trailing edge fairings	
Twist, degrees	-9.0
Airfoil section	Modified NACA 0012
Blade chord, inches (constant)	23.0
Rotor solidity, σ	0.06222
Approximate rotor blade mass constant, γ	9.7
Normal rotor blade tip speed, feet per second	712.0
Normal rotor angular velocity, radians per second	24.2
Test disk loading, pounds per square foot (based on swept area and 32,000-pound test weight)	6.0
Swept disk area, square feet (both rotors)	5486.0

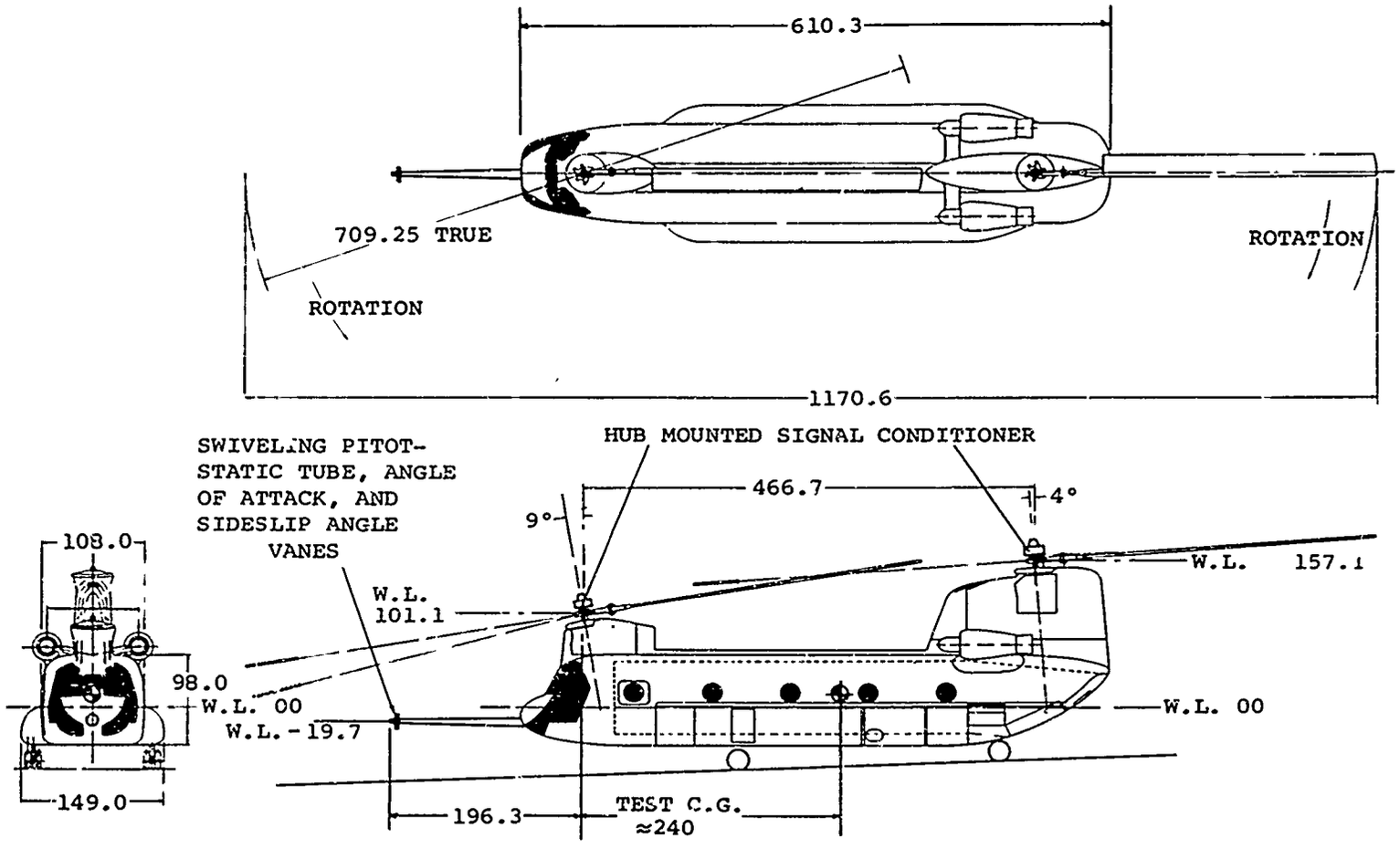

Figure 3. General Arrangement of CH-47A Helicopter as Tested.

TABLE II - Continued

Mass moment of inertia of blade about flap hinge, slug-feet^2	2327.9
Mass moment of inertia of blade about lag hinge, slug-feet^2	1903.4
Mass moment of inertia of blade about pitch axis at zero lag, slug-feet^2	1.91
Static moment of blade about flap hinge, inch-pounds	49,881.5
Static moment of blade about lag hinge, inch-pounds	42,089.2
Hub torque offset, inches	1.58
Lag damper arm, inches	6.9
Pitch arm, inches	10.25
Equivalent viscous lag damping, pound-seconds per inch at 1.5 degrees and $\omega n\zeta$	4522.0
Pitch with lag pin vertical, degrees at r/R = 0.75	10.53
Forward rotor shaft tilt, degrees	9.0
Aft rotor shaft tilt, degrees	4.0

These blades were mounted on CH-47A rotor hubs which have the blade pitch bearings located between the lag hinge and the flapping hinge, as illustrated in Figure 4. Detailed mass and stiffness properties of these blades are given in Volume II of this report.

The instrumented rotor blades were made for this program by utilizing selected materials in order to minimize the effects of the instrumentation. These blades contained and supported the instrumentation wiring internally and provided for the external mounting of the airload pressure transducers as shown in Figure 5. The rotor blade instrumentation consisted of pressure transducers and strain gages as illustrated in Figure 6.

Absolute- and differential-pressure transducers were used to measure the rotor airloads over a chordwise and spanwise array of blade locations. Electrically paired absolute transducers were installed on the top and bottom of the spar section of the blade, while differential units were used on the blade trailing edge fairings. This arrangement was used so that it was not necessary to drill holes in the spars to provide differential-pressure ports. The transducers were attached to the blades by bonding the mounting tabs to the blade surface within recesses provided in external fairing sleeves. An elastic bonding agent was used to mount the transducers so that

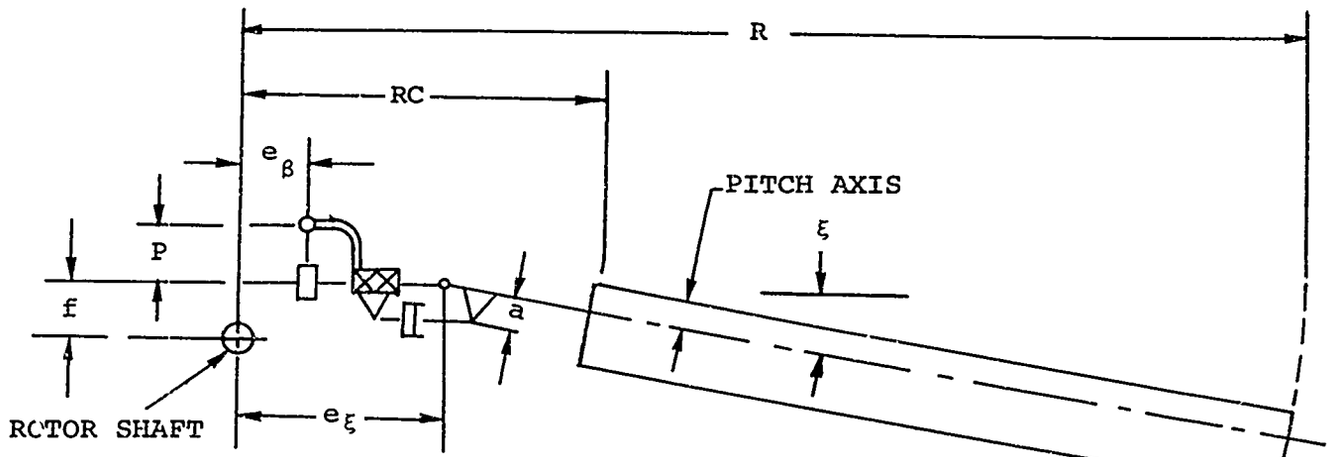

Figure 4. Schematic Diagram of Rotor Blade Geometry.

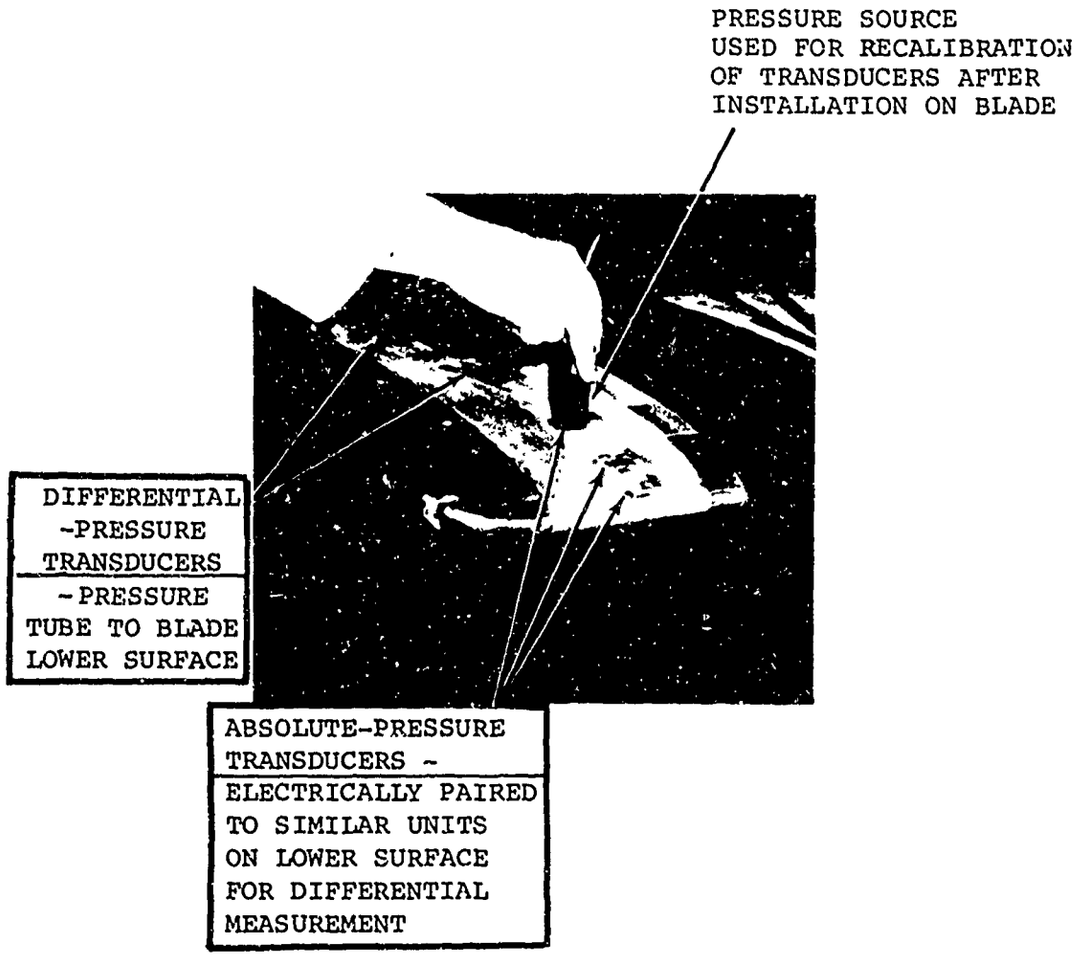

Figure 5. Installation of Pressure Transducers on Rotor Blade Tip.

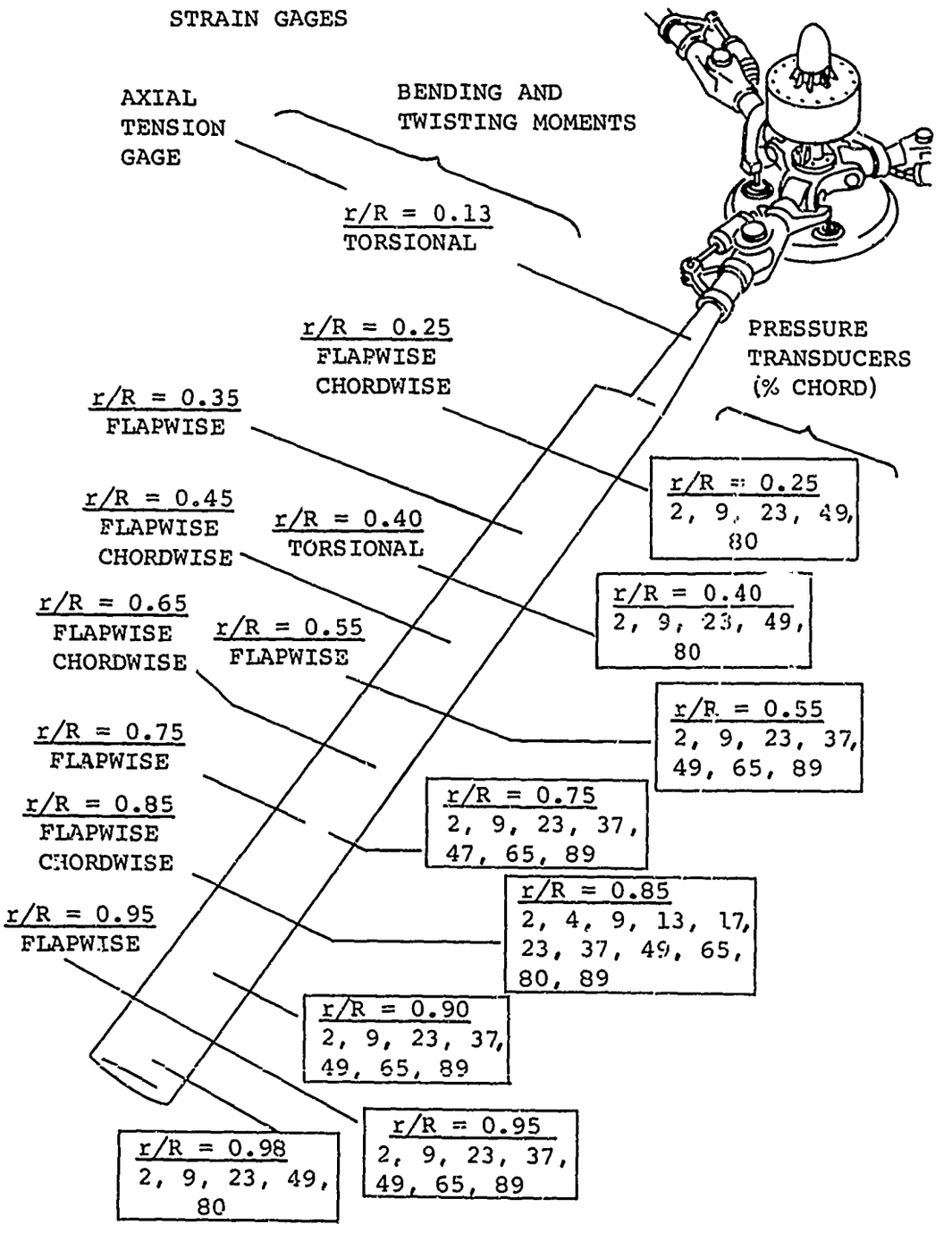

Figure 6. Rotor Blade Instrumentation Locations.

blade surface strain interactions were negligible. The general effect of the transducer installation was to have a series of flush diaphragms with little change in the airfoil dimensions.

It has been shown in other rotor airloads programs that oscillating blade airloads are significantly altered by blade bending. It was therefore important to determine and document the dynamic characteristics of the tested rotor blades. This result was accomplished in this program by means of a coupled flap-torsion bending analysis, an uncoupled chordwise bending analysis, and a static (nonrotating) dynamic response test program. The most significant results of this effort are shown in Figures 7, 8, and 9, which compare the calculated static natural frequencies to the static test data, and which also show the effects of rotation and the control system flexibility on the natural frequencies. It may be noted in Figure 7 that the second flapwise natural frequency was predicted very well but that the third and fourth flapwise frequencies were about 10 percent higher than predicted. This means that the flapwise stiffness of the outer portion of the blades is probably somewhat larger than the values shown in Volume II. The low prediction of the analysis should be considered when interpreting the calculated flapwise natural frequencies. At the normal rotating speed of 230 rpm, it would be expected that the flapwise response would be amplified at 2/rev., 3/rev., 5/rev., 8/rev., and 13/rev., due to the proximity of the flapwise modes to these frequencies.

The data obtained on the torsional response of the blade, shown in Figure 8, show that the primary torsional response should be 5/rev. Chordwise response of the blade should be predominantly 4/rev., as shown in Figure 9. It may be noted in each of these figures that the standard blades with the heavy tip balance weights tend to have a slightly higher natural frequency in all modes of response. This difference is believed to be insignificant for this test program, but it probably increased vibration of the test helicopter due to the lack of symmetry of the rotor hub loads.

As a check on the blade shake testing, the nodes of the flapwise modes of the dynamic response were determined. The nodes were measured with an accelerometer so that the measured locations of zero acceleration were offset from the dynamic response nodes by the rigid blade response. This effect could have been eliminated by more sophisticated instrumentation or by analysis; however, if this offset is

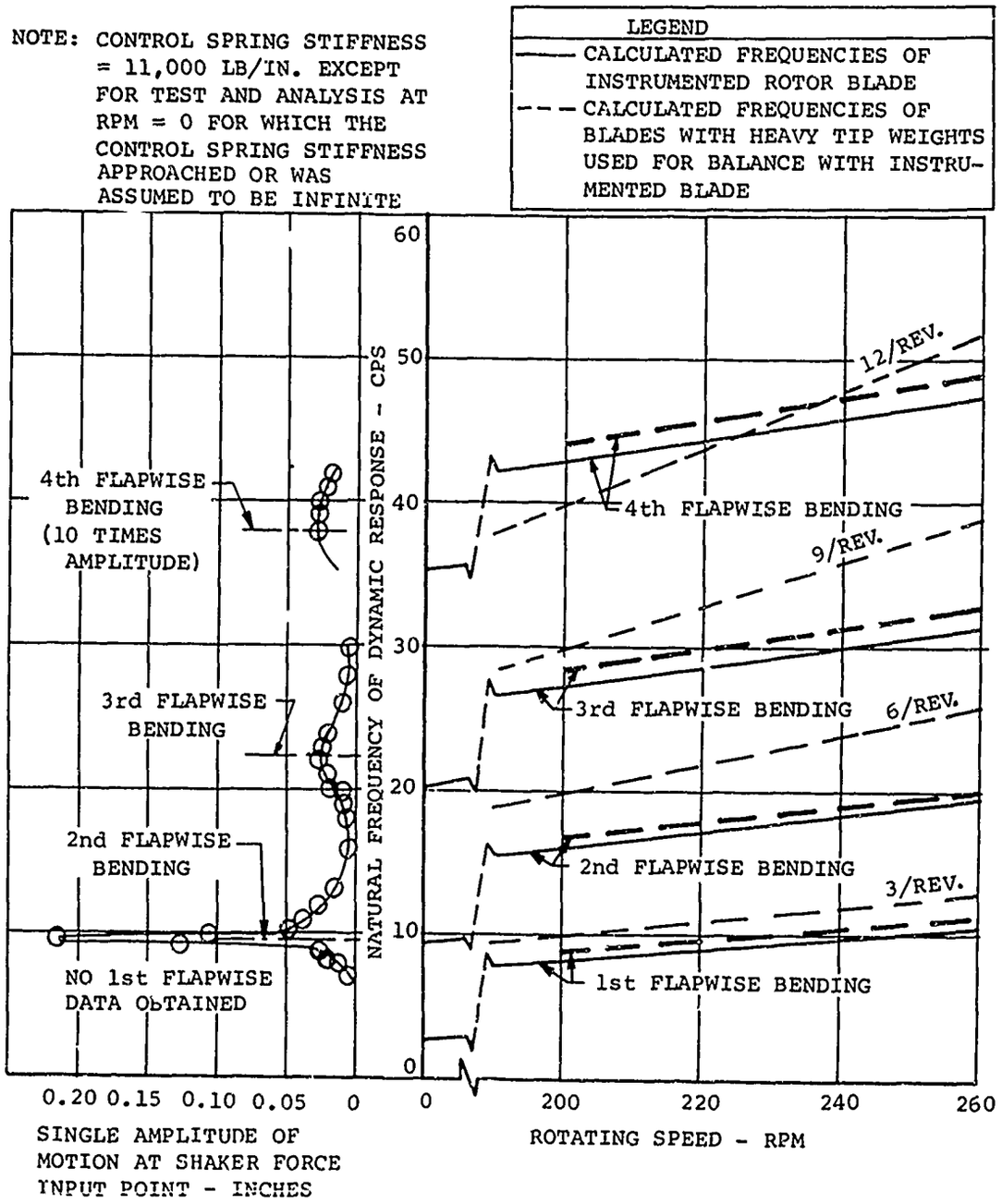

Figure 7. Comparison of Static Shake Test and Calculated Flapwise Rotor Blade Natural Frequencies.

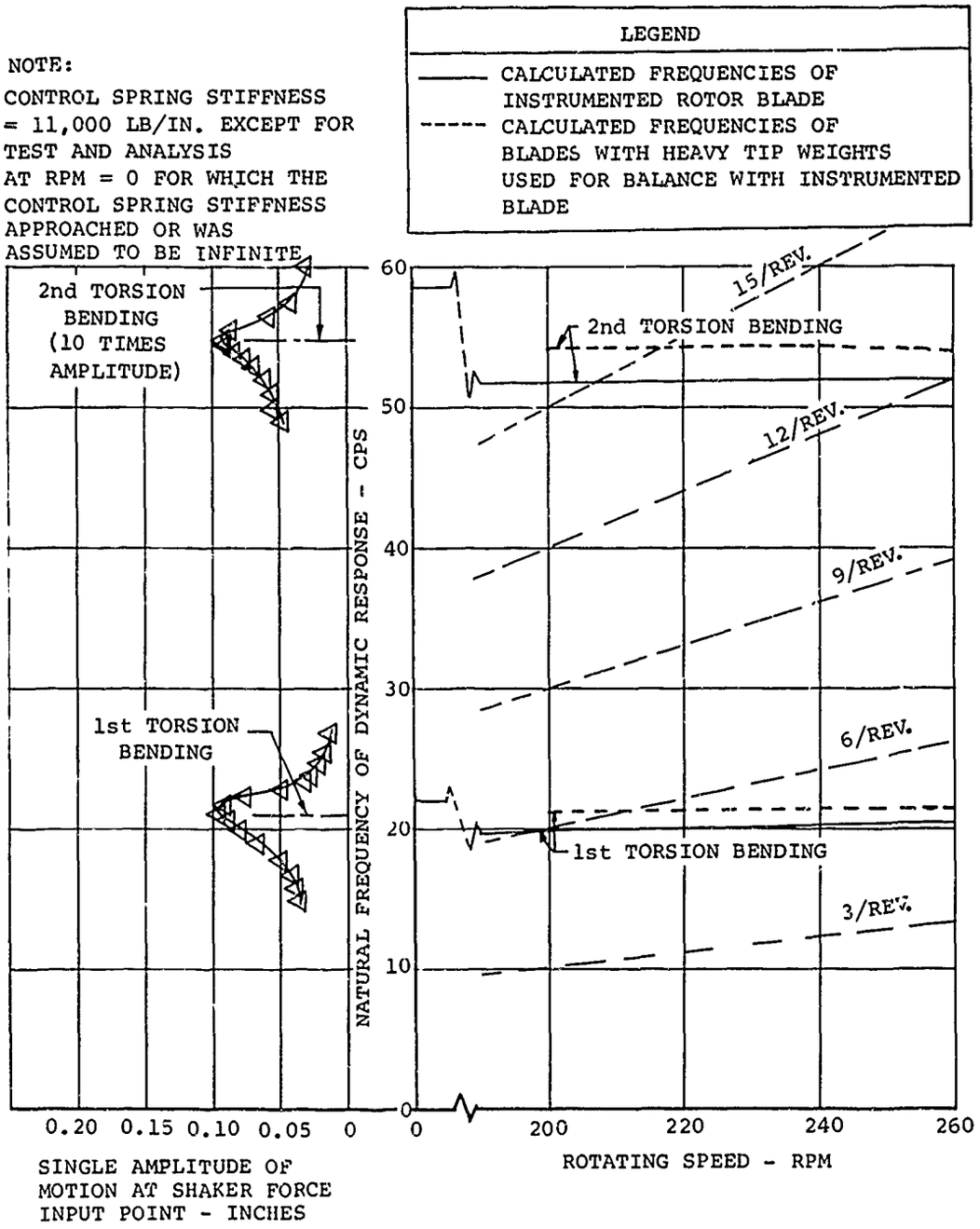

Figure 8. Comparison of Static Shake Test and Calculated Torsional Rotor Blade Natural Frequencies.

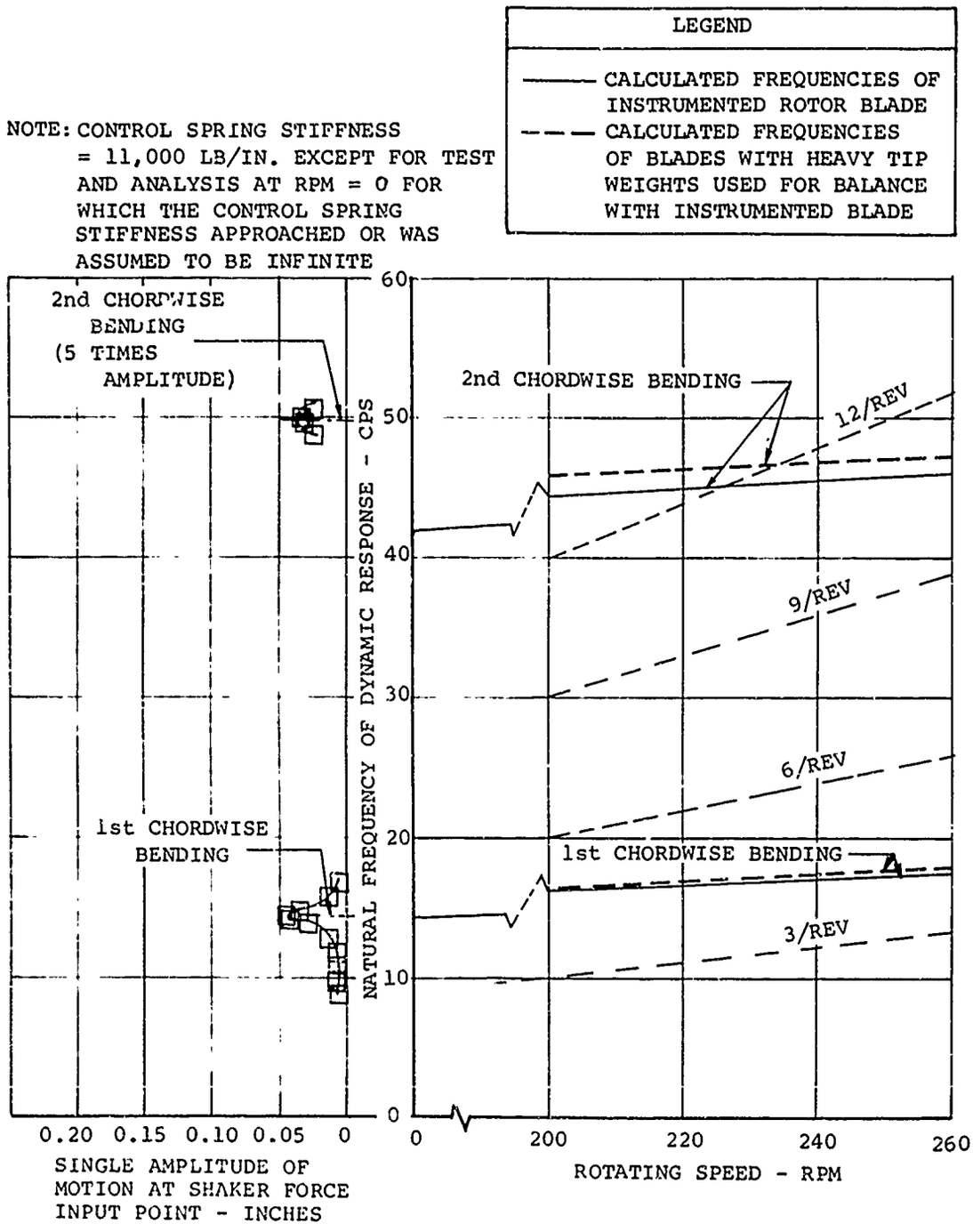

Figure 9. Comparison of Static Shake Test and Calculated Chordwise Rotor Blade Natural Frequencies.

considered, the correlation of the analytical and the measured nodes shown in Figure 10 is good. However, the outboard node of the second flapwise mode is probably offset too much, again showing that the stiffness of the outer blade area used in the calculations was too small. For the purposes of this report, the calculated blade response data are believed to be adequate; but for subsequent detailed analysis, a better resolution of the blade dynamics should be obtained.

ROTOR SHAFTS

Standard CH-47A rotor shafts were strain gage instrumented in the region shown in Figure 11 so that the steady and alternating rotor loads could be measured. Bending moment and shear gages were provided on the shaft in two orthogonal planes. Lift was measured with a gage which measured the entire load and with a gage which was only sensitive to alternating lift loads. A torque gage was also provided.

As a result of the low strain sensitivity of the rotor shafts to shear and lift, these gages have significant interactions which must be identified by calibration and which must be corrected in flight test data reduction. The procedures for these operations are presented in Volumes II and III of this report. In general, the calibration for the shafts results in a 6-by-6 matrix of coefficients. As shown in Volume II, the shaft calibration data were subjected to a detailed statistical correlation and evaluation which produced a well-substantiated calibration of good accuracy.

A significant part of the rotor shaft instrumentation is provided by three rotating accelerometers mounted on each rotor hub, and by an array of accelerometers on the rotor shaft supports. These accelerometers measure the motions of the hub and shaft so that the resultant inertia loads can be isolated. It has been found in previous testing (reference 8) that hub motions can cause significant contributions to third harmonic rotor shaft loads.

ROTOR CONTROL SYSTEM

The control system of the test aircraft was not a production unit but was an experimental unit used to develop an improved production system. This unit is known as the SK system and is geometrically similar to the production system used in aircraft which incorporate Engineering Change Proposal 140/190. An

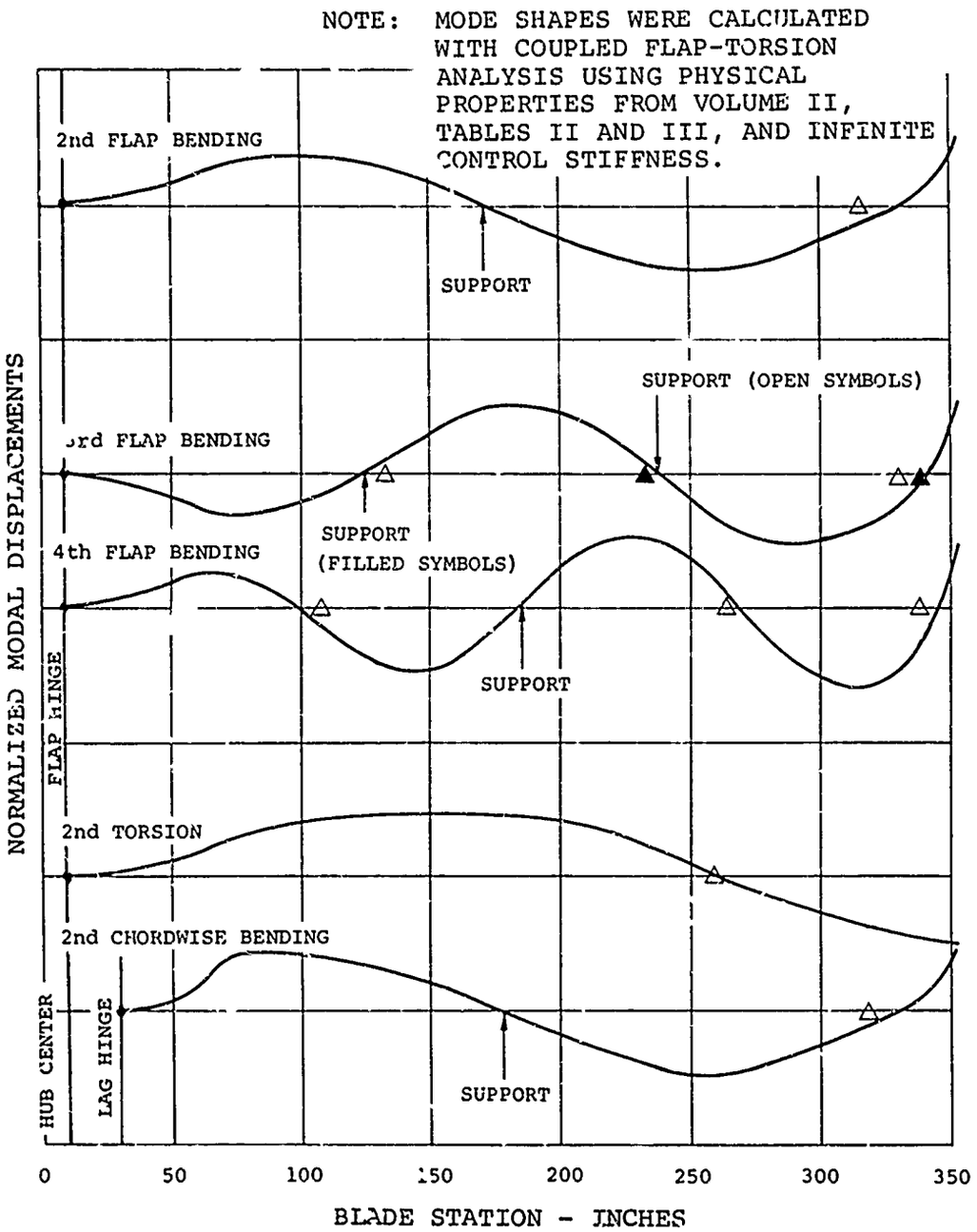

Figure 10. Calculated Blade Mode Shapes and Nodal Points Obtained in Nonrotating Blade Response Tests.

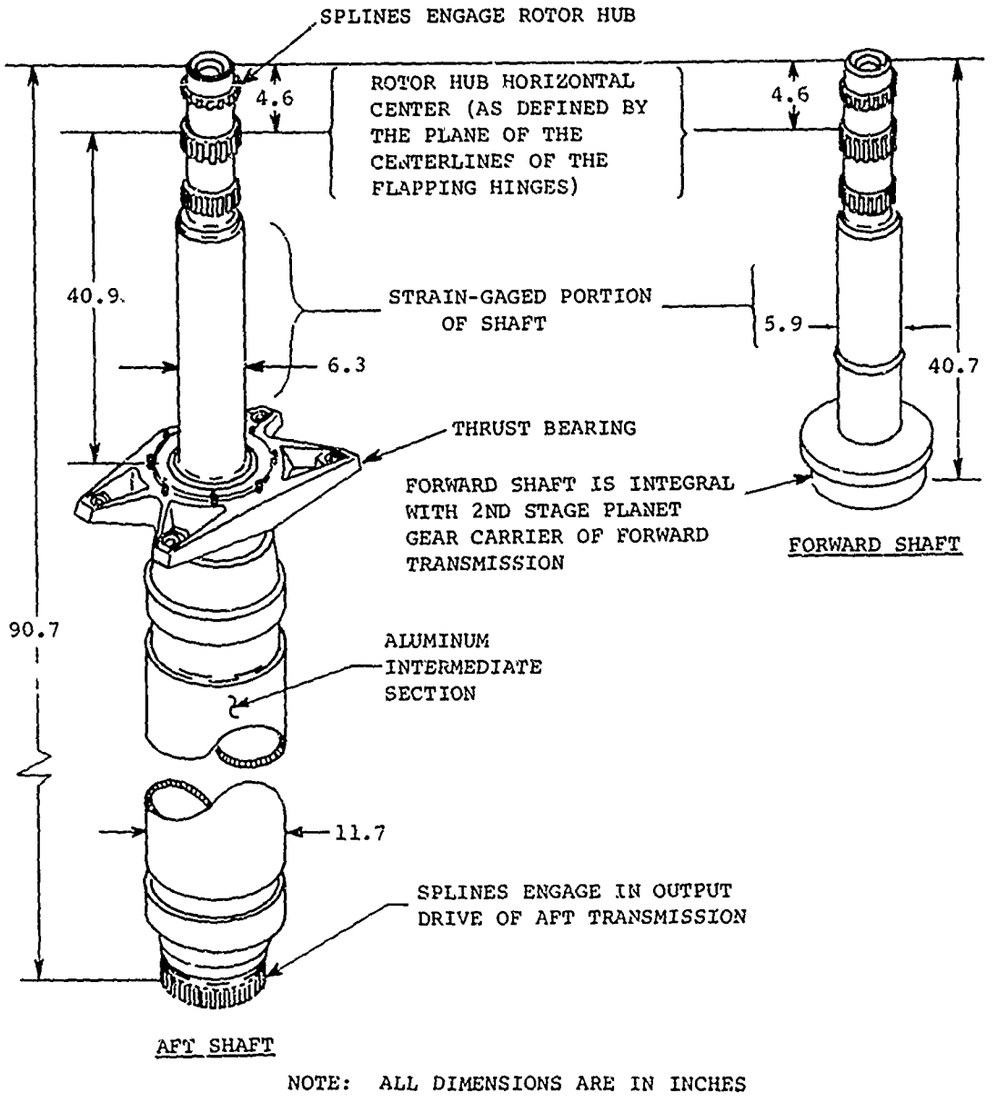

Figure 11. General Arrangement of Instrumented Rotor Shafts.

increase in strength and rigidity is provided by this modification.

Instrumentation for determining control system loads consisted of a strain-gaged pitch link in the rotating control system and three gaged loads which determine the nonrotating control system reactions. The two strain-gaged pitch links were used to control the two instrumented blades. Nonrotating control loads were measured by means of strain-gage bridges on the actuator mounting lugs of the nonrotating swashplate and a strain-gaged fixed link in the longitudinal cyclic trim system.

AIRFRAME

The airframe of the test helicopter caused significant contributions to the dynamics and aerodynamics of this testing, as well as provided its usual mechanical and structural functions. In particular, rotor orientation provided by the airframe has significant bearing on the aerodynamic-dynamic loads. This orientation is shown in Figure 3, and the numerical values of the pertinent geometry features are given in Table III. The CH-47A geometry is highly overlapped with a rotor-to-rotor distance of only 1.32 times the rotor radius. It is rather difficult to evaluate realistically the vertical offset of the rotors due to the inclination of the rotor shafts; however, if the average shaft inclination of 6.5 degrees is used as a basis, there is no vertical offset of the rotors.

TABLE III

DIMENSIONS AND GENERAL DATA OF TEST AIRCRAFT

Tandem Rotor Geometry	
Rotor center to rotor center distance, inches	466.7
Rotor center to rotor center distance/rotor radius	1.32
Vertical offset of rotors (approximate, based on mean shaft tilt)	0
Rotor blade swept overlap/rotor radius	0.69
Rotor Drive System Details	
Transmission ratio (engine to rotor)	65.8 to 1.0
Power plant type	(2) T55-L-7
Engine shaft horsepower, each	2200
Power loading, pounds per horsepower (based on 33,000-pound weight and normal power)	7.5

TABLE III - Continued

Weight and Balance Summary

Structural design gross weight, pounds	33,000
Maximum takeoff gross weight, approved, pounds	33,000
Maximum takeoff gross weight, under development, pounds	36,000
Basic design gross weight, pounds	28,300
Specification weight empty, pounds	18,058
Weight of instrumented aircraft, no fuel or ballast, pounds	19,808

Test weights of aircraft, in pounds, were as follows:

Flight	Crew Weight	Ballast	Fuel	TOGW
384	780	2320	4000	26,900
389	600	9295	4000	33,700
390	600	9295	4000	33,700
391	600	2295	4000	26,700
393	600	11,165	3800	37,273
394	600	9300	4000	33,700
395	600	1596	4000	26,000
397	600	0	3700	24,148
398	600	0	3000	23,448

Note: Ballast consisted of lead pigs which were contained in 12 standard ballast boxes installed at stations 160 (1), 200 (2), 250 (2) 310 (2), 370 (2), 420 (2), and 460 (1). Ballast weights shown above include boxes and all necessary hardware. Boxes were removed when necessary to achieve the desired test weight.

Extreme allowable center of gravity, forward Station 296
Extreme allowable center of gravity, aft Station 344

Test positions of center of gravity at takeoff were as follows:

Flight	CG Station	CG Waterline
384	325	26
389	326	15
390	326	15
391	326	26
393	327	11
394	326	15
395	331	27
397	333	31
398	333	32

Aerodynamically, the airframe of the test helicopter had the capability of producing considerable lift and pitching moment and therefore had a significant influence on trim. The airframe aerodynamic characteristics are shown by Figure 12 to vary almost linearly with fuselage angle of attack. This figure also illustrates the necessity for variation of the longitudinal cyclic trim to minimize the fuselage aerodynamic loads. For example, if the fuselage were allowed to reach -5 degrees (nose-down) angle of attack at the higher speeds tested (TAS = 140 knots), the fuselage lift would be approximately -1500 pounds and the fuselage moment would be about equal to a 6-inch forward shift in the center of gravity.

Structurally, the airframe of the CH-47A aircraft consists of a box-like semimonocoque structure of essentially square cross section. The cockpit enclosure provides a shear web at the forward end of the fuselage. The aft end of the fuselage has an opening for the rear loading ramp. Mountings and drive for the aft rotor are provided in a pylon on top of the aft end of the fuselage. Forward rotor mounting is much more rigid and consists mainly of a reinforcement to the primary airframe structure. To minimize vibratory coupling of the cargo with the airframe, an isolated cargo floor is provided. The mode shapes and natural frequencies of the dynamic response of this airframe are shown in Table IV. It may be noted that the fourth modal frequency listed in this table is very close to the third harmonic rotor frequency (230 rpm = 11.5 cps) and is therefore of importance, since this is a major forcing frequency. Also note that the forward pylon participates in a mode of higher frequency than the aft pylon as a result of its greater structural rigidity. The fuselage of the CH-47A has been analyzed and tested for dynamic response, and, as shown in Table IV, good correlation is obtained between test data and theory. Thus, a good mathematical model of the complex fuselage structure is available for the analysis of the airframe vibration flight test data.

Instrumentation of the airframe consisted of an attitude gyro and angle-of-attack and sideslip vanes to determine trim, and an array of accelerometers to measure airframe dynamic response. The fuselage accelerometers were arranged as shown in Figure 13 to best measure the modes of response shown in Table IV. Additional accelerometer measurements were also provided at the forward and aft rotor shafts by means of the accelerometers which are identified with the rotor shaft instrumentation.

NOTE: DATA OBTAINED FROM REFERENCE 7

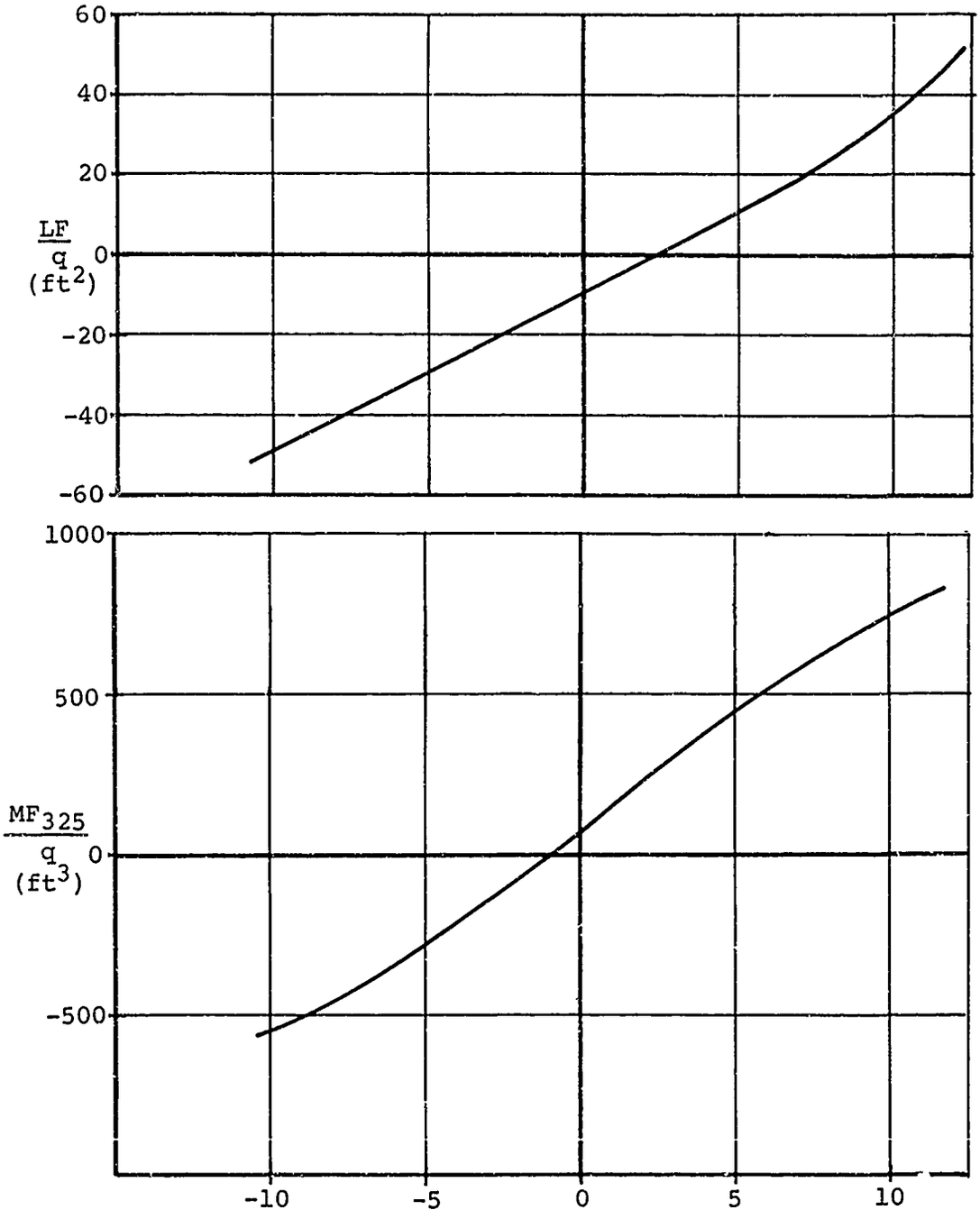

Figure 12. Aerodynamic Characteristics of CH-47A Airframe at Zero Sideslip.

TABLE IV

DYNAMIC RESPONSE CHARACTERISTICS OF CH-47A AIRFRAME

Natural Frequency cps			Description of Mode Shape	Sketch of Mode
Lumped Mass Analysis 1	Unified Structural Analysis 2	Shake Test 3		
7.35	7.68	7.9	Vertical longitudinal motion of structure, forward and aft pylons moving in opposite directions (1st beamwise mode)	
11.15	11.55	11.2	Vertical longitudinal motion of structure, forward and aft pylons moving in same direction (2nd beamwise mode)	
15.53	15.6	13.6	Predominant motion of forward pylon longitudinally	
None	7.38	7.4	Predominant motion of aft pylon laterally	
None	10.62	10.8	Fuselage torsion, forward and aft pylons moving laterally in opposite directions	

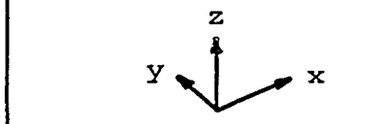

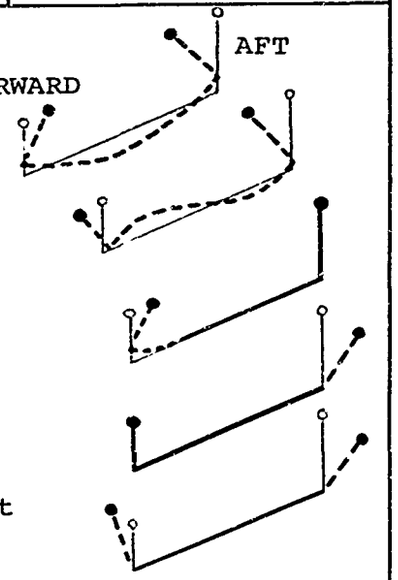

Note: Above data are available from various Vertol documents for the following conditions:

1. Analysis of simplified CH-47A configuration at 28,700-pound gross weight (Computer Program D-29); considered vertical-longitudinal motion only.
2. CH-47A at 25,000-pound gross weight.
3. YHC-1B/HC-1B helicopter standard fuselage at 25,000-pound gross weight (no isolated floor).

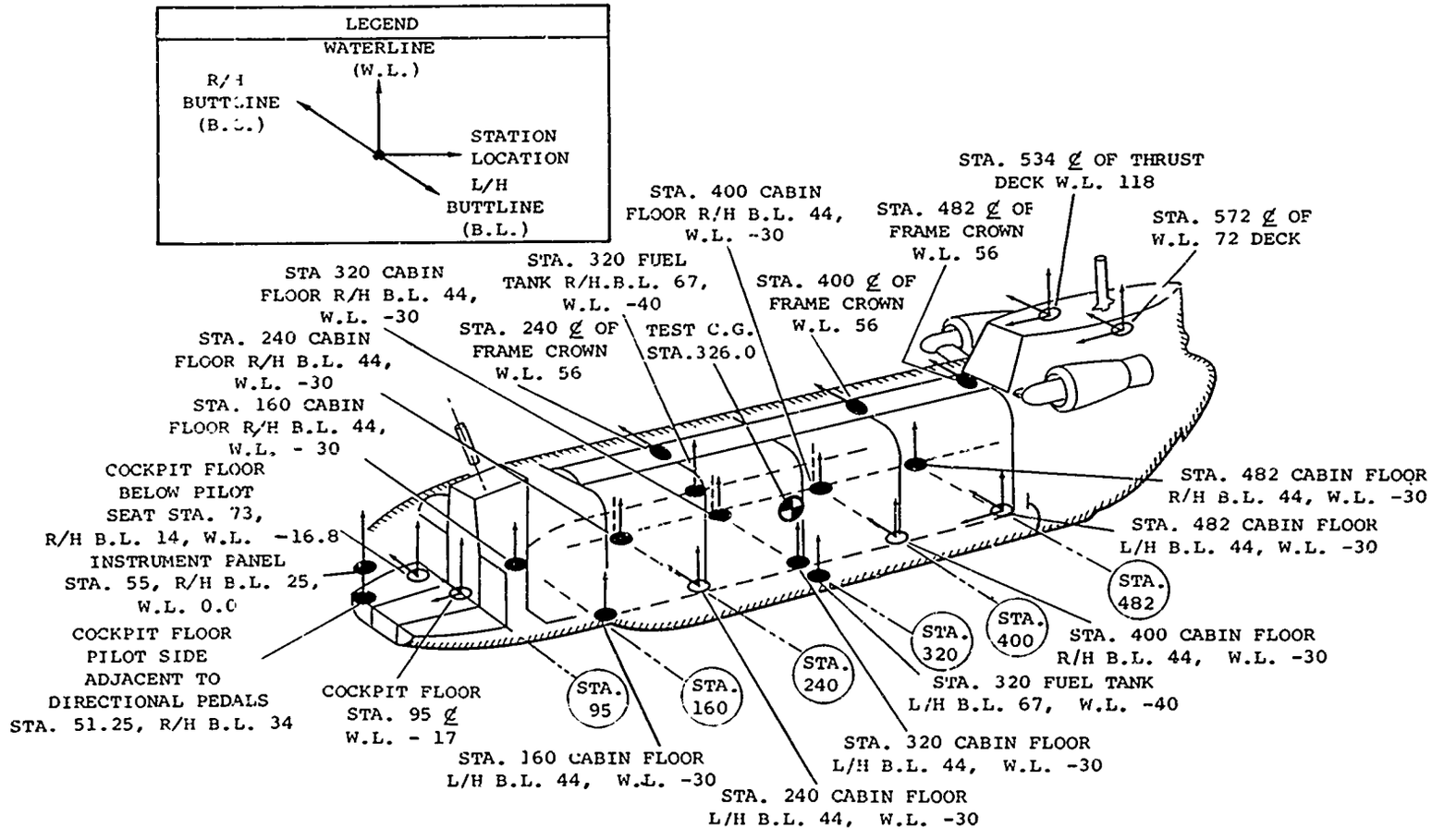

Figure 13. Location and Orientation of Fuselage Response Accelerometers.

GENERAL INSTRUMENTATION CHARACTERISTICS

The instrumentation of the test helicopter provided various measurements along the load path, and if the measurements are considered in a systematic manner, considerable redundancy is provided for data checking. This situation is illustrated in Figure 14, which shows the relationships between the various measurements obtained. As will be discussed, the airloads data obtained in this program have been checked against the blade motion and blade bending data to ensure consistency.

A detailed statistical analysis of the worst-case instrumentation error is presented in Volume I, and the results of this analysis are shown in the Figure 15 bar graph. In this analysis, it is assumed that a temperature change of -40°F occurs between the preflight calibration and data recording. The error coefficients were based on a 2σ deviation and were added vectorially. This approach is believed to be quite conservative, so that a typical or average error in the data should be considerably less than the error values shown. An evaluation of this instrumentation based on the flight test results generally substantiates this analysis, as presented and discussed in a later section of this volume.

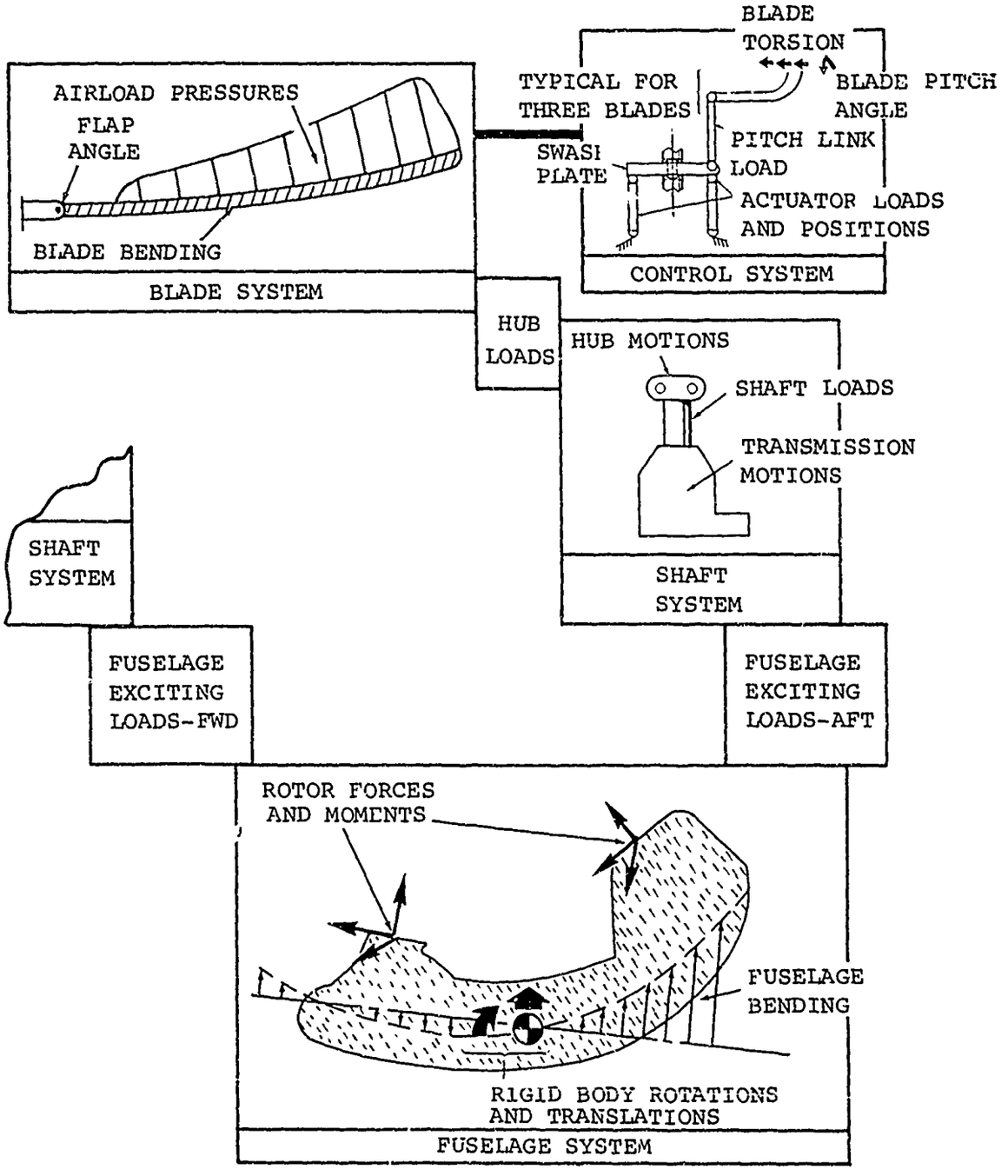

Figure 14. Schematic Diagram of Relationships Between the Various Measurements Obtained.

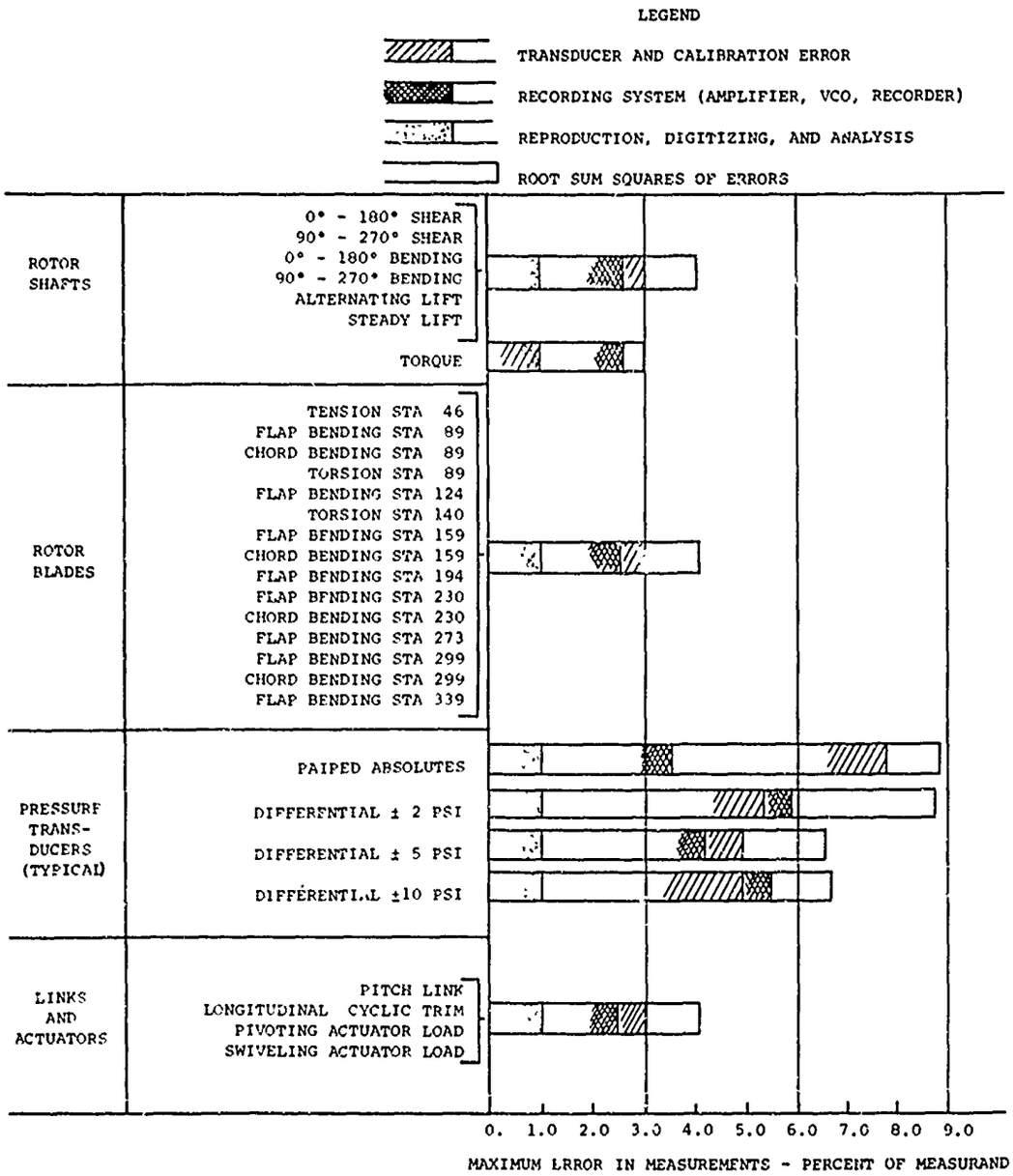

Figure 15. Accuracy of Processed Data as Estimated from Calibrations and Recording/Reproducing System Data.

EXPERIMENTAL PROCEDURE

This testing was an extensive exploration of the experimental flight envelope of the CH-47A and included a thorough in-flight calibration of the airspeed system and sideslip vanes. The test program included gross weight, rpm, airspeed, and cyclic trim variations, as will be discussed. Data acquisition generally followed the test program with minor variations in airspeed and sideslip, but with rather significant variations in altitude and cyclic trim. Average accelerations measured during data acquisition show that steady test conditions were obtained.

TEST PROGRAM

The test program to measure dynamic airloads consisted of a matrix of rotor speeds, helicopter airspeeds, cyclic trim settings, gross weights, and altitudes to explore fully the available range of thrust coefficient, advance ratio, and advancing tip Mach number capability of the test helicopter. The test points defined in Appendix I were obtained using the test program outlined in Table VII. This testing may be summarized as follows:

1. At ,000 pounds nominal test weight, 34 level flight records were obtained; 2 of these were taken in flight conditions which produce high dynamic loads.

2. Also at 26,000 pounds nominal test weight, 33 records were obtained in maneuvers and 2 records were obtained in transition and hover.

3. At 33,000 pounds nominal test weight, 43 records were obtained in level flight, including 23 which were obtained in high dynamic load conditions. One record was also obtained in hover.

4. At 37,000 pounds nominal test weight, 24 records were obtained; 2 of these were at a moderate level flight speed and 1 was in a high dynamic load condition. The remaining 21 records were obtained in hover and transition, including tests in and out of ground effect. The effects of sideslip on transition airloads were also measured.

At the successful conclusion of this testing, it was decided to extend the testing to include higher speeds at lighter gross weights. This extended program, analyzed in Volume V of this report, included approximately 20 test records obtained at 21,000- to 23,000-pound test weights. Data points obtained included a maximum true airspeed of 158 knots.

The achieved test conditions of the level flight portion of the basic flight program are shown in nondimensional form in Figure 16. Accomplished test conditions have included advancing tip Mach numbers greater than 0.9 and advance ratios approaching 0.40. During all these tests, a thrust coefficient-solidity ratio, C_{TW}/σ, greater than 0.06 was obtained. A maximum C_{TW}/σ of 0.11 was tested in transition at 33,000 pounds and 202 rpm rotor speed. Generally, the test conditions either followed the normal operating conditions of the CH-47A, or were selected to produce systematic variations in advance ratio, tip Mach number, or thrust coefficient. These variations can be noted in Figure 16.

The severity of the flight conditions tested is generally reflected by the operating environment of the retreating blade. Presently there is no well-defined criterion for this operating environment which will indicate the severity of the high dynamic loads which have in the past been called blade stall. Figure 17 was prepared to show the uniform downwash-rigid blade angle of attack and Mach number of the retreating blade tip for the conditions tested. These criteria are believed to be wrong and inadequate, but are presented to relate the conditions tested to prior rotor testing and analysis. It should be noted that approximate retreating blade tip angle-of-attack values of 10 degrees or less were tested at various tip Mach numbers.

Of the conditions tested, it is generally believed that the most important data were obtained in transition. Rotor airload effects are particularly severe in transition, especially with sideslip. For this reason, the following data presentations will emphasize these low-speed points. Secondary importance is given here to the high-speed, low-gross-weight data, since these conditions are emphasized in Volume V.

IN-FLIGHT CALIBRATIONS

An extensive airspeed and sideslip vane calibration program was conducted in flight to substantiate the proper operation

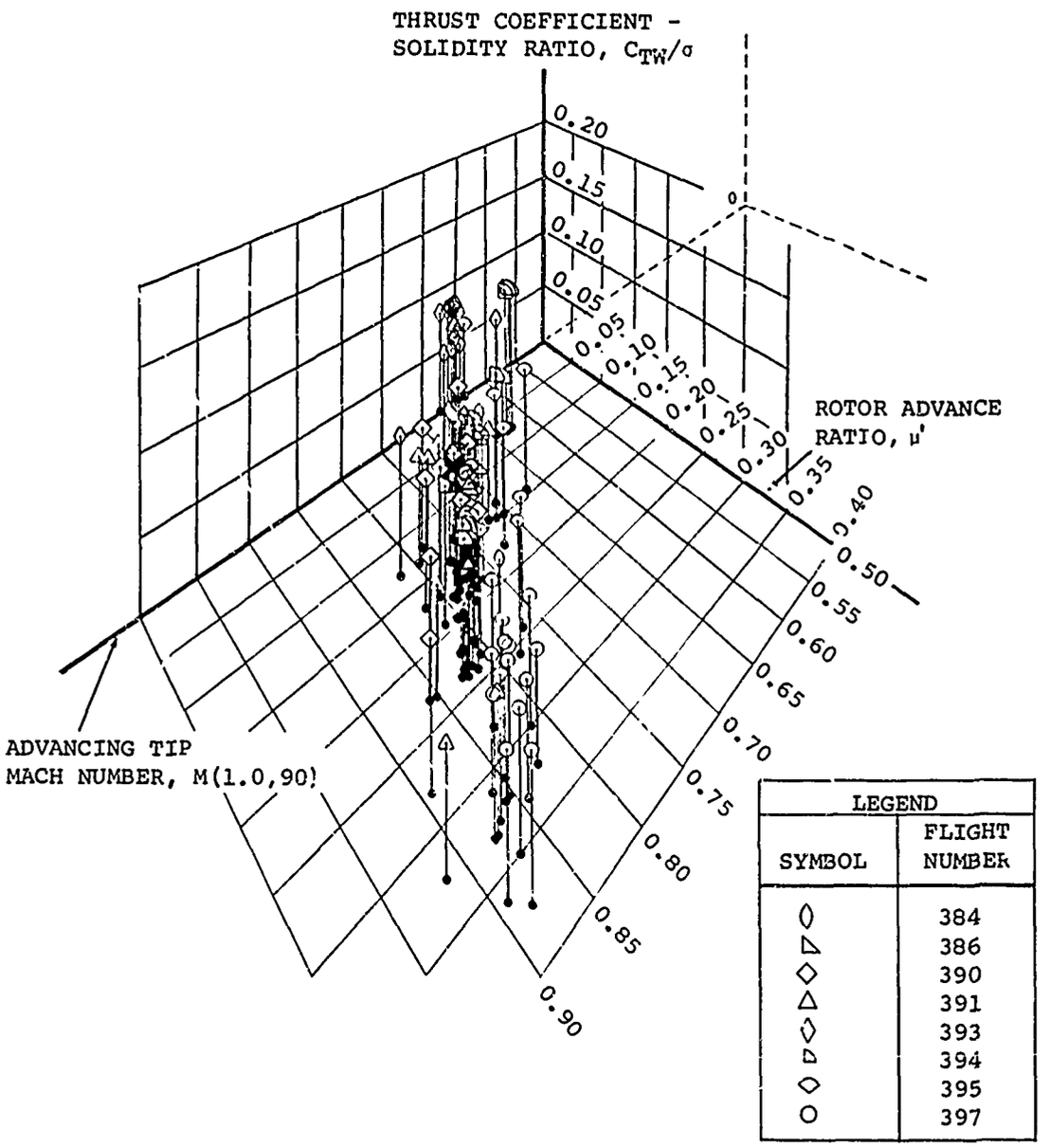

Figure 16. Perspective Illustration of Primary Parameters of Test Conditions.

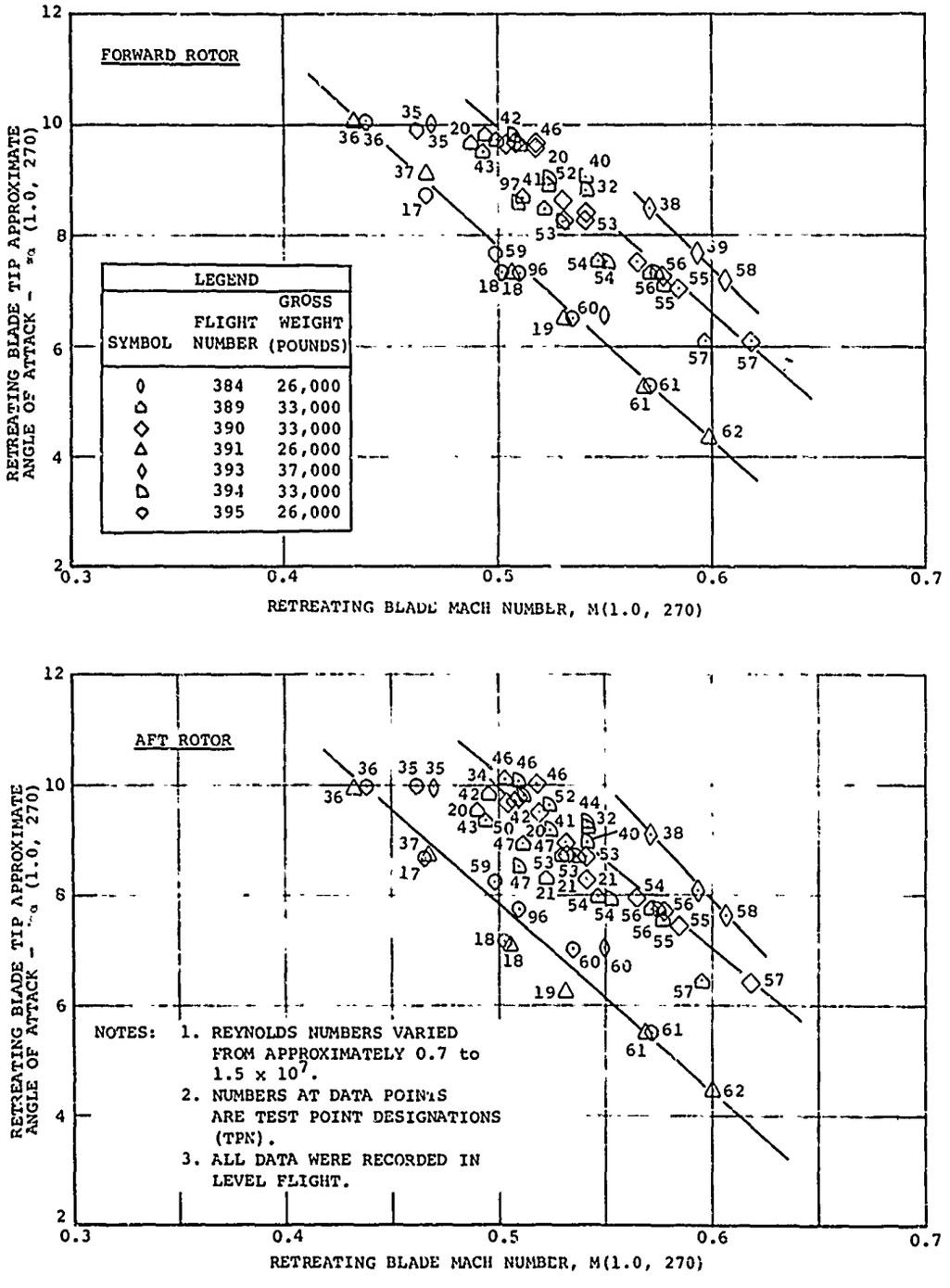

Figure 17. Retreating Blade Tip Operating Conditions Tested.

of the basic flight parameter measuring system. Prior calibrations of such equipment on tandem helicopters indicated that rotor downwash and/or fuselage interference could be significant. Airspeed calibration runs were flown at low altitude with a course marked by two parallel ground reference lines (roads). Sideslip vanes were calibrated using an optical driftmeter installed in the cargo hatch of the helicopter. These calibrations are consistent and are in general agreement with theory.

The airspeed calibration data, presented in Figure 18, show a systematic reduction of the indicated airspeed due to rotor and airframe interference. This position error is apparently predominantly due to rotor and airframe drag, which tends to move the air along with the helicopter. The trend of the interference is to increase slightly with airspeed; this results in a linear calibration for airspeeds above 40 knots. Airspeed data were obtained from the cockpit instrument and from the airspeed data system (dynamic pressure, pressure altitude, and OAT transducers with magnetic tape recording), with essentially identical results. The use of the data system provided a check on the quality of the calibration by indicating the airspeed and sideslip through the calibration run. Typical airspeed data through a calibration run are shown in Figure 19. These data show that the pilot generally held the airspeed within 1 knot. The two apparently separate data measurements taken by the data system are due to in-flight calibration differences ($\pm$0.6 knot) produced by sequencing. (Airspeed was recorded on both of the two sequences, as explained in Volume I of this report.) These calibration data were averaged over a run and are believed to produce final data accurate within 1 knot for the true airspeed range of 40 to 160 knots.

The airspeed position error determined from the calibration is compared, in Figure 20, with the theoretical position error due to rotor interference. The theoretical curve follows a trend with airspeed that is quite similar to the measured curve. A constant increment of the airspeed ratio, which apparently was caused by the airframe parasite drag, occurs between the theoretical and measured curves.

The sideslip vane calibration data obtained at 80 knots, 26,000 pounds gross weight, and 2000 feet altitude are shown in Figure 21. Data are shown to have about $\pm$2 degrees of scatter, and the rotor-hub-mounted vane has a -2-degree zero offset. The boom-mounted sideslip vane data have almost no zero offset.

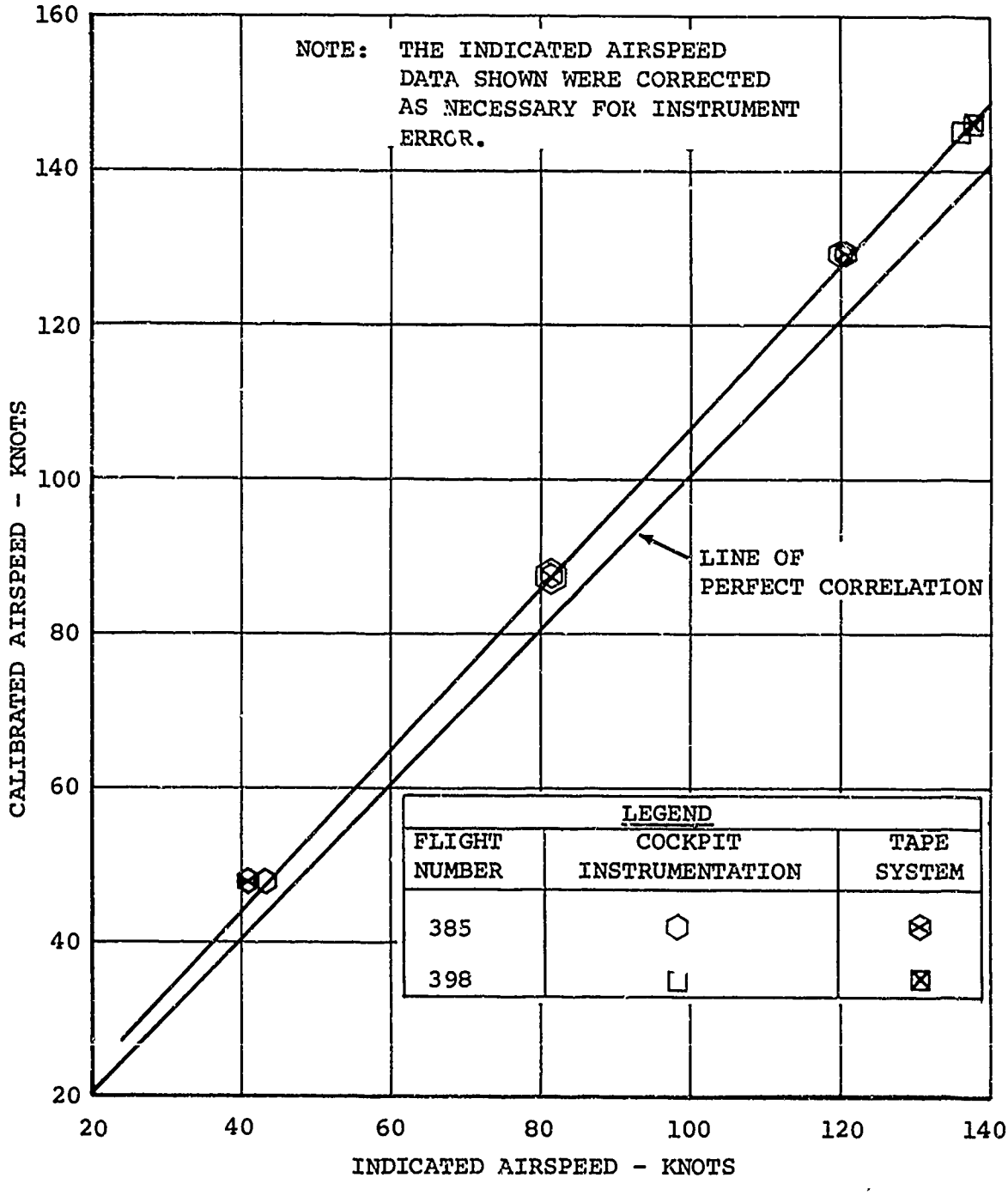

Figure 18. In-Flight Calibration of Boom-Mounted Airspeed Sensor and Airspeed Data System.

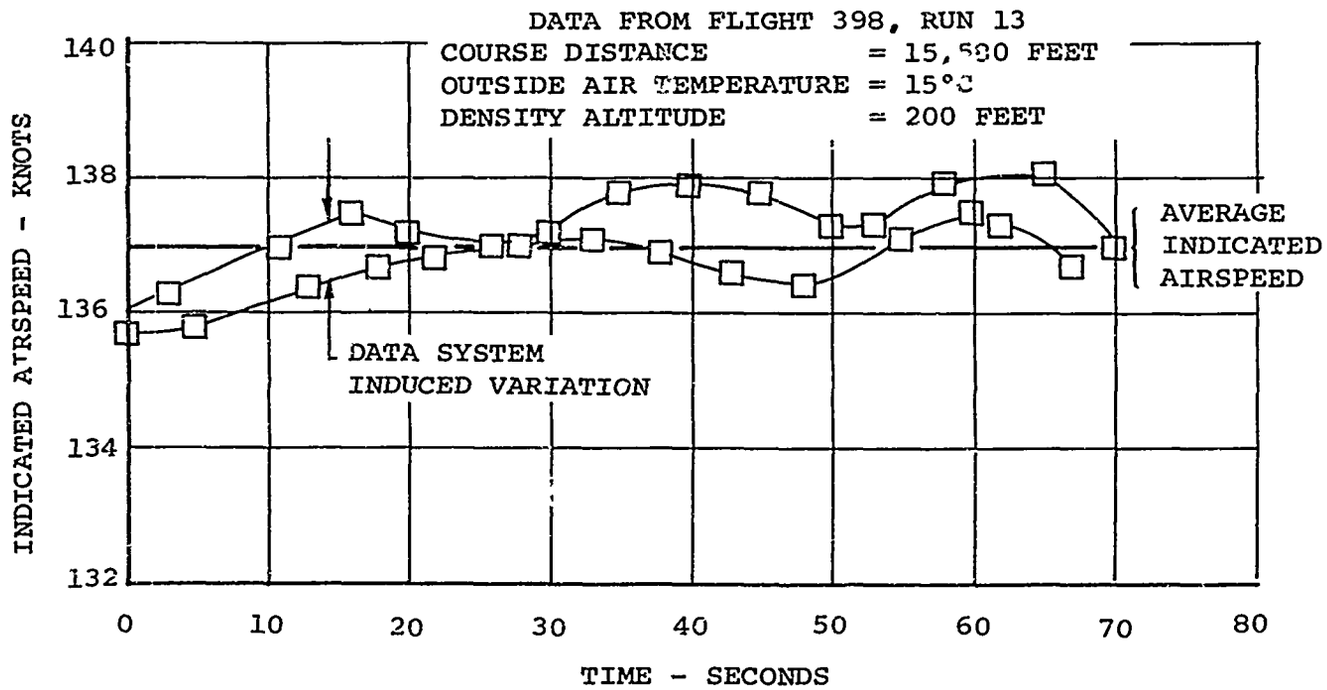

Figure 19. Typical Variation of Airspeed Indications *During a High-Speed Calibration Run.*

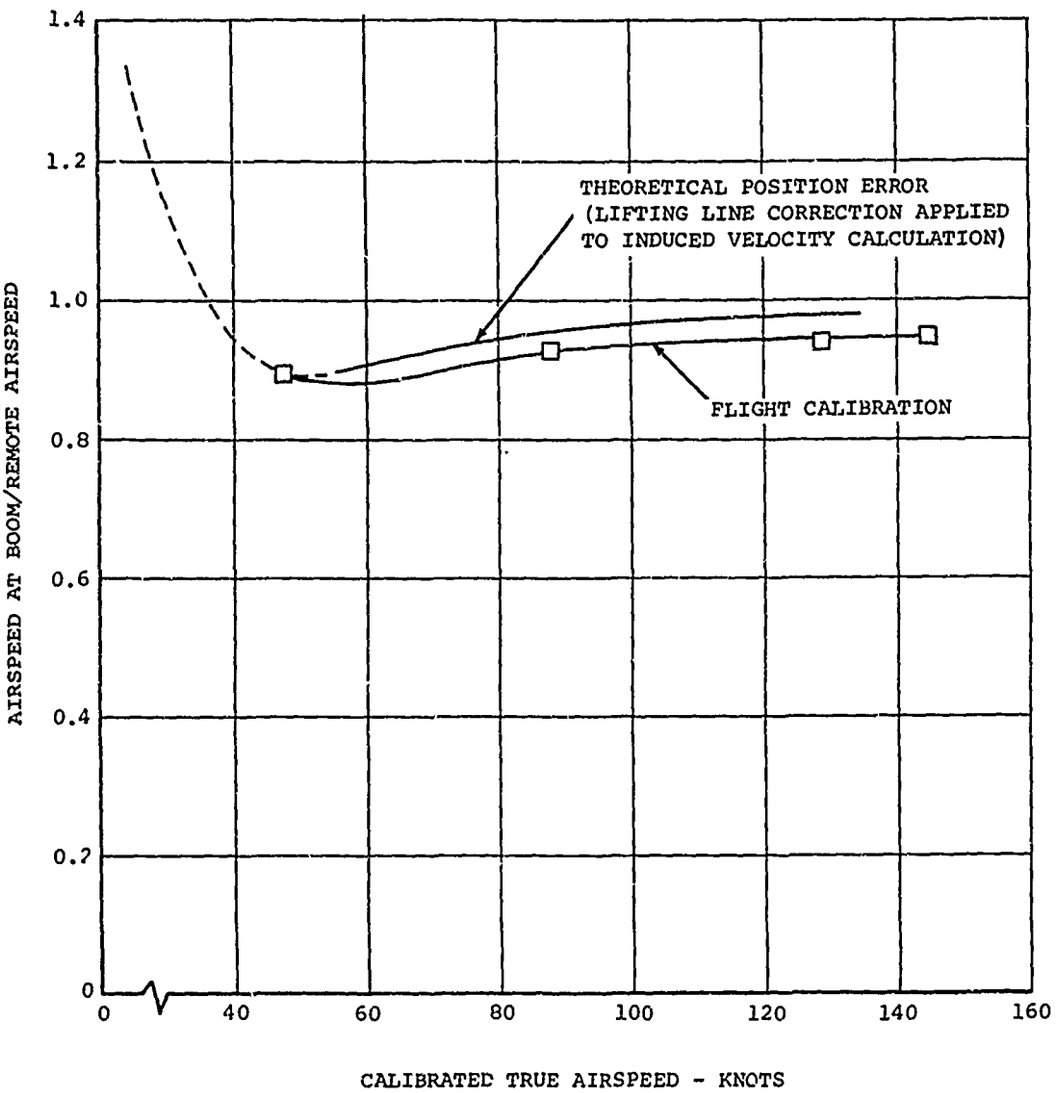

Figure 20. Comparison of Theoretical and Experimental Position Error Variation with Airspeed.

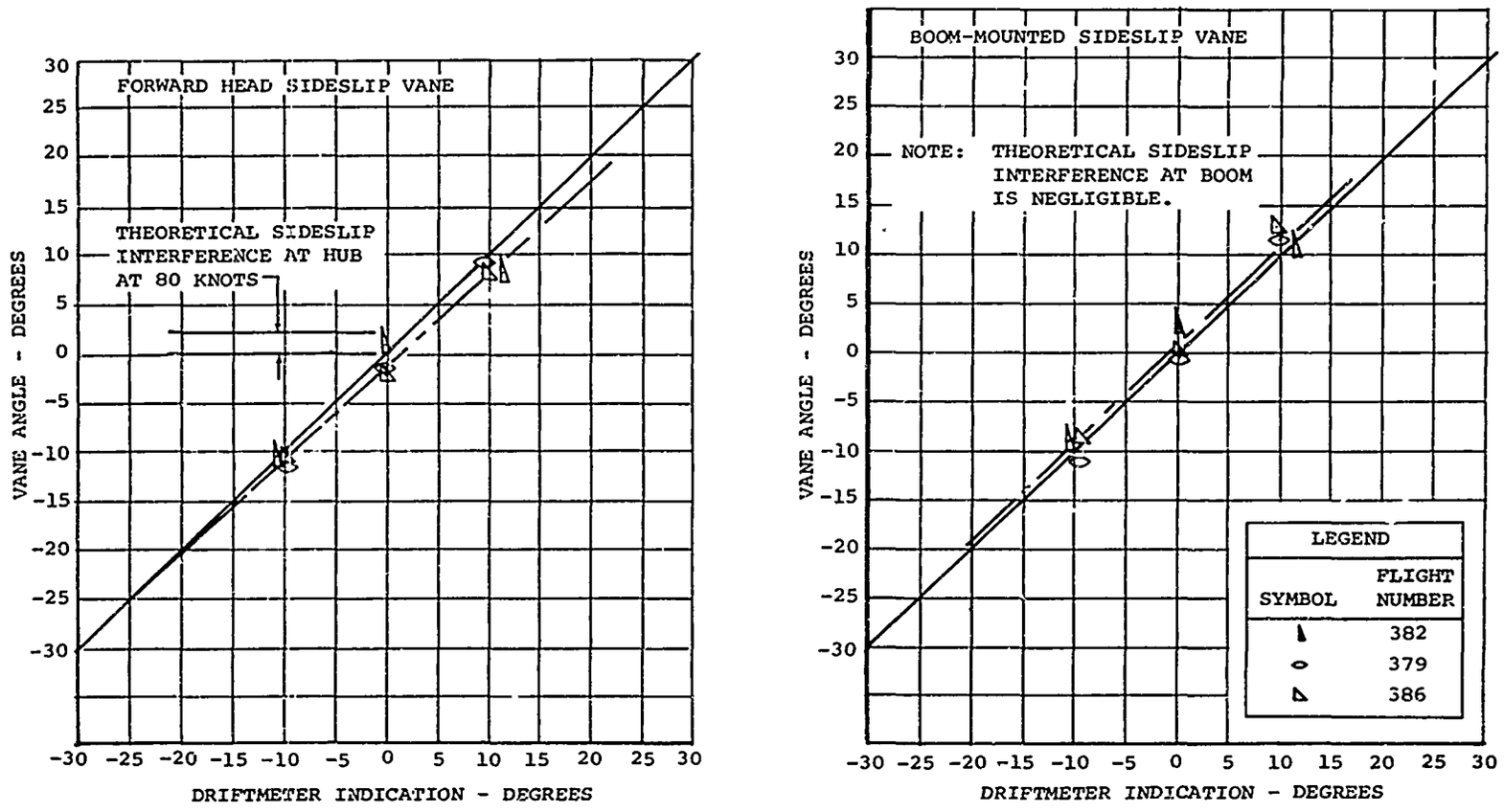

Figure 21. In-Flight Calibration of Sideslip Vanes Against Driftmeter Reference.

Theoretical rotor interference calculations which were made for this condition showed that the rotor should cause a +2-degree offset at the hub and a negligible interference at the boom. The positive sideslip due to the rotor, which is predicted by the theory, can be explained as being due to downwash rotation. The negative sideslip interference measured cannot be explained. All data presented in this report are based on the boom vane indications.

DATA ACQUISITION

The quality of the pilotage during data acquisition is shown by the data given in Figure 22. Generally, the airspeed measured was within 2 knots of the nominal test value, with the accuracy varying inversely with airspeed. Variations of helicopter data with altitude in the 3000- to 5000-foot range are generally very small, so a liberal tolerance was given to the nominal altitude of 5000 feet. This resulted in an average test density altitude of 3000 feet.

A very important parameter to tandem rotor helicopter operations is the sideslip angle. The pilot was provided with a meter which indicated the sideslip angle; but even with this indicator, his performance was rather poor. As shown in Figure 22, the sideslip angle obtained for nominally straight and level flight conditions was generally within ± 5 degrees, but some points were off as much as 10 degrees. Data analysts are cautioned to use the measured sideslip angle for selecting comparative flight conditions, since performance, vibrations, blade bending, and airloads all vary significantly with sideslip.

The longitudinal cyclic trim setting is another parameter which is extremely important but which was poorly acquired in flight testing. Unfortunately, the meters provided to the flight crew for measuring cyclic trim had inadequate resolution, and therefore the desired settings were not obtained. The cyclic trim was measured by the blade pitch transducers, with the first harmonic longitudinal component obtained from the harmonic analysis. A comparison of the measured and nominal cyclic trim settings is shown in Figure 23. The trim setting error was generally less than 1 degree, but many points were obtained with a setting error as large as 2 degrees. It should be noted that all settings were made manually, with the automatic airspeed-sensed trim system disconnected, so there was considerable opportunity for error.

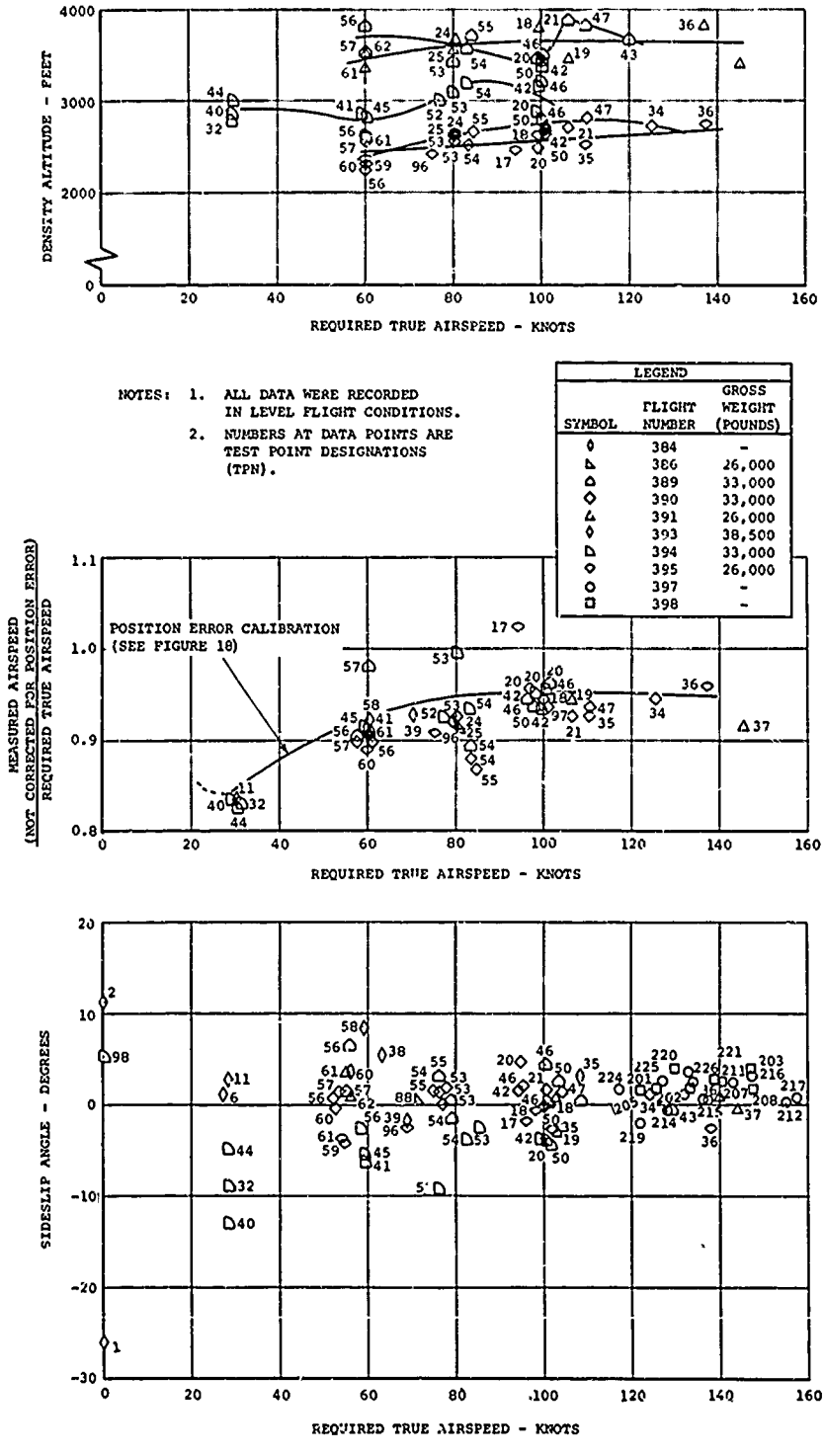

Figure 22. Comparison of Actual Test Conditions with Desired Nominal Test Conditions.

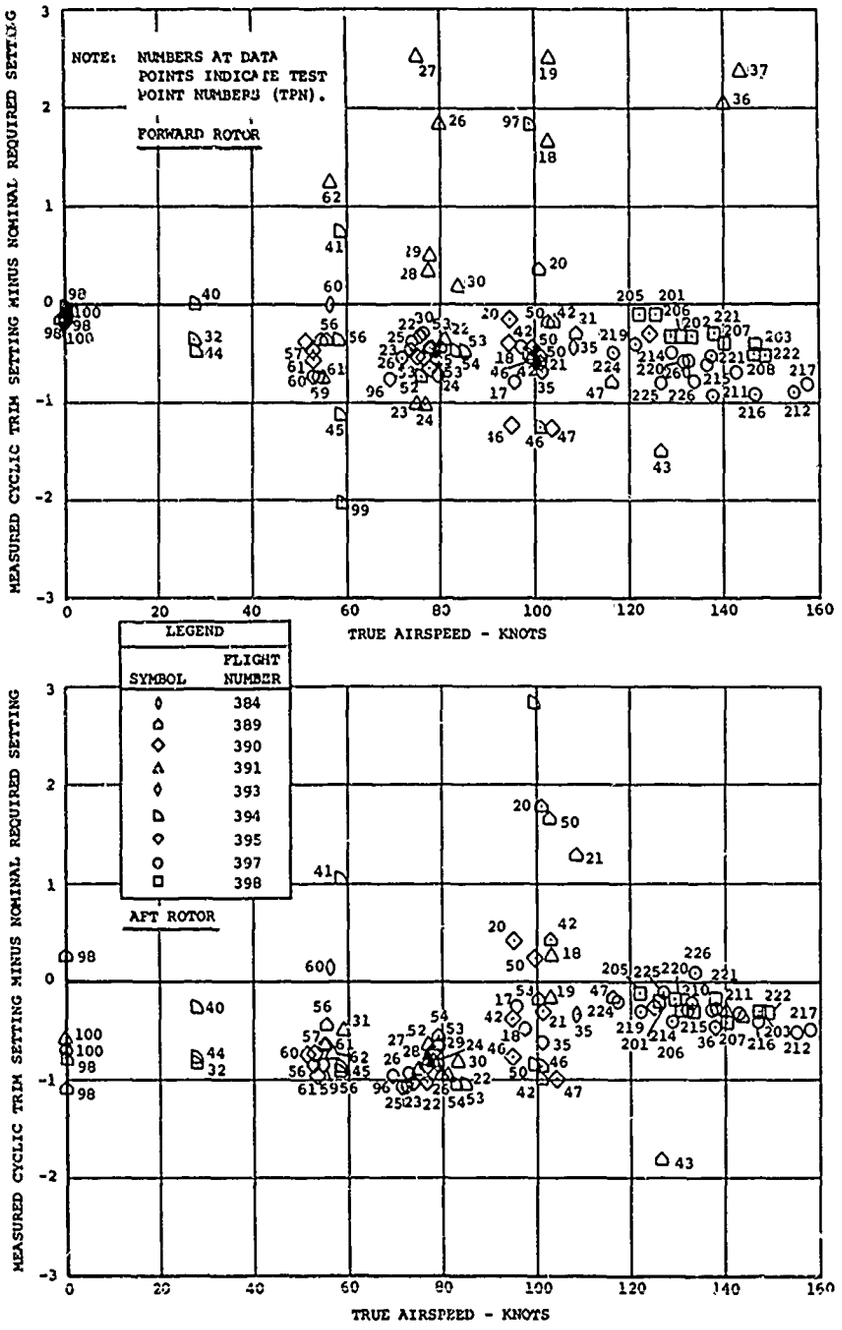

Figure 23. Differences Between Nominal and Achieved Cyclic Trim Settings.

The airframe accelerometer data have been used to check for long-period variations in the trim of the test points. These data are shown in Figures 24 and 25 for the average translational and rotational accelerations measured during data acquisition. These data show that average accelerations over the 15-rotor-cycle (≈4 seconds) data acquisition period were negligible.

It is of interest to note that the sideslip vane data acquired throughout the flight test program tend to substantiate the in-flight sideslip vane calibration. The frequency of occurrence of various differences between the two vane readings is plotted in Figure 26. These data show an average skew or zero offset of about -2 degrees; that is, the average hub vane measurement is -2 degrees if the average boom vane measurement equals zero. This is the same zero offset shown in Figure 21.

The scatter of the vane angle difference data used for Figure 26 is considerably influenced by low-speed operation and by maneuvers. Hovering caused obvious large differences between the readings; these data were eliminated. However, all other data are included. The typical sideslip measurement error is believed to be about ±2 degrees, as shown by the in-flight calibration, rather than the ±4 degrees shown in Figure 26.

DATA PROCESSING

The data system, described in detail in Volume III of this report, utilized the equipment and provided the functions noted in Figure 27. The software of the system consisted of data calibration programs and analysis programs. The data calibration programs prepared corrected, calibrated, and checked test data in harmonic coefficient form for further analysis. The analysis programs were utilized to provide manipulations of the test data, as well as comparisons with theory. A typical example of an analysis program is the Airloads Program which was used to integrate the airload pressures.

Functional testing of the instrumented helicopter showed that signal drifts produced by the instrumentation were corrected by the data system. During flight testing, in-flight calibrations were taken following every in-flight recording to correct for drifts in baseline (zero reference) and sensitivity. Sensitivity changes were usually small, but baseline variations were significant. Functional testing of this data system showed that corrections to the baseline were made with acceptable

accuracy even with large drift. Figure 28 shows typical results from a long-term drift test of the system using the fully instrumented helicopter. The covers of the hub-mounted signal-conditioner packages were alternately installed and removed systematically over a 10-hour period to cause sizable changes in the temperature of the signal conditioners (including the amplifiers). These temperature changes caused large drift in some of the signals, as illustrated by data code 4279 in Figure 28. However, the data system was updated (in-flight calibration procedure) after 3 hours, which corrected the drift except for a -0.6 percent of band edge error. The majority of the signals had considerably less drift than data code 4279 and more closely resembled the signals shown as average drift or low drift. As noted in Volume III of this report, following updating, the mean drift was 0.55 percent with a 2σ distribution of 1.16 percent. While this drift correction is very good, it also establishes the minimum resolution of the data system as 1.16 percent of band edge or 20 counts. This means that signals with a sensitivity calibration which was small as compared to 20 counts were subject to excessive drift and had to be deleted. A list of data deleted for this reason is included in Appendix II of this volume.

It should be noted that the data presented in this report were not processed completely, as described in Volume III. These data have not been corrected for blade bending interactions, and the steady airload pressures were integrated using a forced-fit routine. The blade bending moment interactions correction procedure was not adequately developed at the time of this writing. The blade pressure integration procedure change was made to minimize instrumentation drift further, as will be described later.

The work described in Volume II showed that blade bending interactions were significant, but these effects are not accounted for in the data presented in this volume. The development of the extrapolation procedures described in Volume III, which are required to estimate the interaction loads, was not completed in time for utilization. Rather than present data which were uncertain, it was decided to postpone the completion of this development and present all blade bending data uncorrected but checked against experience with similar instrumentation installations on the CH-47A. It is therefore suggested that apparent blade flapwise-to-chordwise bending coupling be attributed to uncorrected gage interactions. This recommendation should be tempered by consideration of the proximity of the natural

frequencies of the first chordwise bending mode and the second flapwise bending mode, which would cause these modes to be highly coupled for 5/rev. oscillations. The magnitude of the interaction of chordwise bending on flapwise bending was about 0.15 ± 0.05 inch-pound of flapwise bending per inch-pound of chordwise bending, with the variation in interaction depending on the blade station considered. Flapwise bending had a considerably larger interaction with chordwise bending.

The modified steady airloads integration procedure was found to be necessary when the data were evaluated, as will be described later in this volume. The procedure utilized was to force the chordwise distributions of the azimuthal average (steady) airload pressures to be similar to a two-dimensional airfoil. The theoretical pressure distribution of a 0012 airfoil was obtained from reference 1. It was found that this pressure distribution could be represented with engineering accuracy by the relation

$$p(x) = K_1 \ (_x - 0.215) + K_2 \ . \qquad (1)$$

The modified integration procedure utilized the 5, 7, or 11 steady pressure values, p(x), available at each blade radial station. A least-squares fit was made to solve for the constants K_1 and K_2. Equation (1) was then integrated analytically to determine the lift per unit span and the pitching moment per unit span for the steady terms. Linear integrations were used for the harmonics.

The form of the output of this program has led to some confusion, but this situation can be avoided by noting two definitions. These definitions are illustrated in Figure 29, and involve the Fourier coefficients used for the harmonic analysis and the definition of the alternating value used in preliminary data sorting. The alternating value is commonly used in evaluating stress data and is defined as one-half the excursion of the value from the highest peak to the lowest peak encountered within any one rotor cycle. In this program, five rotor cycles were evaluated. The Fourier coefficient definitions utilized are defined by the following equations for any arbitrary parameter, Y:

$$Y = \text{Steady } (Y) + \sum_{K=1}^{n} (B_K \sin K\psi + A_K \cos K\psi) \qquad (2)$$

or

$$Y = \text{Steady } (Y) + \sum_{K=1}^{n} R_K \sin (K\psi + \phi_K). \qquad (3)$$

These definitions are straightforward and have general acceptance, but the coefficients can produce rather startling results if the definitions are confused.

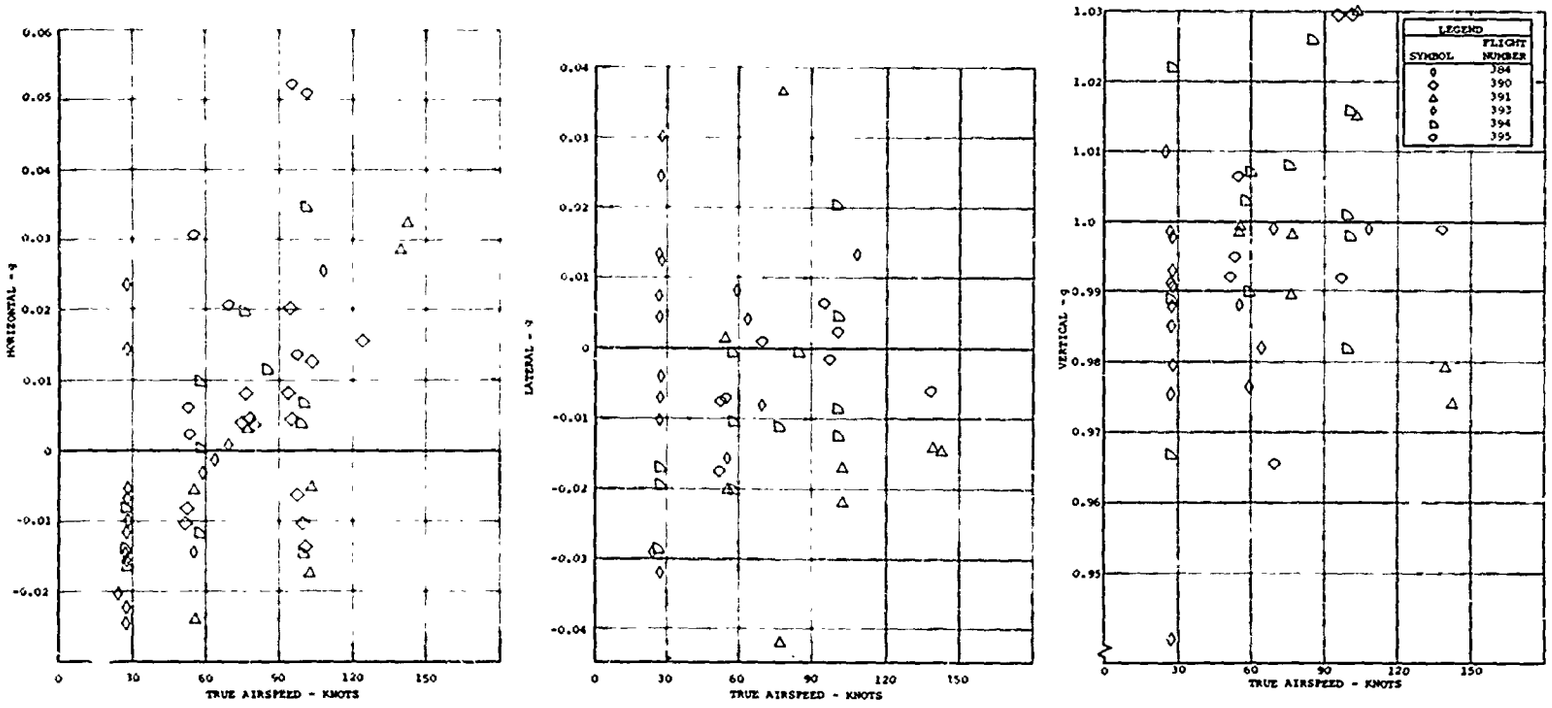

Figure 24. Average Translational Accelerations of Test Aircraft During Steady Test Point Data Acquisition.

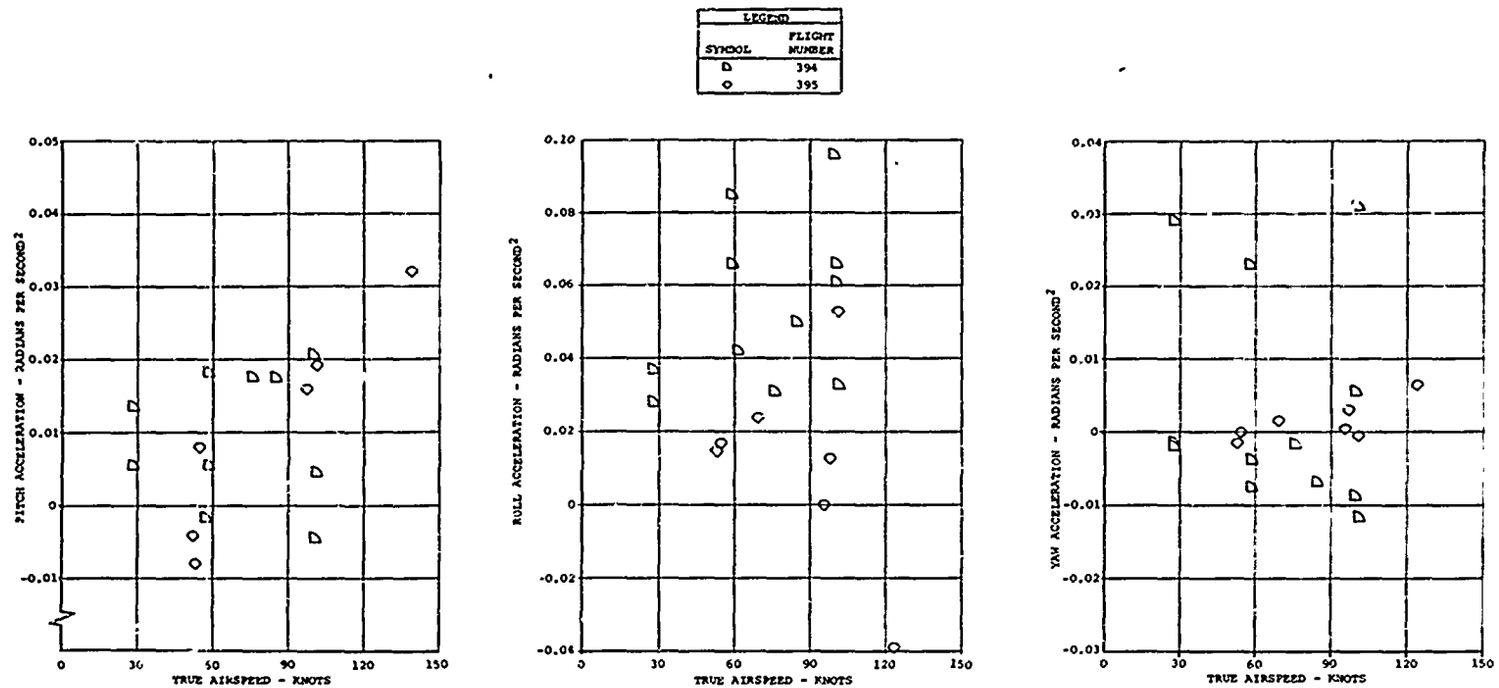

Figure 25. Average Rotational Accelerations of Test Aircraft During Steady Test Point Data Acquisition.

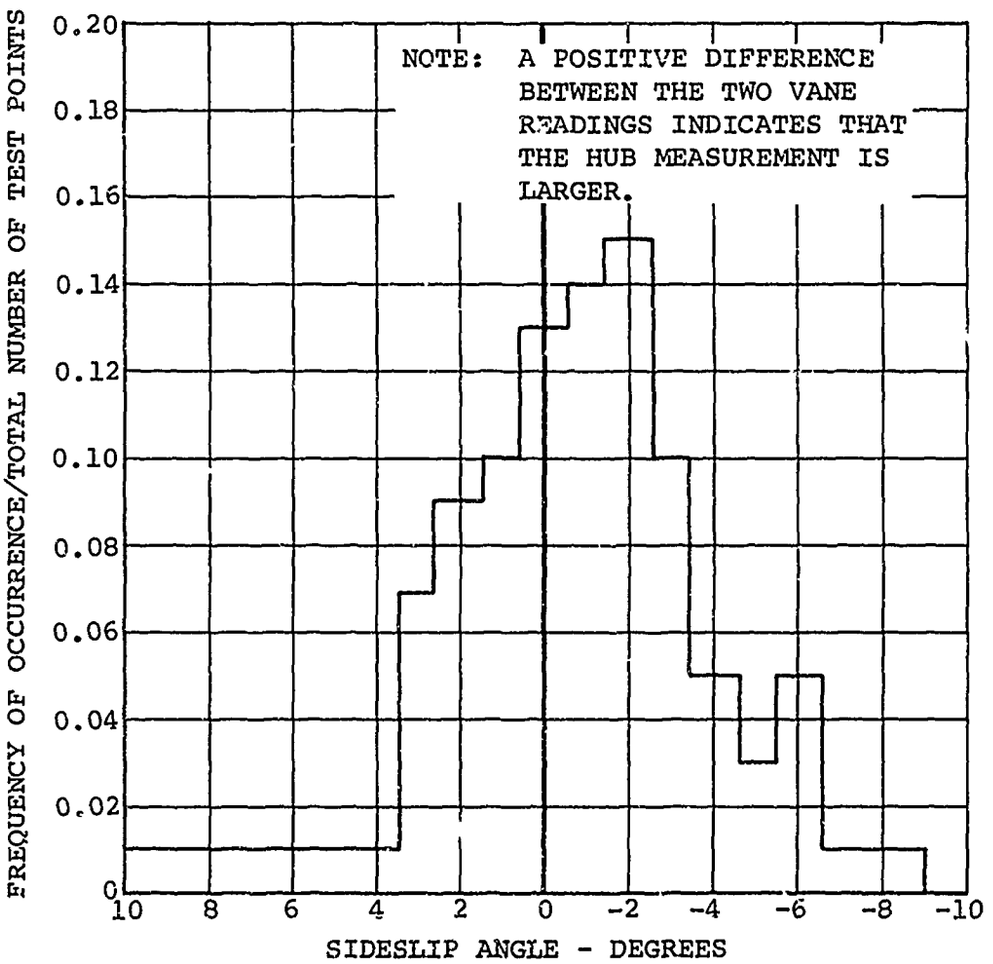

Figure 26. Comparison of the Two Sideslip Vane Readings Showing Statistical Confidence of Measurements.

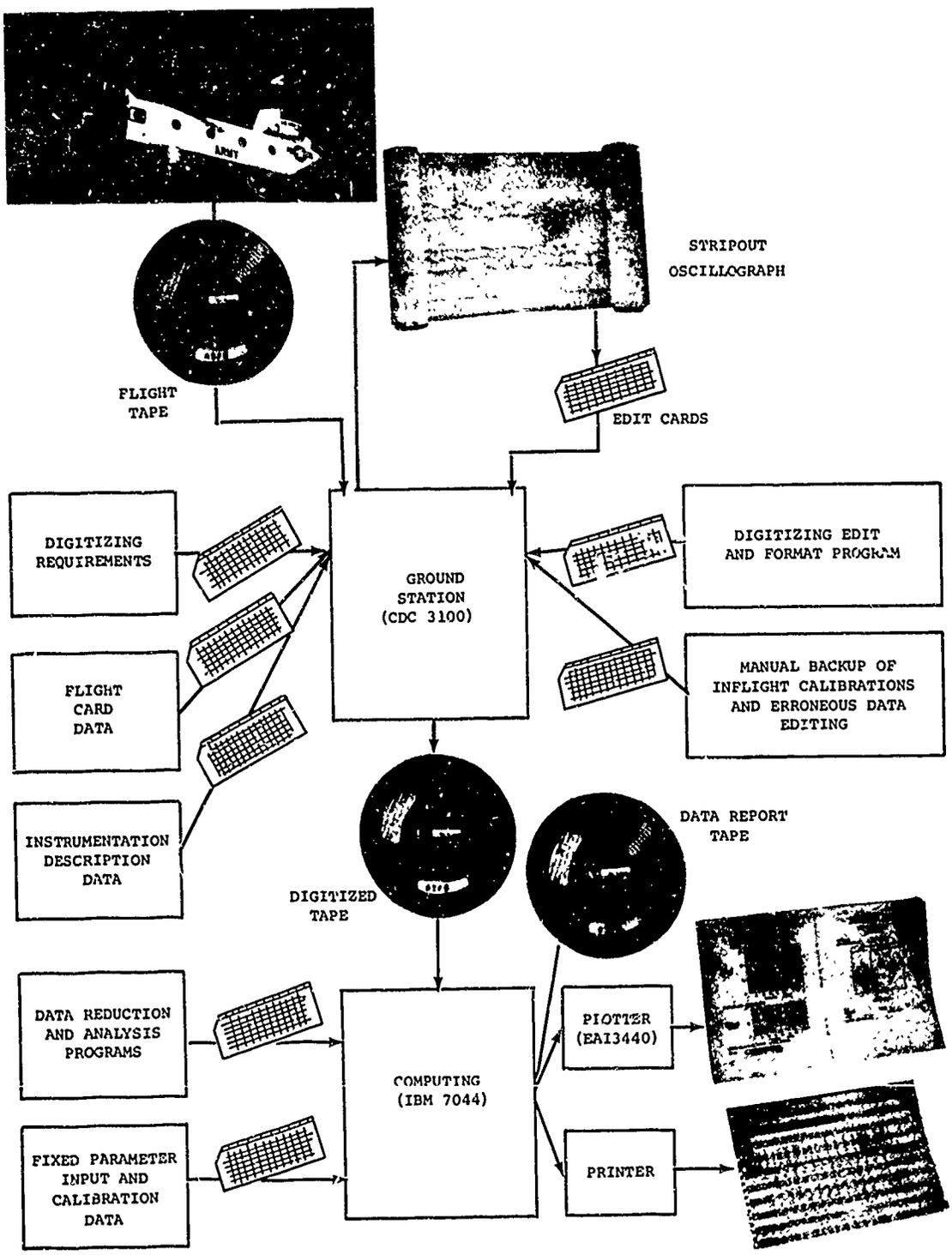

Figure 27. Data Flow Schematic Diagram.

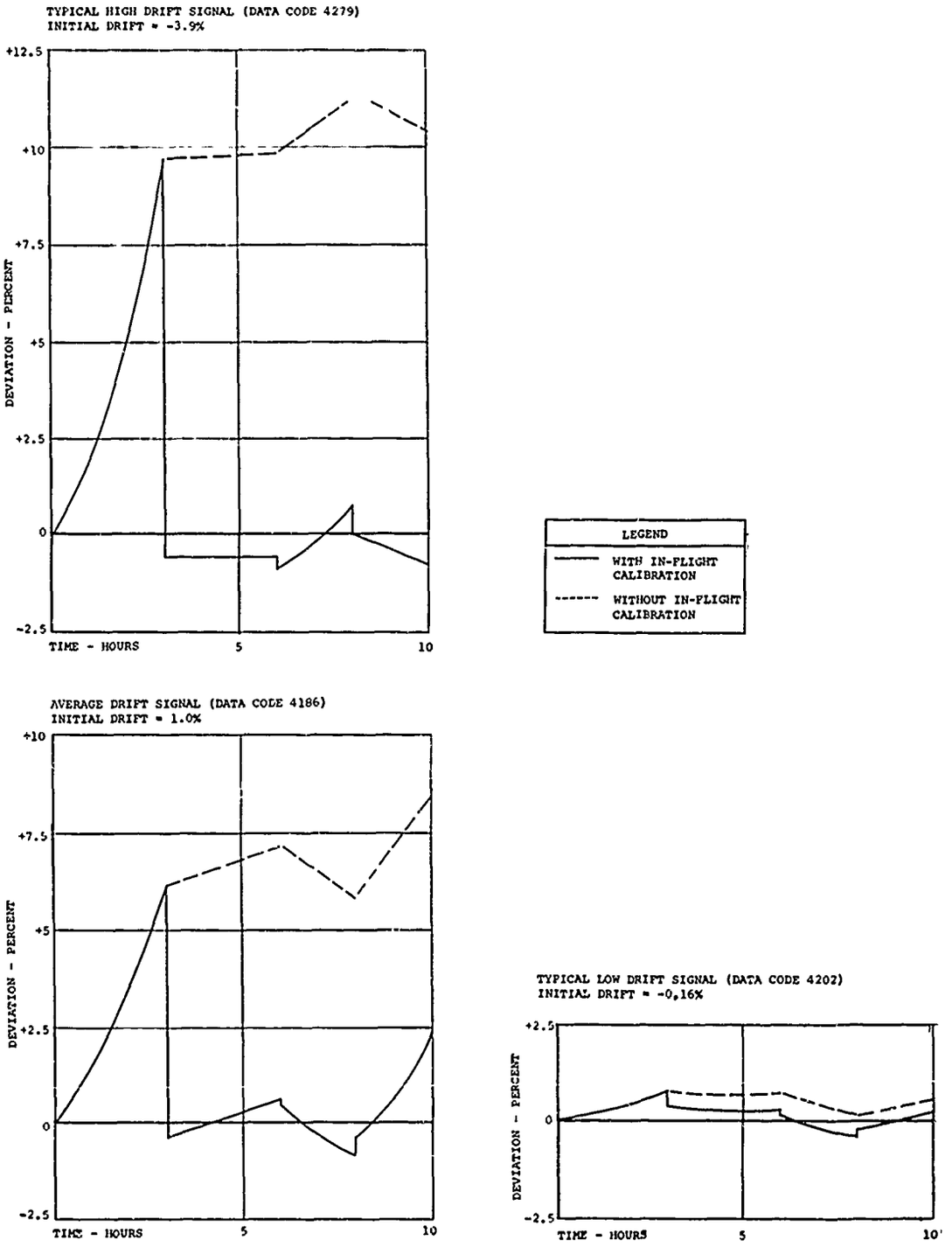

Figure 28. Drift Corrections Achieved in Ground Functional Testing.

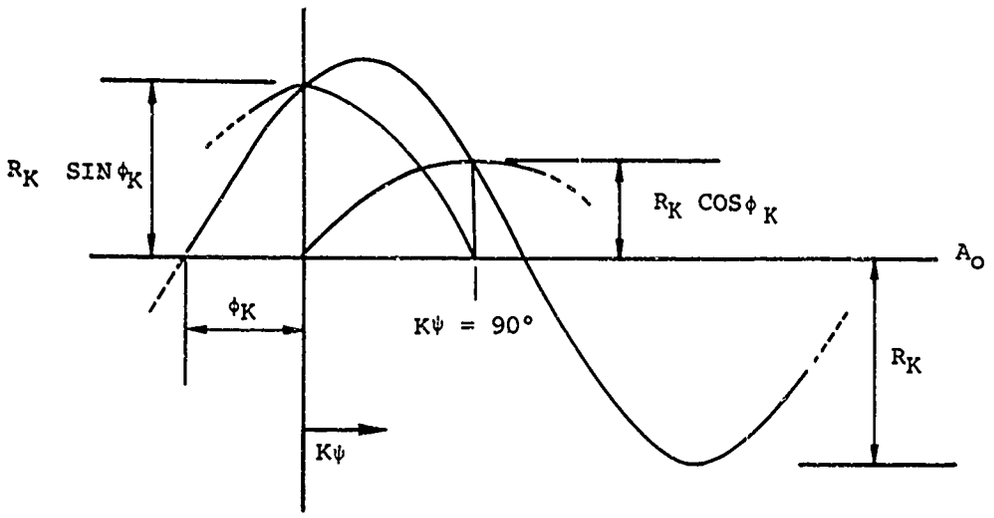

A. FOURIER SERIES TERMS (SKETCH FOR Kth HARMONIC)

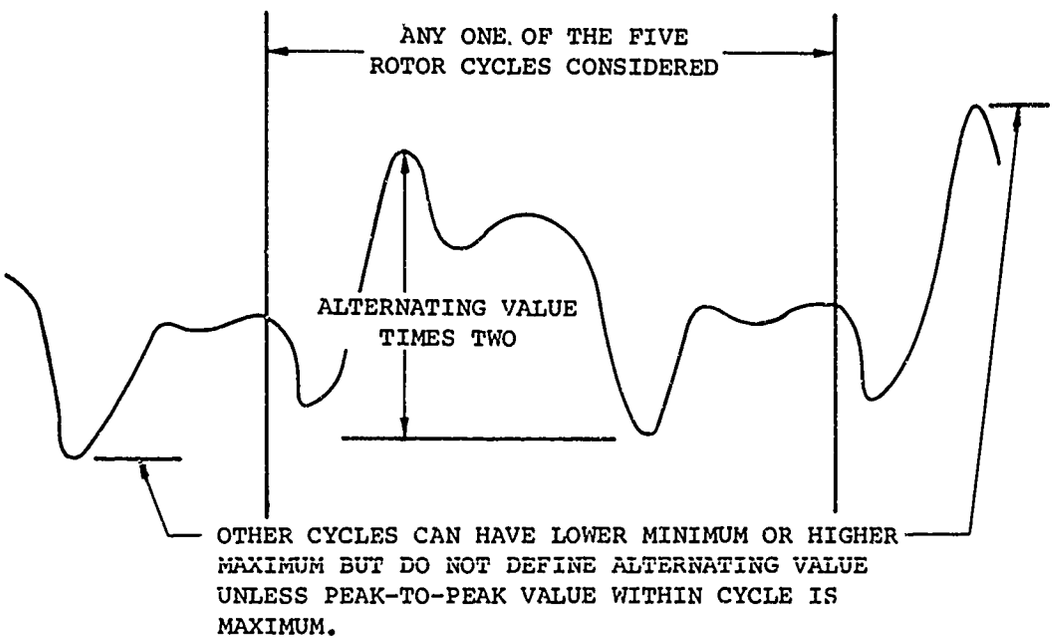

B. ALTERNATING VALUE DEFINITION

Figure 29. Illustration of Fourier Series Terms and Definition of Alternating Value Used for Data Preparation.

EXPERIMENTAL RESULTS

An attempt has been made in this presentation of results to illustrate some of each type of data obtained. It is hoped that this display provides some visibility as to what is available and helps to provoke future utilization of the data. The general approach differs, depending on the type of data presented, as follows:

1. Rotor airloads - These data presentations have received emphasis, with the data being given in many different forms.

2. Rotor blade bending - The data illustrate the variation with flight conditions; emphasis is placed on the bending which influences the airloads.

3. Control system loads - The presentation is brief but important, since the flight envelope of the test helicopter tends to be limited by control loads.

4. Rotor shaft loads - The data which illustrate trim are emphasized; vibratory data are also presented.

5. Airframe vibration - A large volume of data is available, but the presentation is brief.

6. Trim and performance - Emphasis is placed on the data which show the consistency and the quality of the data acquisition.

These presentations were initiated with the purpose of being illustrative and brief; however, it is believed that even with this approach, considerable new fundamental knowledge of tandem rotor aerodynamics and dynamics was uncovered. The need for further analysis is obvious. One example of the beginning of additional analysis is the investigation of blade stall aerodynamics described in Volume V of this report. Similar efforts are necessary to obtain the latent value from the other dynamic data obtained in this program.

ROTOR AIRLOADS

Airloads data are informative when considered in at least four forms. Details of the local flow are indicated by local blade differential pressures measured near the leading edge. The similarity of blade section performance to a two-dimensional

airfoil is indicated by the chordwise distribution of airload pressures. For indicating overall performance and the vibration excitation of the rotor, the airload pressures should be considered after chordwise integration and harmonic analysis. Finally, the chordwise integrated airloads - that is, the lift per unit span - can be reduced to coefficient form for comparison with other airloads data and with theory.

Airload Pressure Data

Local airload pressure data are available as pressure ordinates that are a function of azimuth, as steady and alternating values, and as harmonic coefficients. The pressure data, which are a function of azimuth, are relatively difficult to handle, since they are least compact, but they show rotor flow variations with clarity. These data illustrate the effects of trim and sideslip, and are also used later to show chordwise distributions. The alternating pressure values give a quick overall look at the data, and have been used for showing the effects of airspeed, gross weight, sideslip, trim setting, and maneuvers. Harmonically analyzed pressure data are of value to determine whether a parameter can affect the blade or airframe dynamics.

The effect of wind direction on airload pressure harmonics when hovering (stationary with respect to the ground) is shown in Figure 30. These bar graphs show that there are variations in airload pressures in hover which are independent of the wind and are apparently due to rotor-rotor interference. These variations are approximately 0.2 psid, which is about 5 percent of the steady airload at the blade location considered. The data show that the wind has a significant effect on the airload presure harmonics, particularly at the lower harmonics which have a strong influence on vibration. Wind from the left causes the largest first and second harmonics on the aft rotor and the largest first harmonic on the forward rotor. This tendency cannot be explained at present; however, as the nonrigid wake-nonuniform downwash theory is developed, this type of data should be of increasing value.

A summary of data on the alternating airload pressure, measured at the 85-percent radius and the 4-percent chord in steady level flight, is shown in Figure 31. These data usually are of smallest magnitude at 80 knots, and increase with either increased or decreased airspeed. Alternating airloads pressures tend to be about 30 percent (1 psid) larger on the aft rotor than on the forward rotor. The effect of run gross weight is

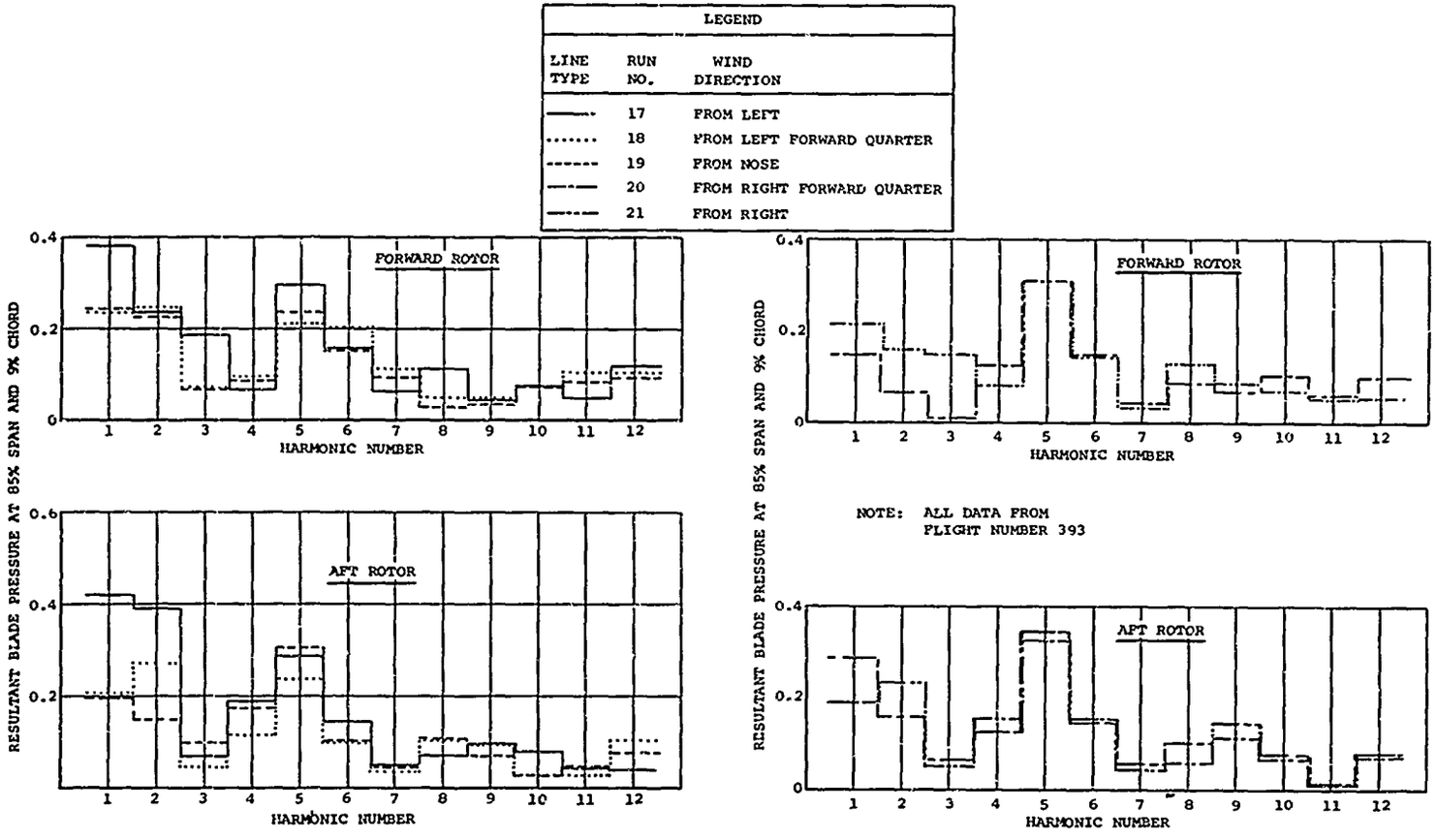

Figure 30. Variations in Harmonics of the Airload Pressures at 95-Percent Radius and 9-Percent Chord Due to Wind Direction While Hovering.

NOTES: 1. ALL DATA SHOWN WERE MEASURED AT 85-PERCENT SPAN AND 4 PERCENT CHORD.
2. OPEN SYMBOLS WERE OBTAINED AT ≈ 26,000 LB., FILLED SYMBOLS AT ≈ 33,000 LB.

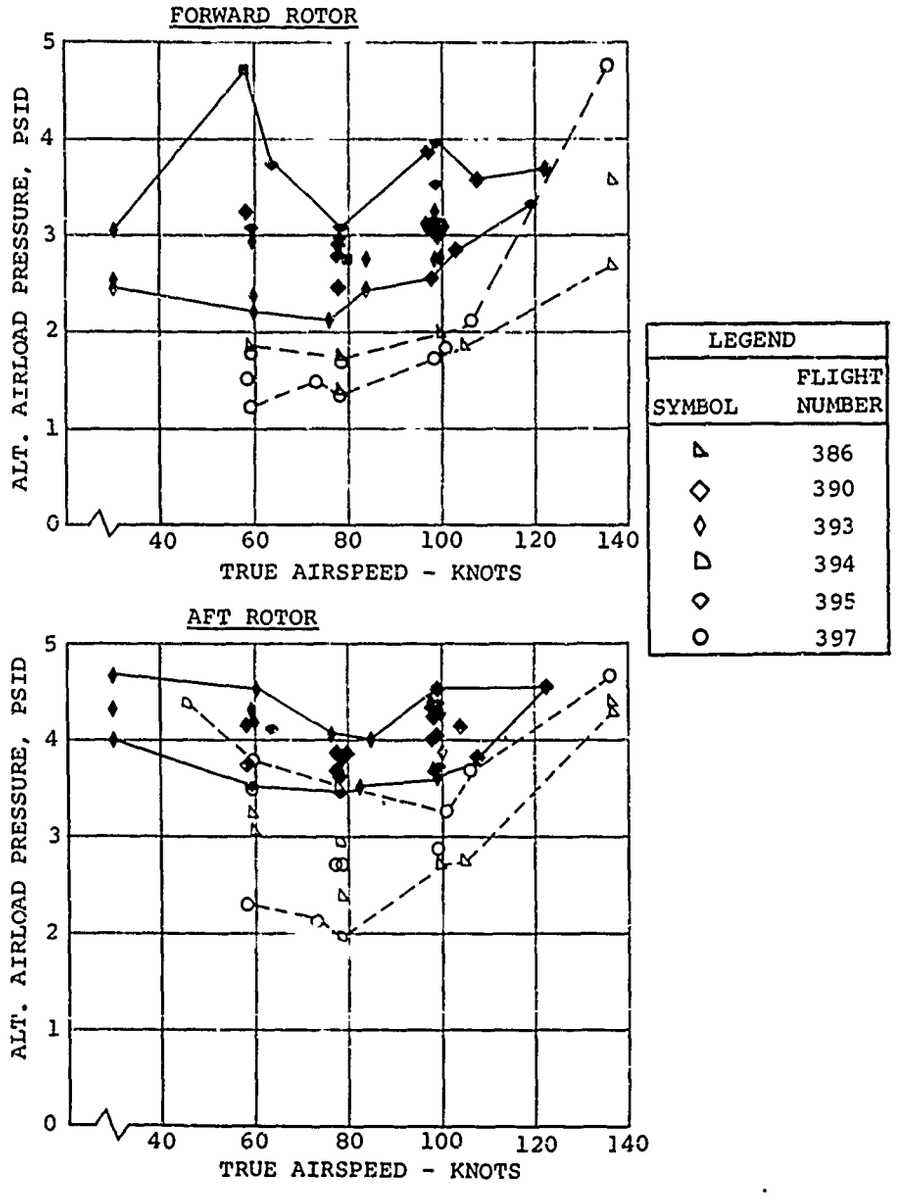

Figure 31. Alternating Local Blade Pressure Values at 85-Percent Radius and 4-Percent Chord for a Summary of Level Flight Conditions.

shown to be significant at lower speed; but at 120 knots, essentially the same alternating pressure values were obtained at 26,000 pounds and at 33,000 pounds. It should be noted that the data shown in Figure 31 were obtained with various rpm values and trim settings, which probably accounts for the scatter shown.

As will be shown later, the tandem rotor helicopter experiences severe aft rotor loads during sideslip in transition (30 knots). These loads tend to be slightly more severe when the helicopter is flying in ground effect (10-foot wheel height). Airloads data were obtained for these conditions, and typical data are shown in alternating pressure form in Figure 32. These data show how the alternating values can be misleading, with essentially no significant variations apparent between the forward or aft rotor data in or out of ground effect. The pattern with sideslip is shown to be uncertain and ill-defined. As will be shown, these data are consistent and illustrate a definite pattern when considered as a function of azimuth or as azimuthal harmonics.

The effect of sideslip at 80 knots on alternating airload pressures is also shown in Figure 32. The aft rotor data vary significantly, with almost no change shown in the forward rotor data. These 80-knot data were obtained at 26,000 pounds gross weight, and therefore the alternating pressure values shown are smaller than the transition sideslip data, due to the effects of both increased speed and reduced weight.

A systematic variation of longitudinal cyclic trim setting was tested at 100 knots and 33,000 pounds. Again, the 85-percent radius, 4-percent chord pressure value was taken as typical, and the alternating values are shown in Figure 33 as functions of forward rotor cyclic trim. It can be noted that 2 degrees of forward cyclic trim has no significant effect on the airloads, but that an increase in trim to the -3/-5-degree (forward/aft rotors) setting causes a noticeable decrease in forward rotor alternating pressures and a comparable increase on the aft rotor. As will be noted later, the effects of cyclic trim in causing changes to the fuselage attitude are nonlinear, and this effect is reflected in the alternating airload pressures.

The effect of maneuvering at 80 knots on the alternating airload pressure is shown in Figure 34. It is interesting that the largest alternating airloads were caused by rolling the helicopter. The roll to the right, which was at 13.4 degrees

per second (as shown in reference 25), caused an alternating pressure of about 4.5 psid, which is about the same alternating pressure measured at 135 knots. The symmetrical pullup (1.5 g) or the steady 30-degree banked turns were expected to cause the largest alternating pressures.

This presentation on alternating airload pressures shows a general overall review of typical data, but gives no information as to possible effects of the alternating data. As noted, significant parameters can be overlooked if too much importance is given to the alternating values. Waveforms of the data to be presented next are of considerably more value, but are hard to evaluate and summarize. The use of harmonics, to be presented later, is perhaps the best compromise, but harmonics can also be misleading due to the impulsive nature of rotor airloads.

Typical azimuthal variations in local airload pressures are shown in Figure 35 for arbitrary selected locations along the chord of the blade at the 85-percent radius. Generally, the forward rotor data are similar to single rotor measurements, but have additional abrupt changes due to interference with the aft rotor. By comparison, the aft rotor data generally contain fewer higher harmonic oscillations than the forward rotor, but are characterized by a large impulsive vortex interference spike. For this particular test condition, this spike occurs at the 120-degree azimuth, as expected from the rigid wake tip vortex pattern. As an illustration of the consistency of these data, Figure 35 contains all the data measured during five separate rotor cycles. The envelopes of data are about ± 5 percent of the mean for any azimuth, which is believed to be excellent repeatability considering the variations in flight path and helicopter motions which are possible. The data of Figure 35 also show that the largest variations in pressure due to vortex interference occur at 13 percent of the chord rather than at the leading edge. This is not in accord with expectations based on static two-dimensional airfoil data. The expected responses of the 9-percent and 37-percent chords are 1.3 and 0.5 of the 13-percent-chord response; however, the airload pressures measured at 85-percent radius indicate that these response ratios are about 0.9 and 0.2. Aft of the 37-percent chord, there is essentially no change in pressure due to vortex interference.

Data from the same flight and run as Figure 35, but for the 98-percent radius, are shown in Figure 36. It is rather surprising that the tip vortex interference spike and the higher harmonic pressure variations are smaller at this radius. The

general trend of these data is similar, with a decreasing pressure in the first 90 to 120 degrees and then an increasing trend to reach the maximum pressure at 360 degrees. A small vortex interference bump is present at 40 degrees and at 300 degrees on the forward rotor at the 98-percent radius (Figure 36), with similar but considerably larger bumps occurring at the 85-percent radius. The aft rotor data have a similar bump at about 300 degrees azimuth at both radii; but do not have the bump at 40 degrees azimuth apparently due to forward rotor downwash interference. The rather large vortex interference spike that is shown in the aft rotor data of about 120 degrees azimuth in Figures 35 and 36 is due to the vortex trailed by the blade tip of the forward rotor blade. This spike is smaller at the 98-percent radius than at the 85-percent radius, apparently due to the influence of the blade on the vortex, or to the increased angularity of the blade-vortex intersection at the 98-percent radius. From the rigid wake geometry, the vortex would first collide with the blade at about the 70-percent radius, and therefore this blade station should have the largest vortex spikes. It is believed that further review and detailed analysis of these data would shed light on the problem of rotor noise generation due to vortex intersection; however, this study is beyond the scope of the present effort.

The reduction in the higher harmonic pressure variations with increased radius from the 85- to 98-percent radius is apparently due to the increased elastic response of the blade tip. As will be shown later, most of the higher harmonic excitation is applied over the outer region of the blade; however, as shown in Figure 10, the 85- and 98-percent radii are on opposite sides of the outer nodes of the higher harmonic blade bending modes. It appears from a comparison of Figures 35 and 36 that the blade bending velocity is in phase with the airloads at 90-percent radius, so that the higher harmonic loading is small. Obviously, then, the 85-percent radius station would have a bending velocity which is out of phase with the applied airloads, so that blade bending increases the higher harmonic pressure variations. This situation could not be expected to apply always, since it depends on the phasing between two rather loosely coupled phenomena: the rotor wake geometry and the blade bending response.

Longitudinal cyclic trim is shown in Figure 37 to have a pronounced effect on rotor-rotor interference. The aft rotor interference spike is shown to be significantly reduced when the cyclic trim is zero. With zero cyclic trim, there is the largest spacing between the rotors, and this spacing apparently allows the vortexes to pass the aft rotor without causing

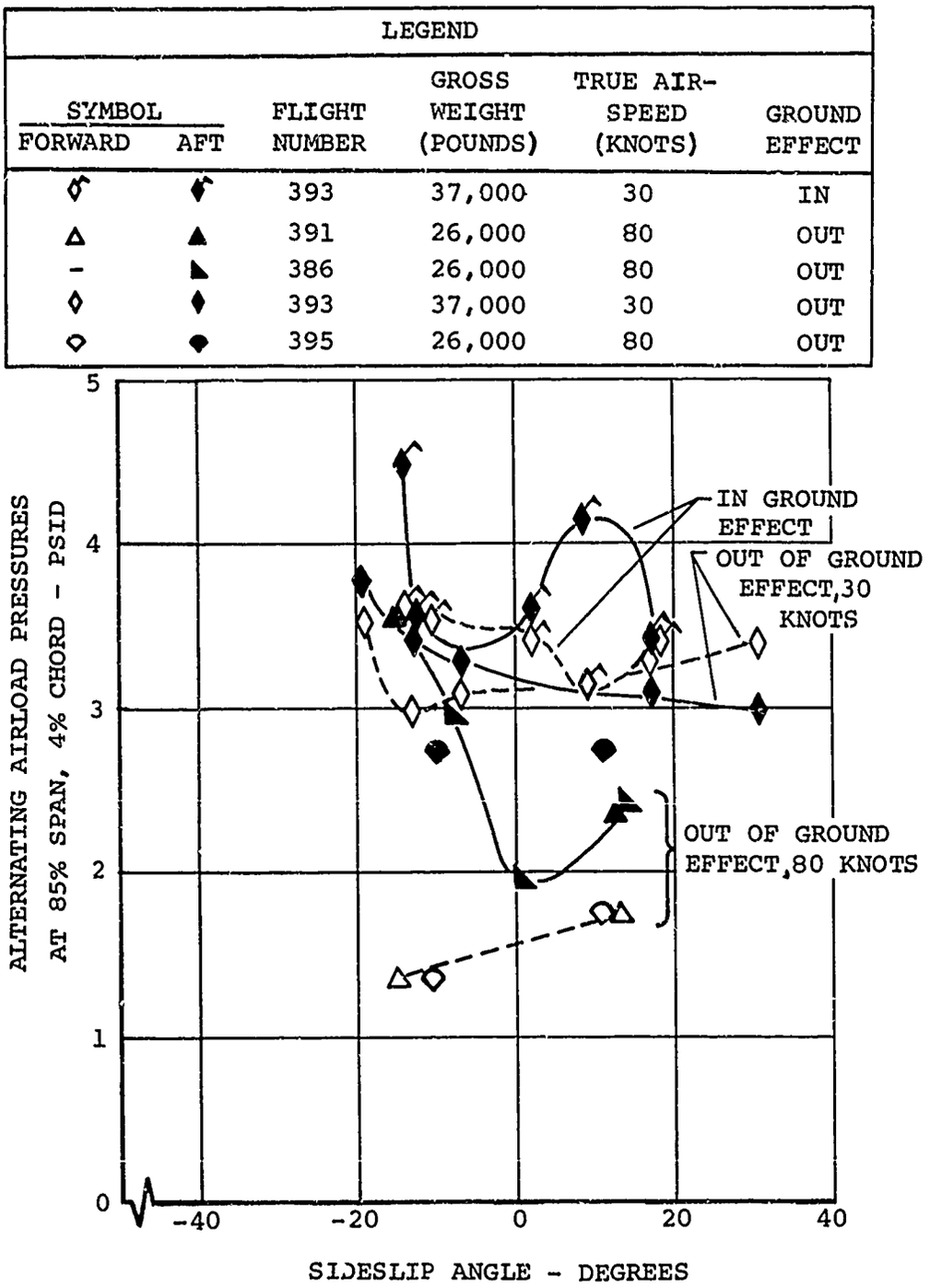

Figure 32. Effect of Sideslip on Alternating Airloads in Transition and at 80 Knots.

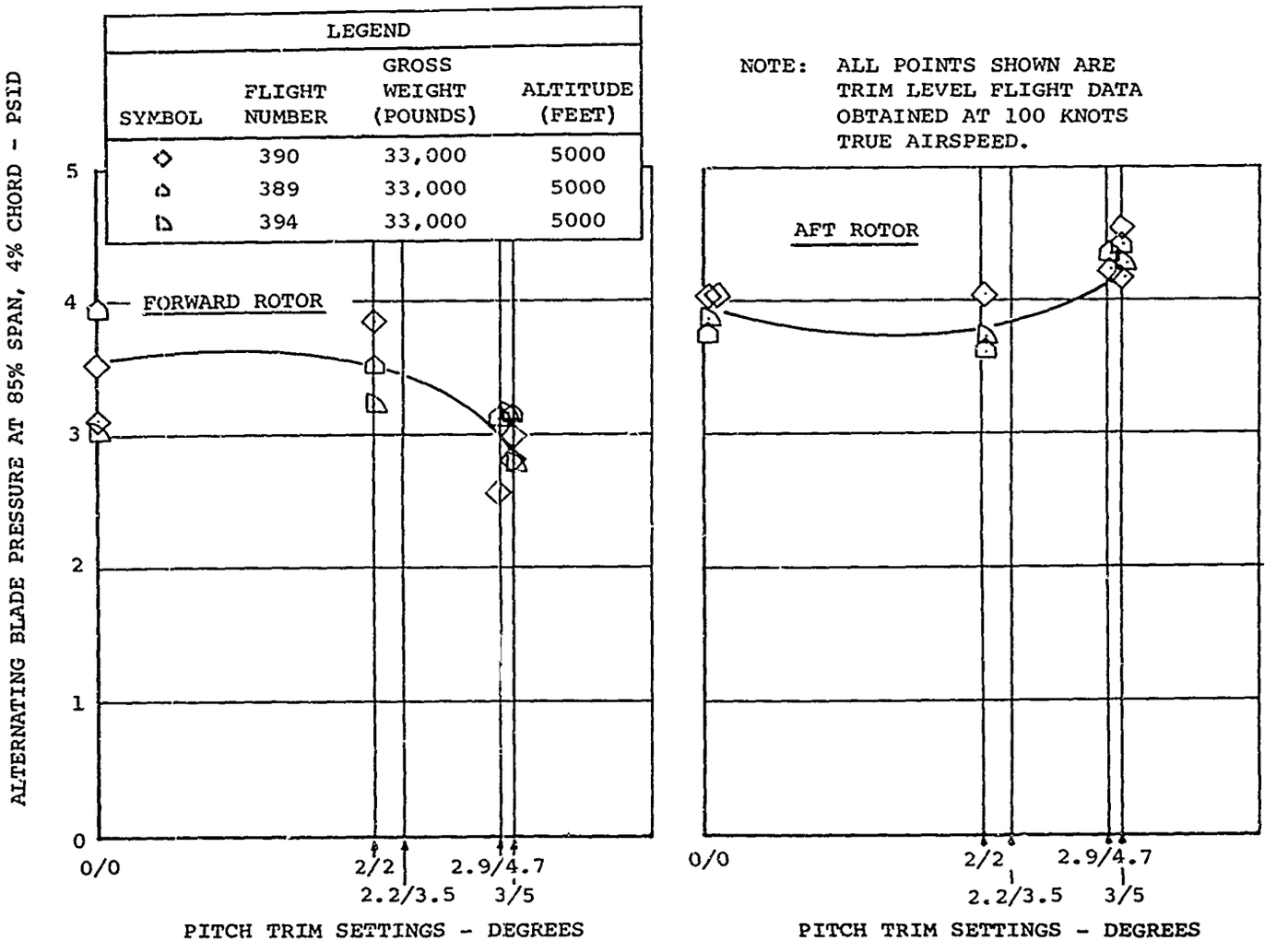

Figure 33. Variation of Typical Alternating Airloads with Cyclic Trim Setting.

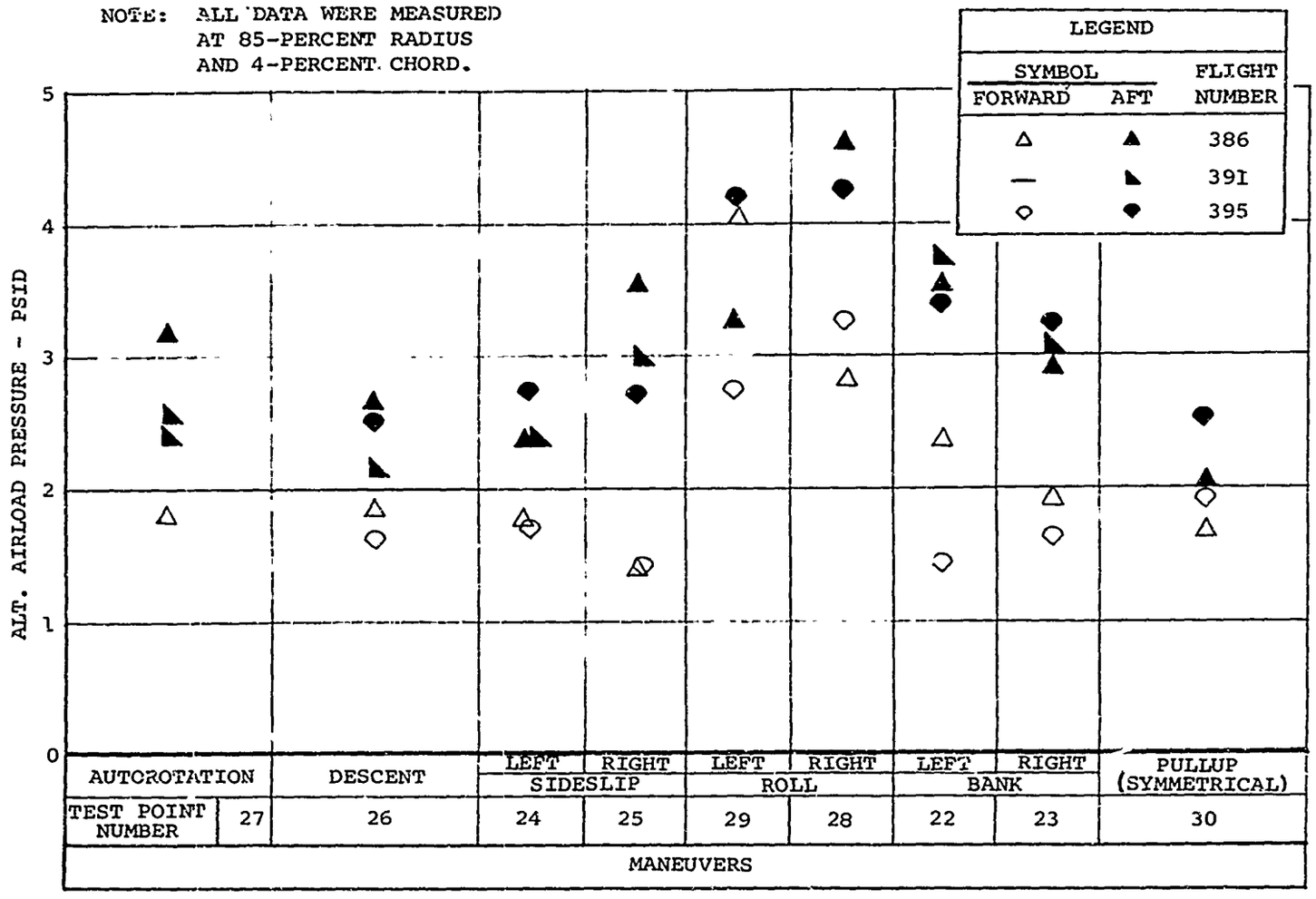

Figure 34. Measurements of Alternating Airload Pressures Obtained During Maneuvers at 80 Knots.

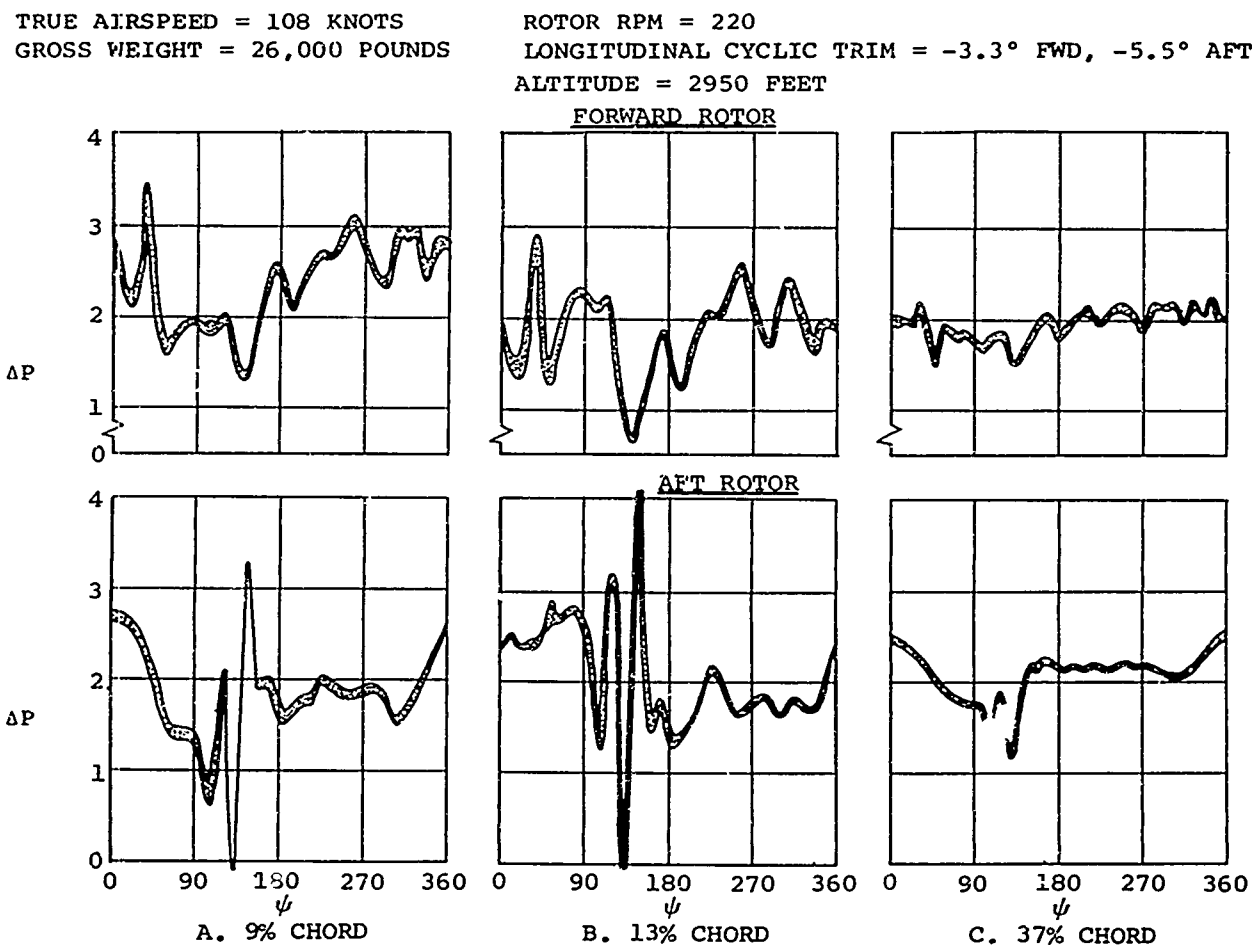

Figure 35. Azimuthal Variation of Airload Pressures at 85-Percent Radius for Three Chordwise Locations for a "Spiking" Trim Condition.

NOTES: 1. DATA RECORDED ON FLIGHT NUMBER 384, RUN 4, TEST POINT NUMBER 35
2. TRUE AIRSPEED 108 KNOTS, ROTOR RPM 221, GROSS WEIGHT 25,900 POUNDS

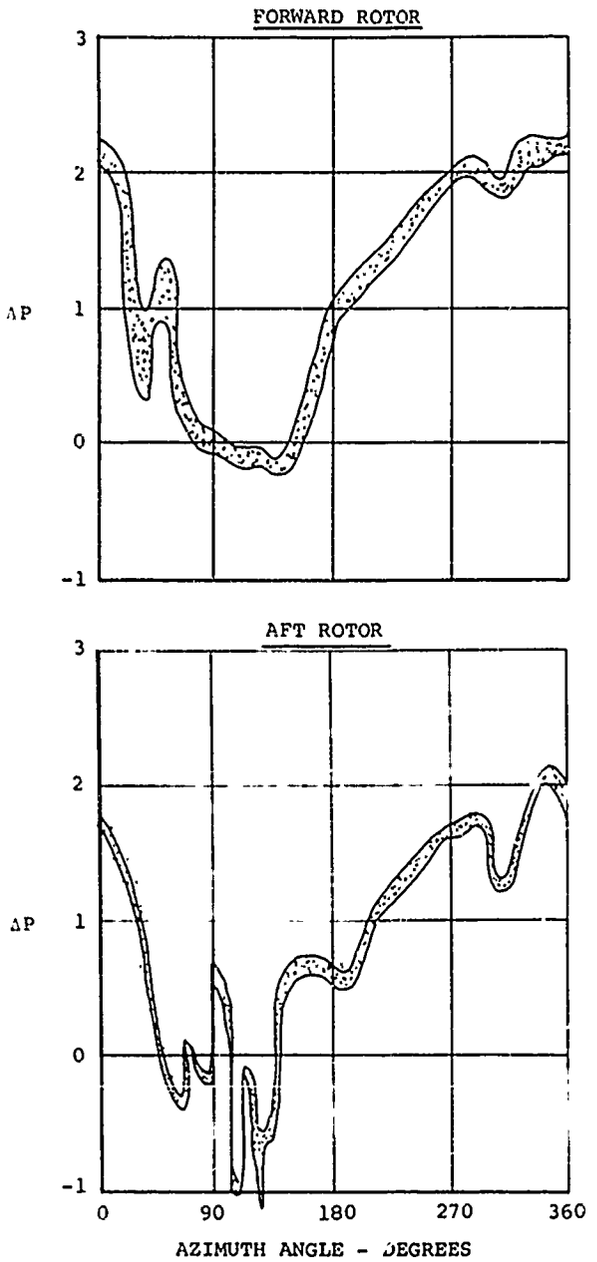

Figure 36. Azimuthal Variation of Airload Pressures at 98-Percent Radius and 9-Percent Chord.

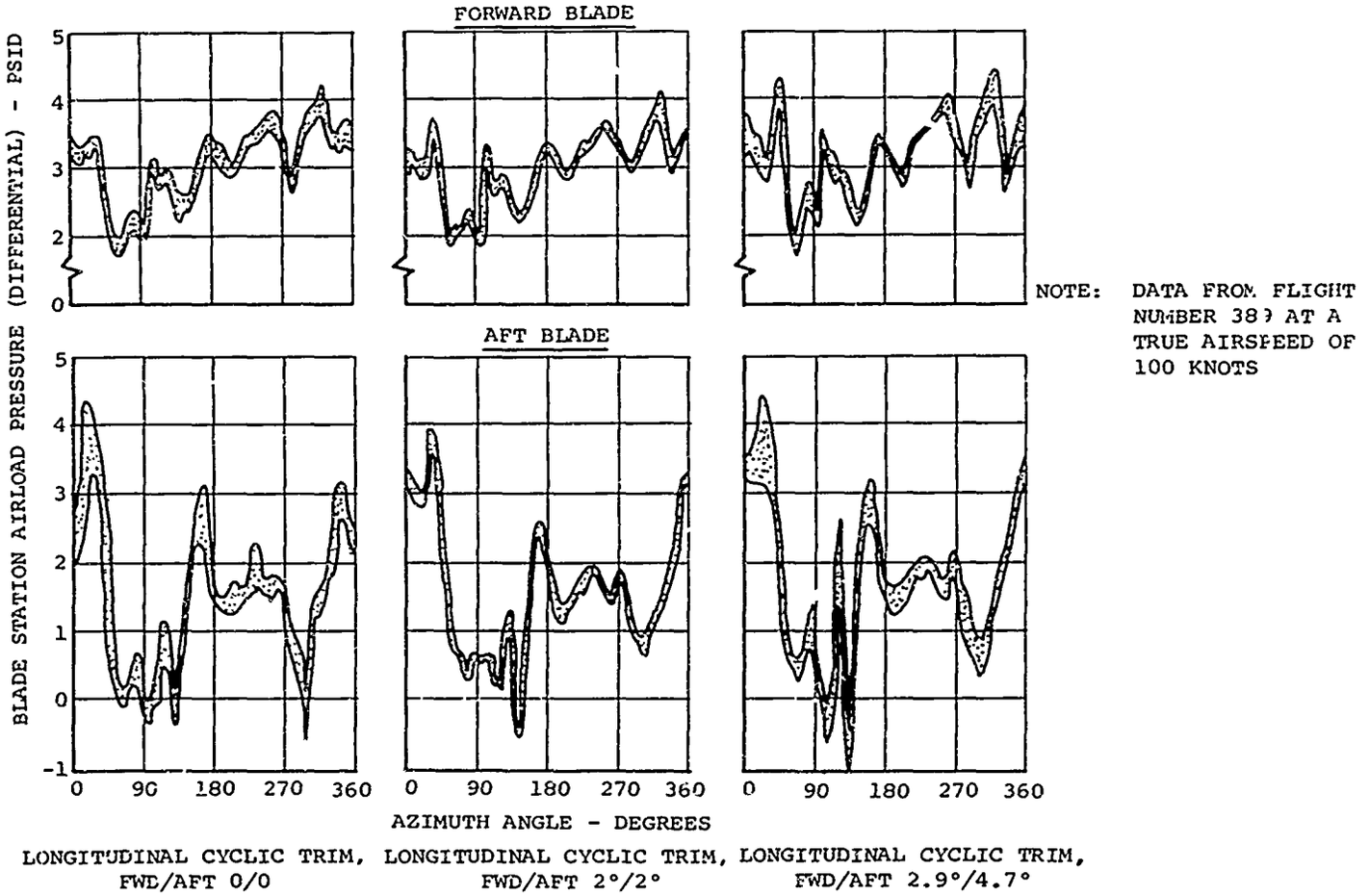

Figure 37. Effects of Longitudinal Cyclic Trim on Azimuthal Variation of Airload Pressure at 85-Percent Span, 9-Percent Chord.

significant disturbance. For reasons of performance, rotor shaft stresses, and other variables, it is desirable to fly with extended trim; however, as shown in Figure 37, increases in cyclic trim cause a continual increase in rotor-rotor interference on the aft rotor for this condition of airspeed and gross weight. It is significant to note, however, that while the spiking at 120 degrees is increased, the peak-to-peak airload pressures remain essentially unchanged. This is due in part to a reduction in the negative pressure peak at the 300-degree azimuth by the extension of the trim. The forward rotor data are shown to be essentially unchanged due to cyclic trim; however, an increase in the pressure bump in the overlap region, 40 degrees azimuth, can be observed as the trim is extended. A comparison of the data of Figure 37 to the data given previously in Figure 35 shows that a similar level of spiking occurred with the lower gross weight, slightly higher airspeed, and slightly further extended trim. The effects of cyclic trim must obviously vary with the flight conditions; however, the data generated apparently can be used to devise a cyclic trim schedule that will minimize vortex interference spiking. This schedule would not necessarily be optimum, since the blade generally does not respond to the spiking loads; there are also other considerations. Noise and local blade stresses would probably be diminished by this minimum interference trim schedule.

It is noteworthy that, as the gross weight is increased and the speed is decreased, the airload pressure variations increase significantly. Airload pressure data obtained at a run gross weight of 35,973 pounds and at 60 knots illustrate this trend (see Figure 38). The forward rotor data show surprisingly little variation in pressure due to aft rotor interference over the 300- to 60-degree azimuth angle region of the rotor overlap. Large pressure bumps are shown at 130 and 260 degrees, apparently because of interference with the vortex from the preceding blade of the same rotor. The aft rotor pressure bumps are much harder to interpret, but again appear to be due mostly to intrarotor effects. The large pressure bump at 270 degrees is most likely caused by the preceding blade of the aft rotor. Similar bumps are shown at 40 and 190 degrees, which cannot presently be explained. Obviously, wake distortion is more significant with reduced airspeed and with the more intense vortexes caused by increased weight. The development of a wake distortion-nonuniform downwash analysis should benefit considerably from these data.

When the airspeed considered is about 30 knots, the flight condition is known as transition. An extensive test program was conducted in transition, since this condition causes the most severe blade bending loads. The azimuthal variations in local airload pressure, measured at selected sideslip angles during the in-ground-effect testing, are shown in Figure 39. These data illustrate the large airload pressure variations caused by transition and the sizable effect of sideslip on the aft rotor pressures. Forward rotor data show a pressure peak at 110 degrees azimuth, apparently due to interference with the vortex from the preceding blade, and are almost unchanged due to sideslip. The aft rotor data are similar to the forward rotor data at zero sideslip, with intrarotor interferences most prominent as evidenced by peaks at 20, 90, and 160 degrees, with a minimum at 60 degrees. A positive sideslip (nose-left) of 17.3 degrees causes an extremely large pressure peak at 170 degrees azimuth; a negative sideslip of 13.8 degrees causes an extremely large pressure peak at 30 degrees azimuth. These very large peaks certainly would be expected to produce the large increases in blade bending which are caused by sideslip. No effort has yet been made to explain the source of these pressure peaks or to isolate these effects. It is expected that these pressure peaks are due to local angle-of attack conditions which would be indicative of blade stall. Blade torsion loads and pitch link loads are also very high in sideslip conditions, giving further indication that stall is occurring. Since it is not practical to build a helicopter that cannot fly through transition, and since it is difficult to fly a tandem helicopter through transition at zero sideslip, these data should receive considerable further analysis. This problem should be resolved before future tandem helicopter configurations are defined, since it is not obvious why zero sideslip does not cause large pressure variations.

The previously given azimuthal variations in airload pressures are highly responsive to all the variations in the local operating conditions; however, most of these variations are local and the blade responds only to much smoother effects. Automatic contour plots tend to be somewhat smoothed due to the analysis required for a two-dimensional fit of the data, and therefore show the more important aspects of the pressure variations. This tendency can be noted by comparing Figures 40 and 41, which show the 9-percent-chord pressure data for the forward and aft rotors for the same test point as shown in Figures 35 and 36. These data show significant differences when the local pressures are plotted against azimuth; however, the two concour

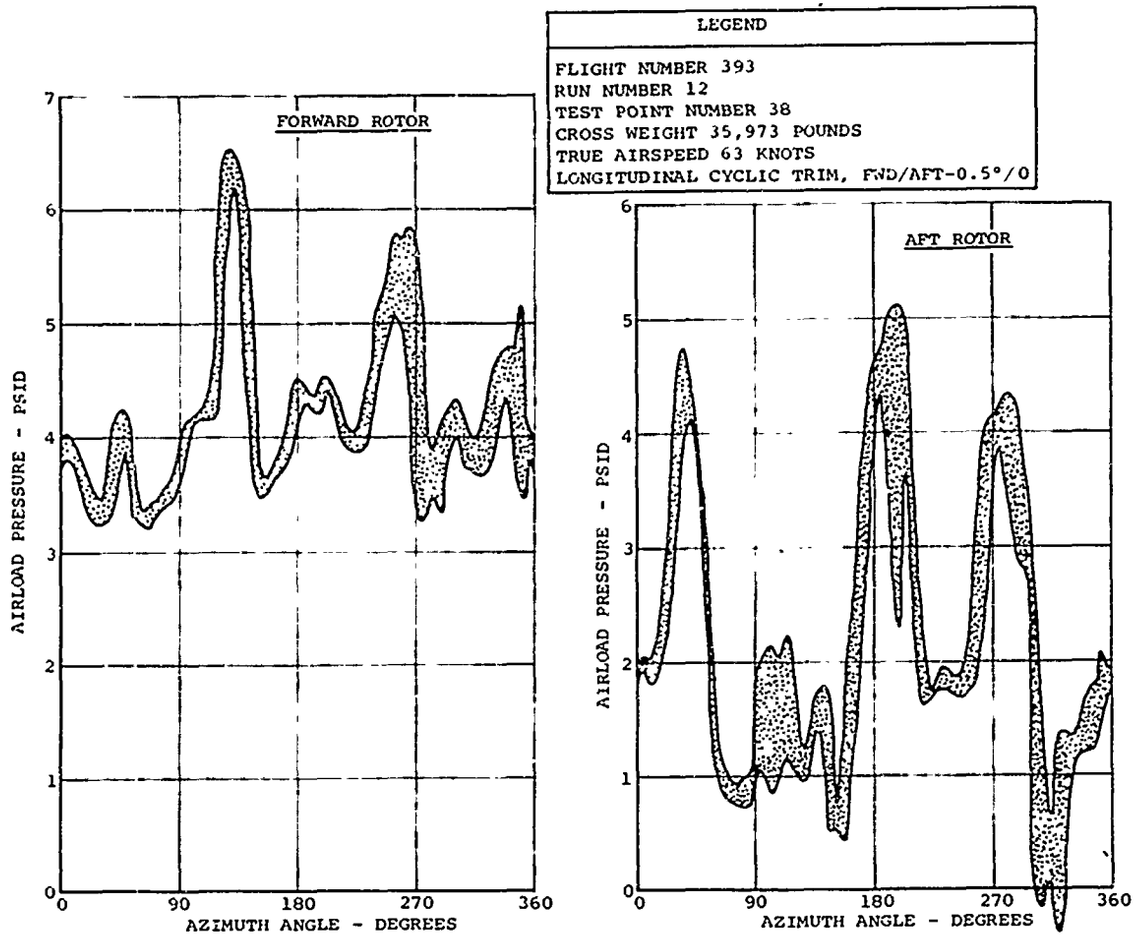

Figure 38. Azimuthal Variation of Airload Pressure at 85-Percent Span, 9-Percent Chord for a High-Gross-Weight Low-Speed Flight Condition.

FORWARD ROTOR

NOTES: 1. ALL DATA FROM FLIGHT NUMBER 393, RUNS 1, 3, AND 5, TEST POINT NUMBERS 6, 7, AND 9, WITH AIRSPEED NEAR 30 KNOTS AND RGW APPROXIMATELY 37,000 POUNDS.

2. DATA FOR AFT ROTOR AT A SIDESLIP ANGLE OF 17.3 DEGREES WERE SHIFTED 4 PSID TO CORRECT FOR A BAD IN-FLIGHT RECALCULATION. THESE DATA HAVE BEEN DELETED FROM THE FINAL DATA REPORT.

AFT ROTOR

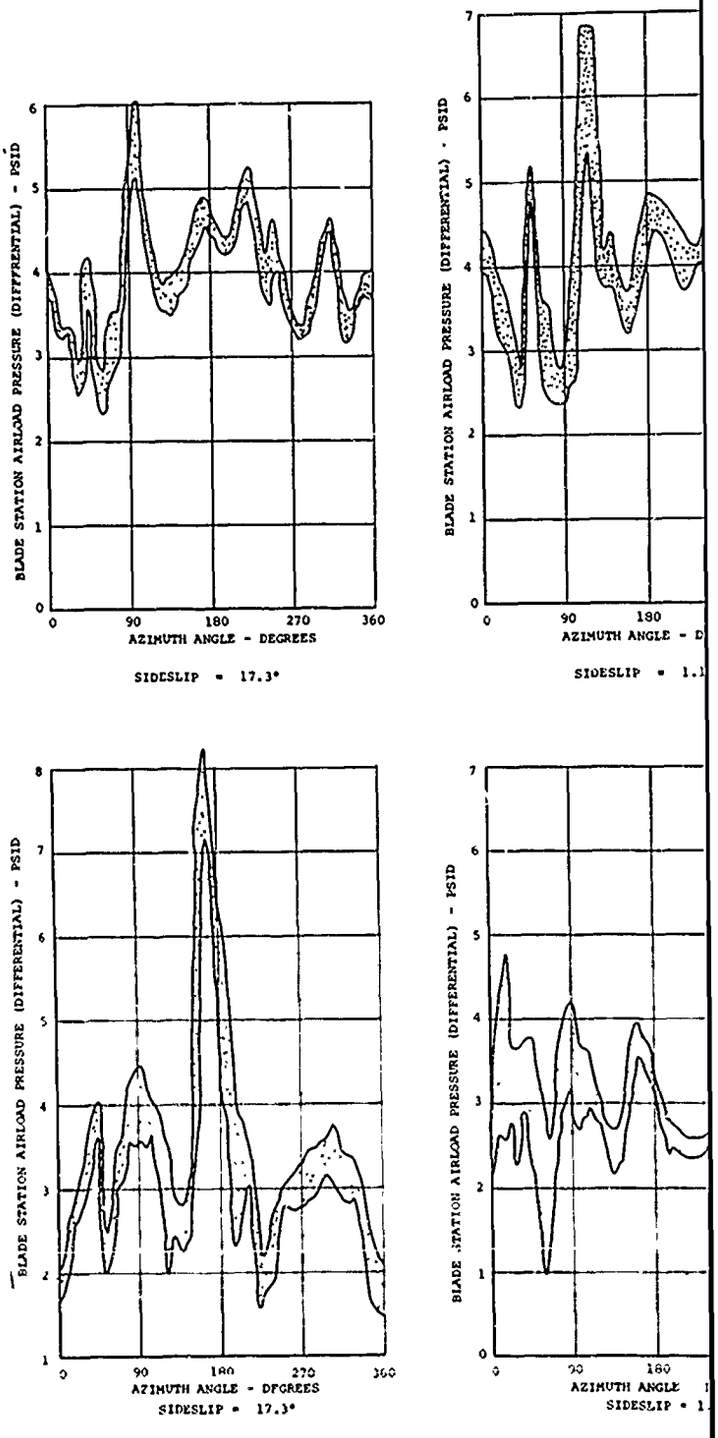

Figure 39. Effects of Sideslip in Transition on Azimuthal Variation of Air and 9-Percent Chord.

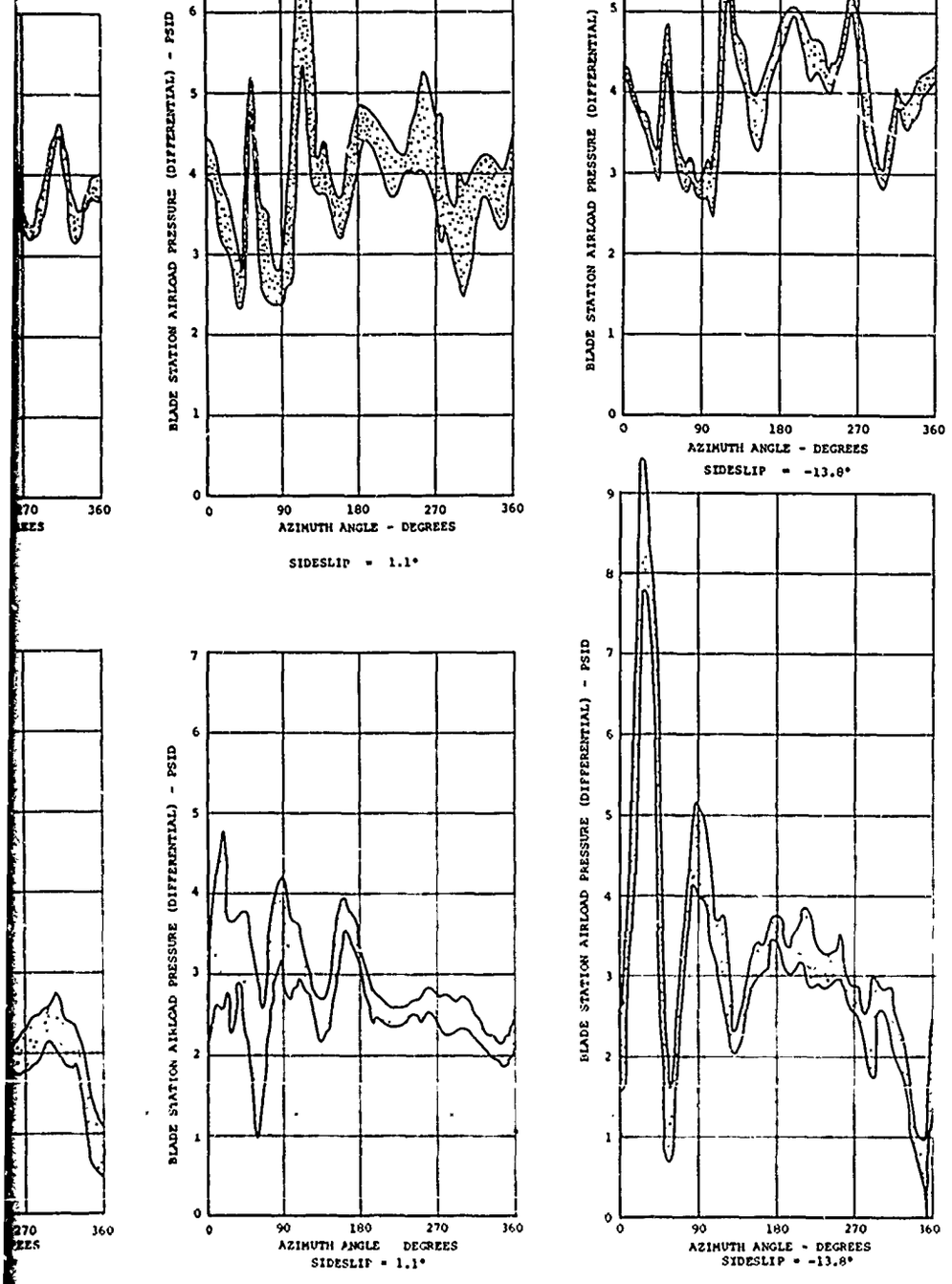

imuthal Variation of Airload Pressure at 85-Percent Radius

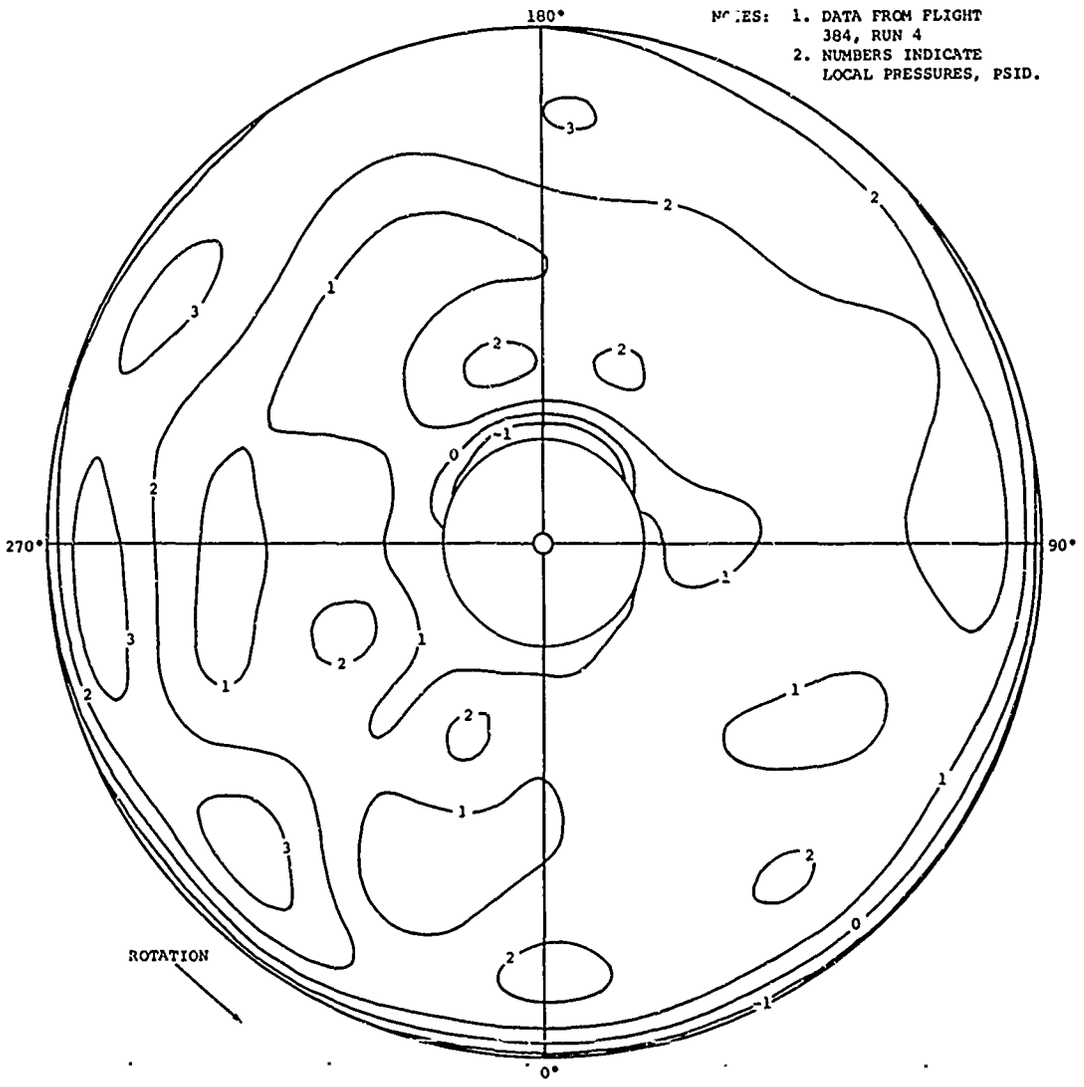

Figure 40. Contour Plot of Airload Pressures at 9-Percent Chord of the Forward Rotor at 108 Knots.

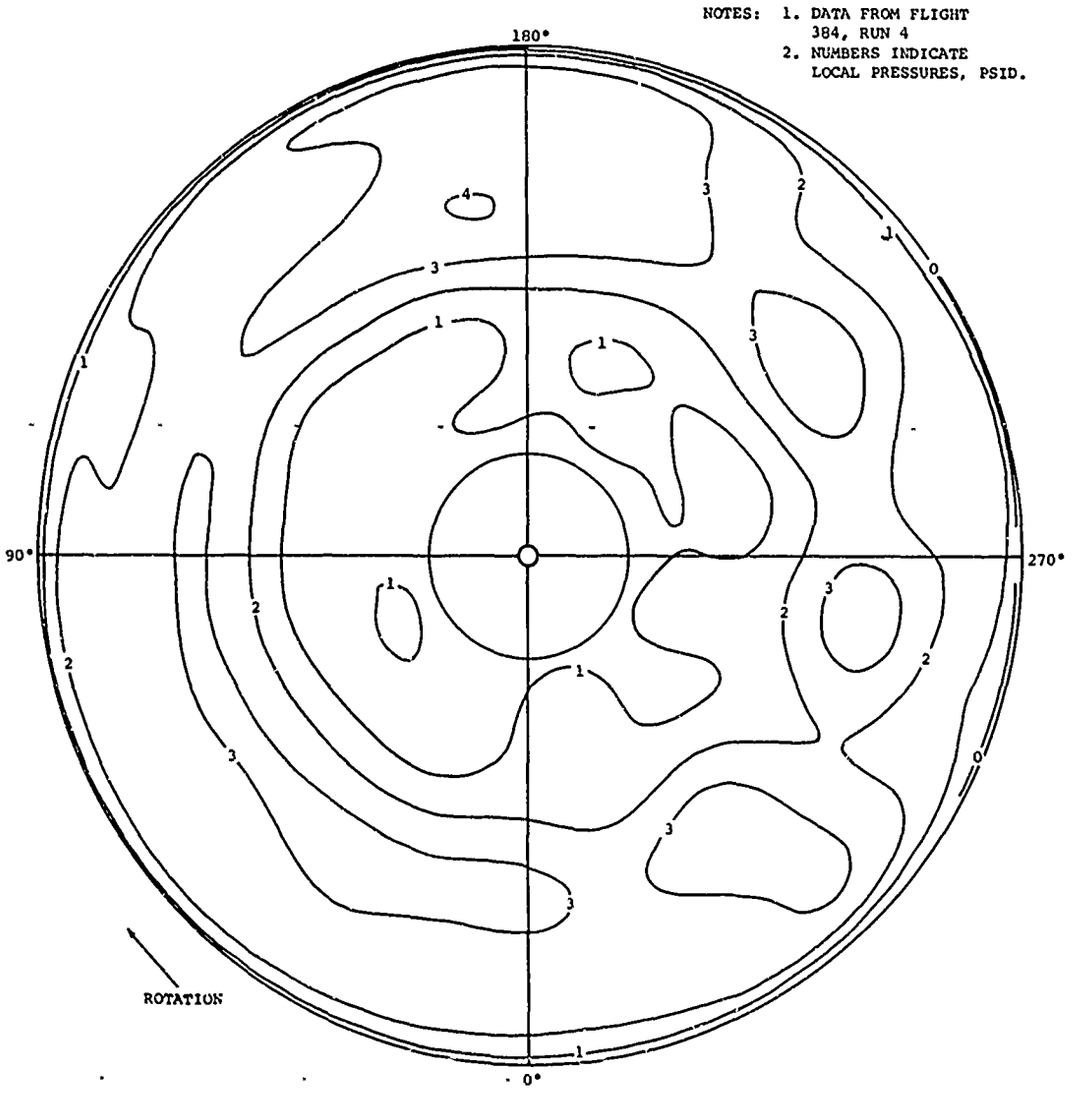

Figure 41. Contour Plot of Airload Pressures at 9-Percent Chord of the Aft Rotor at 108 Knots.

plots of the same data show only small differences. Outer blade pressures are shown to be fairly constant on the advancing side of the disk, with three regions of higher pressure (about a 6/rev. variation) on the retreating side. The overall pressure distributions differ in that the forward rotor has larger pressures inboard than the aft rotor. In addition, the forward rotor has lower pressures in the overlap region ($\psi \approx 0°$), while the aft rotor has higher pressures in the overlap region ($\psi \approx 180°$). These differences in local pressures are believed to be reflections of the average rotor-rotor interference which will be discussed in conjunction with the integrated airloads data.

Chordwise Pressure Distributions

The presentation of airload pressure measurements as chordwise pressure distributions shows the regions in which the blade sections do not act as two-dimensional airfoils. Typical data are shown in this manner in Figures 42 and 43 for the advancing and retreating sides of the rotor disk. After the azimuth angle increases to about 30 degrees, the chordwise pressure distributions on both rotors are irregular on the advancing side, as shown in Figure 42. This effect is believed to be due to the combined effects of compressibility and the interference of the tip vortex from the preceding blade. The azimuthal area over which the airfoil pressures are disturbed by these effects is considerably larger than expected. From theoretical inviscid-incompressible considerations, the airfoil pressure distribution is expected to be stable and highly damped. These data show that the pressure distribution recovers slowly from a disturbance.

There are two especially interesting features of the data of Figure 42. First, it appears that the influence of the vortex pressure field on the blade airload pressures near the trailing edge has been measured. Note that at an azimuth angle of 120 degrees, the aft rotor data show a pressure bump at 89-percent chord. This pressure bump is apparently due to the tip vortex from the preceding blade of the forward rotor, which causes considerable disturbance to the aft rotor blade at this azimuth. It appears that this bump is the remnant of the pressure spike which moves off the blade quite rapidly. These data are expanded in Figure 44 to show the persisting effects of previous disturbances at 113 degrees azimuth and the increased distrubance at the leading edge of the blade at 124 degrees after the vortex pressure bump (shown at $\psi = 120°$) has disappeared. The irregularities of the pressure distribution after the spike loads are past are shown to be significant and persistent.

The second particularly interesting detail of Figure 42 is the clear evidence of the effects of blade section sweep (radial flow) in the data taken at 180 degrees azimuth on the forward rotor. The chordwise pressure distribution shows much higher pressures aft of the midchord than expected. This distribution is quite similar to that measured on yawed wings at high angles of attack. The significance of this phenomenon in reducing blade stall is discussed in reference 11 and in Volume V.

For typical flight conditions, the pressure distributions on the retreating portion of the rotor disk are not significantly different from those of a two-dimensional airfoil. This general conclusion is supported by the data shown in Figure 43; however, it is suspected that this general conclusion does not apply for blade section radii which experience reversed flow ($r/R \leq \mu'$), or when stall occurs. The effects of stall are presented in Volume V and are not generally considered in this volume. It is recommended that reversed flow effects also be investigated separately.

The significant implications of the relative smoothness of the retreating blade airloads are either that tip vortex proximity does not occur, or that when tip vortexes are nearby, the local Mach number is sufficiently low that the pressure distribution is not disturbed. Wake distortion would have to be significant to prevent tip vortex proximity on the retreating blade. If wake distortion is the mechanism which prevents retreating blade vortex proximity, it is expected that there would be flight conditions or rotor trim settings for which the distortion was not enough to prevent the tip vortexes from coming near the following blades. Except for transition, this situation has not been found to occur, so tip vortex proximity effects apparently are a compressibility coupled phenomenon. The extensive analysis of this phenomenon is also recommended. Rotor performance and control loads will undoubtedly be improved when the performance of the airfoil sections is more thoroughly understood.

The irregularities in the chordwise pressure distributions apparently are not of a harmonic nature but are impulsive. Therefore, the rotor blade section environment is reflected in non-airfoil-like pressure distributions if the airload pressures are considered as harmonics. Figures 45 and 46 show typical results of first and second harmonic airloads data when prepared as nondimensional airload pressure distributions. A hyperbolic variation of pressure with chord typical of

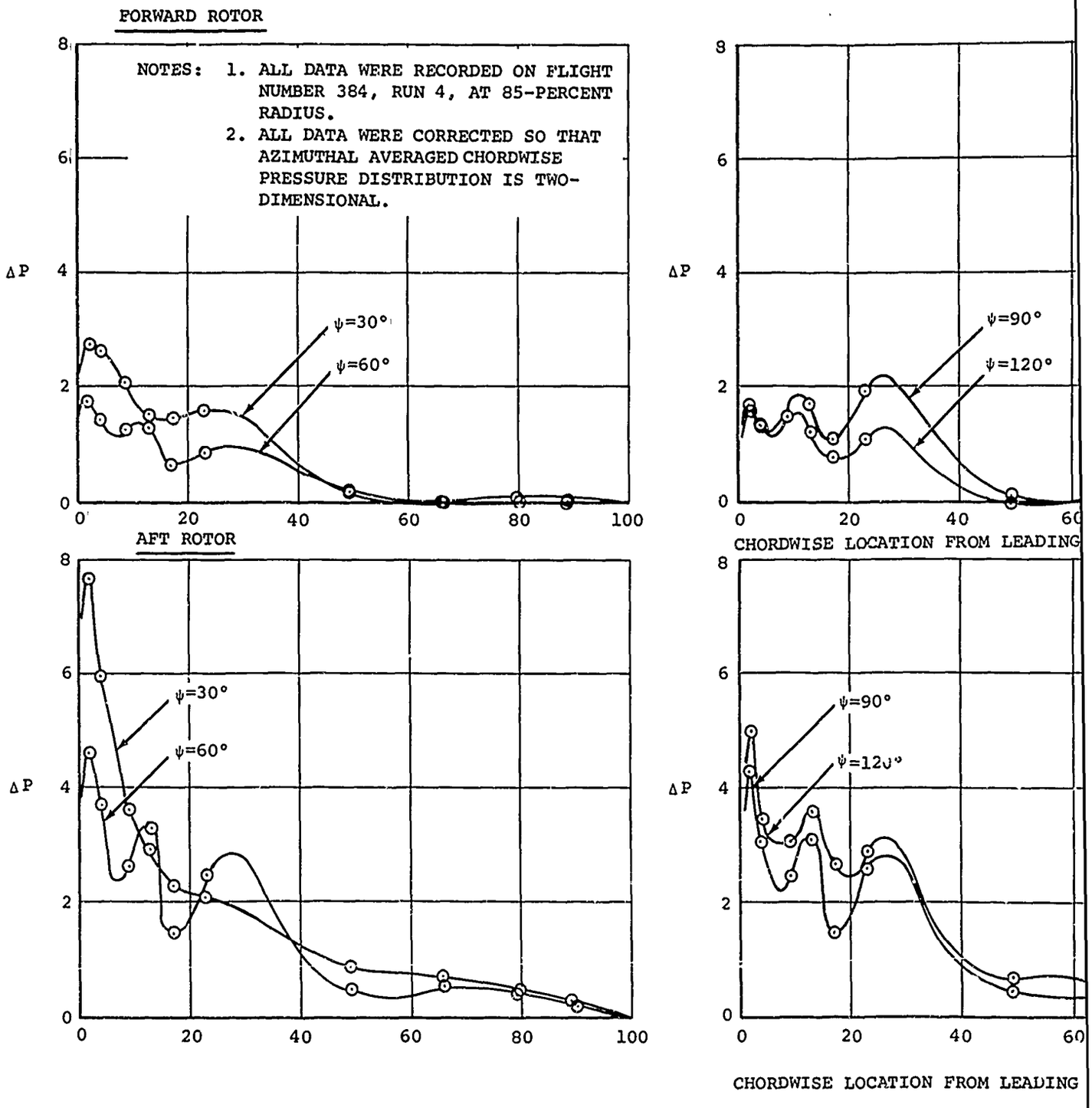

Figure 42. Chordwise Pressure Distributions Measured on Advancing Side of Rotor Disk at 108 Knots Airspeed and 26,000 Pounds Gross Weight.

A

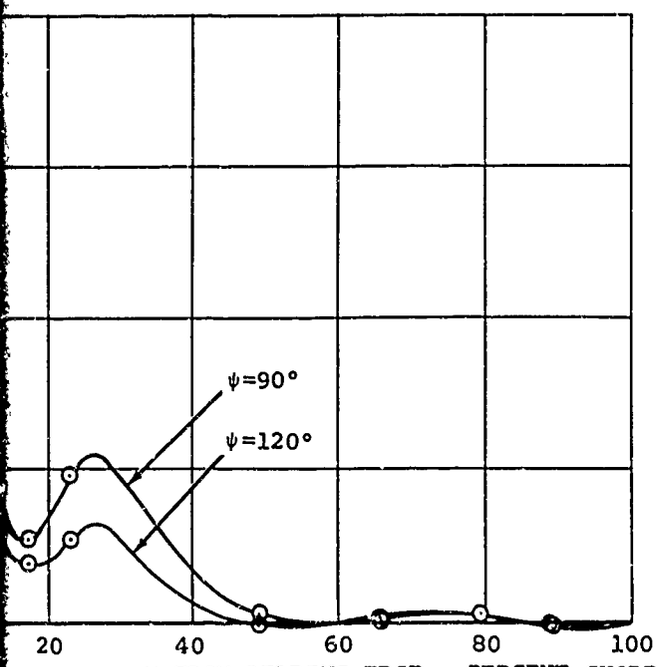

E LOCATION FROM LEADING EDGE - PERCENT CHORD

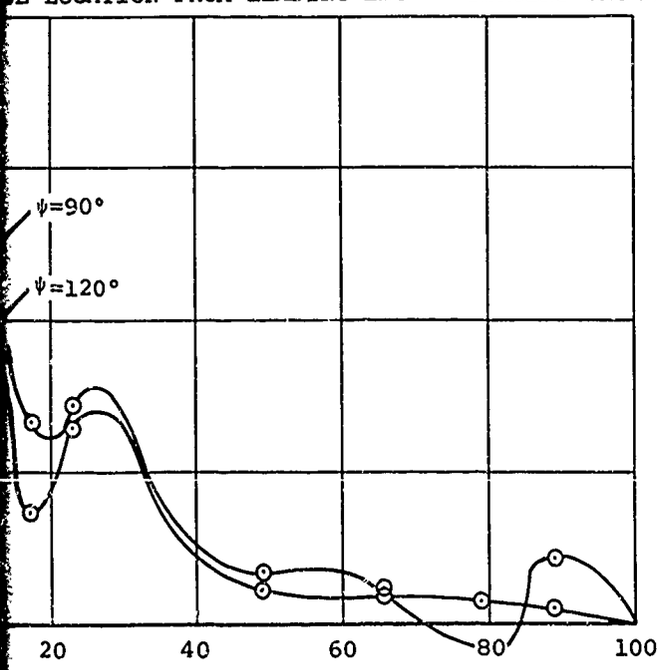

E LOCATION FROM LEADING EDGE - PERCENT CHORD

ΔP

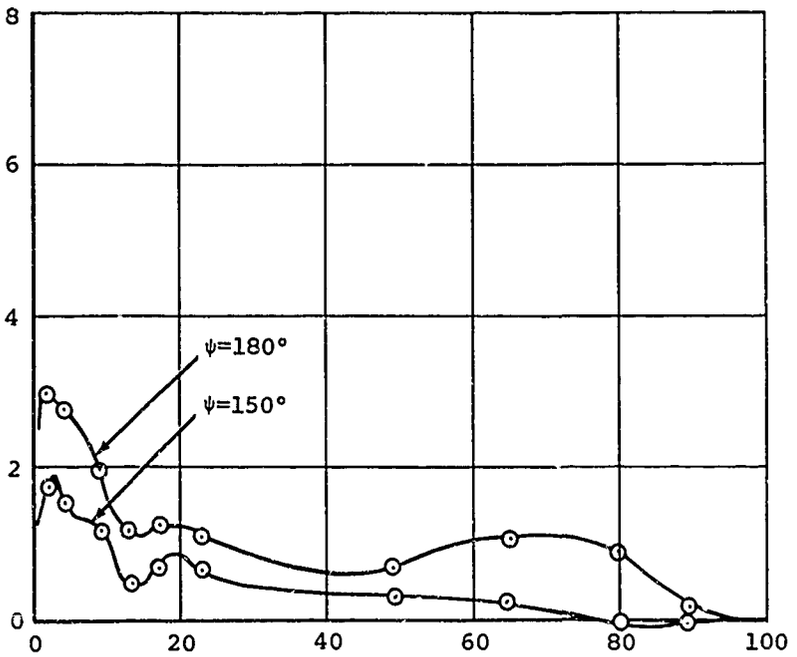

ΔP

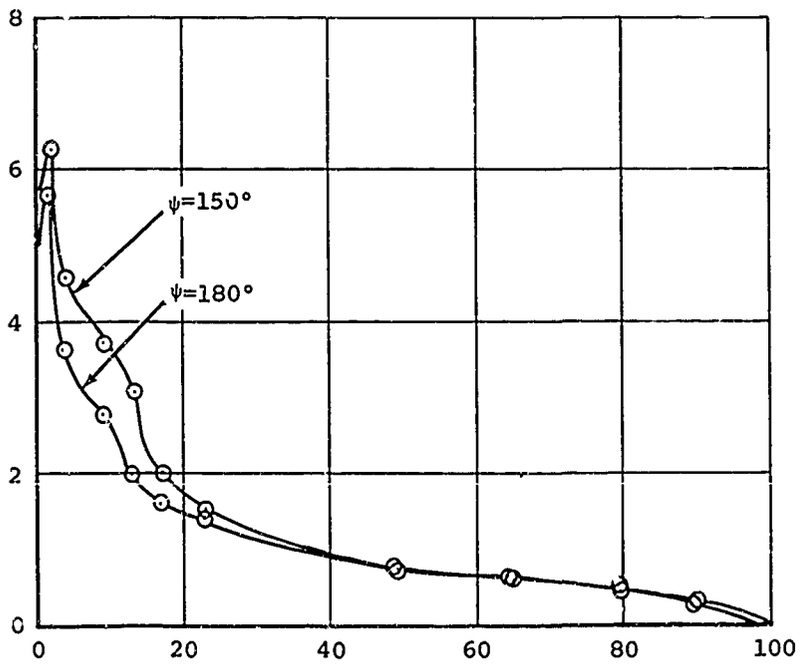

B

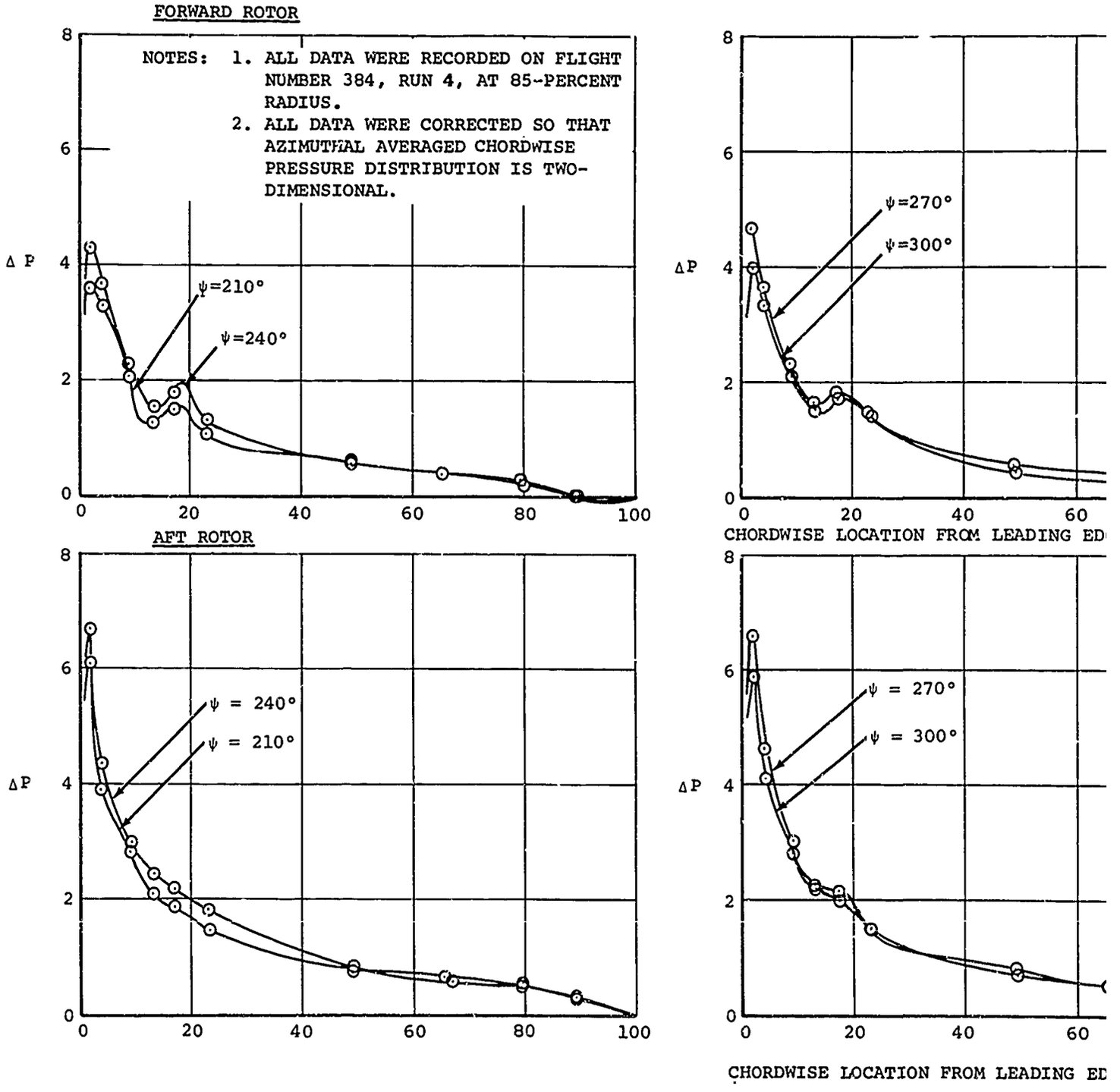

Figure 43. Chordwise Pressure Distributions Measured on Retreating Side of Rotor Disk at 108 Knots Airspeed and 26,000 Pounds Gross Weight.

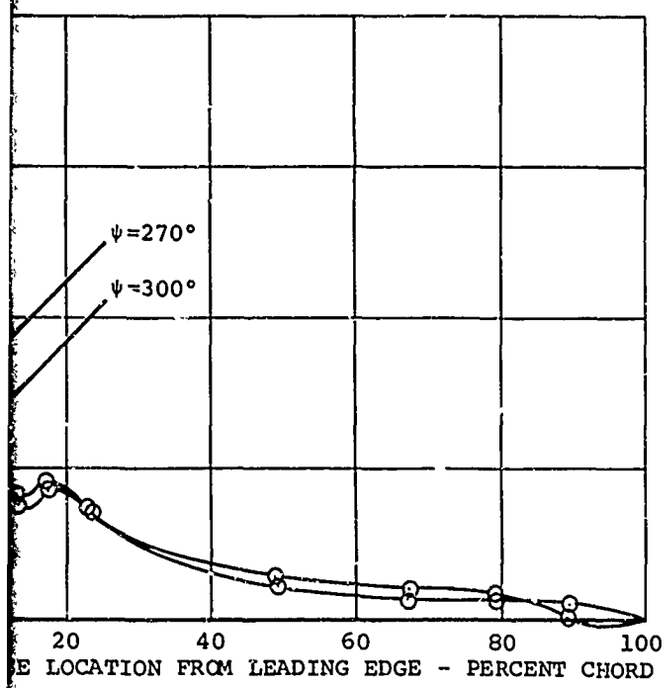

E LOCATION FROM LEADING EDGE - PERCENT CHORD

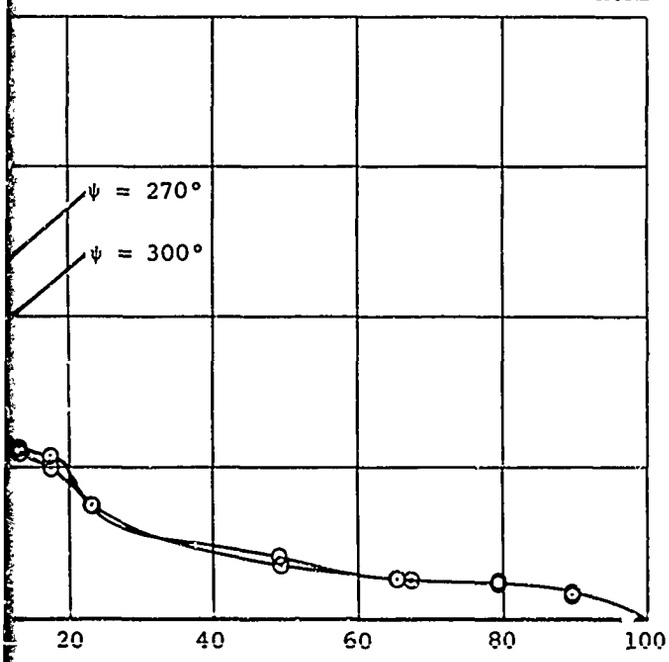

SE LOCATION FROM LEADING EDGE - PERCENT CHORD

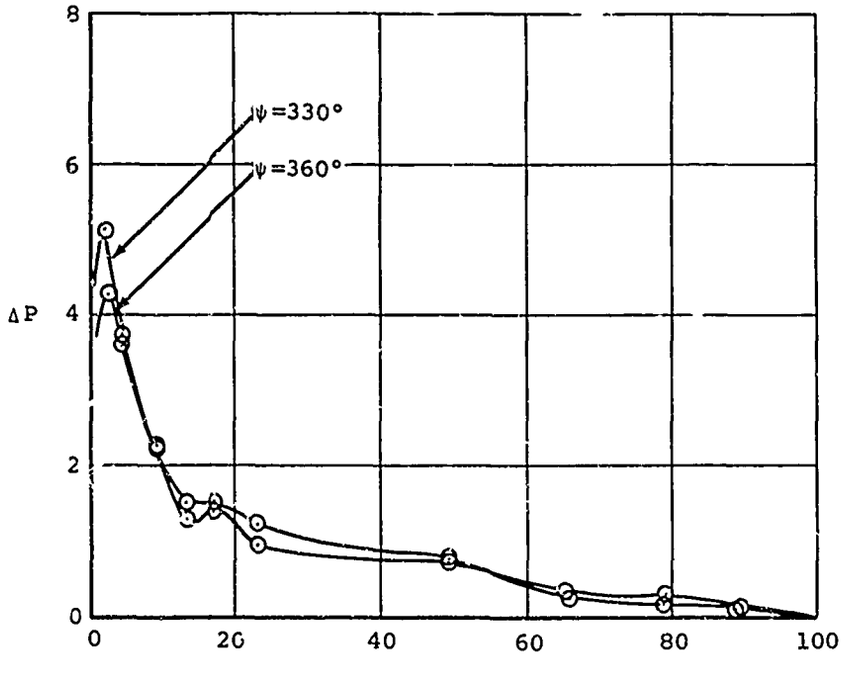

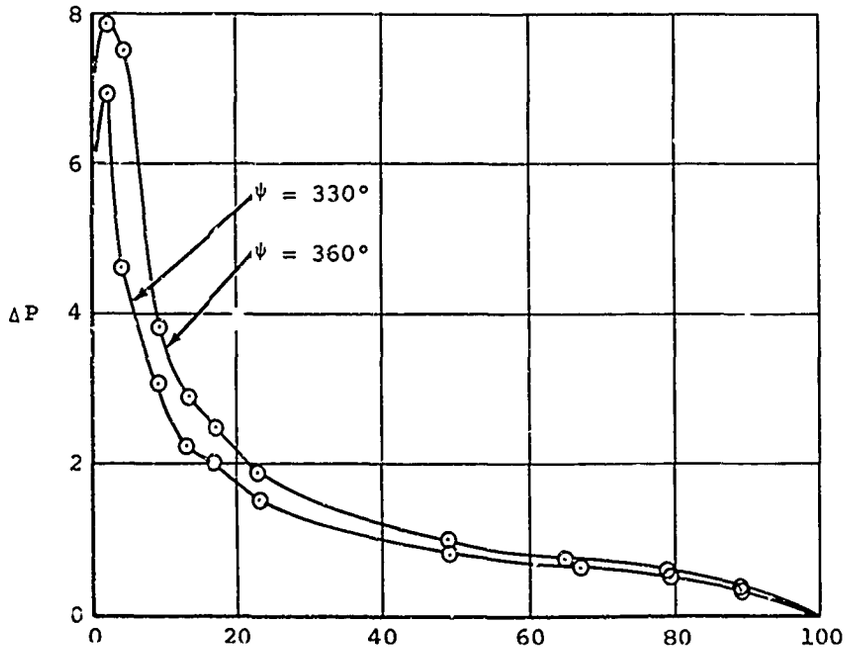

B

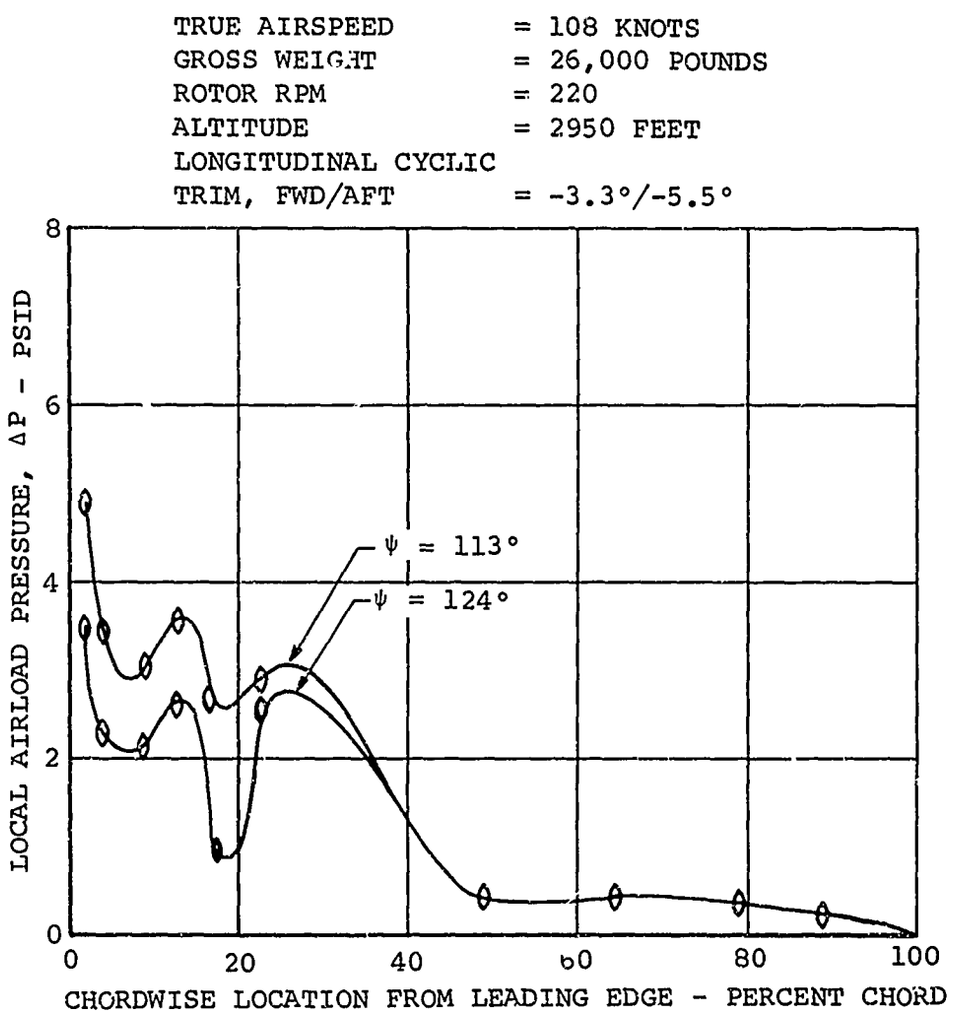

Figure 44. Typical Chordwise Pressure Distributions of Aft Rotor When in Proximity of Forward Rotor Tip Vortex.

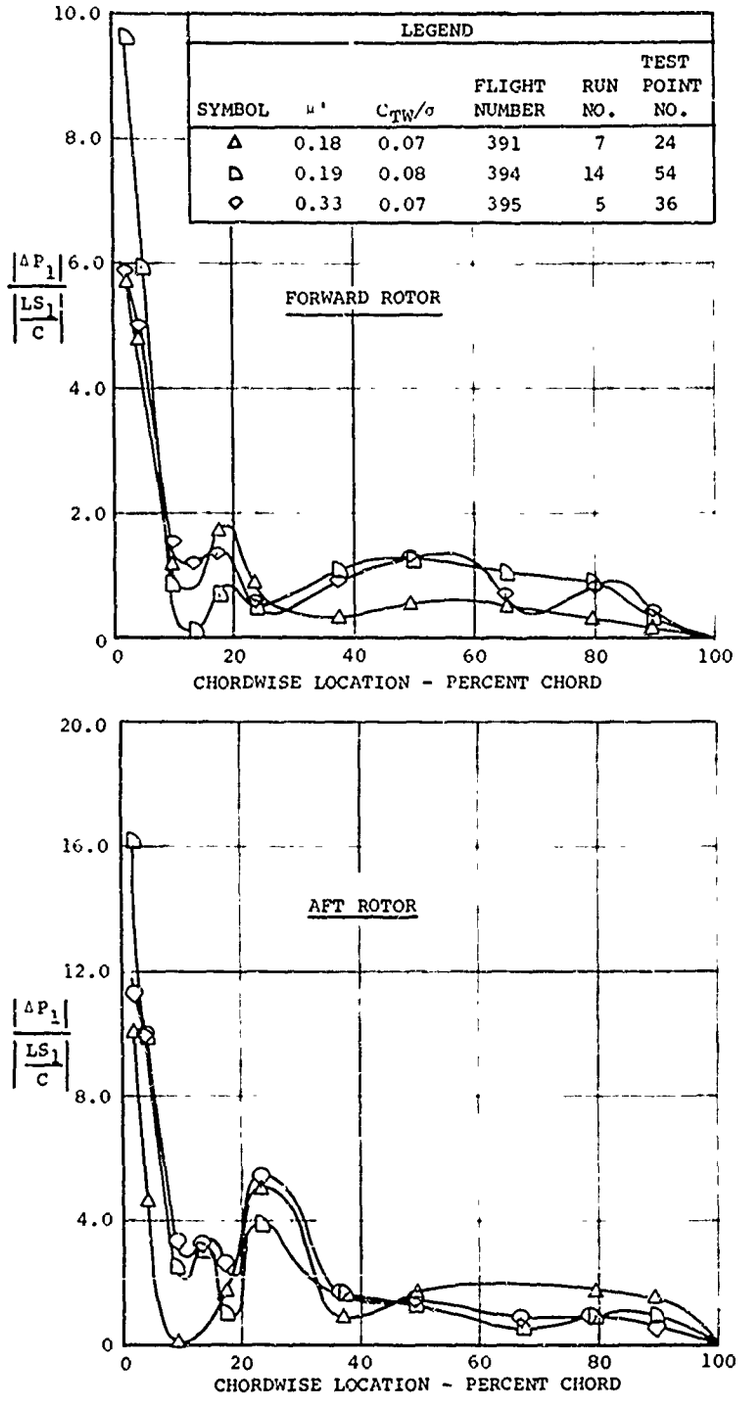

Figure 45. Chordwise Distribution of First Harmonic Airloads at 85 Percent of the Blade Radius for Three Tests.

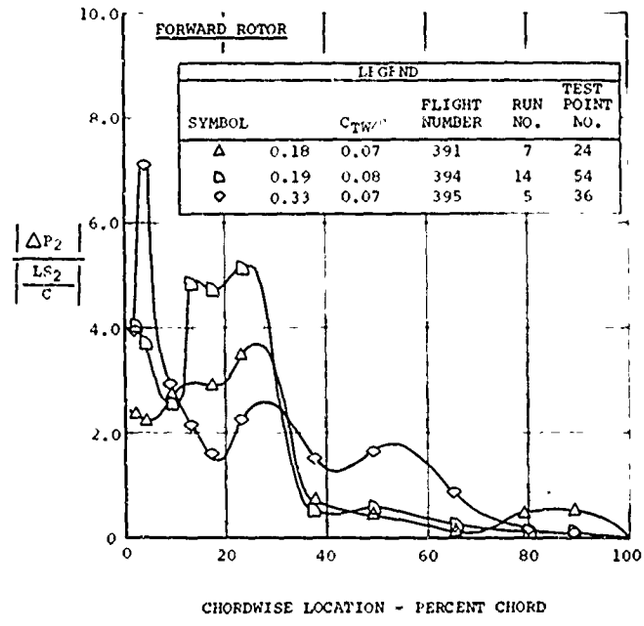

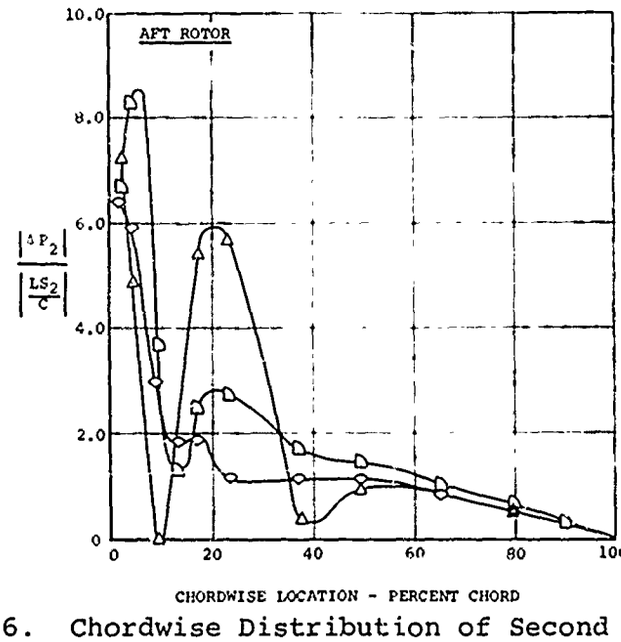

Figure 46. Chordwise Distribution of Second Harmonic Airloads at 85 Percent of the Blade Radius for Three Tests.

two-dimensional airfoils would be expected of airloads data prepared in this manner; however, these figures show significant irregularities. The data shown were obtained at a moderate speed well above transition but well below the region of high dynamic loads (stall), so these effects probably do not contribute to the irregularities. Later in this volume, these data are compared with other rotor airloads data obtained at lower advancing blade Mach number but at similar thrust coefficients and advance ratios which show almost no irregularities in the harmonic blade section loading. Thus, the effects of sweep, reversed flow, and first-order time-dependence (potential flow damping effects) are apparently harmonic in nature or are relatively small. Also, the effect of tandem rotor interference apparently is not significant, since Figures 45 and 46 show similar harmonic loadings for both rotors with only slightly larger irregularities in the aft rotor data. The significant parameter of this non-airfoil-like performance is apparently the advancing blade Mach number.

Lift per Unit Span

The airload pressure measurements have been integrated over the chord to determine the local lift per unit span at the various blade stations. Obviously, this value is of considerably more interest than the individual local pressures, since the contributions of the various blade sections to lift, propulsion, and blade bending excitation are indicated. These data have been prepared as azimuthally averaged values, plots showing the azimuthal variations, contour plots, and illustrations of various harmonics of airloads.

Typical azimuthal averaged lift-per-unit-span data are shown in Figures 47 and 48. Forward flight is shown to produce a considerably different radial distribution of average airloading on the forward and aft rotors. The forward rotor apparently operates in an upwash region caused by the aft rotor. This upwash increases the average loading on the inboard area of the forward rotor. The aft rotor has an average airload distribution which is typical of an isolated rotor, except for a rather large tip loss. Figure 48 includes three typical hovering test points (of the eight hovering test points obtained) and shows the significant effect of relatively small wind velocities. It should be noted that at a run gross weight of 35,123 pounds and with the wind (9 knots) from the left side, the average loading on the two rotors is almost identical and is like an isolated rotor. At lighter gross weights and with the wind

SYMBOL	TRUE AIRSPEED (KNOTS)	LONGITUDINAL CYCLIC TRIM (FWD/AFT)	RUN NUMBER	TEST POINT NUMBER
◇	54	-1.1/-0.9	3	61
◆	98	-3.3/-5.2	4	18
◇	138	-3.9/-5.4	5	36

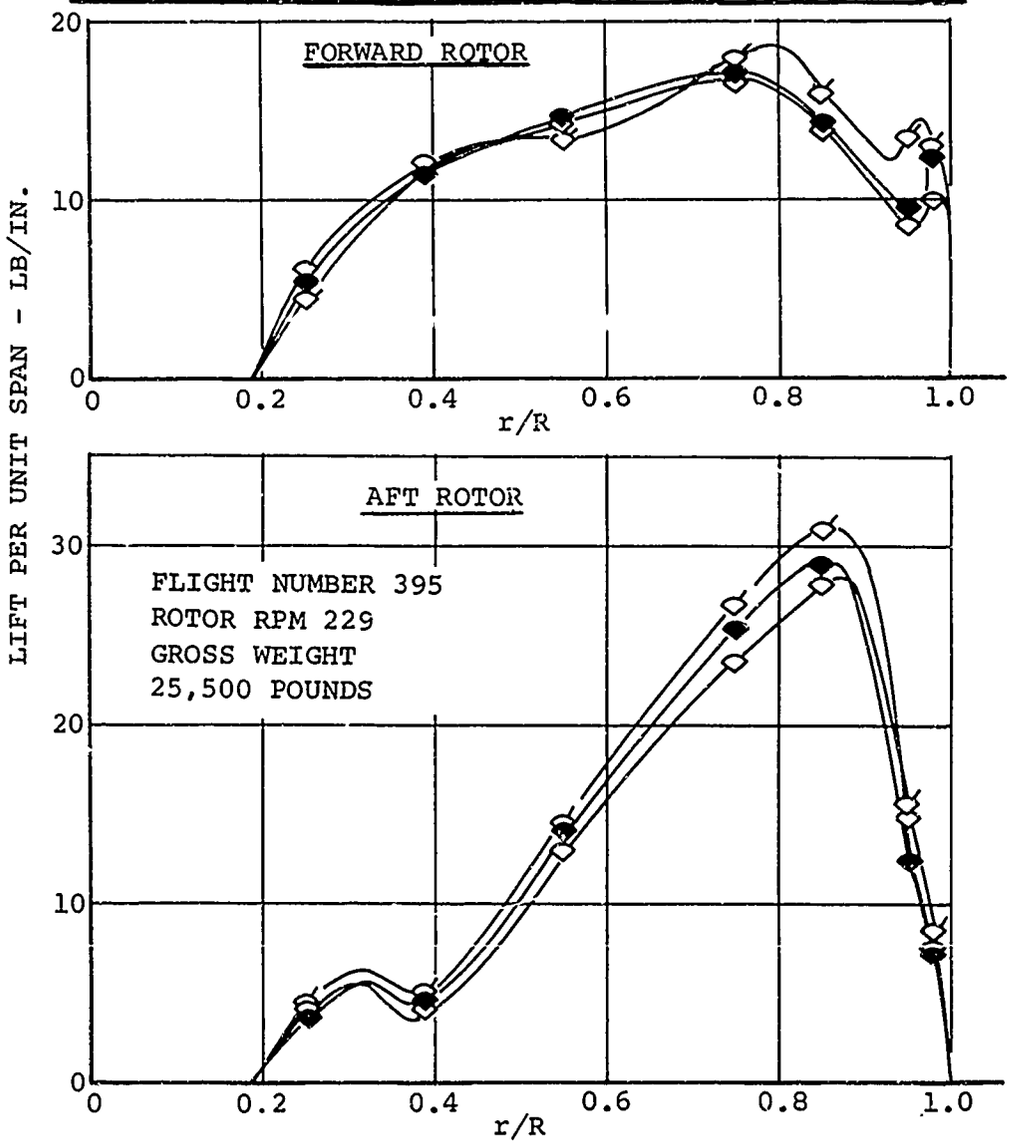

Figure 47. Effect of Forward Speed on the Radial Distribution of the Azimuthal Average Lift per Unit Span.

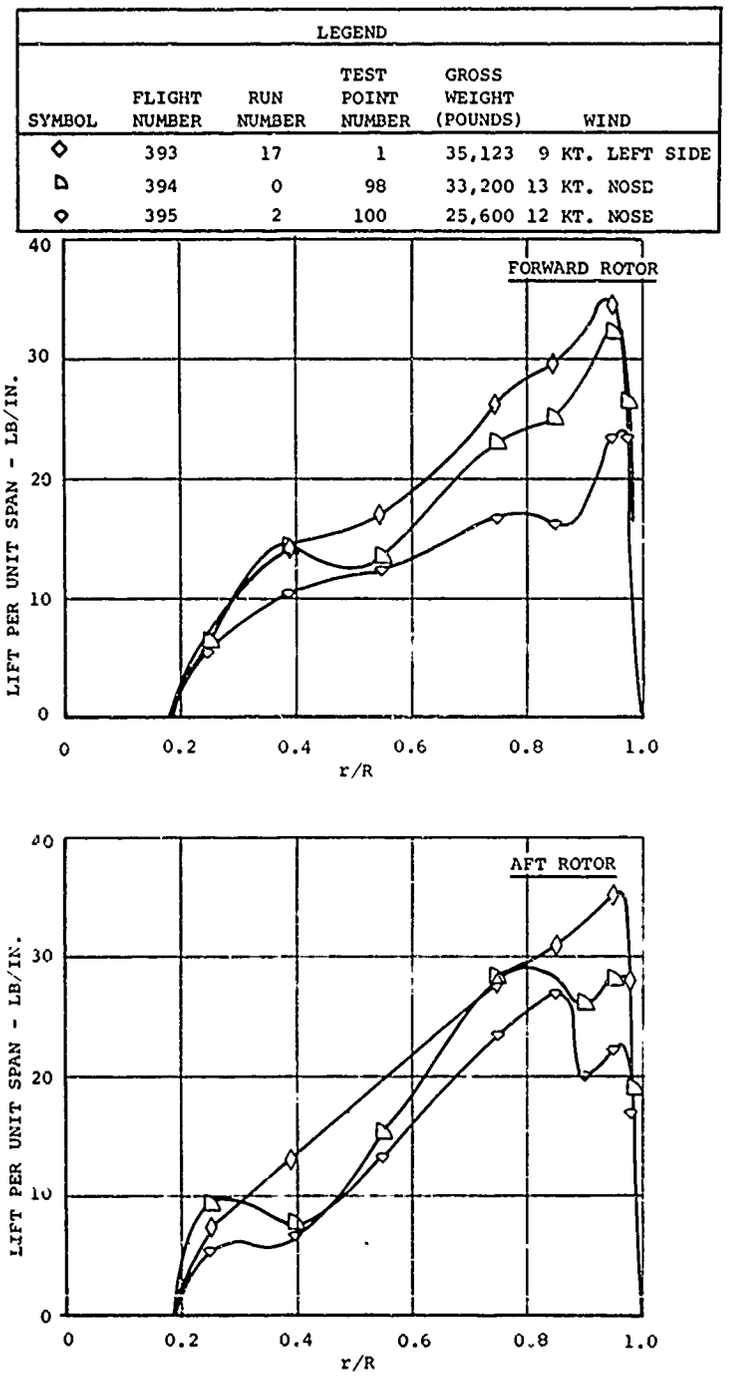

Figure 48. Azimuthal Average Lift per Unit Span in Hover at Three Gross Weights.

on the nose, the effects of rotor-rotor interference are evident.

Azimuthal variations of lift per unit span for the three most outboard blade stations measured are shown in Figures 49 and 50. These data are for a test weight of 33,300 pounds and include four airspeeds. The lower airspeed data show an interesting lift spike at the 60- to 90-degree azimuth on both rotors. This spike is the predominant feature of the azimuthal variations at low speeds, especially at the more outboard blade stations. It is believed that this spike is due to intrarotor interference with the vortex from the preceding blade tip. Wake distortion is apparently more significant at low speed and keeps this vortex near the rotor on the advancing side.

At 110 and 124 knots airspeed, the forward rotor airloads variations are predominantly 1/rev. with a small 12/rev. ripple. It is interesting to note that at 124 knots the aft rotor has a significant region of negative lift on the advancing blade tip and a large 6/rev. oscillation. This oscillation in the airloads may be due to the blade torsional (twisting) motions at its first mode natural frequency, since the amplitude of the oscillation increases with radius. These data indicate that a nonlinear blade twist should be considered for the aft rotor to avoid the negative lift region on the advancing blade tip.

Lift-per-unit-span data obtained at 26,000 pounds gross weight and 108 knots are shown as contour plots in Figures 51 and 52. These data differ significantly from the 33,300-pound data in that the forward rotor has the larger variations in loading. Forward rotor blade twist appears to be too large for this condition, with several negative lift regions shown, particularly on the advancing side. Aft rotor blade twist appears to be too small for this condition, with a rather large blade tip loading occurring at 90 degrees azimuth. This apparent sensitivity of the optimum twist to the gross weight was unexpected and should be thoroughly evaluated. The data presented in this report are believed to be typical, but an extensive study of these data for twist optimization should be conducted.

There appears to be a connection between the extensive 6/rev. on the aft rotor at 33,300 pounds and 124 knots and the forward rotor lift variations shown in Figure 51 for 26,000 pounds and 108 knots which also are about 6/rev. These lift oscillations appear to be related by the negative lift region on the advancing blade, which apparently excites the blade torsional

(twisting) motions. This response produces control load variations and helicopter vibrations which, of course, should be avoided. Blade design improvement and cyclic trim schedule optimization can apparently reduce this response.

The contour plots (Figures 51 and 52) also show the regions of the rotor disk which contribute the differences in the average loading on the rotors shown in Figure 47. Figure 52 shows that, for the aft rotor, the area inboard of the 60-percent radius produces lift-per-unit-span values which are always less than 20 pounds per inch, and a rather sizable region of negative lift is shown. The forward rotor data in Figure 51 show 5 regions of 20 pounds per inch inboard of the 60-percent radius, and only a few small regions of download. This pattern of loading generally substantiates the average loading data given in Figure 47.

The lift-per-unit-span data are also of considerable interest when prepared as harmonic amplitudes. Since blade bending response amplifies those airload harmonics which are near a bending natural frequency and the rotor hub only allows passage of blade integer harmonics of vertical loads (if the blades are identical), the third harmonic loading is of primary significance in producing vibration of the test helicopter. Blade bending is produced by all harmonics of the airloads but, of course, the effect is amplified or attenuated depending on the frequency and phase relationships. The radial distribution of the airloading is also important in that a distribution which has the same shape as the modal response will produce a larger bending with the same airloading amplitudes. Since rotor blades are generally pin-free beams, the blade tip is an antinode for all modes of response; therefore, the loading at the blade outboard end tends to have a large influence on blade bending. As will be shown in the following series of illustrations, the harmonic airloads also tend to be concentrated outboard on the blade. Thus, improved blade tip design, such as a sharp planform taper near the tip, should be expected to reduce blade bending loads and vibration significantly.

The effect of sideslip in transition on third harmonic airloads is shown in Figure 53. As noted previously, there is essentially no effect of sideslip on the forward rotor airloads, but the aft rotor loads vary markedly. The largest aft rotor third harmonic airloads were measured at -19.0 degrees sideslip, with large amplitudes measured both inboard and at the tip. Since blade bending is the predominant problem caused by

transition sideslip - not vibration - the other harmonics of the airloading should also be studied.

The effects of cyclic trim on third harmonic airloads measured at 100 knots and 33,000 pounds test weight are shown in Figure 54. The variations with trim are shown to be small except at the tip of the aft blade. When the trim was fully retracted (0/0), very large third harmonic airloads were measured on the aft tip. This large change is believed to be due to a tip vortex intersection. Plots such as those shown in Figure 42 should be made for the pressure measurements at 98-percent radius to determine if a vortex spike does occur for this condition. This investigation was considered beyond the scope of the present report.

The effect of a change in thrust coefficient on the rotor airloads at a moderate advance ratio of about 0.15 is shown in Figure 55. This advance ratio is equivalent to about twice that of transition and one-half of the advance ratio for high-speed conditions, so that rotor-rotor interference effects would be expected to be moderate. These data indicate that the forward rotor harmonic loading is systematically reduced with increased thrust coefficient. Aft rotor harmonic loading is shown to decrease significantly when the thrust coefficient was increased from a C_{TW}/σ of 0.070 to 0.078, but no further decrease was produced when the thrust coefficient was increased further. This effect is believed to be due to the closer position of the forward rotor wake to the aft rotor when the thrust coefficient is 0.70. When the thrust coefficient is increased, the forward rotor wake interference is reduced, but other disturbances limit the reduction in third harmonic loading.

The effects of advance ratio on third harmonic airloads at a C_{TW}/σ of about 0.070 are shown in Figures 56 and 57. Generally, for the inboard stations, third harmonic airloads are shown to decrease with advance ratio, turning up somewhat as the highest speeds are reached. Airloads at outboard stations of the forward rotor vary significantly with advance ratio, generally turning up sharply above an advance ratio of 0.27. The aft rotor data in Figure 57 show similar trends but are larger to start with a low μ' for the outboard stations, so that the increase at high μ' is relatively small.

The effect of advance ratio on the sixth harmonic airloads at C_{TW}/σ near 0.070 is shown in Figure 58. The sixth harmonic is also passed by the rotor hub as a vertical vibratory force and

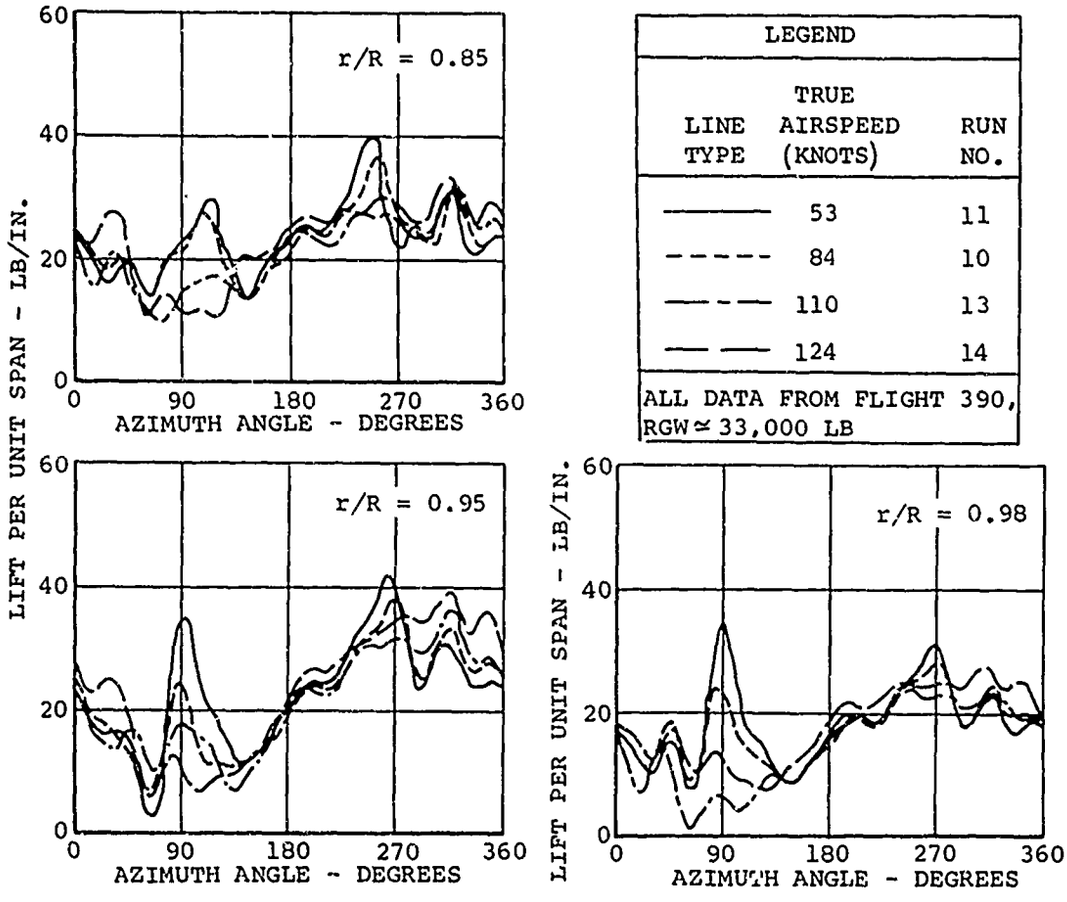

Figure 49. Typical Azimuthal Variation of Lift per Unit Span for Three Outboard Stations of Forward Rotor Blade.

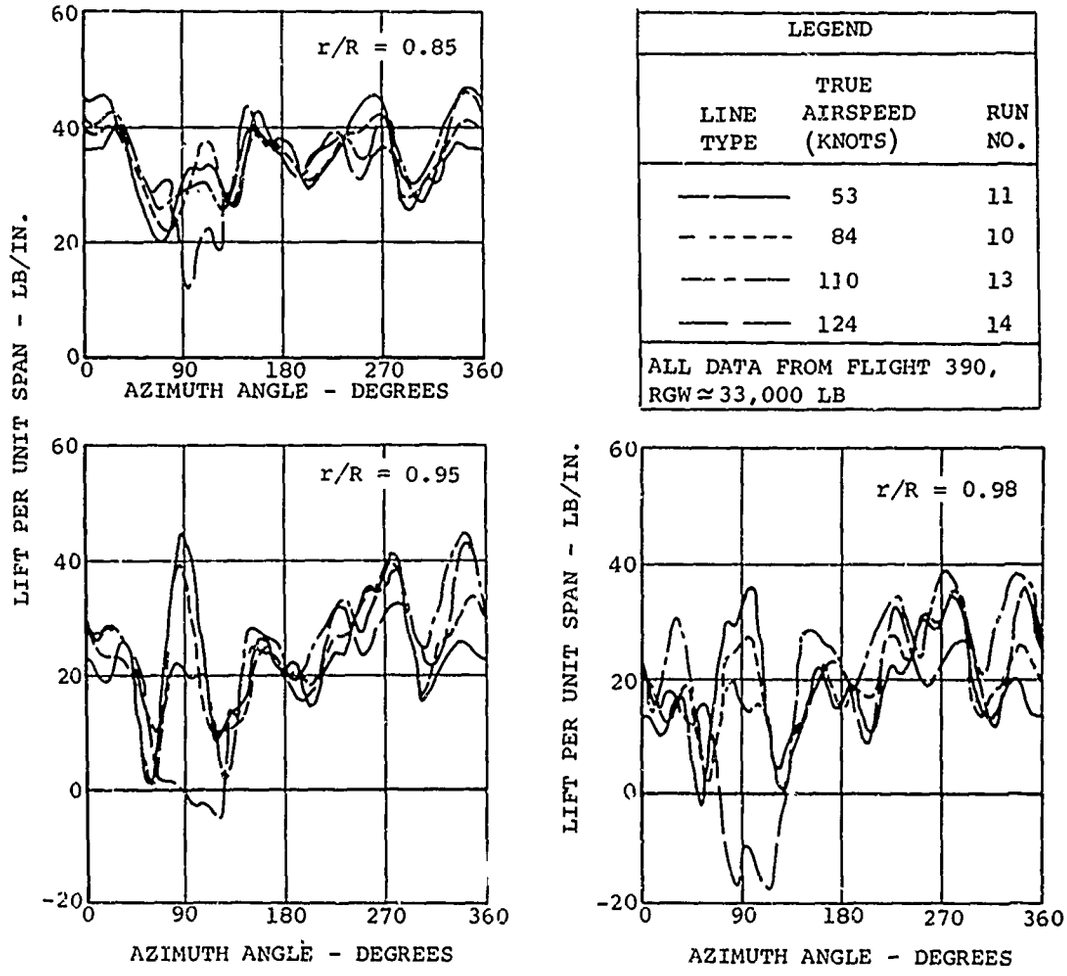

Figure 50. Typical Azimuthal Variation of Lift per Unit Span for Three Outboard Stations of Aft Rotor Blade.

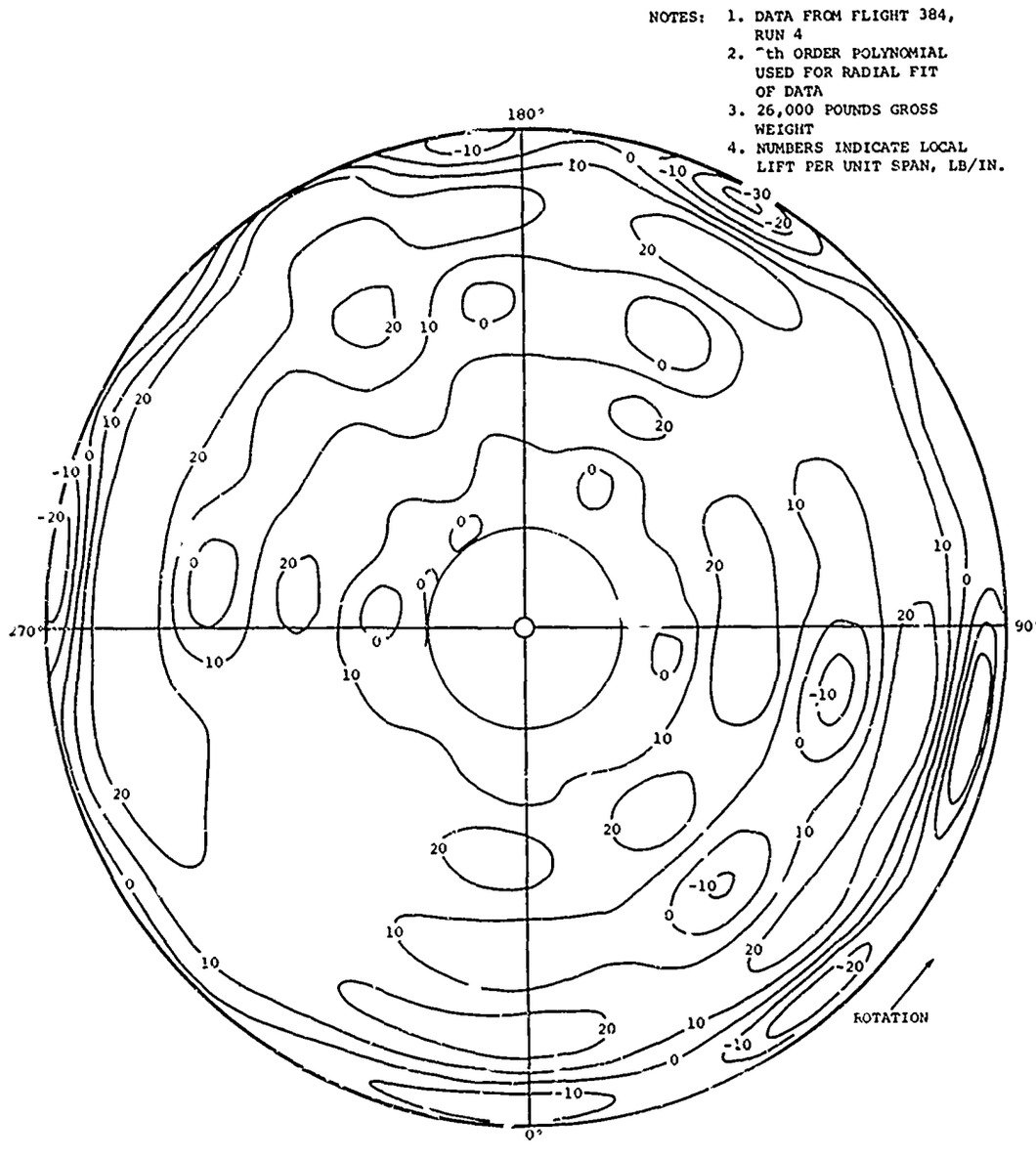

Figure 51. Contour Plot of Lift per Unit Span for Forward Rotor at 108 Knots.

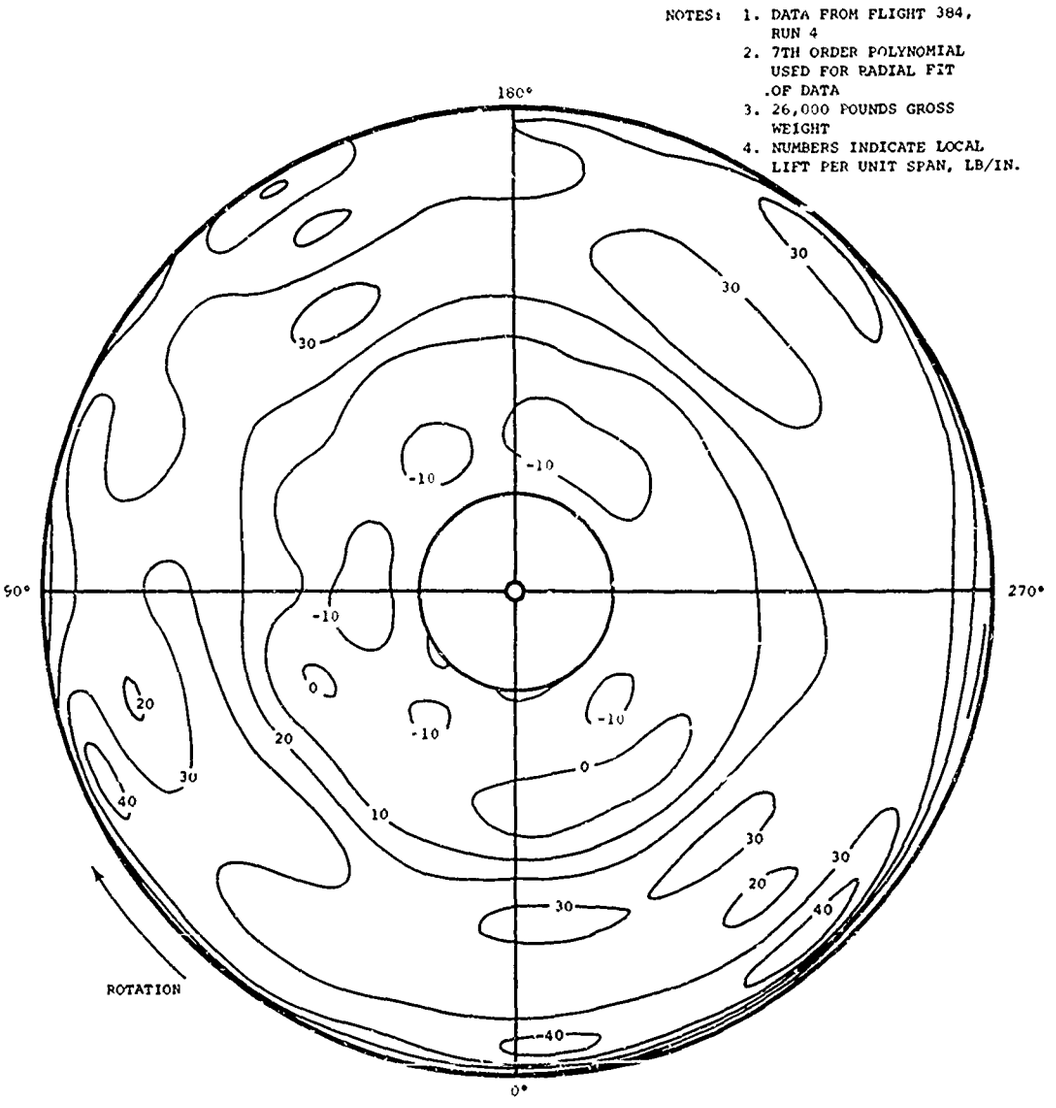

Figure 52. Contour Plot of Lift per Unit Span for Aft Rotor at 108 Knots.

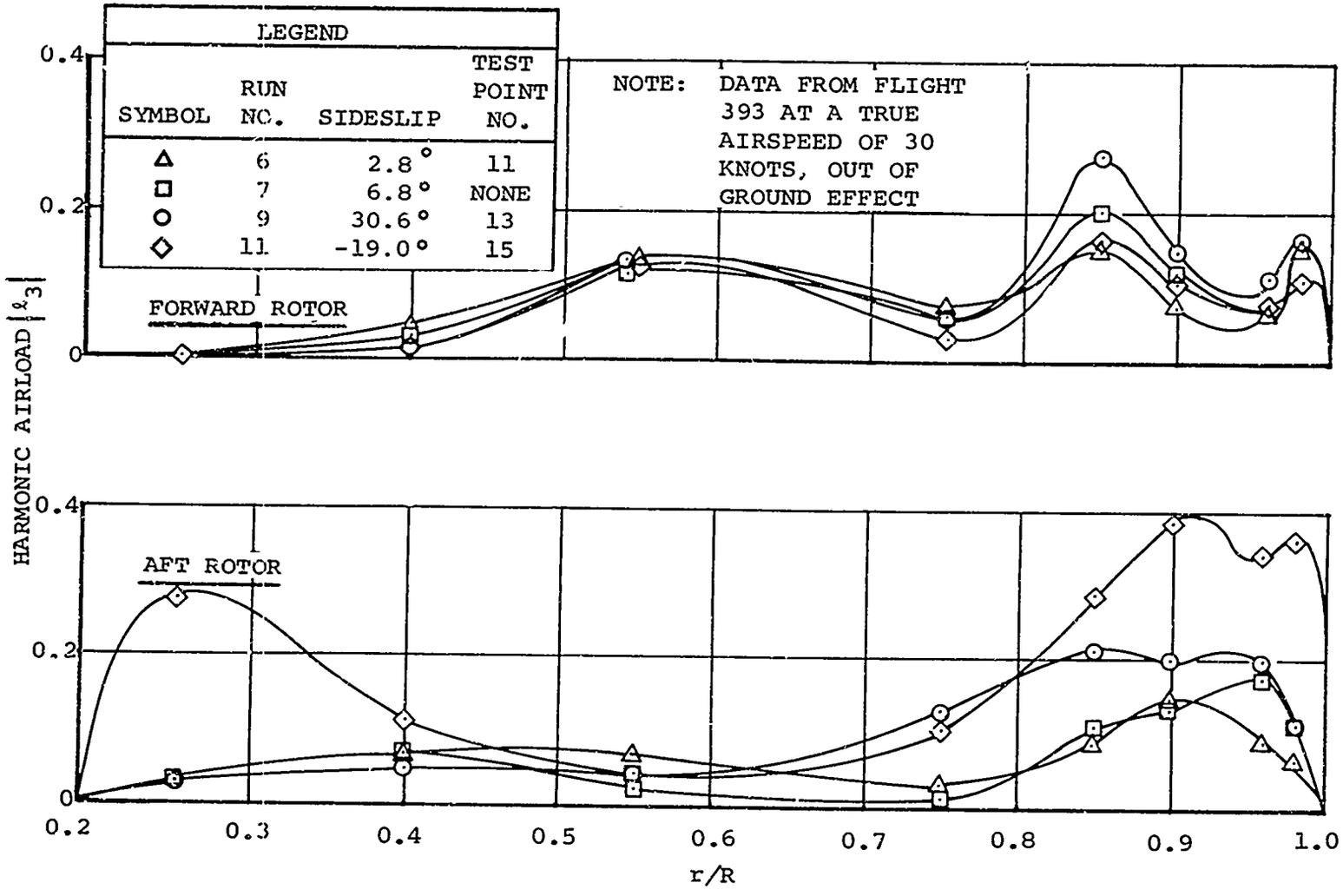

Figure 43. Effects of Sideslip in Transition on Third Harmonic Airloads.

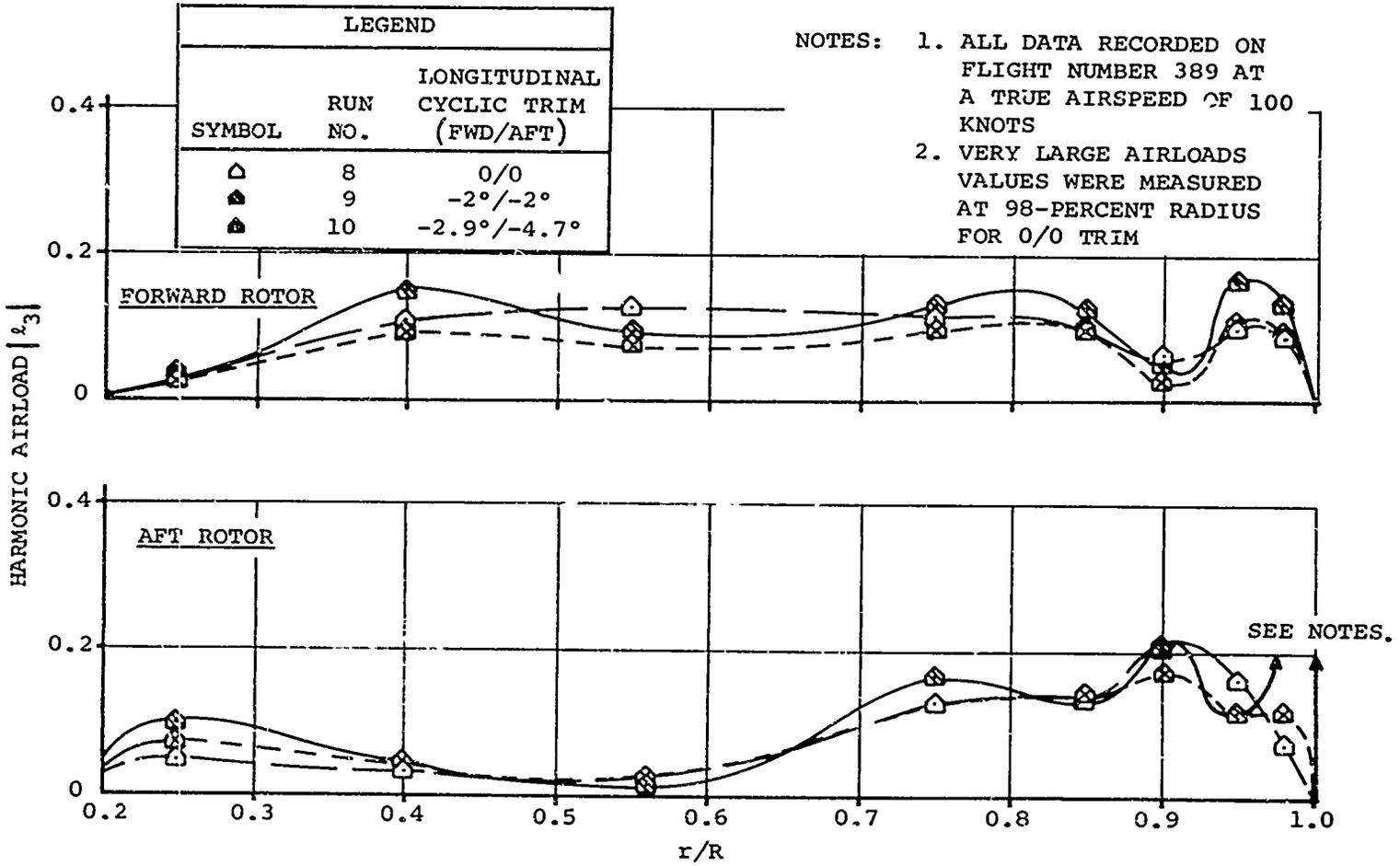

Figure 54. Effects of Cyclic Trim on Third Harmonic Airloads Measured at 100 Knots.

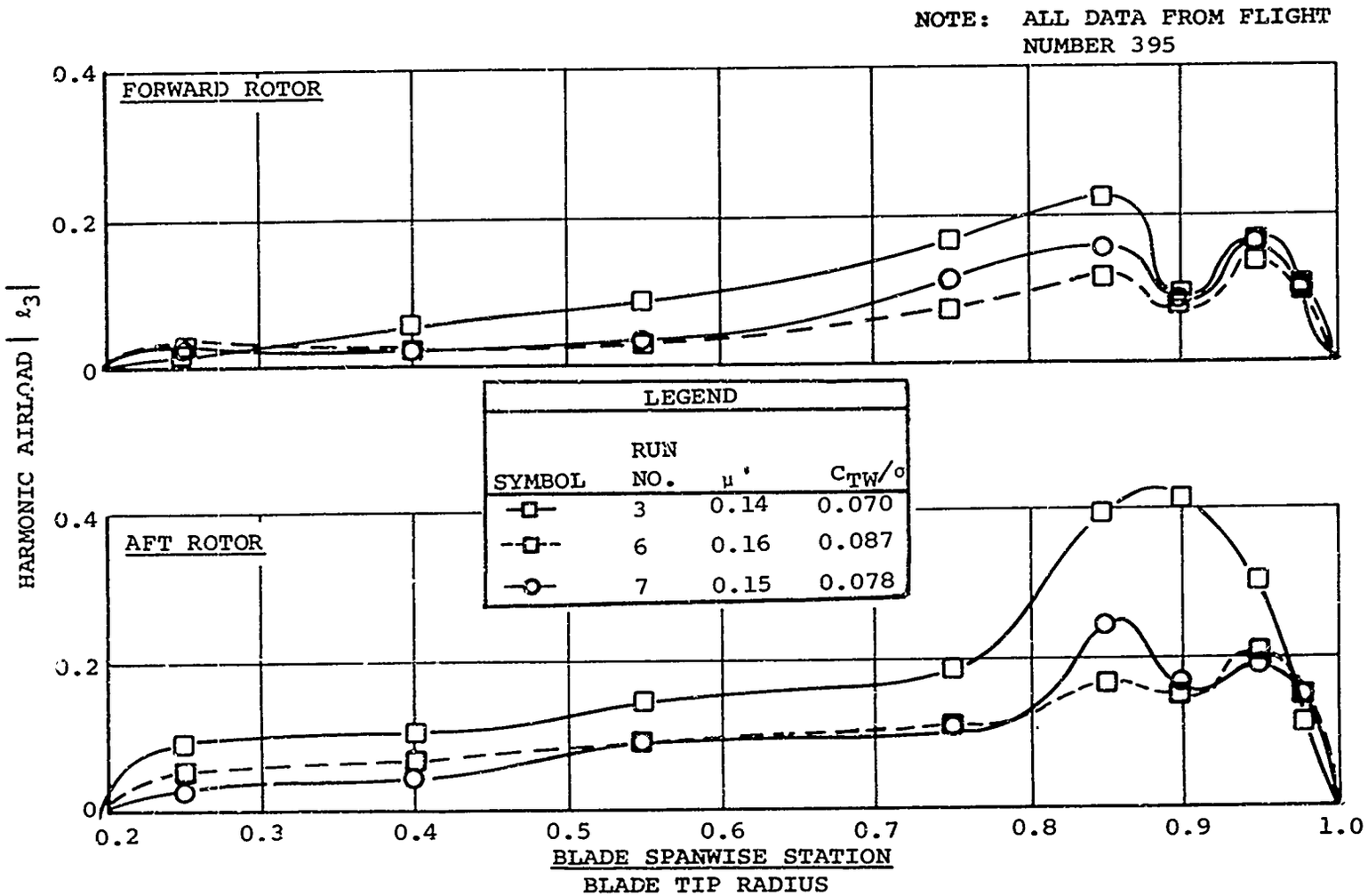

Figure 55. Effects of Thrust Coefficient on Third Harmonic Airloads at an Advance Ratio Near 0.15.

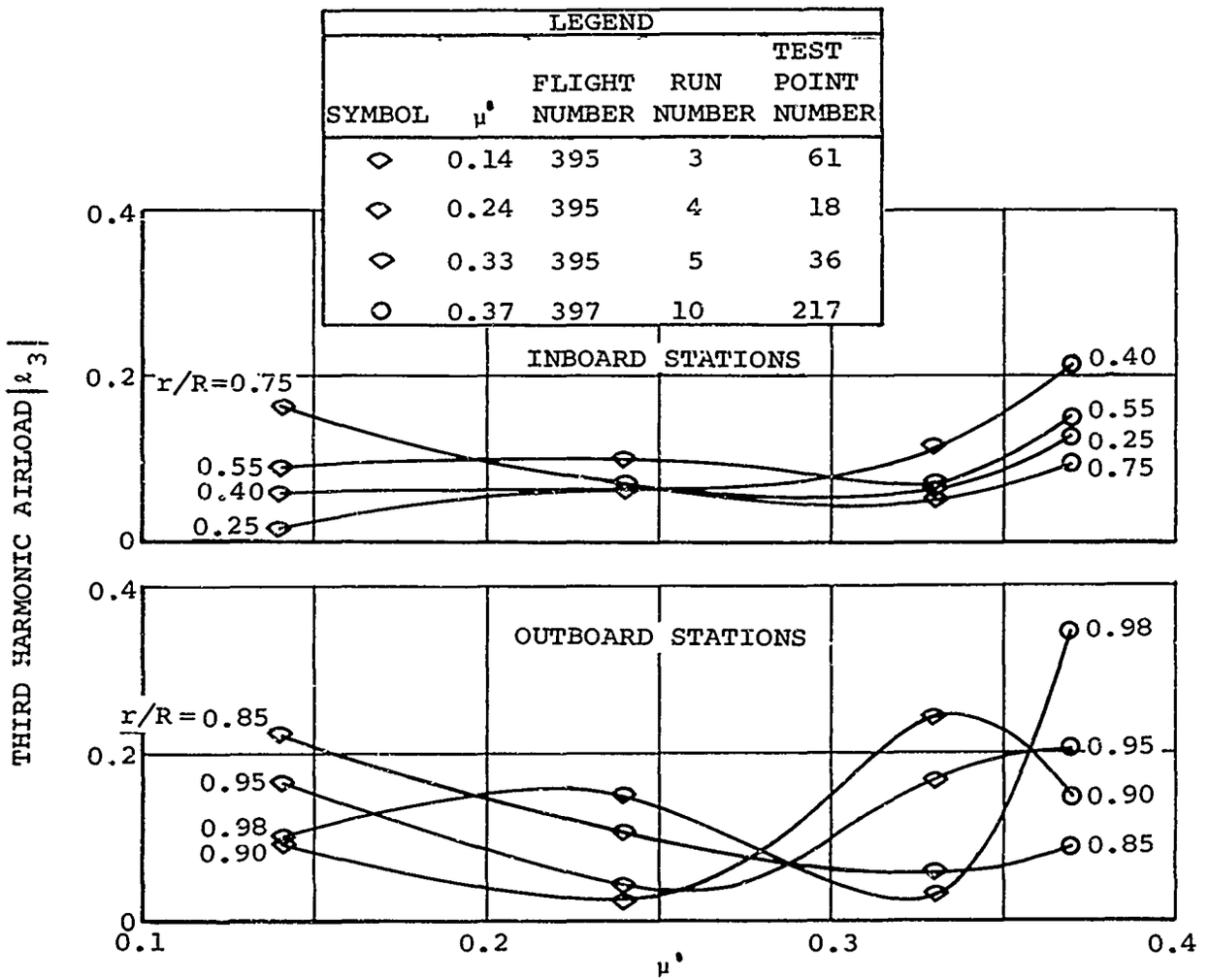

Figure 56. Effects of Advance Ratio on Third Harmonic Airloads of Forward Rotor (C_{TW}/σ = 0.070).

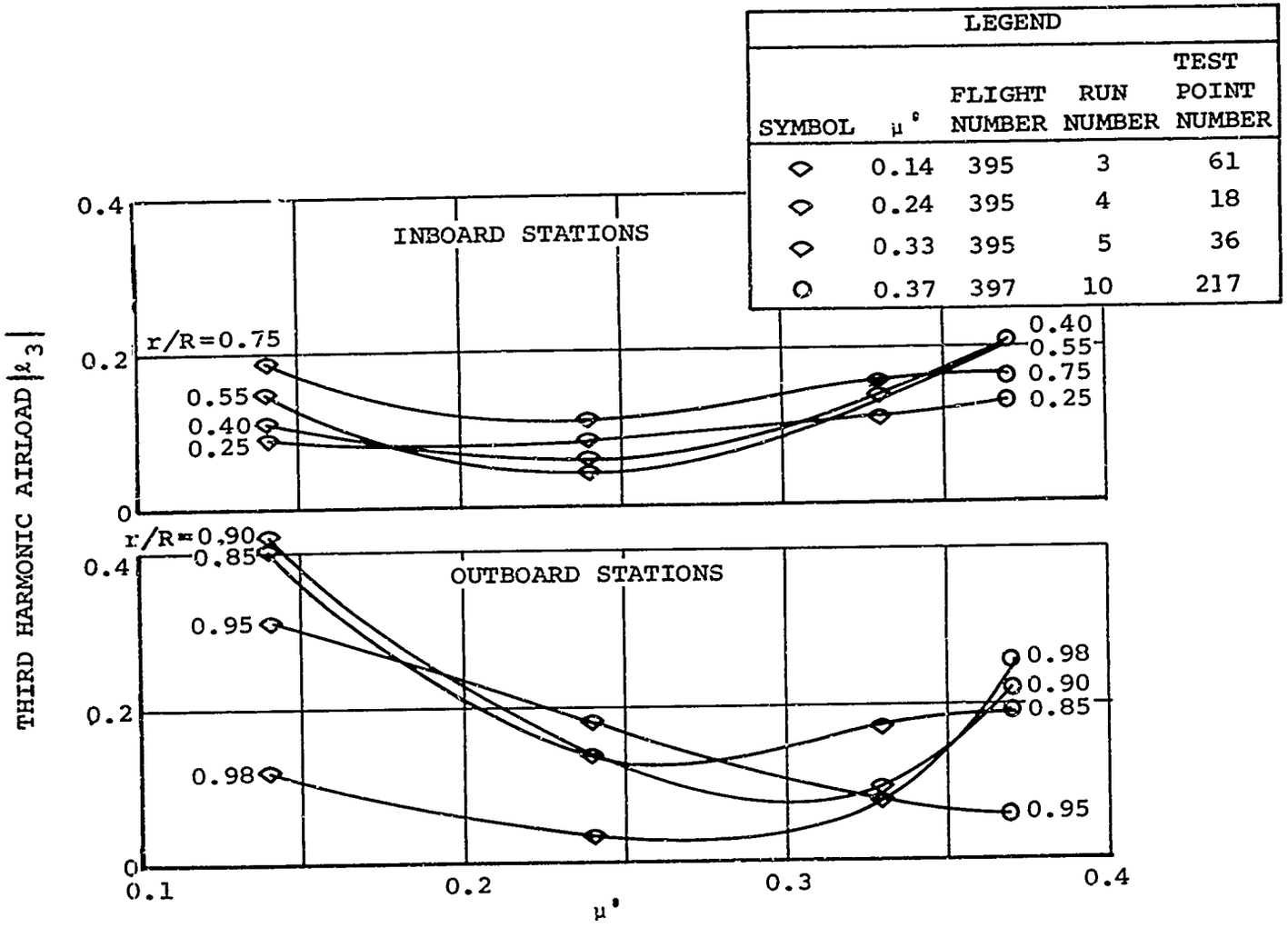

Figure 57. Effects of Advance Ratio on Third Harmonic Airloads of Aft Rotor (C_{TW}/σ = 0.070).

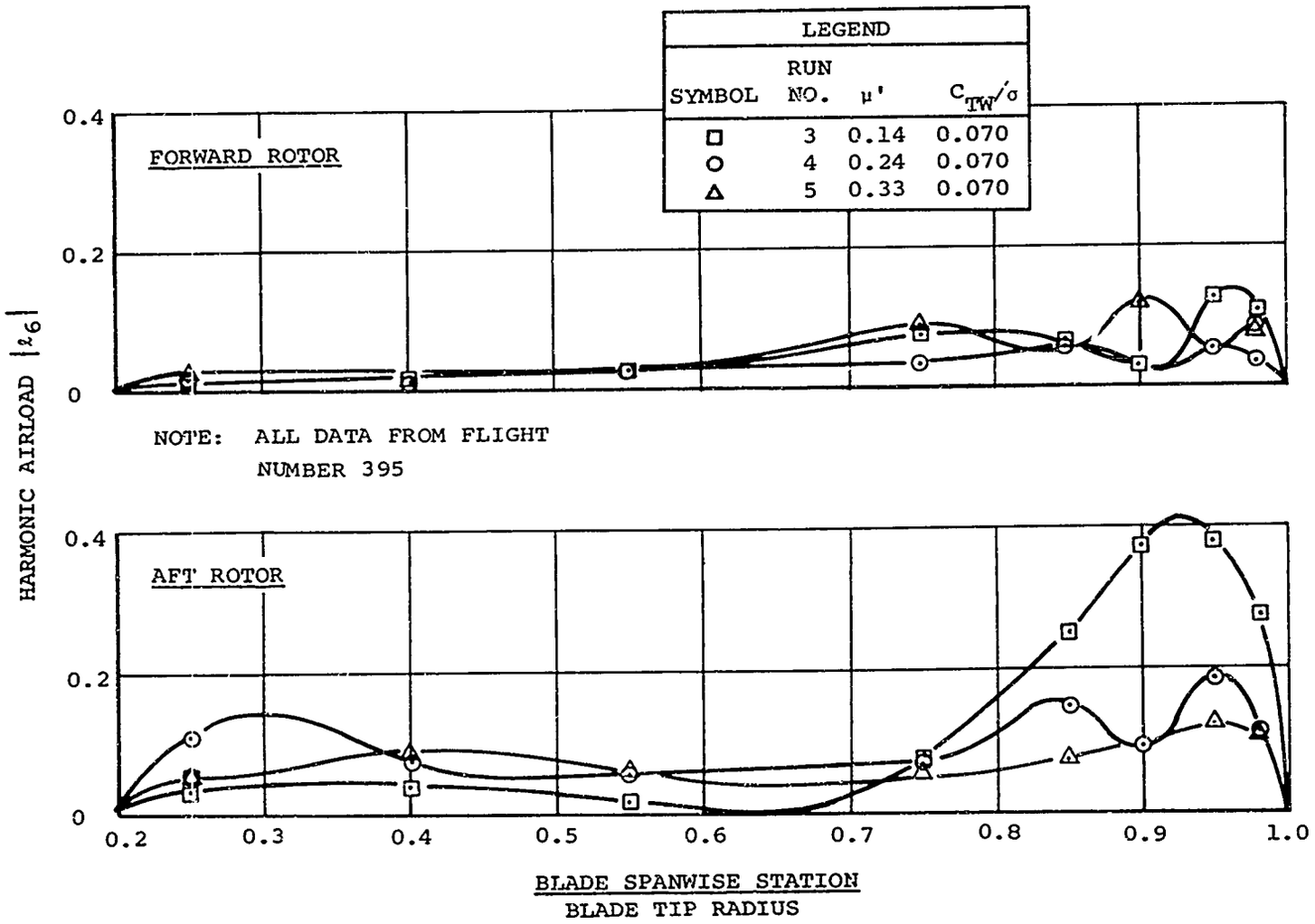

Figure 58. Effects of Advance Ratio on Sixth Harmonic Airloads.

is amplified by the second mode flap bending response of the blade; therefore, it is also significant in producing helicopter vibration. The data of Figure 58 show that, at low advance ratio ($\mu' = 0.14$), surprisingly large sixth harmonic loadings occur. At the tip of the aft rotor, the sixth harmonic loading is as large as the previously given third harmonic loadings. Forward rotor sixth harmonic loading is shown to be small, first decreasing and then increasing with increases in advance ratio. Aft rotor data values decrease significantly as the advance ratio increases.

To offset the tendency to overemphasize the blade integer harmonics, an example of the first ten harmonics of airloads is shown in Figures 59 through 63. This particular example is for a C_{TW}/σ of 0.085, μ' of 0.25, and trim settings which cause vortex interference at the tips of the blades of both rotors. Interference is apparently intrarotor, since it occurs on both rotors in a similar manner. Note that data for the 5 separate rotor cycles measured are presented in these figures rather than the 5-cycle averages given previously; however, there is essentially no variation between cycles, except at the blade tips which experience very large loadings at all harmonics. This situation is apparently due to the impulsive-type loading from tip vortex interference which is not well represented by harmonics. Also, the tip vortex pattern is not stable and therefore does not influence each rotor cycle in the same manner. While the cycle averaged data given previously for the third and sixth harmonics are believed to be representative, this example of the separate cycles of all harmonics is presented to caution the users of these data in the variations which should be expected.

Pitching Moment per Unit Span

The rotor airload pressure measurements probably have the largest potential value when used to determine the aerodynamic pitching moment imposed on the blades. This moment can cause prohibitive control loads, apparently due to the reduced (or negative) pitch damping which occurs at stall. There also tends to be an aerodynamic moment spike on the advancing side of the disk due to compressibility effects. These data are reviewed in some detail in Volume V of this report, and therefore the presentation in this section is of an introductory nature. For this report, all aerodynamic moment data are referred to the blade pitch axis (19.5-percent chord), since this is the axis about which the control load is reacted. The Volume V

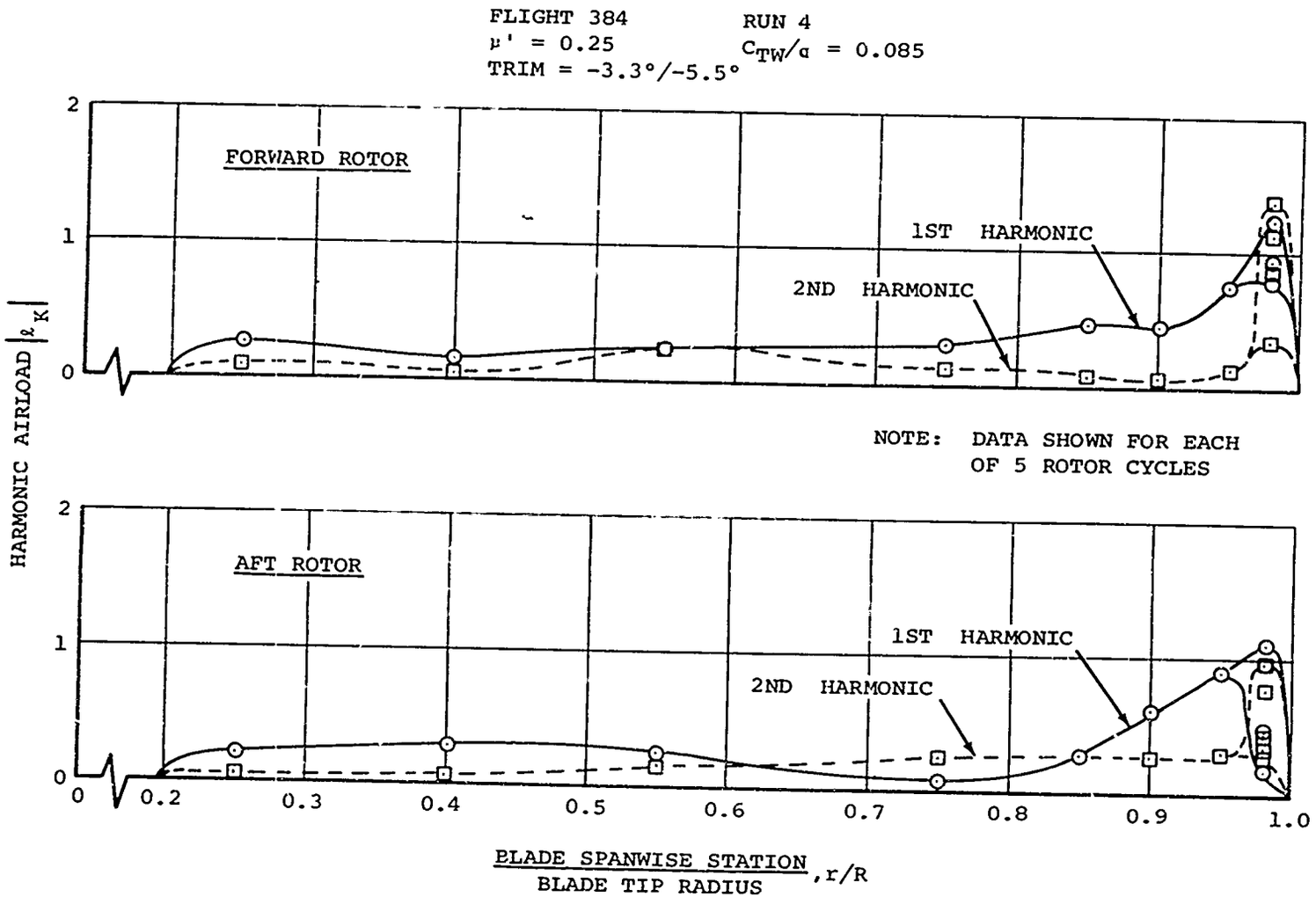

Figure 59. Typical First and Second Harmonic Airloads at an Advance Ratio of 0.25.

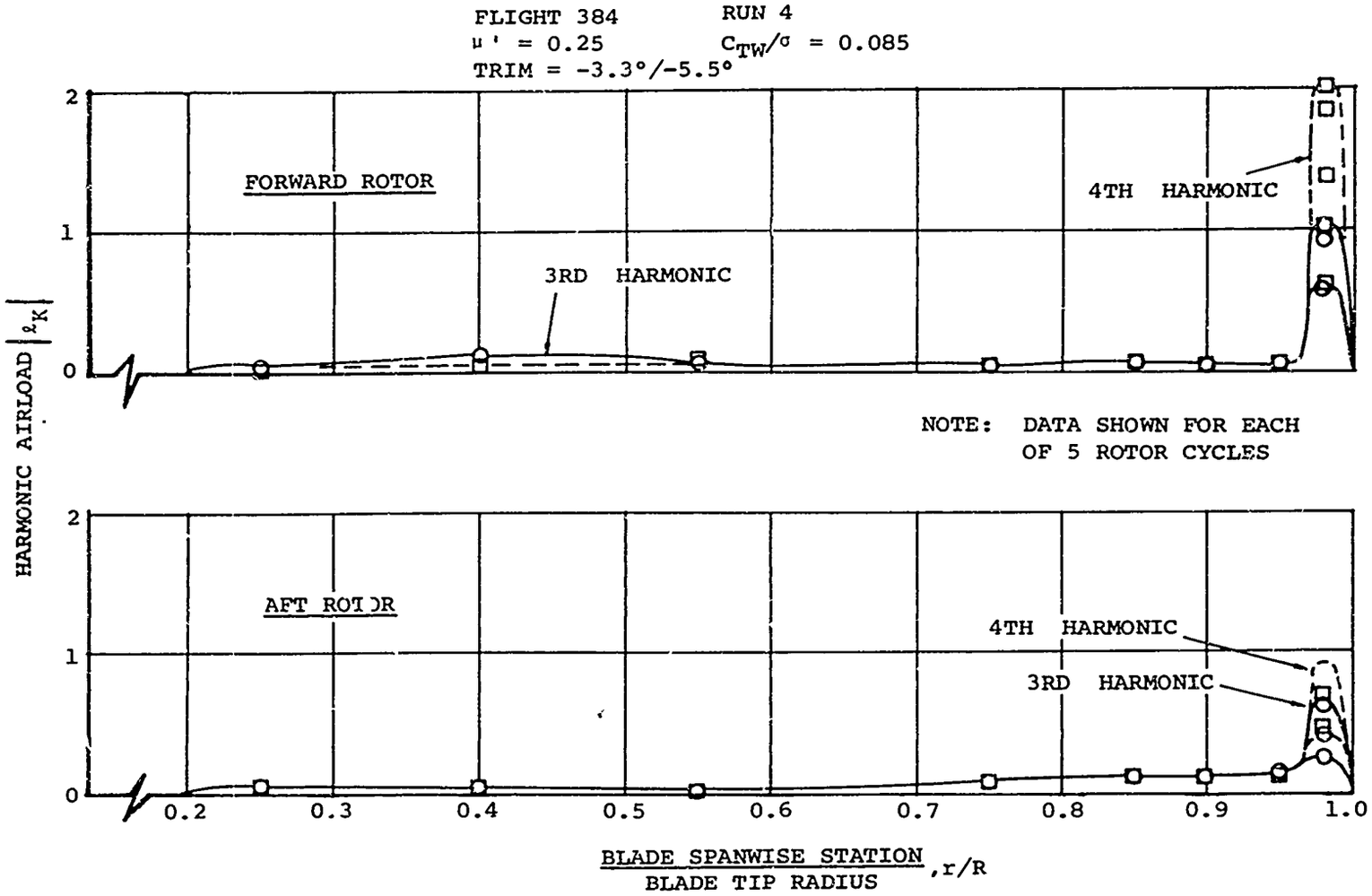

Figure 60. Typical Third and Fourth Harmonic Airloads at an Advance Ratio of 0.25.

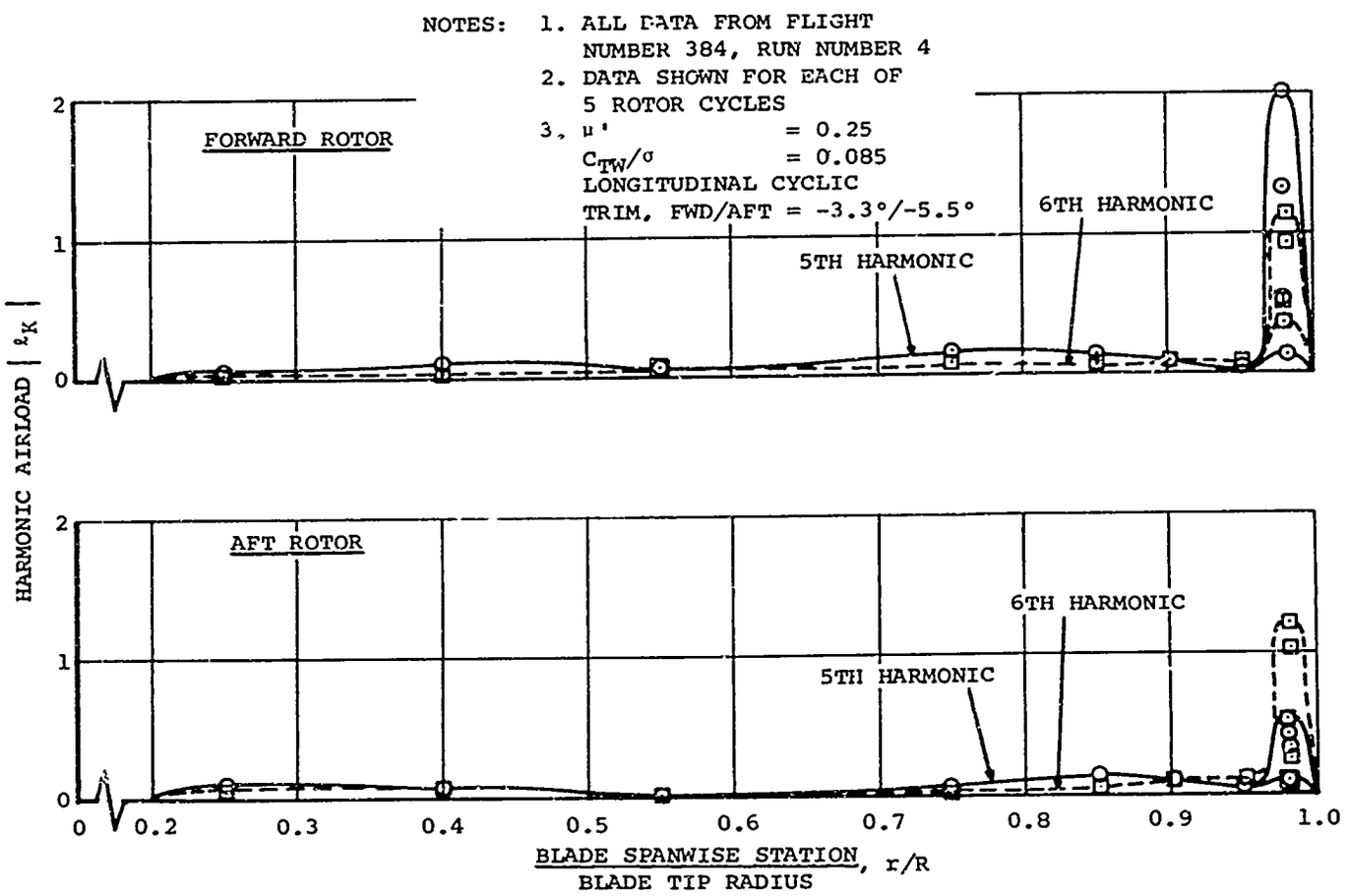

Figure 61. Typical Fifth and Sixth Harmonic Airloads at an Advance Ratio of 0.25.

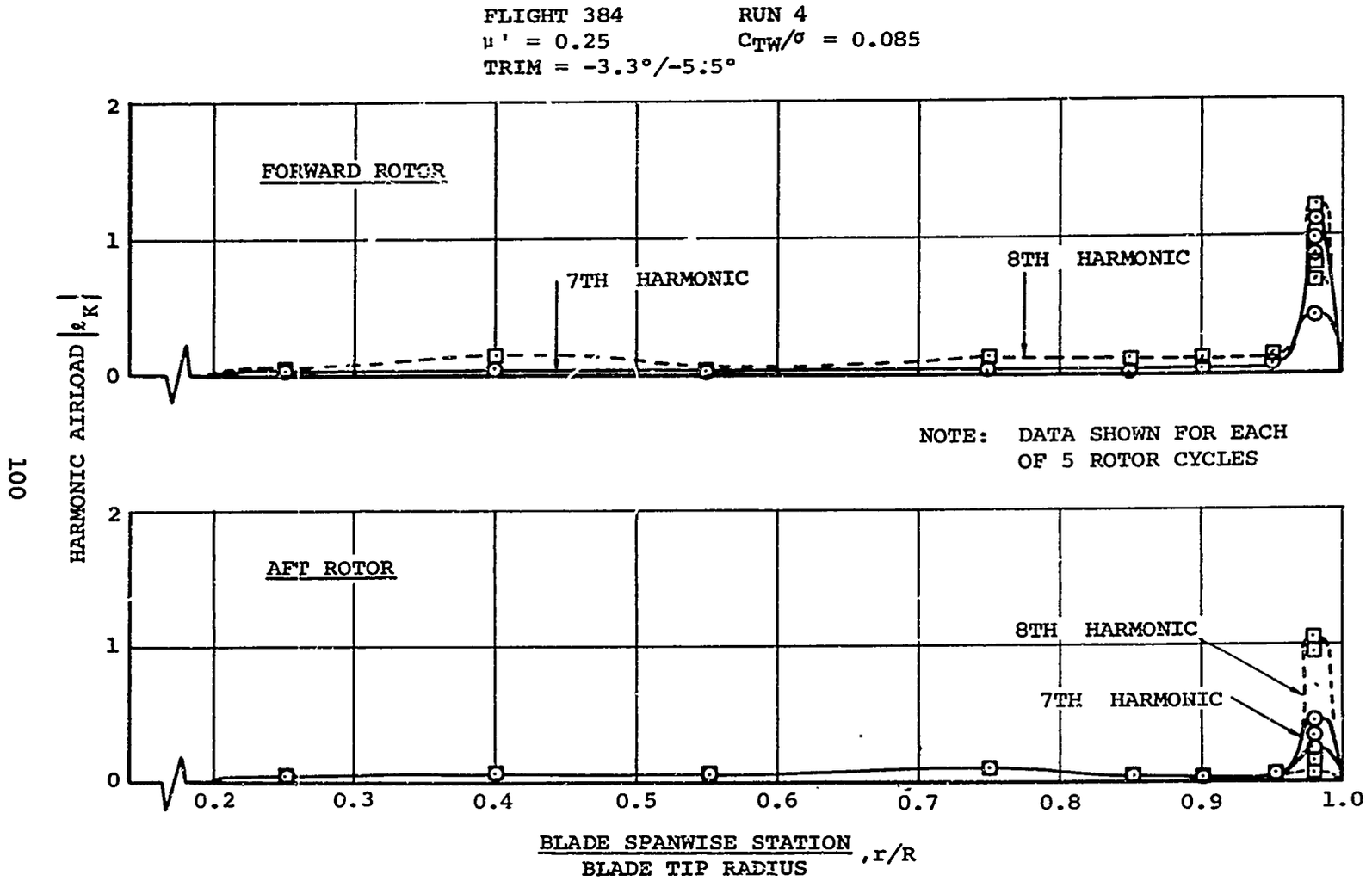

Figure 62. Typical Seventh and Eighth Harmonic Airloads at an Advance Ratio of 0.25.

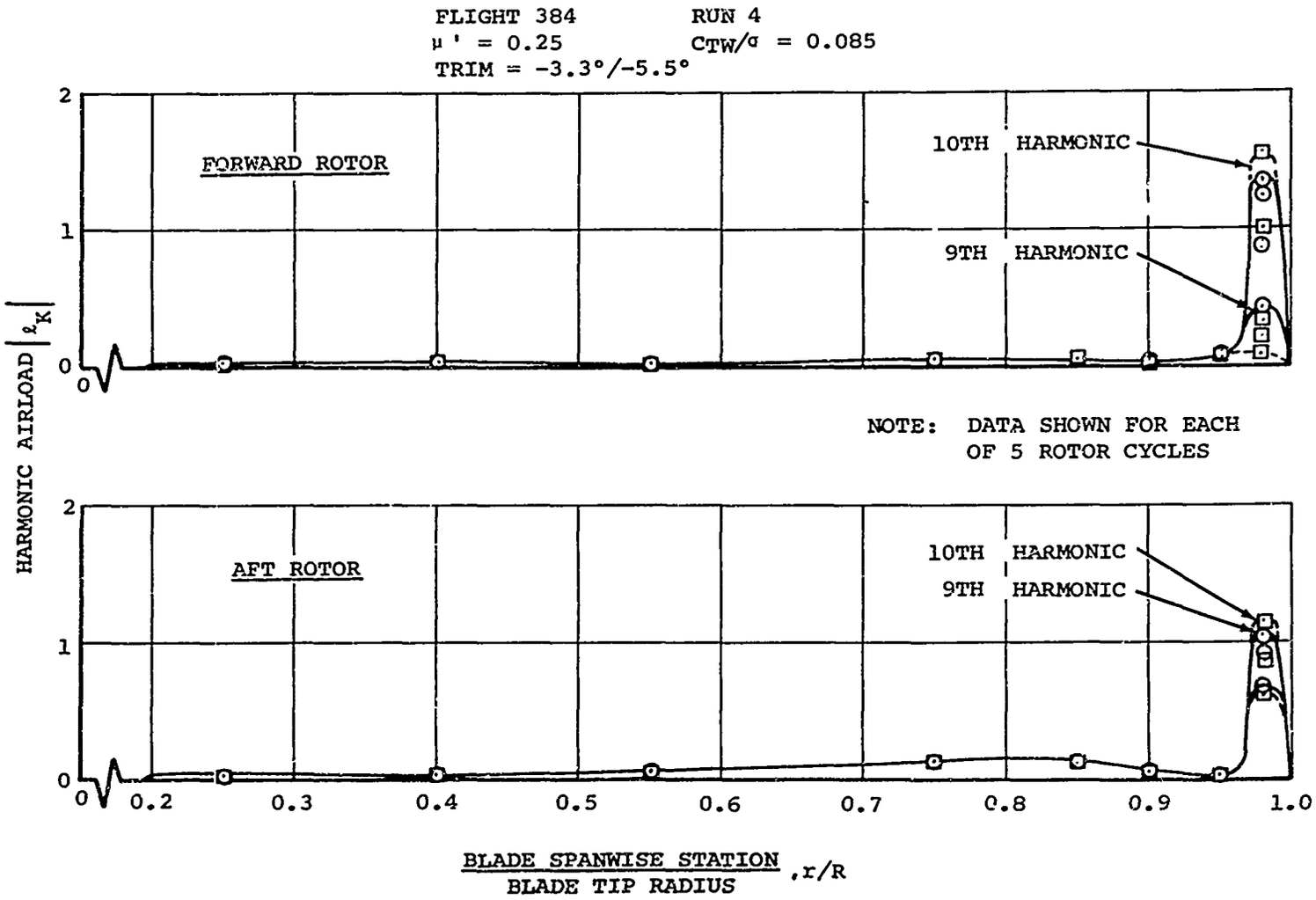

Figure 63. Typical Ninth and Tenth Harmonic Airloads at an Advance Ratio of 0.25.

presentations show the relation of data prepared using this moment reference to the more common quarter-chord reference.

Typical pitching moment data for the three most outboard stations of both rotors are shown in Figure 64. Data are shown for a test weight of 33,000 pounds at four typical airspeeds. Forward rotor data are shown to contain significantly less higher harmonic excitation than the aft rotor data. Except for 98-percent radius, these data all show a nose-up spike on the advancing blade to some degree. This was expected, since the advancing tip Mach number reached 0.91 at 124 knots with the 243 rpm tested. The large 12/rev. oscillation in the aft blade moment data may be due to blade twisting in the second torsional mode. Oscillations at 6/rev. which dominate the aft rotor data and which are significant in the forward rotor data are believed to be due to blade twisting in the first torsional mode. The first harmonic variation which dominates the forward rotor moment data is probably due to the first harmonic variation of the rotor blade lift which is acting at the quarter chord of the blade. Obviously, these data should be the subject of considerable review and analysis.

The significant effect of test weight on the forward rotor blade tip loading, which was mentioned previously in regard to lift per unit span, is most obvious in the pitching moment data, as shown in Figure 65. At the lighter gross weight, the blade tip produces negative lift on the advancing side so that compressibility causes a nose-down moment. This effect causes considerable blade twisting and is reflected in a rather large first and sixth harmonic oscillation. At a test weight of 32,650 pounds, the blade lift at the advancing tip is positive and the compressibility spike makes it more positive. This effect causes large 6/rev. and 12/rev. oscillations. The first harmonic oscillation for the higher test weight is of reversed sign due to the change in the first harmonic lift oscillation. These data indicate that forward rotor blade design optimization needs careful consideration, since the normal flying weight variations of the test helicopter cause significantly different operating conditions at the forward blade tips. This conclusion also applies to the aft rotor for significantally different gross weights and flight conditions.

The distribution of the oscillating pitching moment (steady moment suppressed) over the two rotor disks for the 26,000-pound-gross-weight test data is shown in the contour plots of Figures 66 and 67. These plots substantiate the previous data with the first

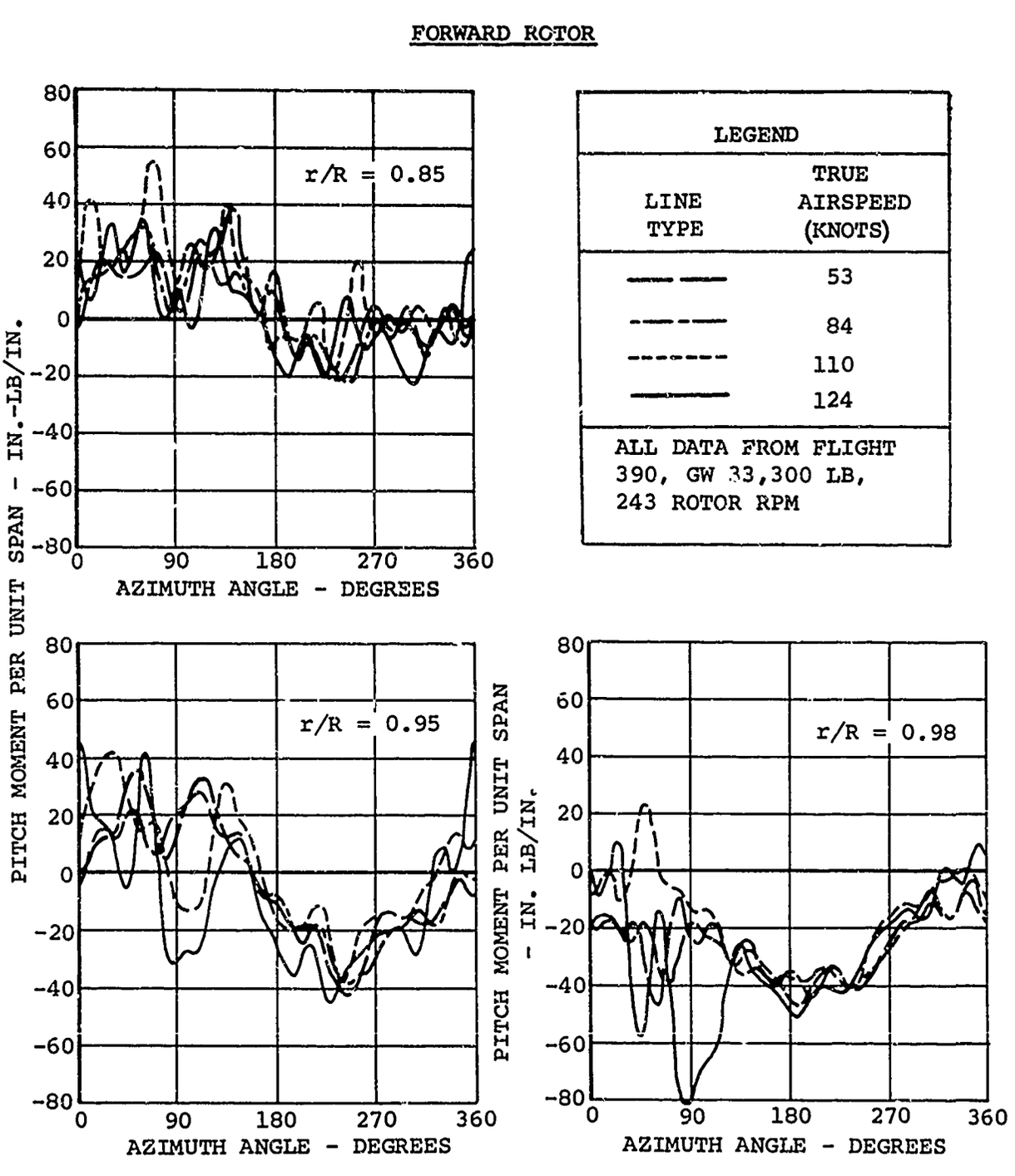

Figure 64. Azimuthal Variation of Pitch Axis Pitching Momen of Rotor Blades.

AFT ROTOR

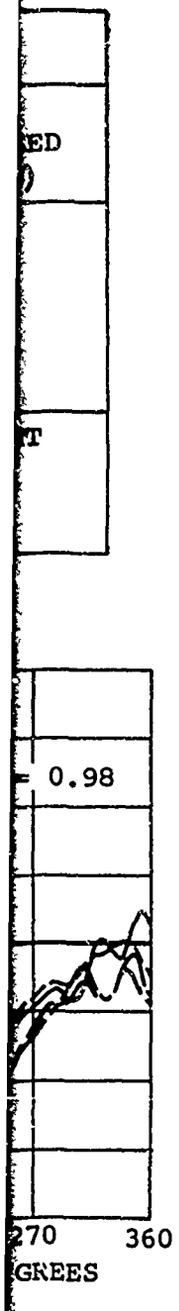

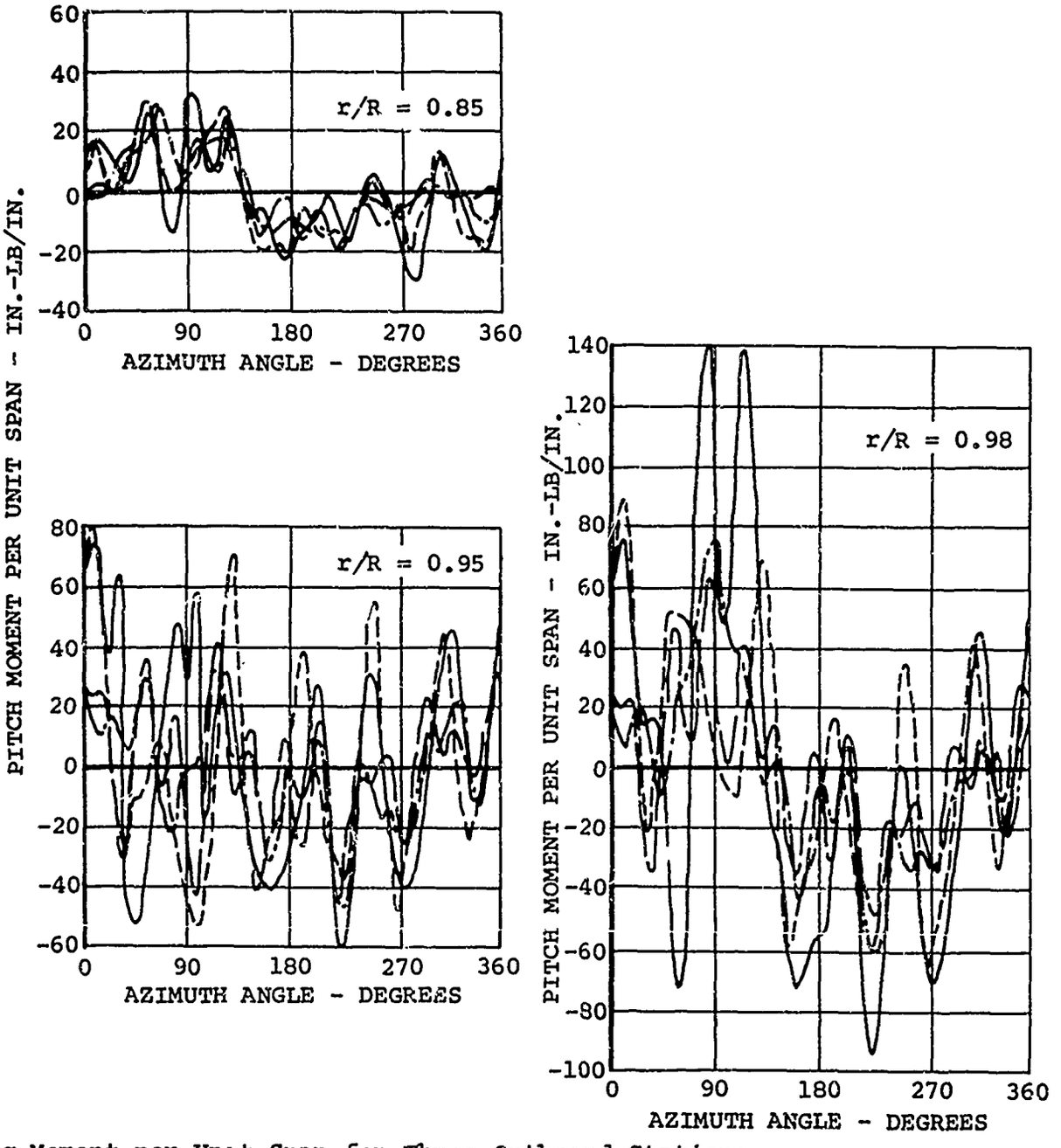

ch Axis Pitching Moment per Unit Span for Three Outboard Stations

B

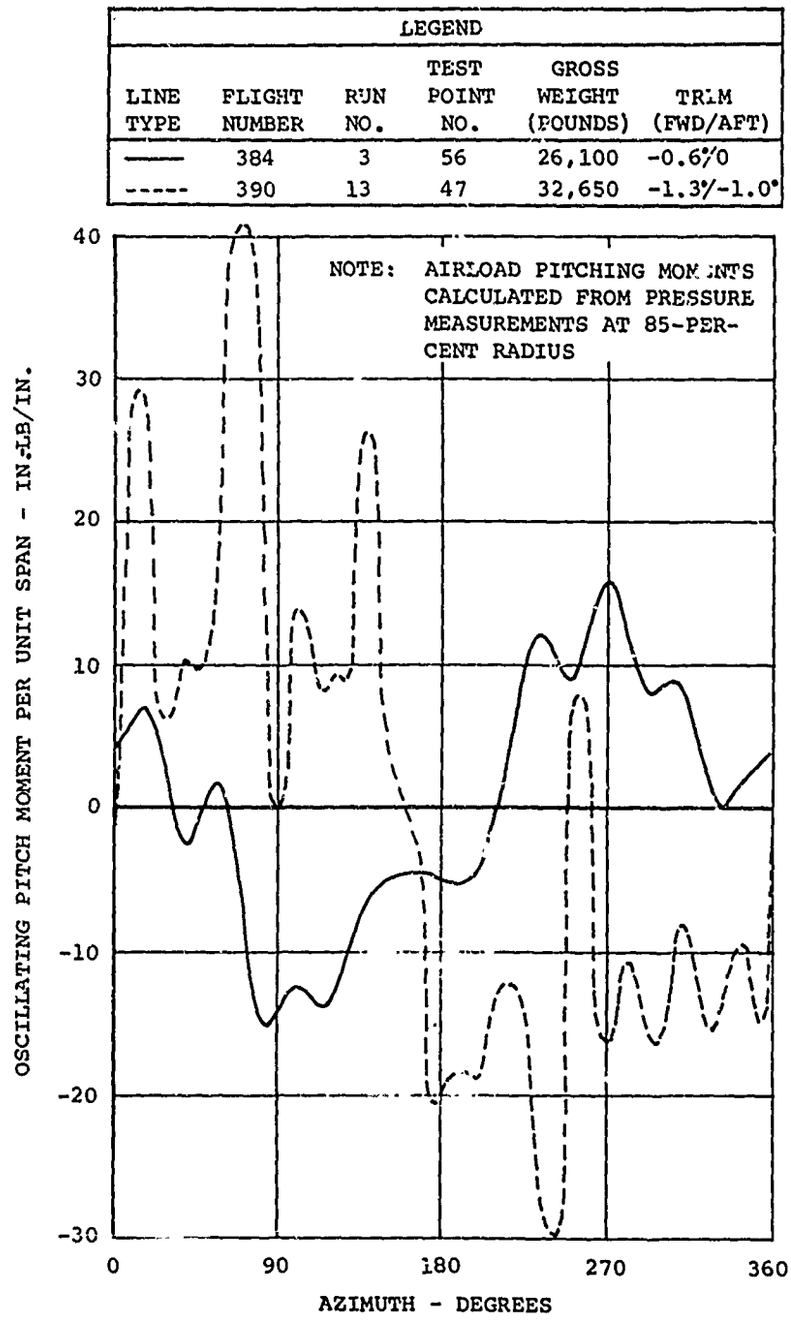

Figure 65. Effect of Gross Weight on Pitch Axis Pitching Moment per Unit Span of Forward Rotor Near 110 Knots Airspeed.

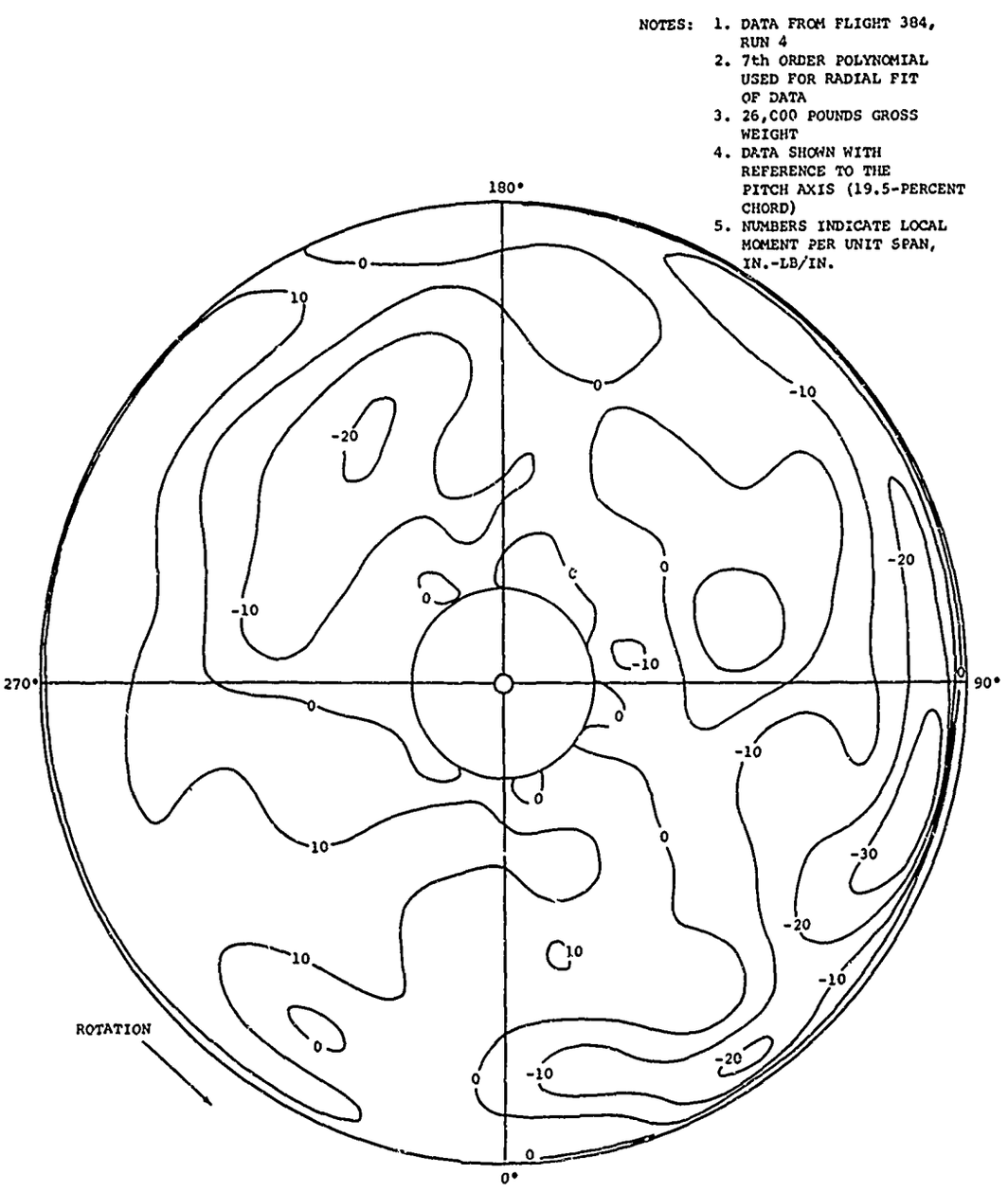

Figure 66. Contour Plot of Oscillating Pitch Axis Pitching Moment per Unit Span for Forward Rotor at 108 Knots.

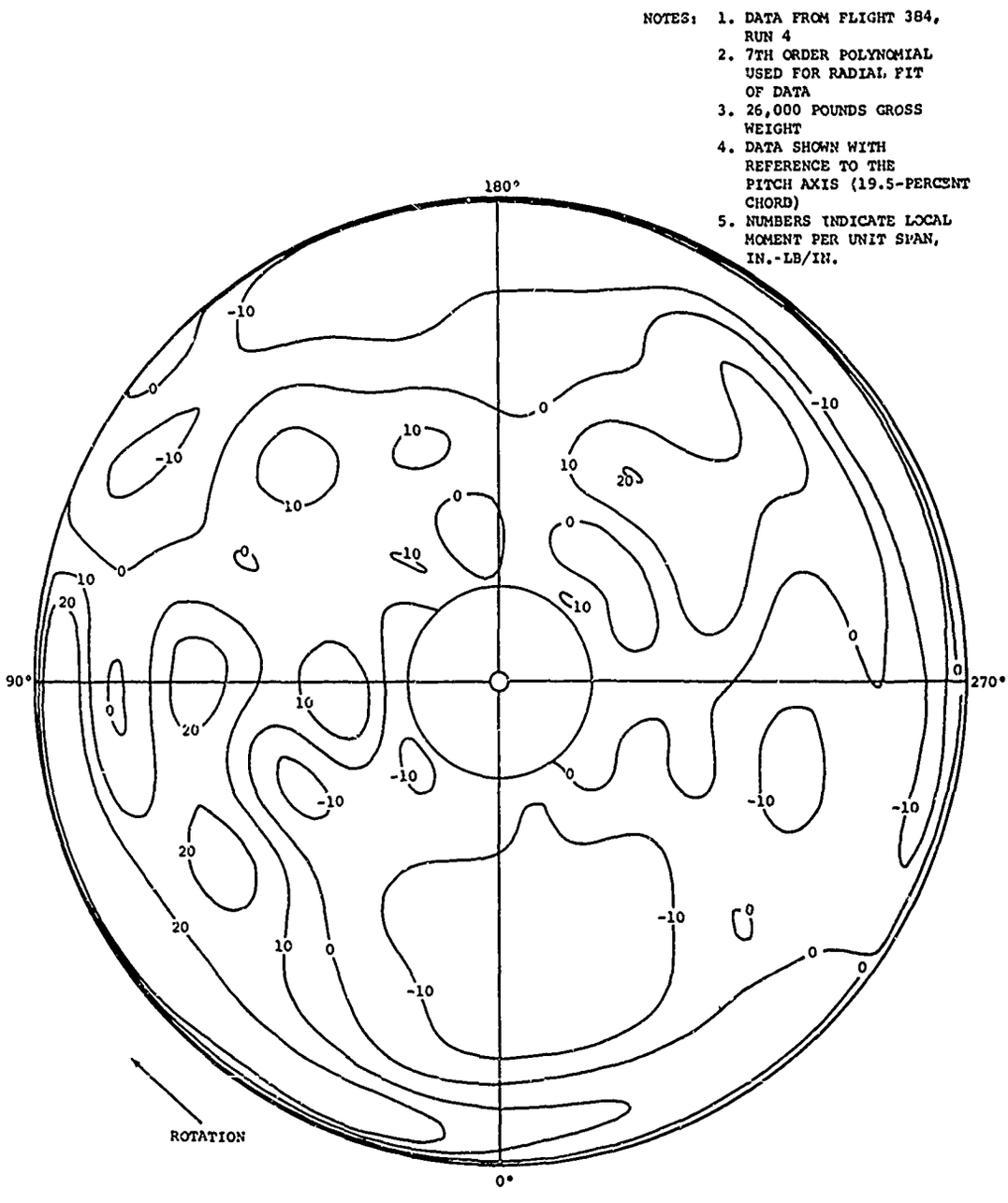

Figure 67. Contour Plot of Oscillating Pitch Axis Pitching Moment per Unit Span for Aft Rotor at 108 Knots.

quadrant blade tip loadings shown to be a significant nose-down moment on the forward rotor and a nose-up moment on the aft rotor. The aft rotor data show a rather sudden moment reduction at 110 to 120 degrees azimuth, apparently due to interference with the tip vortex from the forward rotor. After this disturbance, the oscillating moment at the tip does not become positive again until the third quadrant. It should be noted that this negative oscillating moment at the blade tip does not indicate that the total pitching moment is nose down, since the steady load at the tip is probably about 20 inch-pounds per inch.

It is hoped that this introduction to these pitching moment data helps to stimulate further analysis of these data. All the rotor airloads data available from this and other programs should be used to calculate pitching moment, and these data should be reduced to moment coefficient form. Analysis of these moment coefficients will probably show the source of the high dynamic loads which presently limit helicopter operations.

ROTOR BLADE BENDING

The rotor blades of the test helicopter experienced flapwise bending and torsional deflections which significantly influenced the airloads data. The blades also deflected in the chordwise direction to a lesser extent. Blade bending and twisting moment data obtained from the strain gage instrumentation are illustrated in this section to indicate the magnitude of these deflections. It is again noted that the blade bending moment data presented have not been corrected for load interactions. The effect of flap bending interactions on the chordwise bending data is believed to be significant. Other interactions are 15 percent, or less, of the actual moment. Blade bending gage interaction details are discussed in Volume II of this report. These interactions are linear and predictable and should be accounted for in the data before detail correlation with theoretical predictions is attempted. These corrections are generally small enough to be neglected for first-order considerations such as those made in this report.

Blade bending data are usually considered as stress problems so these data were first analyzed to determine the alternating values of the bending moments. The data obtained in straight level flight are shown in Figure 68 as boundary curves of the

data for all flight conditions tested (about 100 test points); data points are shown for a typical test point at 32,600 pounds gross weight and 124 knots airspeed. It is emphasized that these data are for straight level flight, since, as will be shown, sideslip causes a significant increase in aft rotor blade bending. Blade stall at high speed also tends to slightly increase outboard blade bending, and these data are included in Figure 68. The coincidence of the typical aft rotor data, which probably include the effect of some aft rotor stalling, with the upper boundary of the data envelope at the 90-percent radius illustrates the effect of stall. A theoretical prediction of the alternating blade bending moment distribution is also shown for the aft rotor. This aeroelastic rotor analysis, the Leone-Myklestad method, is generally used for blade design at the Vertol Division but is shown to be quite conservative. Due to the very high bending which occurs in sideslip transition and which cannot be predicted, this conservatism is warranted.

The effect of airspeed on the straight level flight data is shown in Figures 69 and 70 for two stations on the forward and aft rotor blades. The forward rotor data (Figure 69) show that blade alternating bending is high in hovering due to wind and overlap effects. These data show that transition causes increased bending at 25-percent radius, except when in ground effect, even with no sideslip. At 100 knots airspeed, about 20 test points were obtained at various trim settings, rotor speeds, and gross weights; these three variables are shown to have caused a significant variation in forward rotor inboard bending. It is believed that the longitudinal cyclic trim setting and run gross weight are the predominant parameters which cause this variation.

The dominant effect of sideslip on aft rotor bending moments is shown in Figure 71. Aft rotor alternating flapwise bending at 25-percent radius is shown to double in transition if the sideslip is about 20 degrees. The data obtained at 33,000 pounds gross weight and a very low rotor speed of 202 rpm show higher flap bending than the data for 37,000 pounds, and also show a greater sensitivity to sideslip. These test data had the largest thrust coefficients tested, which apparently caused large bending amplitudes. Ground effect is shown to cause a small decrease in flap bending at small sideslip angles. These alternating flap bending data obtained in sideslip transition are the largest flap bending data obtained in any steady flight condition. With the possible exception of high-speed or

maneuver-induced stall conditions, it appears that these loads are the most severe that tandem rotor helicopter blades can experience. These data should be analyzed to determine the source of the increased loads, and blade design compromises to minimize these loads should be seriously considered. Negative (nose-right) sideslip gives improved low-speed performance which is particularly important in one-engine-out operation, so flight in sideslip transition is performed routinely.

The azimuthal variation of flapwise blade bending is typical of the data shown in Figures 72 and 73. These data were obtained at 33,000 pounds gross weight at 60 and 124 knots. A large 5/rev. oscillation is shown in the 60-knot data for both rotors and also in the 124-knot data for the aft rotor. The forward rotor data for 124 knots show a predominant 1/rev. oscillation and an 8/rev. oscillation. The 5/rev. oscillation indicates that the blades are bending predominantly in their second flapwise bending mode. The significant 8/rev. oscillation is due to excitation of the blades in the third flapwise bending mode.

The actual harmonic content of these flapwise bending data for 124 knots and 33,000 pounds is illustrated in Figure 74. The predominance of 2, 4, and 8/rev. oscillations due to the first three bending modes is evident, especially at the 25-percent radius. Since the more outboard stations are near the nodes of the higher mode bending, the flap bending data measured at these stations contain various amounts of these higher harmonics.

The steady flapwise bending data are particularly interesting since they substantiate the steady blade loading airloads data. Figure 75 shows the radial distribution of steady flap bending at 60 knots and in hover with a gross weight near 33,000 pounds. In hovering, the blades of both rotors are shown to have similar bending moment distribution. When the airspeed is 60 knots, the bending of the inboard region of the forward blade has become more negative (concave downward) and the aft blade has become less negative. This indicates that the lift shifts inboard on the forward blade as the airspeed is increased. The steady flap bending data at the 55-percent radius give a good indication of this effect, and therefore these data are plotted in Figure 76 as a function of airspeed. Forward rotor bending is shown to drop sharply between 30 and 55 knots, indicating that the lift has shifted inward. An outward shifting tendency is also shown starting at about 80 knots; however,

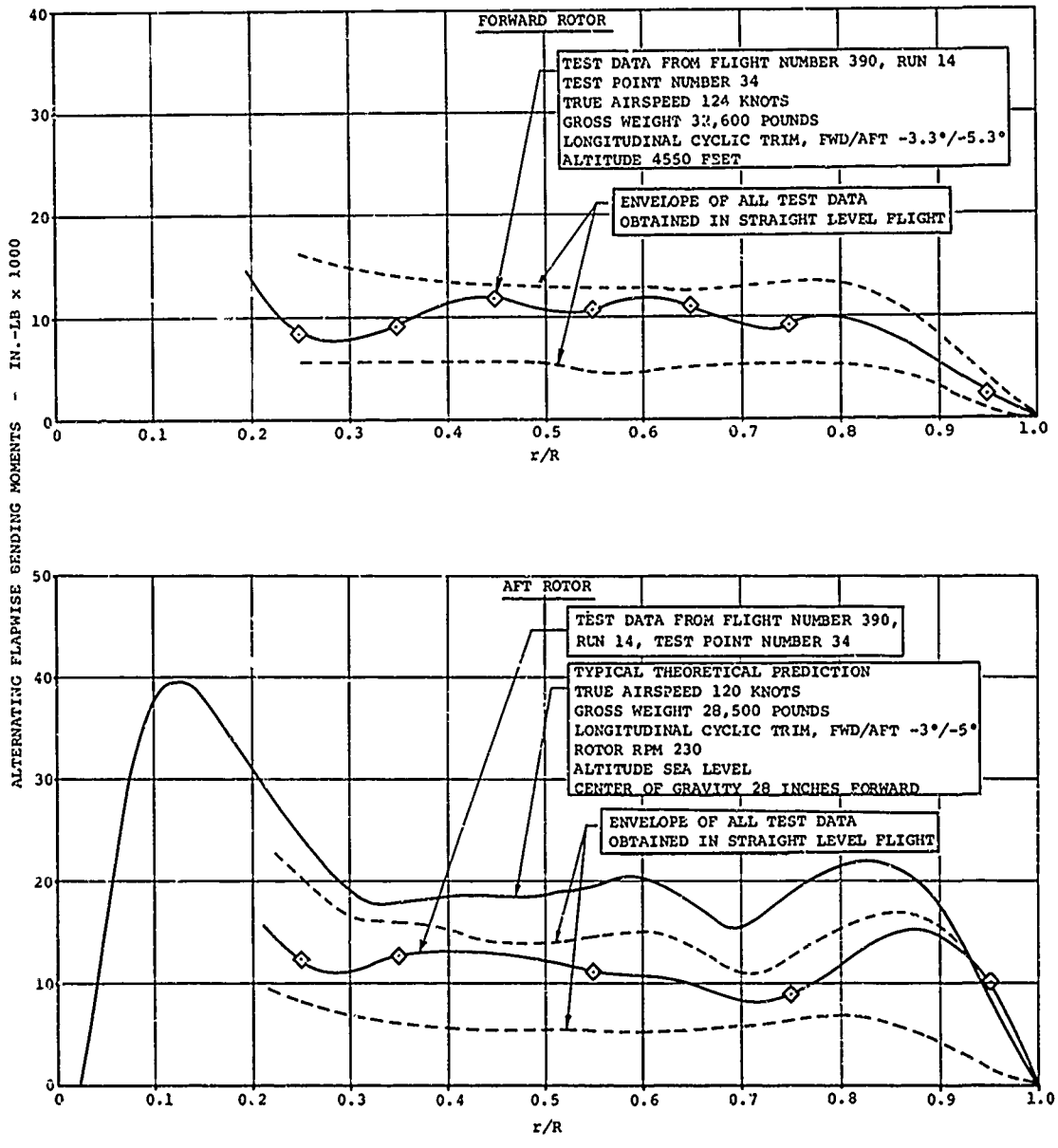

Figure 68. Typical Variation with Radius of Alternating Flapwise Bending Data Obtained in Level Flight.

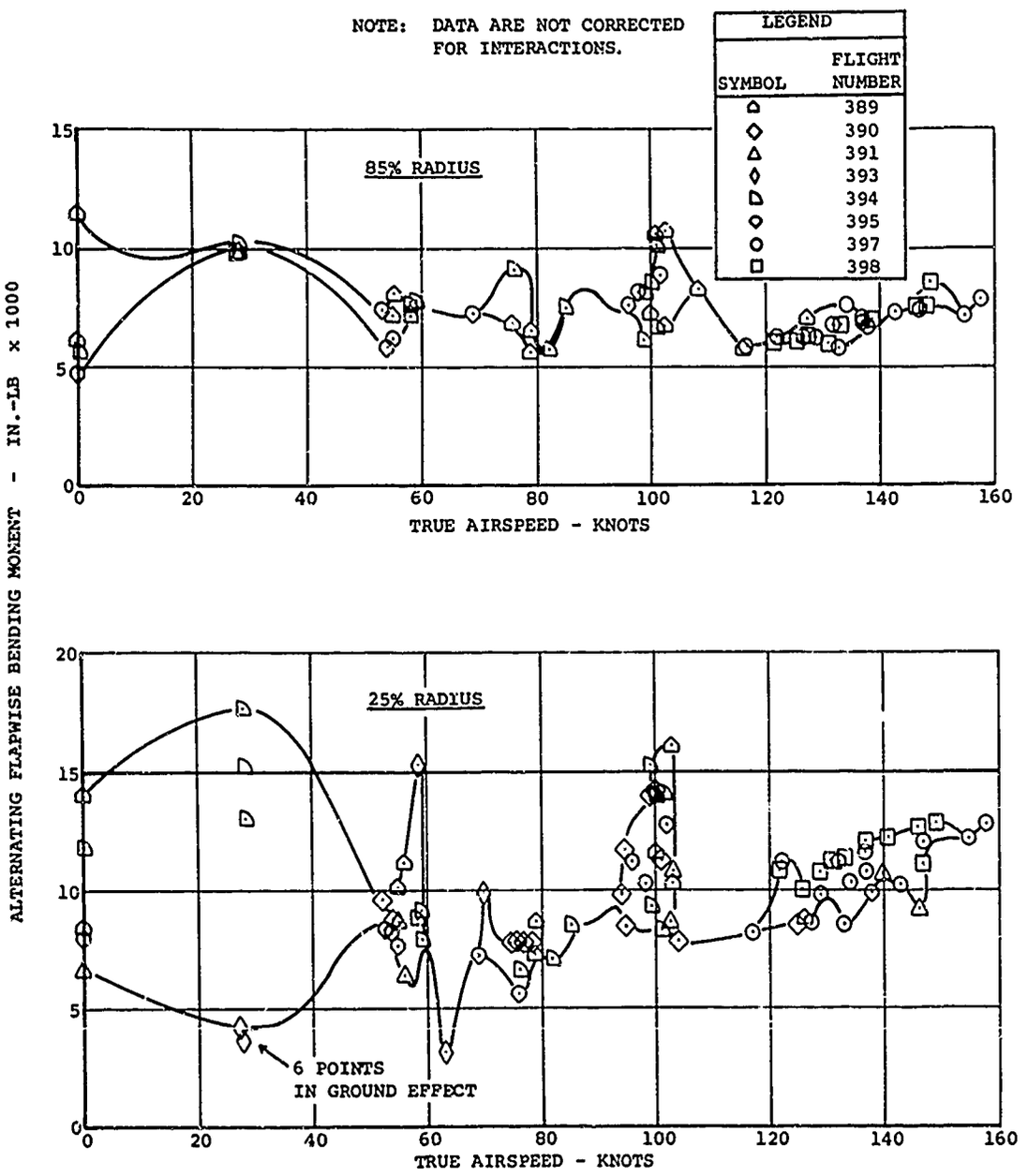

Figure 69. Effect of Airspeed on Alternating Flapwise Bending of Forward Rotor Blades in Level Flight.

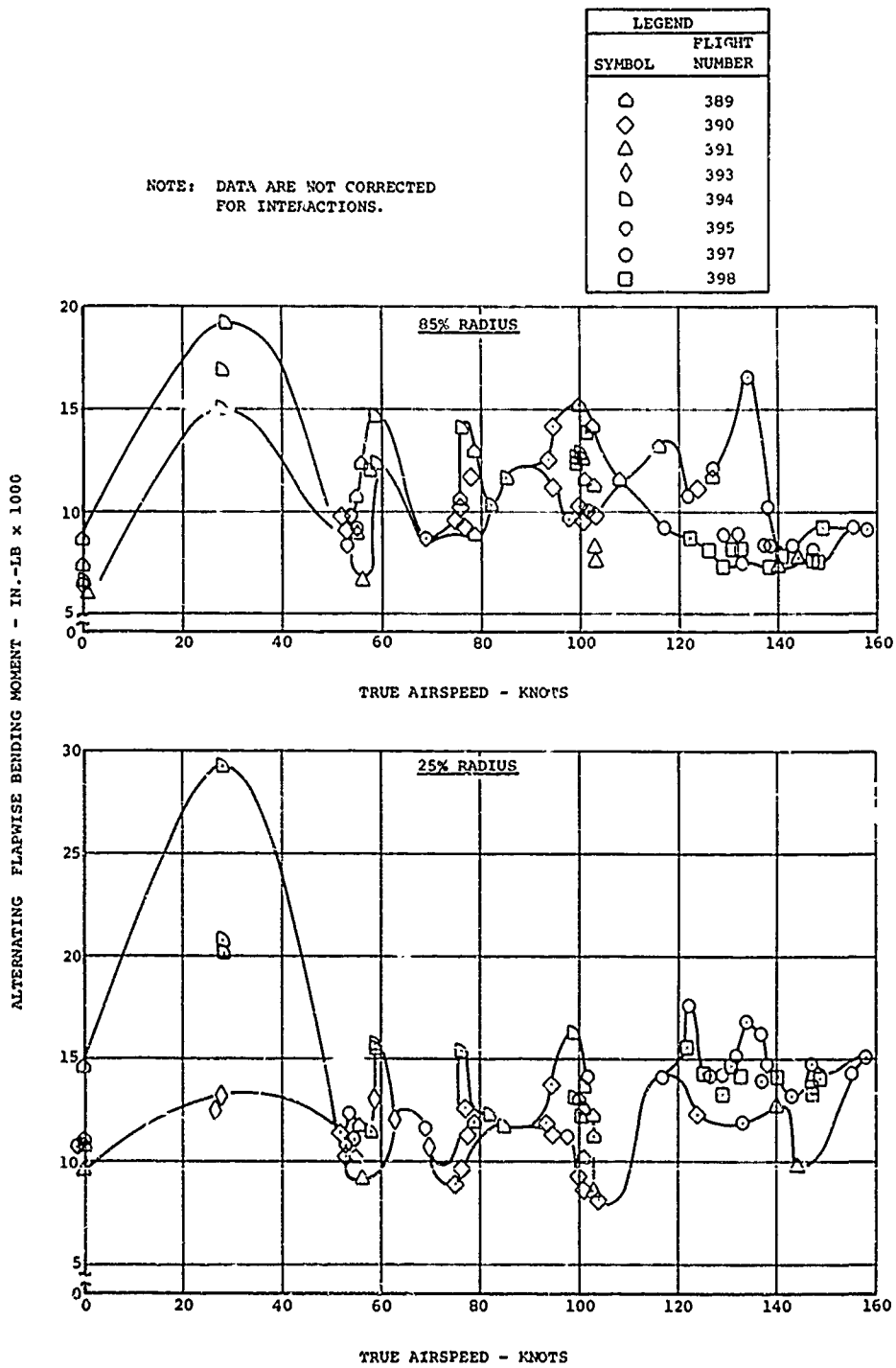

Figure 70. Effect of Airspeed on Alternating Flapwise Bending of Aft Rotor Blades in Level Flight.

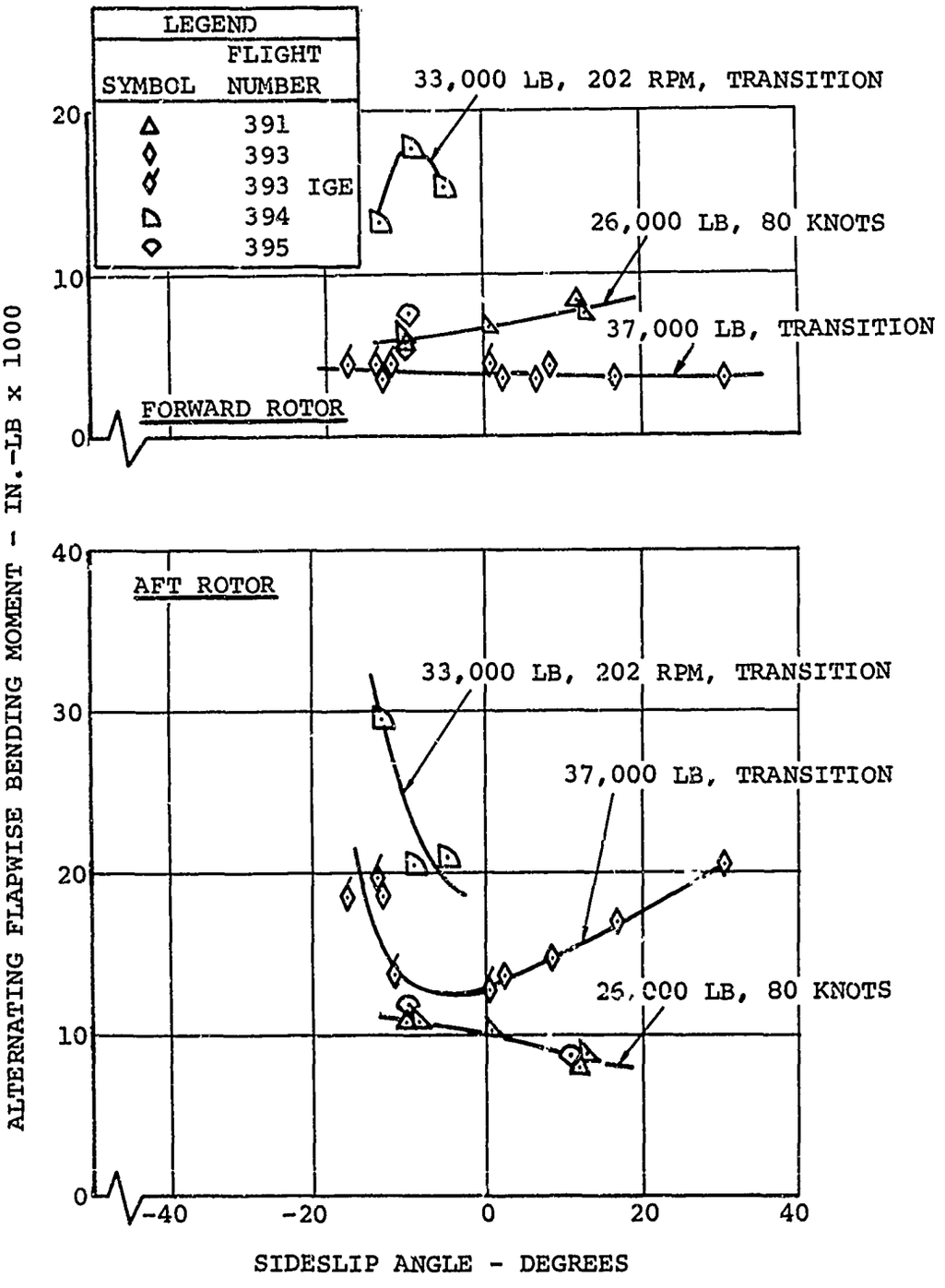

Figure 71. Effect of Sideslip on Rotor Alternating Flapwise Bending at 25-Percent Radius in Transition and at 80 Knots.

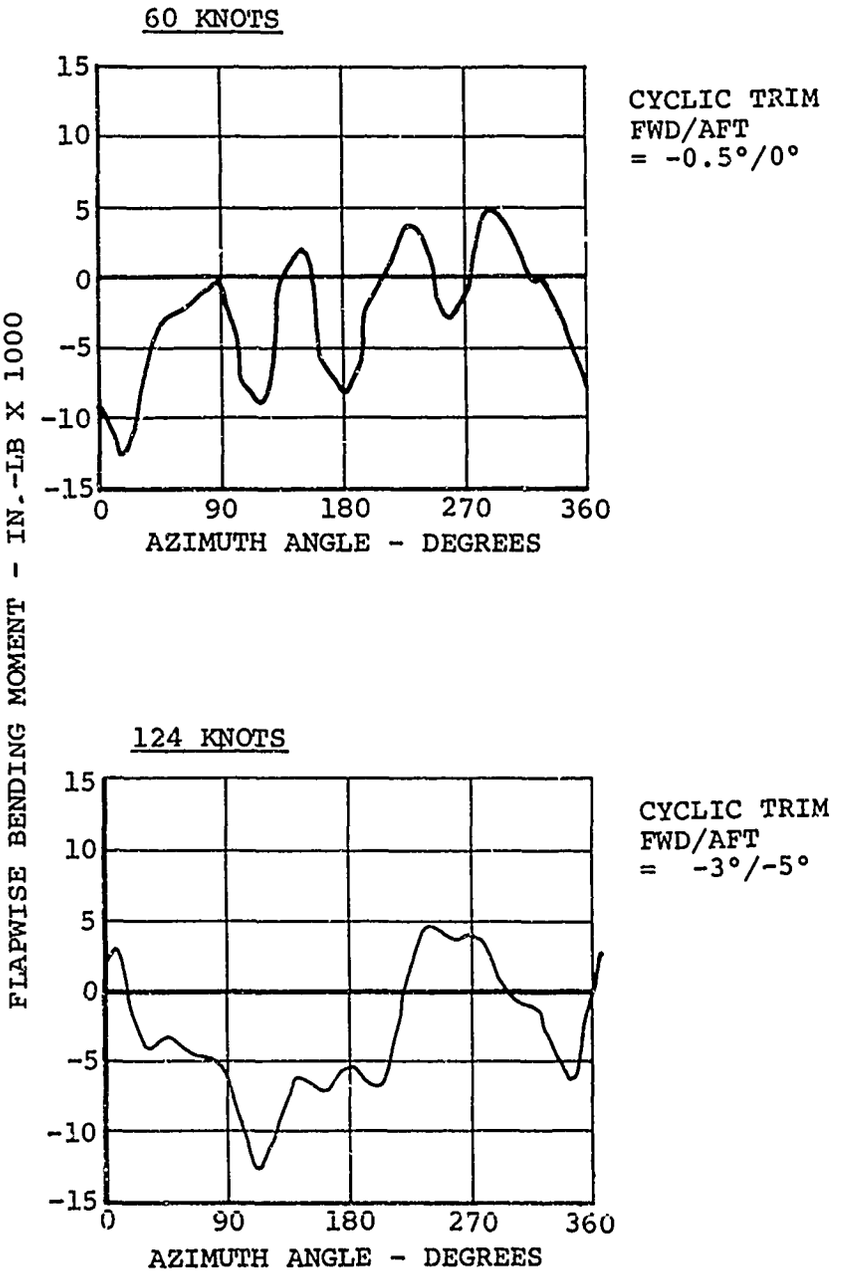

Figure 72. Azimuthal Variation of Blade Flap Bending Measured at 25-Percent Radius of the Forward Rotor.

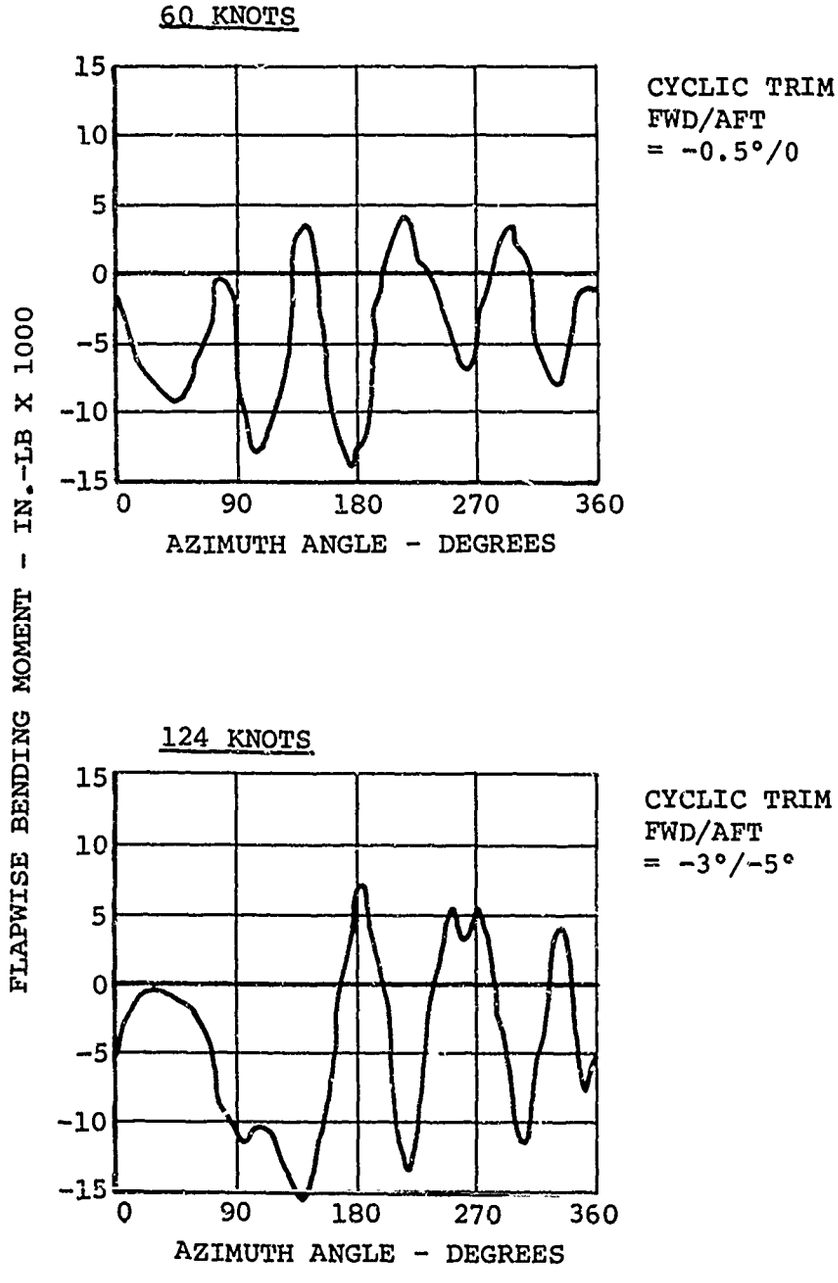

Figure 73. Azimuthal Variation of Blade Flap Bending Measured at 25-Percent Radius of the Aft Rotor.

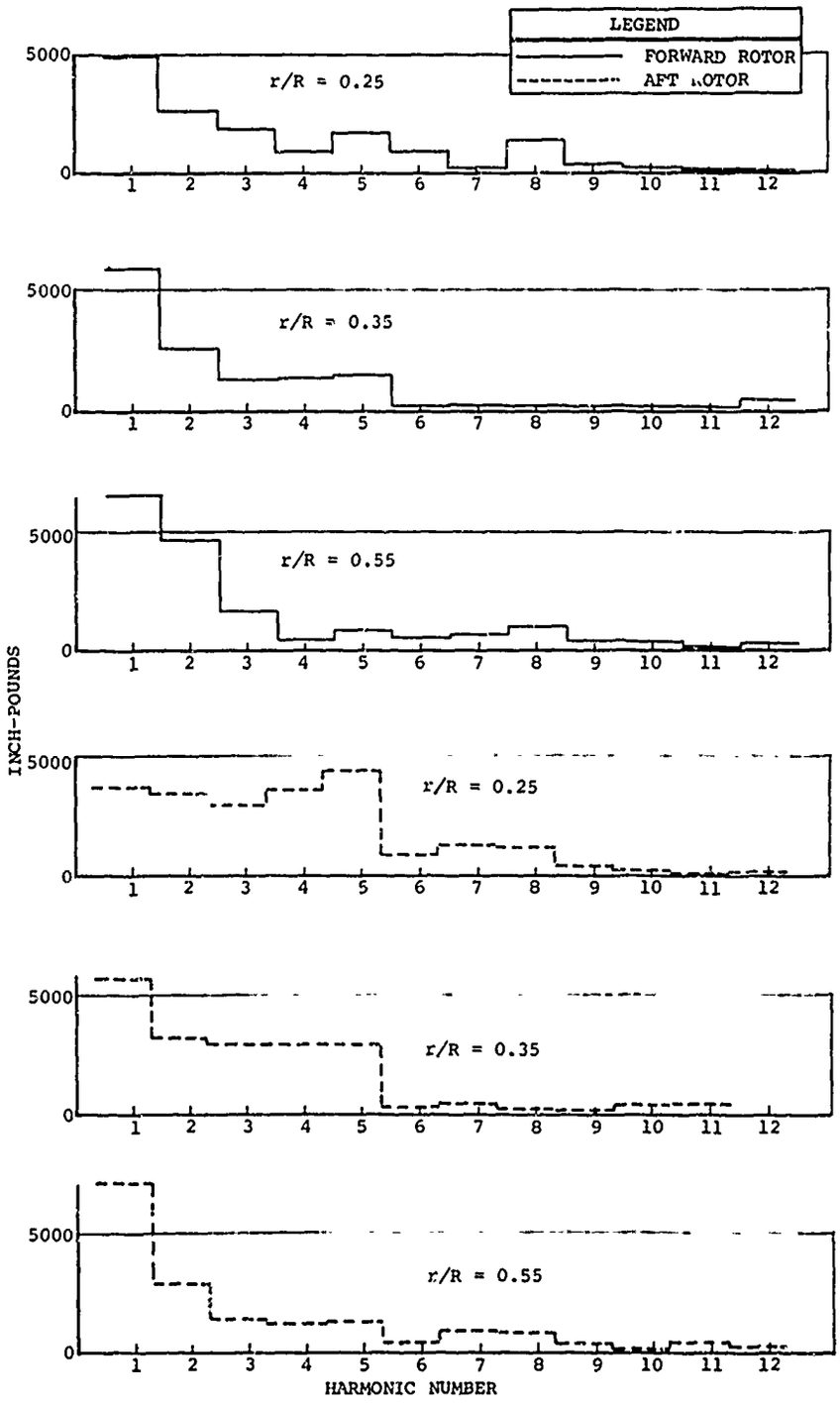

Figure 74. Harmonic Content of Flapwise Bending Moments at 124 Knots Airspeed and 33,000 Pounds Gross Weight.

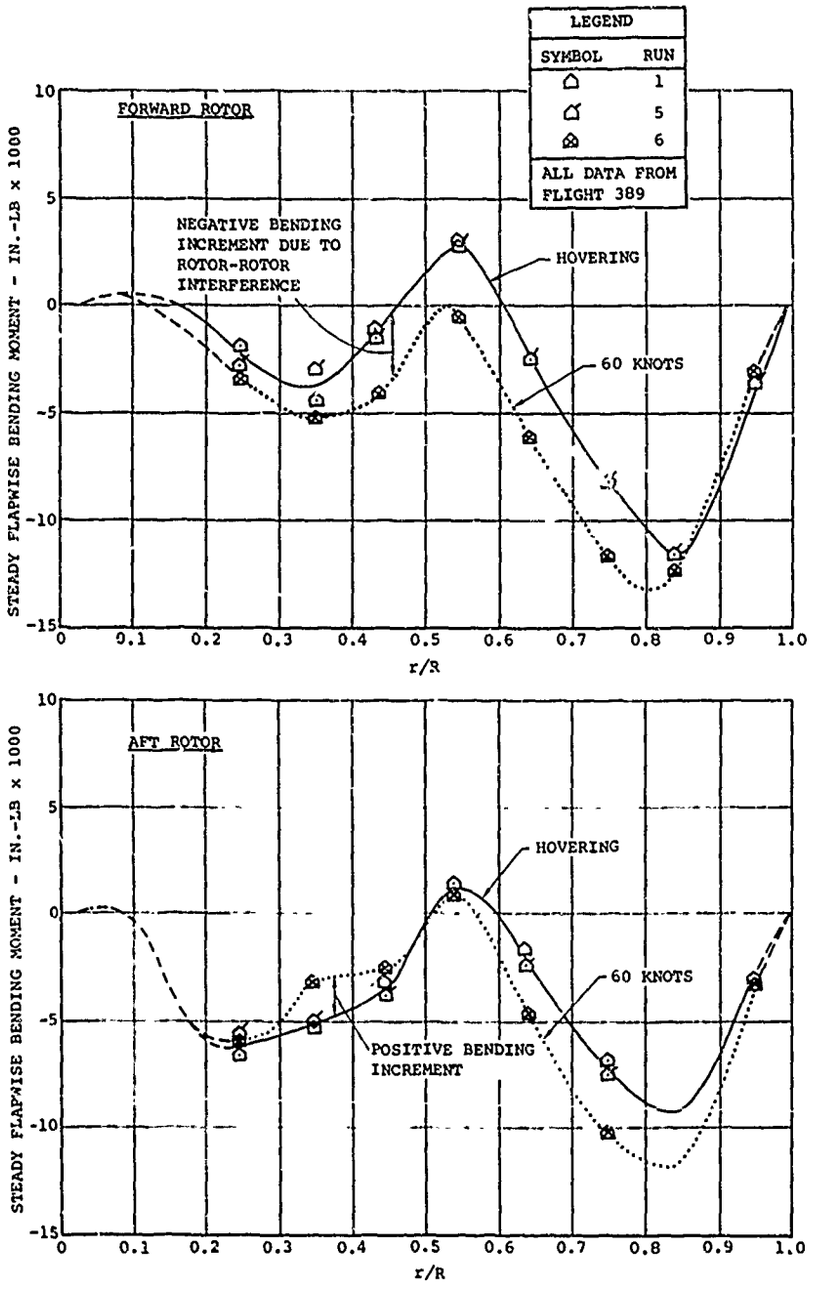

Figure 75. Steady Flapwise Bending Moment Distribution in Hovering and at 60 Knots with a Gross Weight of 33,000 Pounds.

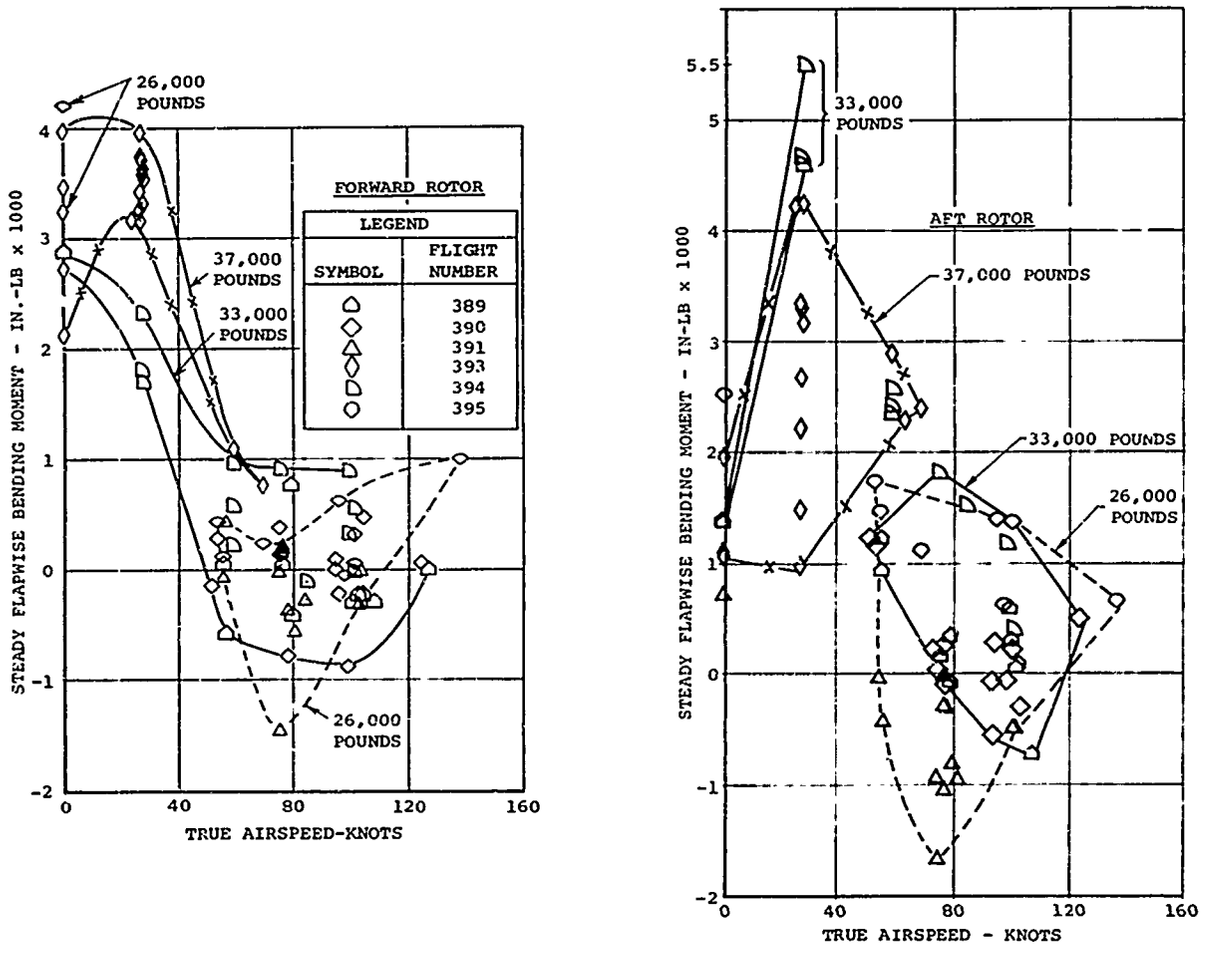

Figure 76. Effect of Airspeed on Steady Flapwise Bending Moments at 55-Percent Radius.

even with an airspeed of 158 knots, the bending moment is not as large as it is in hovering. The aft rotor data shown in Figure 76 show a sharp increase in bending in transition and then drop back to about the same level as in hovering when the airspeed is above transition.

A first-order comparison of the oscillating blade bending and the oscillating airloads can be made by comparing these measurements at an antinode of the blade bending. This comparison is obviously first order, since the bending is caused by the distributed airload; however, the comparison indicates that the data are consistent, and some insight into the airload-bending relation is shown. Figures 77 and 78 show the ratio of the second harmonic airloads and bending at the 40- and 45-percent radii respectively. This region of the blade is near an antinode of the first mode blade bending which has a natural frequency ratio of about 2.5/rev. In spite of the relatively crude nature of this comparison, the data are surprisingly consistent except for the forward rotor at about 60 knots. The general consistency is apparently due to a direct relationship between the second harmonic airloads at 40-percent radius to the airloads on the remainder of the blade. This relationship apparently does not hold near 60 knots for the forward rotor. The phase relationship between this single station airload measurement and the blade bending response is also surprisingly consistent. Forward rotor data again show the largest variations, which occur at 100 knots.

Similar data for the fifth harmonic load-response ratio at the 75-percent radius are shown in Figures 79 and 80. The 75-percent radius is near an antinode of the second bending mode which has a natural frequency ratio of about 4.5/rev. These data are much more consistent, with a systematic trend of the loading ratio with airspeed shown for both rotors. Another indication of consistency is that the phase angle ratio is very near unity for almost all airspeeds.

The azimuthal variation of the blade chordwise bending moments measured at the 45-percent radius with a gross weight near 33,000 pounds is shown in Figure 81. These data show the predominance of 1/rev. and 4/rev. response, which is expected since the chordwise blade loading is mostly 1/rev.; but, as shown in Figure 9, the natural frequency of chordwise bending is about 4/rev. The actual harmonic content of these data is shown in Figure 82 to consist of fairly large 3, 4, 5, and 6/rev. as well as the large 1/rev. The fourth and fifth

harmonics are largest, since the natural frequency is somewhat larger than 4/rev.

Blade torsion moment data are particularly important, since blade twisting causes an otherwise unmeasured control input to the rotor. The harmonic content of the blade torsion data obtained at 33,000 pounds gross weight and 124 knots is typical and is shown in Figure 83. Torsion loads are shown to be predominantly 1, 2, and 3/rev., with a resonant amplification of the 5 and 6/rev. due to the first torsion mode. The magnitude of the twisting of the blades can be estimated by assuming that the moments at the 40-percent and the 13-percent radii are in phase, and that the change in moment per unit length between these radii is constant. The blade torsional stiffness data required for this estimate are presented in Volume II of this report. With these data and assumptions, the total blade twist is calculated to be about 0.6 degree.

The excitation of the blade twisting in its first mode due to blade stall (resulting in so-called stall flutter) is of considerable interest. A first look at the possible existence of this phenomenon has been made with the plotting of the fifth harmonic blade torsion moment against airspeed for a large number of the test points obtained in level flight. These plots are presented in Figure 84 and show no sign of a divergence of any kind. The forward rotor data increase slightly with speed above 120 knots; but the aft rotor, which is expected to stall first, experienced a decrease in fifth harmonic torsion in this range. These data are further explored in Volume V to isolate the effects of stall.

CONTROL SYSTEM LOADS

The serious effects of blade torsion loads are generally manifested in requirements for a heavy rotor control system. Blade loads themselves are generally acceptable due to the blade strength required to withstand centrifugal force loads. Thus, the alternating pitch link load data of Figures 85 and 86 are of considerable interest. The data are shown to increase with the square of the airspeed as expected, with some variations due to maneuvers, changes in gross weight, and altitude. The aft rotor data also show a sizable increase in control load due to sideslip in transition, and the high-speed, light-gross-weight test data show the effects of blade stall as discussed in Volume V.

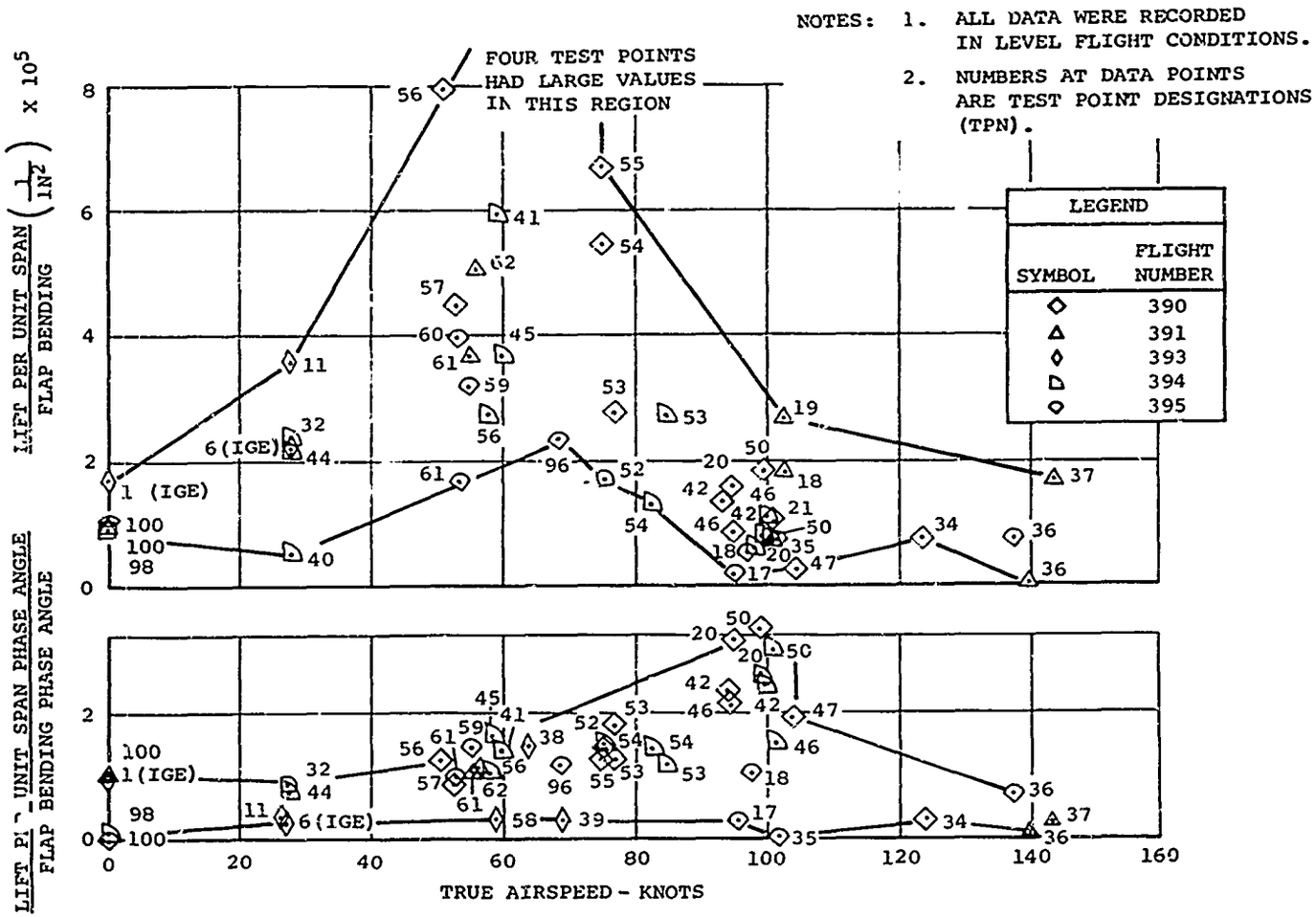

Figure 77. Comparison of Second Harmonic Amplitudes of Flapwise Bending and Lift per Unit Span as Measured Near Antinode of First Flapwise Bending Mode for Forward Rotor.

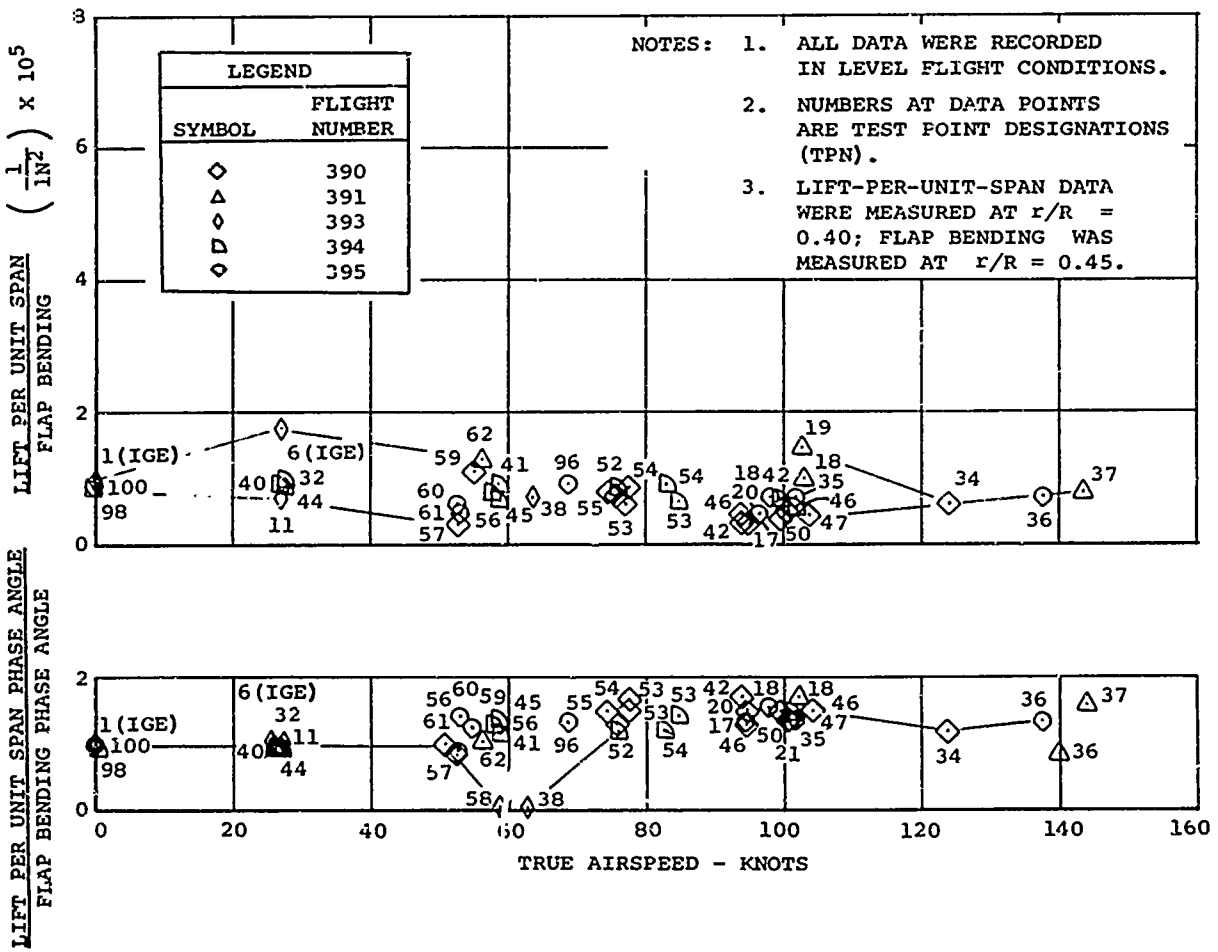

Figure 78. Comparison of Second Harmonic Amplitudes of Flapwise Bending and Lift Per Unit Span as Measured Near Antinode of First Flapwise Bending Mode for Aft Rotor.

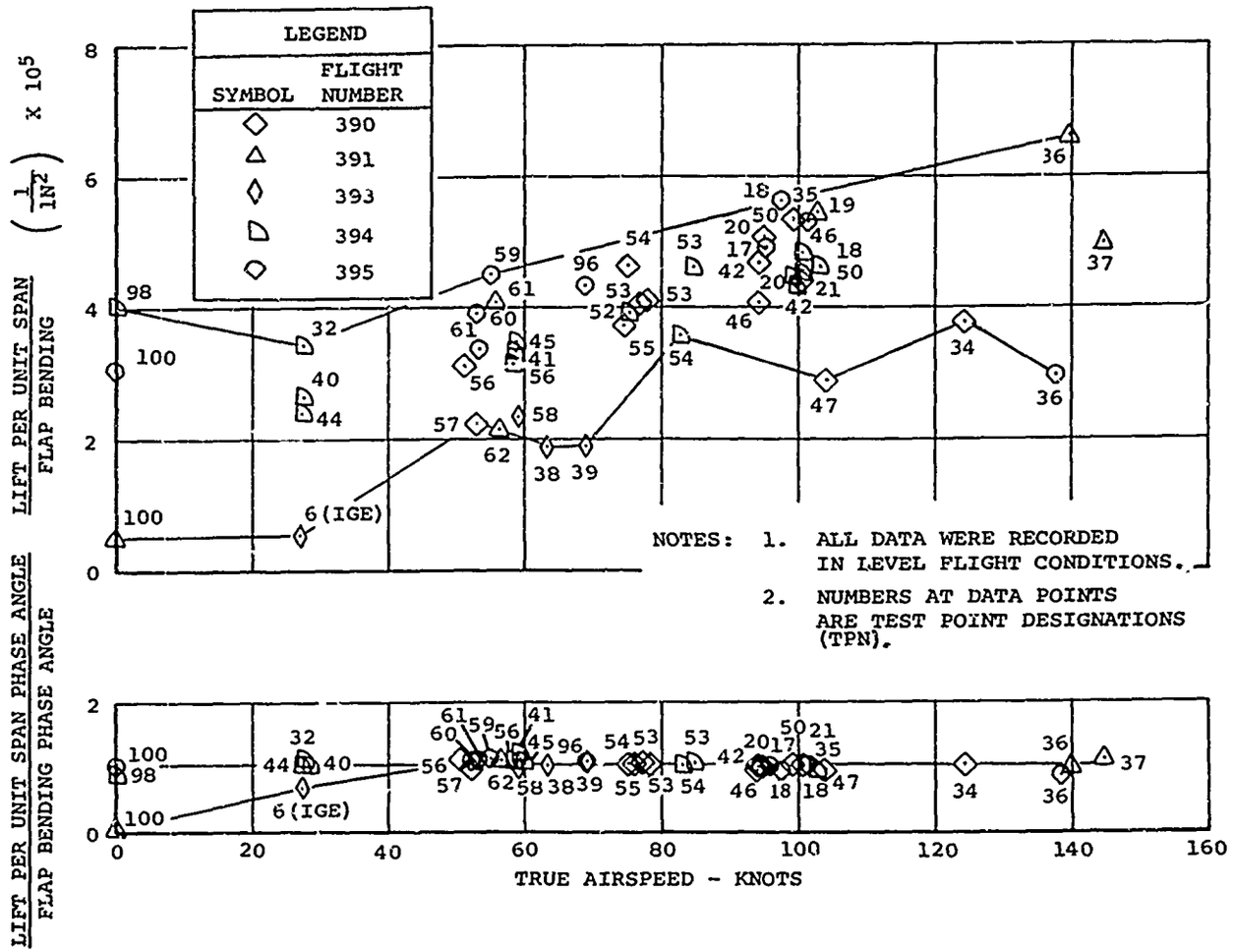

Figure 79. Comparison of Fifth Harmonic Resultants of Lift per Unit Span and Blade Bending Near the Antinode of Second Flap Bending Mode for Forward Rotor.

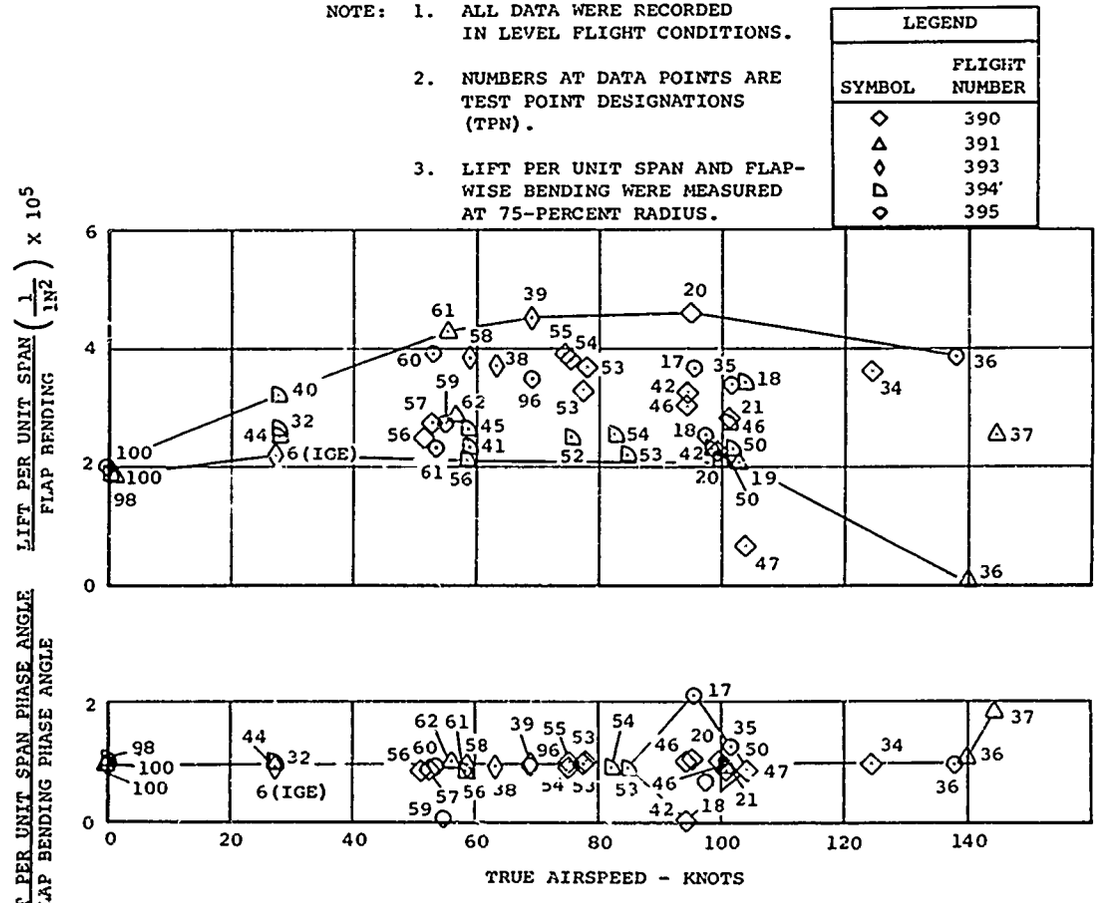

Figure 80. Comparison of Fifth Harmonic Resultants of Lift per Unit Span and Blade Bending Near the Antinode of Second Flap Bending Mode for Aft Rotor.

AIRCRAFT CH-47A NO. B5
FLIGHT NUMBER 390
GROSS WEIGHT 33,300 POUNDS
TOCG 5.3 INCHES
ROTOR RPM 243

r/R = 0.45

LONGITUDINAL CYCLIC TRIM, FWD/AFT = 3°/5°

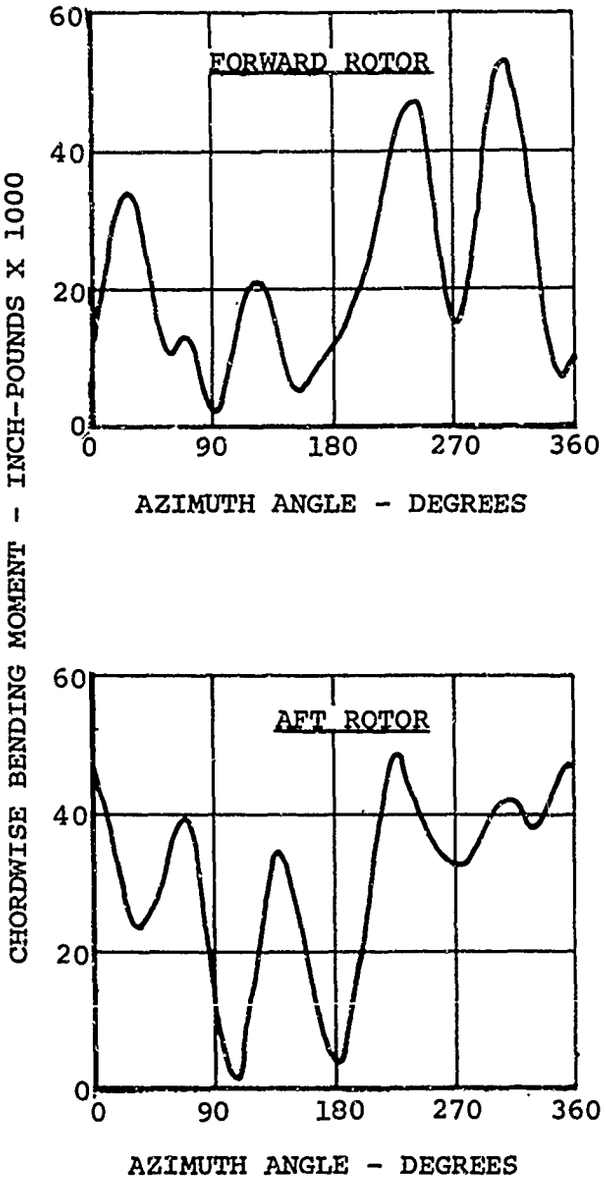

Figure 81. Azimuthal Variation of Chordwise Blade Bending Moments at 124 Knots.

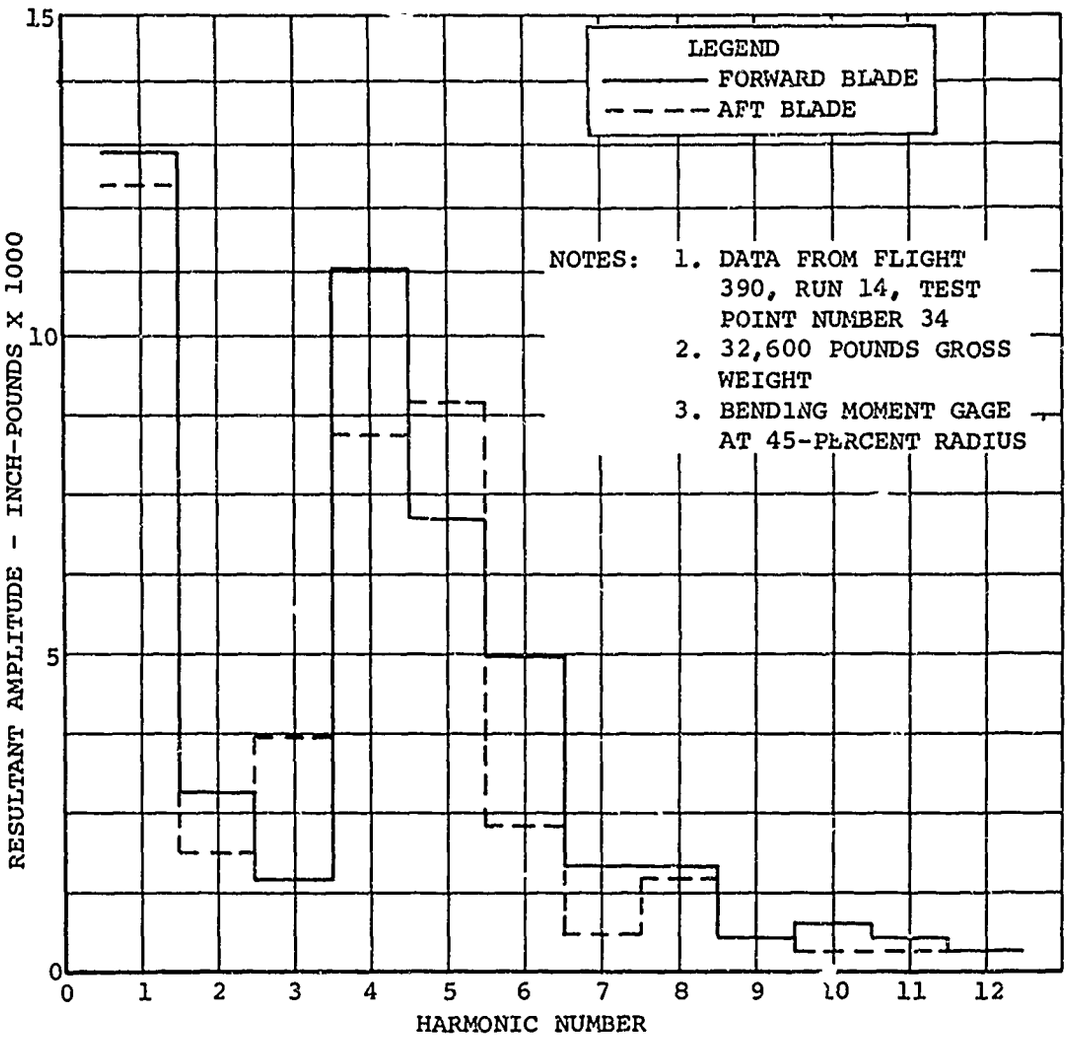

Figure 82. Harmonic Content of Chordwise Blade Bending Moments at 124 Knots.

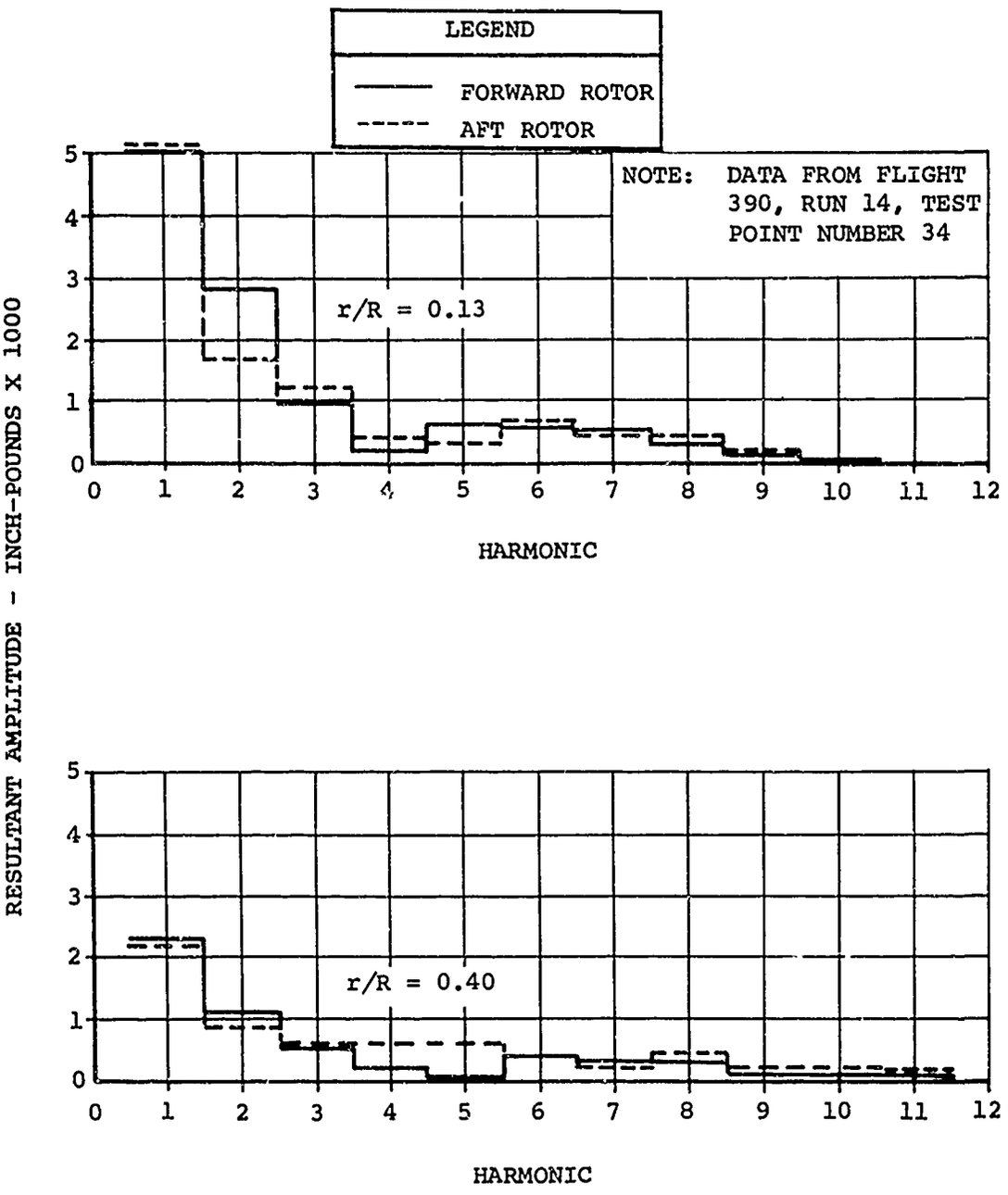

Figure 83. Harmonic Content of Torsional Moments at 124 Knots.

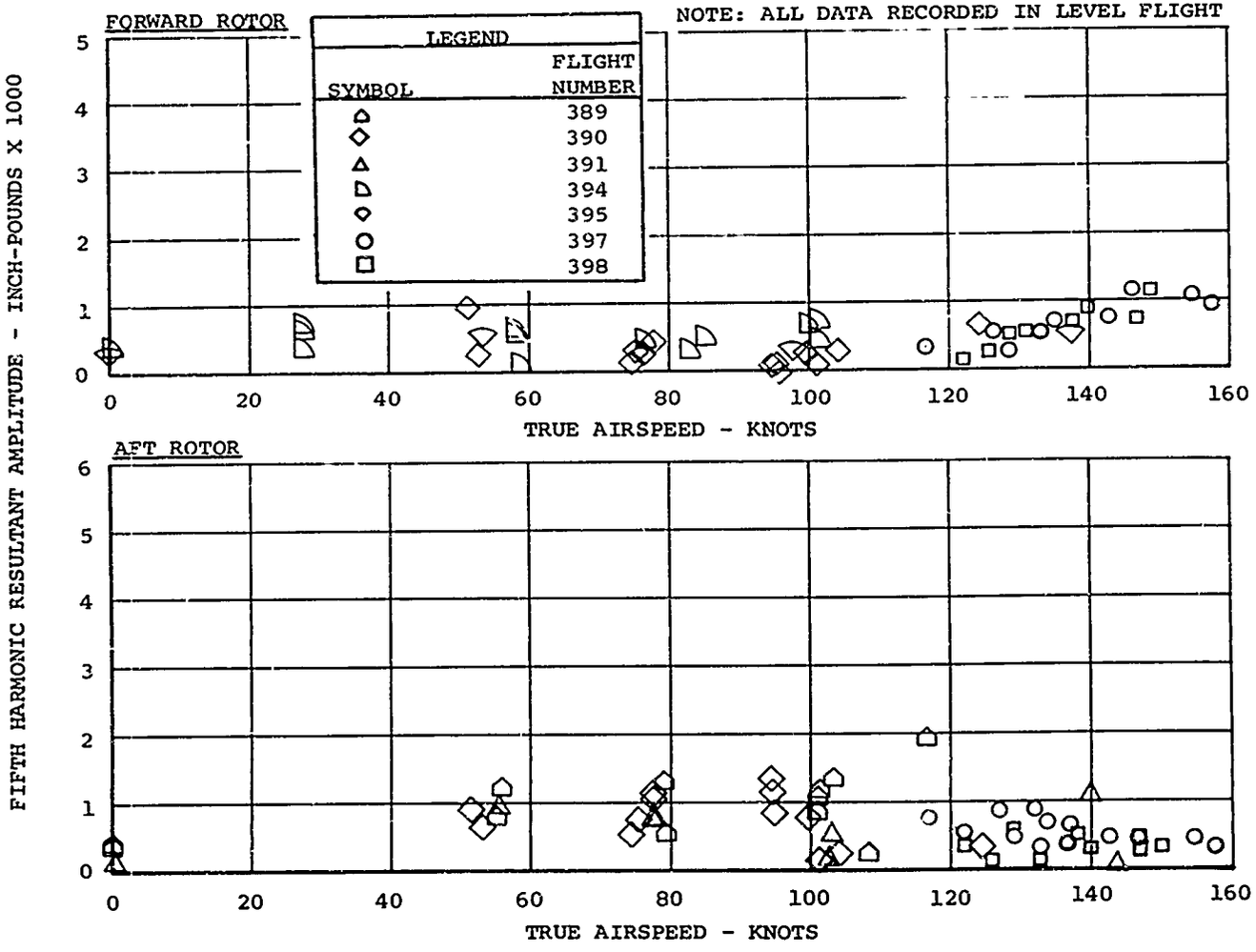

Figure 84. Fifth Harmonic Torsional Moments at 13-Percent Radius as Measured in Level Flight.

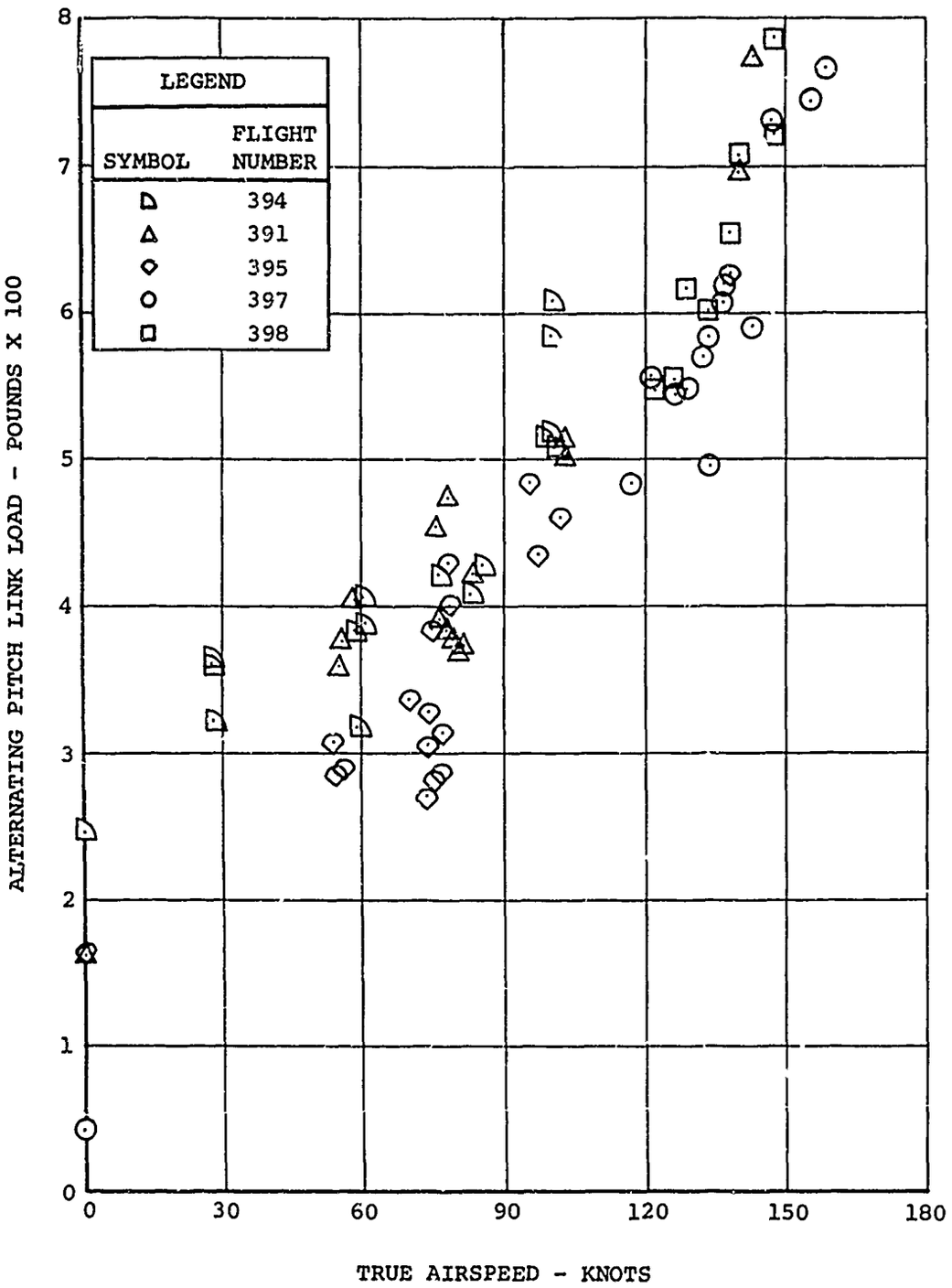

Figure 85. Alternating Control Loads Produced by Forward Instrumented Rotor Blade.

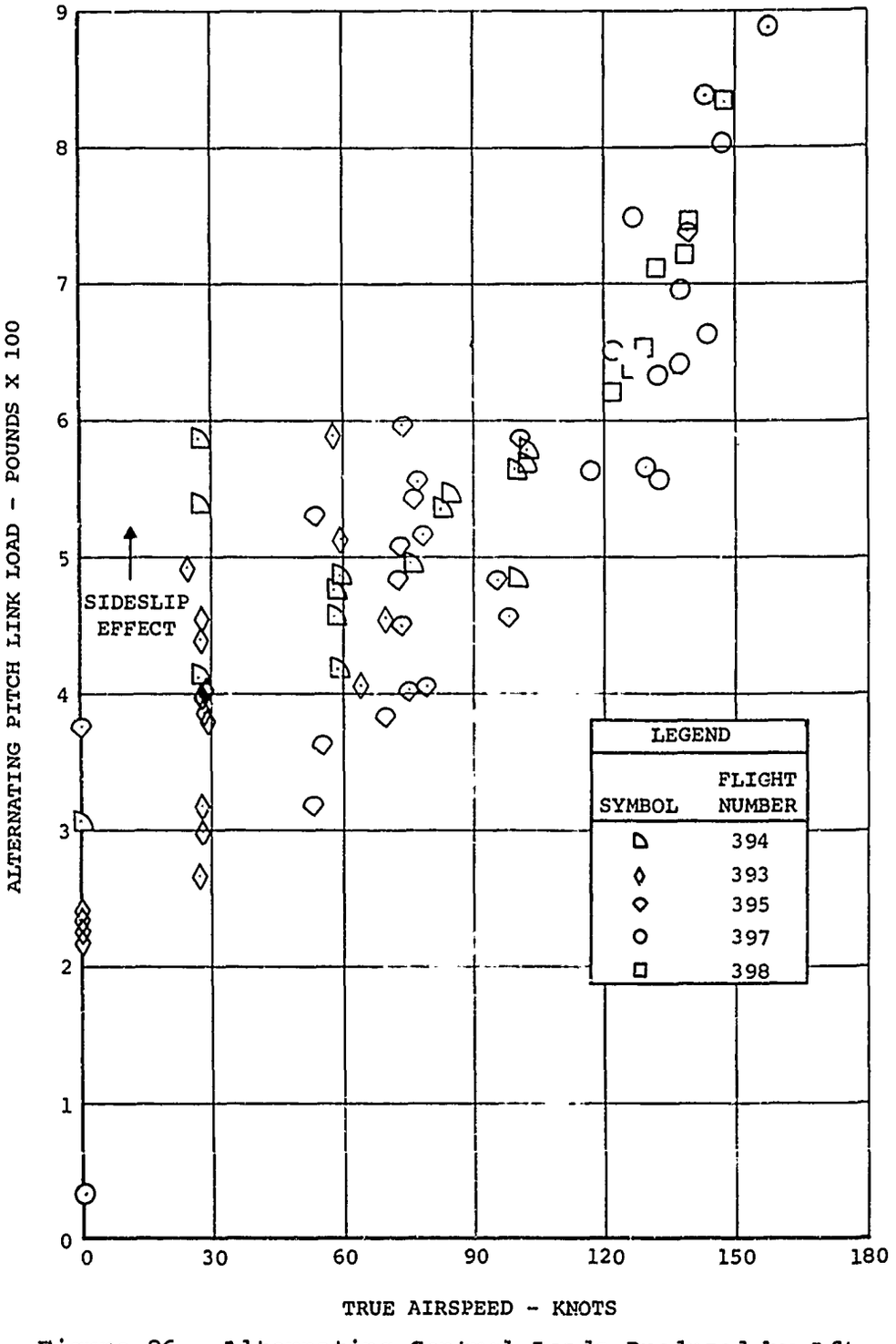

Figure 86. Alternating Control Loads Produced by Aft Instrumented Rotor Blade.

The harmonic content of typical pitch link load data at three airspeeds is shown in Figure 87. Large increases in the first and second harmonic loads with increased airspeed are shown. However, the fifth harmonic loads on the aft rotor decrease with airspeed in agreement with the blade torsion data of Figure 84. This may indicate that there was no stall for these test data, which were obtained at a gross weight of 26,000 pounds.

ROTOR SHAFT LOADS

The rotor shaft loads which were measured included shear and moment in two planes, rotor thrust, and torque. Shaft bending moment data are rather routine, so none of these data were prepared for this report. These moment data are of excellent quality and are available in the reference 4 data report. Rotor torque is considered as a performance parameter and is discussed later. The rotor shaft shear data obtained are unique to this program and are of good quality, as will be illustrated. Rotor thrust measurements had inadequate resolution of the steady values which were deleted.

From performance and trim considerations, the most important shaft shear data are the first harmonic longitudinal shear components. These data are shown in Figure 88 for various longitudinal cyclic trim settings. While there is some scatter in the data, fairly consistent, nearly linear variations of the longitudinal shear with advance ratio are shown. In hovering and at low advance ratio with 0.5-degree trim, the forward shaft shear is negative; that is, it is directed forward. As the speed is increased, the rotor and hub drag increases and causes the shaft shear to be directed aft. Extension of the cyclic trim reduces the shaft shear, since the rotor thrust is directed forward; however, at advance ratios larger than 0.1, the shaft shear is always positive. As shown in Figure 89, the variation of shear with trim is linear at a given advance ratio. The slope of the shear-trim variation is also shown to be greater at a lower advance ratio. These data should be reviewed in detail to aid in the understanding of tandem rotor performance. It is unfortunate that adequate fuselage attitude data were not obtained, since these data could be converted to the rotor lift-drag ratio if the shaft inclination were known.

Rotor shaft shear data are also of value in understanding fuselage vibration. The harmonic content of some typical test data is shown in Figure 90 for three airspeeds. As expected,

the first harmonic shear caused by rotor drag is the largest harmonic component. The large 4 and 2/rev. shears of the forward rotor shown in these data combine to produce a fixed-orientation 3/rev. in the nonrotating system. The relatively large 5/rev. in the aft shaft data cannot presently be explained. Since these rotor shaft shear data are consistent and are of good quality, they should be analyzed in detail.

AIRFRAME VIBRATION

A large volume of airframe vibration data was generated by this program which should be of special value to the CH-47A project due to the unusual conditions which were flown and due to the simultaneous measurements of blade loads, shaft loads, and vibration. There are large variations in these data due to the large range of rpm, trim settings, and gross weights which was tested. Typical test data for this test program are shown in Figure 91, which illustrates this large variation in the data. The general trend shown, with small vibration in hover, sharply increasing vibration in transition, and then decreasing until speeds above 120 knots are reached, is fairly typical of the tandem helicopter.

As would be expected from the rotor loads data given previously, fuselage vibration varies significantly with sideslip. This effect starts in hover with the data showing significantly increased vibration due to wind from the left side (equivalent to negative sideslip). Figure 92 shows the effect of sideslip on 3/rev. cockpit vibration at three airspeed ranges. A fairly systematic reduction with sideslip is shown at each speed, with about 0.05 g reduction in vibration caused by a 10-degree sideslip (nose-right). This variation of vibration with sideslip is more pronounced toward the aft end of the helicopter, since sideslip affects aft rotor loads, not forward rotor loads.

Figure 92 also shows some data obtained at reduced rotor rpm. Apparently due to the proximity of the second beamwise fuselage natural frequency (11.2 cps, Table IV) to 3/rev. excitations at normal rotor rpm, there is a pronounced reduction of vibration when the rotor rpm is reduced. A reduction of vibration by reducing rpm would be practical for low-speed operation, but would lower the limits on the high-speed operation of the helicopter. Fuselage stiffening to increase the fuselage natural frequencies has been considered.

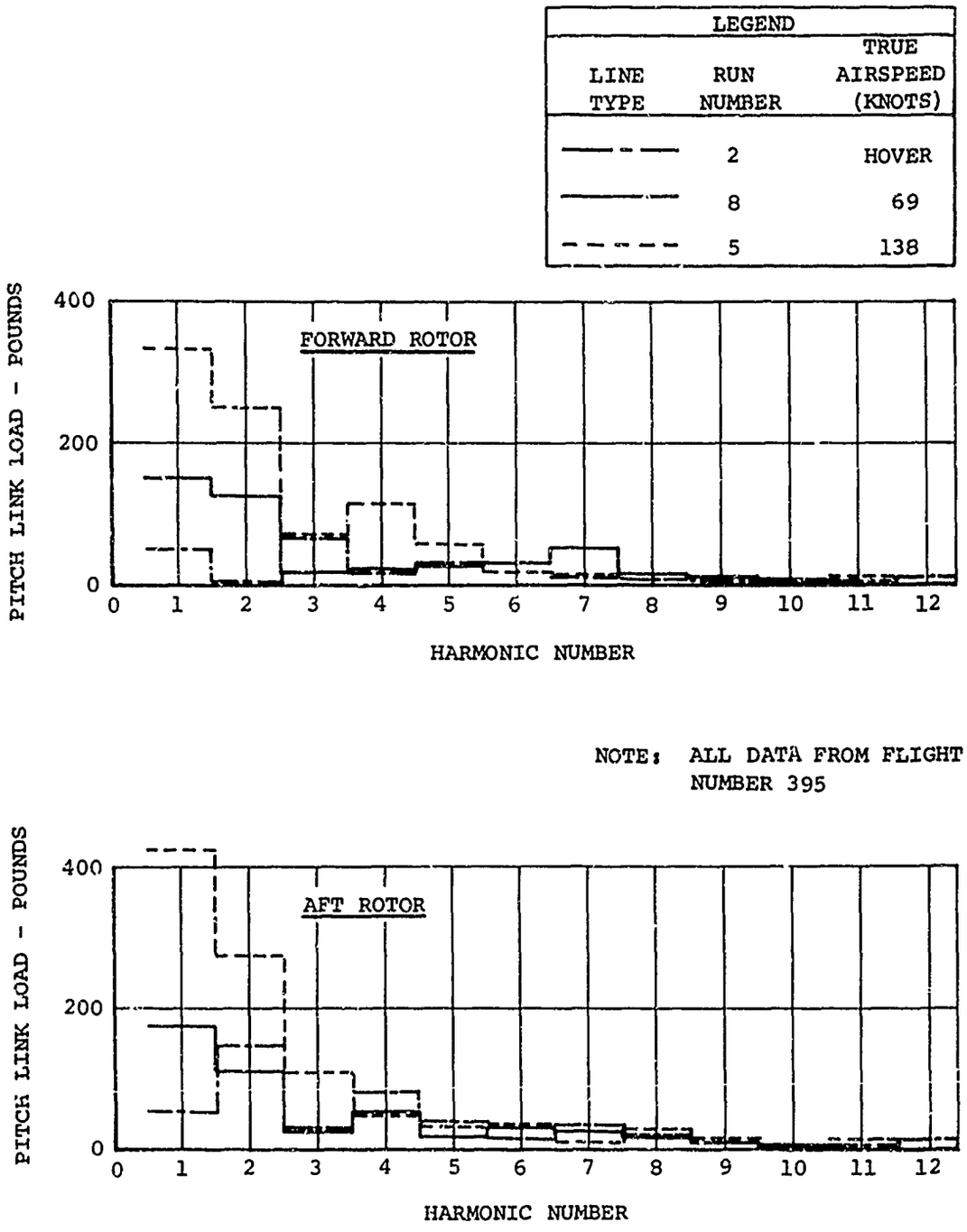

Figure 87. Harmonic Content of Rotor Pitch Link Loads at Three Airspeeds.

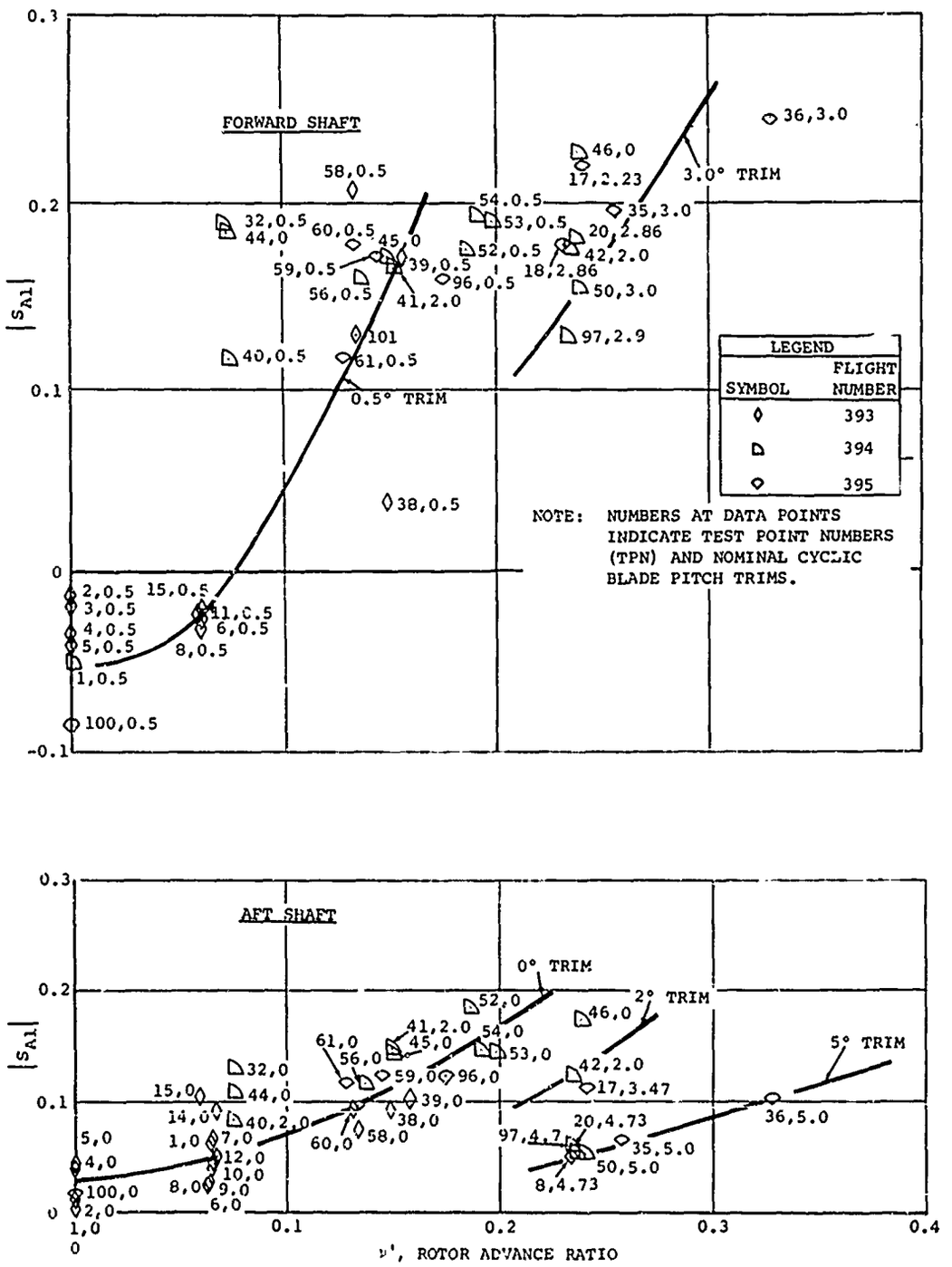

Figure 88. First Harmonic Shaft Shear Data Measured in Level Flight.

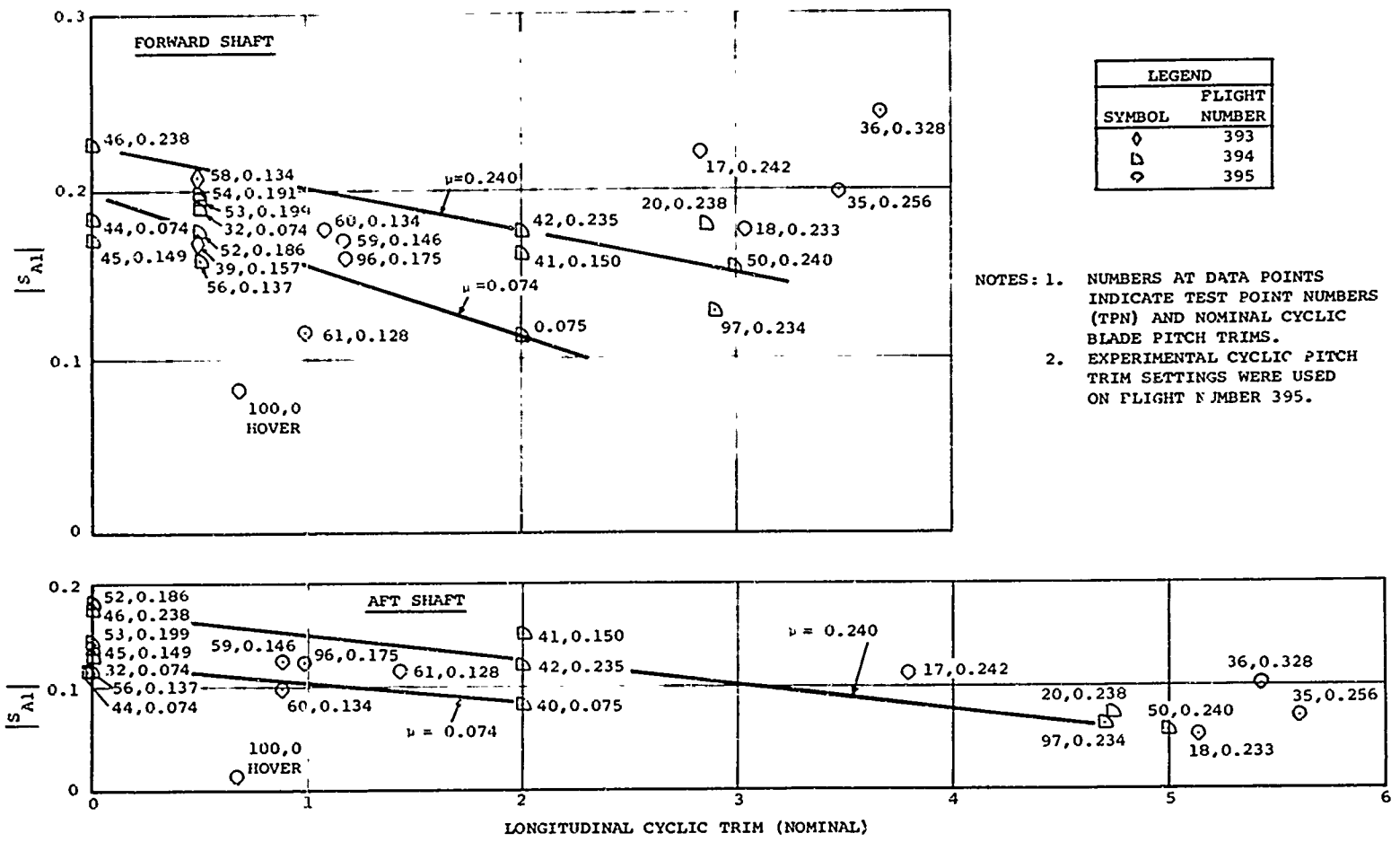

Figure 89. Effect of Cyclic Trim on First Harmonic Longitudinal Shaft Shear.

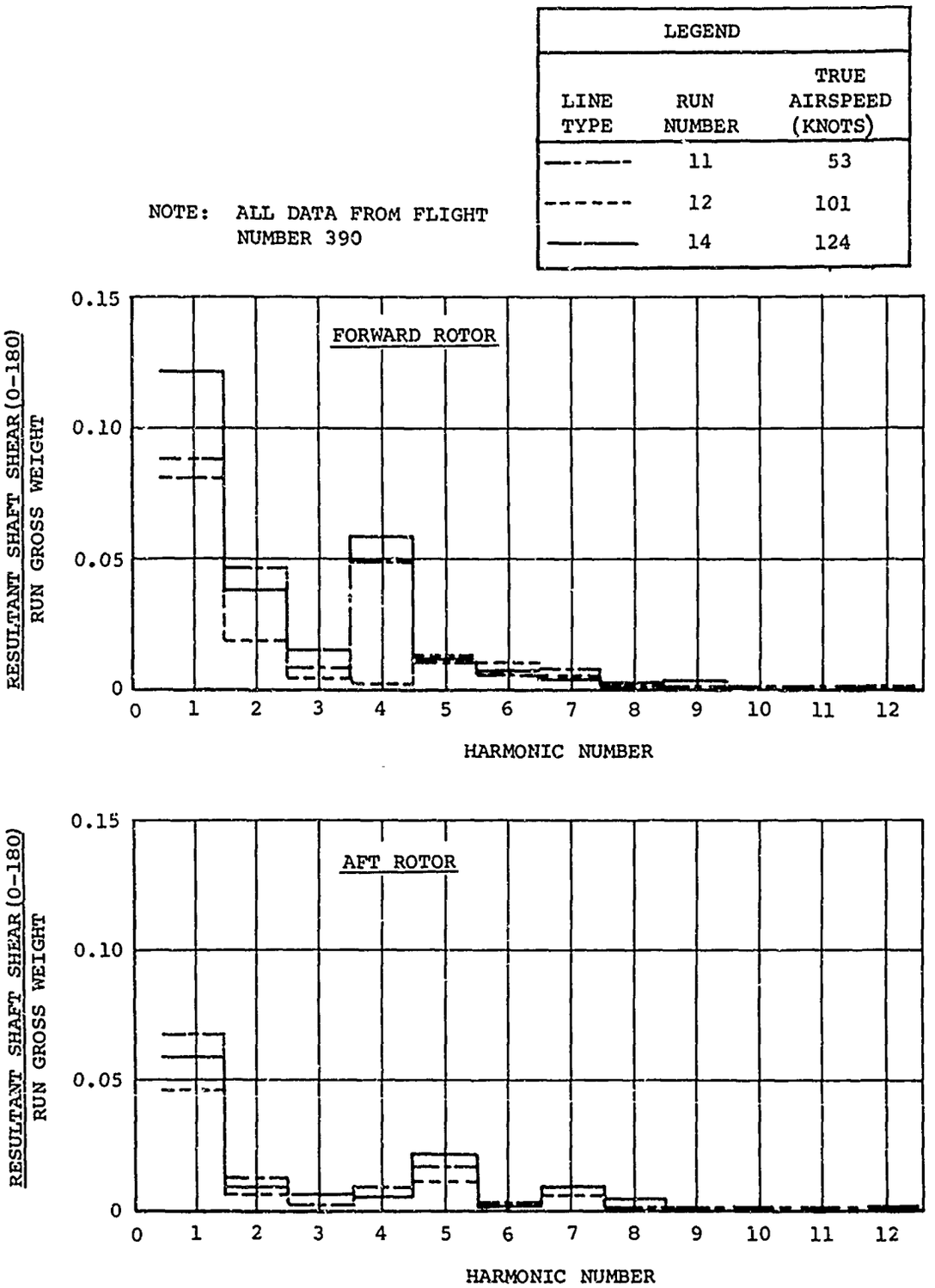

Figure 90. Harmonic Content of Typical Shaft Shear Data.

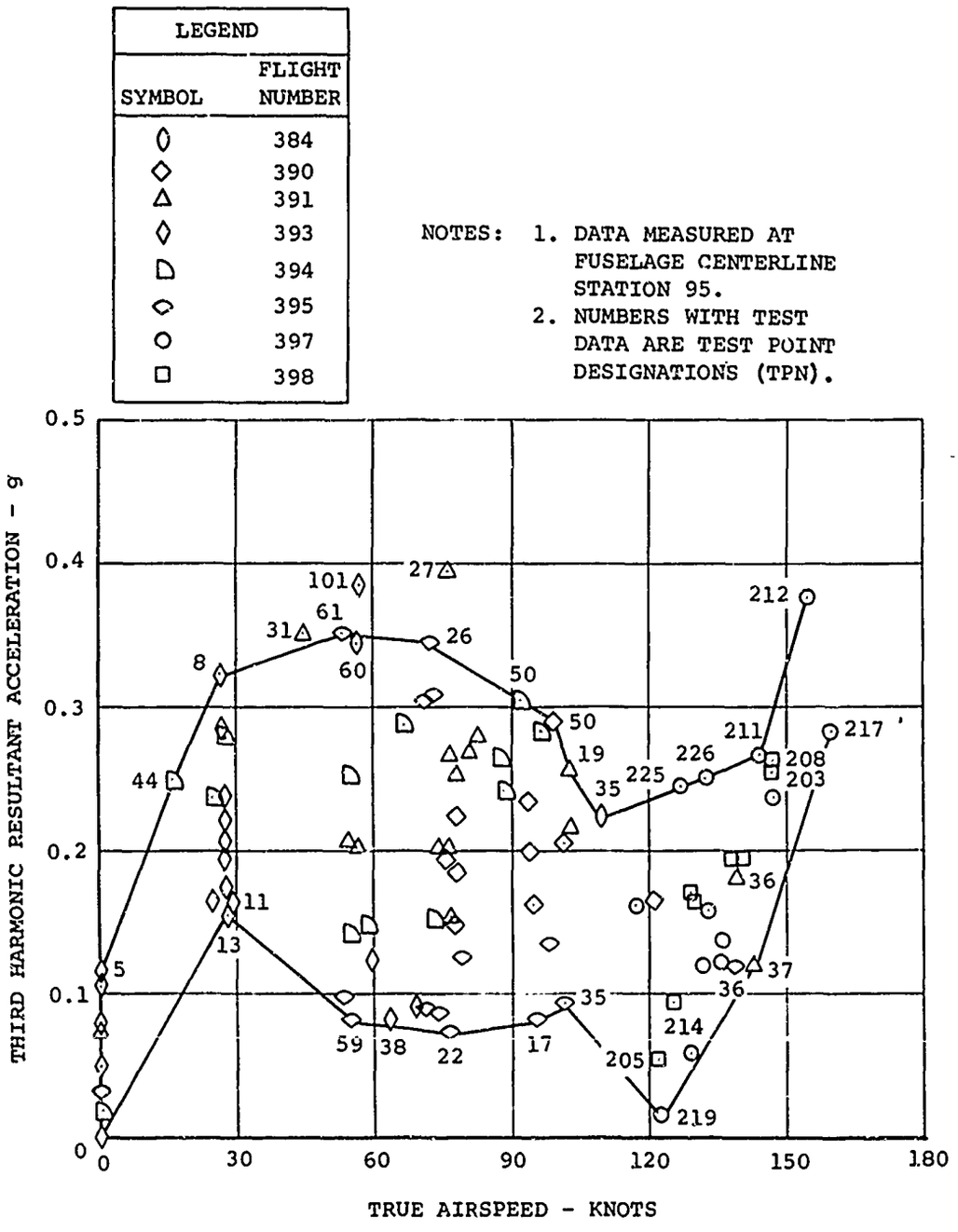

Figure 91. Third Harmonic Cockpit Vibration of Test Aircraft in Level Flight.

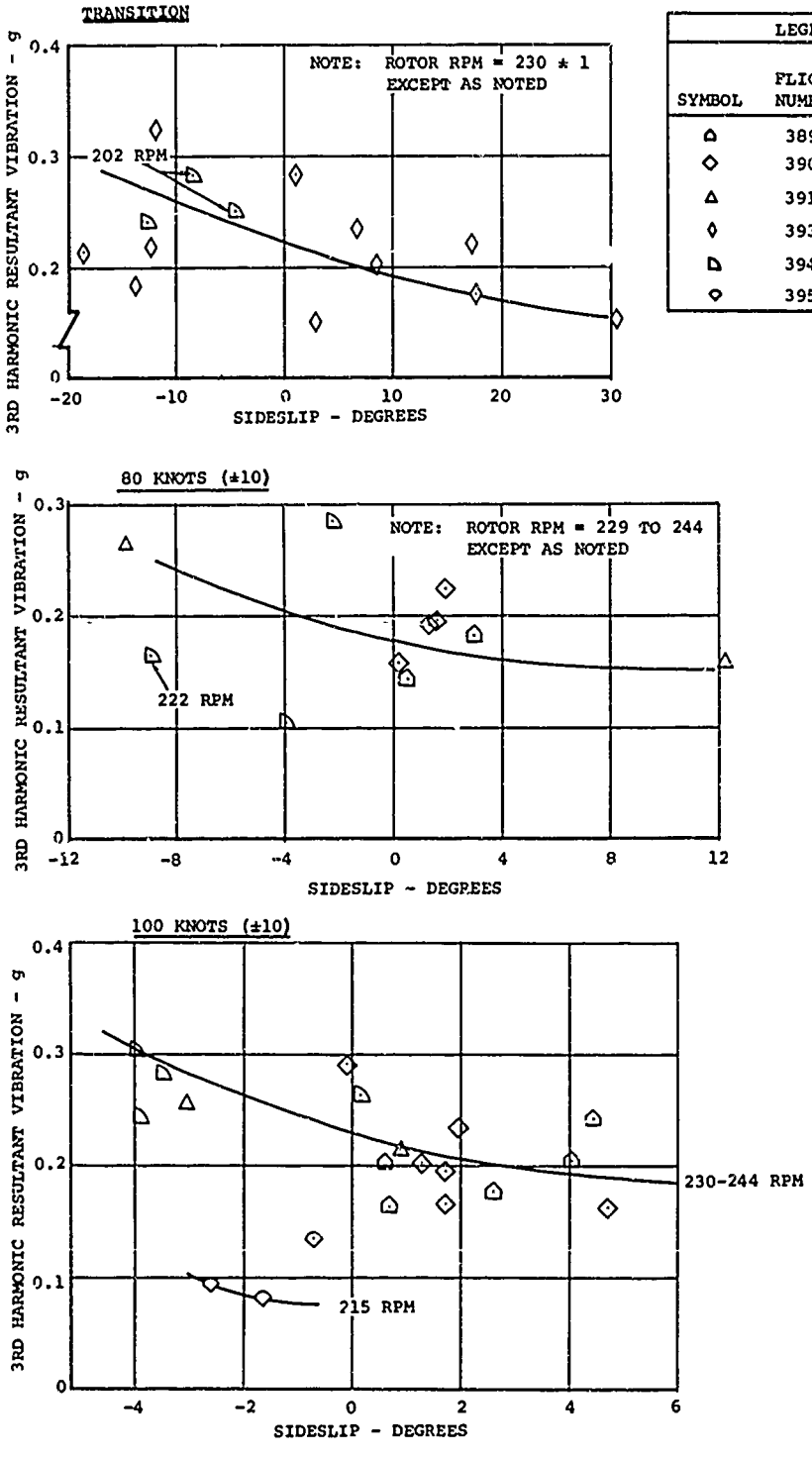

Figure 92. Effect of Sideslip on Cockpit Vibration.

The distribution of third harmonic vertical vibratory bending of the airframe is shown in Figure 93 for one test point. The first and second beamwise bending modes, the forward pylon longitudinal (bending) mode, and a lateral fuel tank-fuselage-fuel tank (mammary) mode are evident. No calculations are available on the lateral modes of the CH-47A, but there are shake test data which show that this mode varies significantly with the fuel level. This parameter further complicates the analysis of these fuselage vibration data. The longitudinal modes are essentially as described in Table IV and are predictable by analysis.

PERFORMANCE AND TRIM

The rotor torque measurements obtained in this program have been prepared as a nondimensional power coefficient-thrust coefficient ratio following the data presentation of the tandem rotor model test of reference 14. These data are shown in Figure 94, and indicate that the tandem helicopter has considerably better performance than the referred data indicate. It can be shown that this coefficient ratio is made up of the following terms:

$$C_P/C_{TW} = K_i(C_{TW}/2\mu') + c_{do}\sigma/8C_T + C_{PP}/C_{TW} , \qquad (4)$$

where

K_i is an induced power factor resulting from nonuniform downwash and

c_{do} is an average rotor profile drag coefficient.

The referred wind tunnel test data were prepared with no propulsive force, so that the parasite power coefficient ratio, C_{PP}/C_{TW}, was zero. To provide equivalent data, the parasite power which would be required if each of the rotors produced one-half of the required propulsion ($f = 21$ ft^2) was subtracted from the faired curve of the test data. A test weight of 33,000 pounds was conservatively assumed for this calculation, even though most of the high-speed test data shown were obtained at about 26,000 pounds. The resulting corrected power coefficient ratio data are shown to substantiate the reference data for the forward rotor for advance ratios of 0.12 to the highest advance ratio tested in reference 14, 0.28. Below an advance ratio of 0.12, the forward rotor requires considerably less power than this reference indicates, except in hovering, where the results again are identical. For the aft rotor, the power

required is considerably less than reference data indicate at all advance ratios tested, except for three points obtained at 37,000 pounds test weight. It is believed that this difference in performance between the two-blade teetering rotors of the model and the flight test data may be due to the induced power advantages of more blades. Reduced sensitivity of the full-scale rotor blades to the disturbances of the tandem rotor downwash may also reduce c_{do} for the full-scale test data.

The effects of sideslip on performance are shown in Figure 95. Minimum aft rotor torque is shown to exist at about -5 degrees (nose-right) sideslip. This appears to be due either to an induced power advantage or to reduced rotor profile power resulting from having the advancing blades operating in less disturbed air. At 80 knots, there is also a small performance advantage to flying with nose-right sideslip.

The effect of variations in longitudinal cyclic trim setting on required rotor power is shown in Figure 96. With small extensions of the cyclic trim, the forward rotor power increases, indicating that more propulsive force is being provided by the forward rotor. Extension of the trim to about 2 degrees forward and aft causes essentially no change in fuselage attitude. Larger extensions of trim cause significant changes in attitude which shift the propulsive force requirement onto the aft rotor. This is shown by an increase in the aft rotor torque and a decrease in the forward rotor torque. The effect of increased cyclic trim in causing a shift of the propulsive force to the aft rotor is somewhat substantiated by the rotor thrust measurements obtained by integrating the steady airload pressures. The following data from flight 390 show that the forward rotor thrust remains constant with trim and the aft rotor thrust varies as follows:

Trim Setting		Aft Rotor Thrust per Blade
Forward	Aft	(Pounds)
-3°	-5°	5720
-2°	-2°	5520
-1°	-1°	5210

The instrumentation provided to indicate the steady trim of the aircraft was either unreliable at best or completely inadequate. Figure 96 shows the effect of longitudinal cyclic trim setting on trim and illustrates the scatter in the data. Surprisingly, the fuselage angle-of-attack vane, which was expected to give

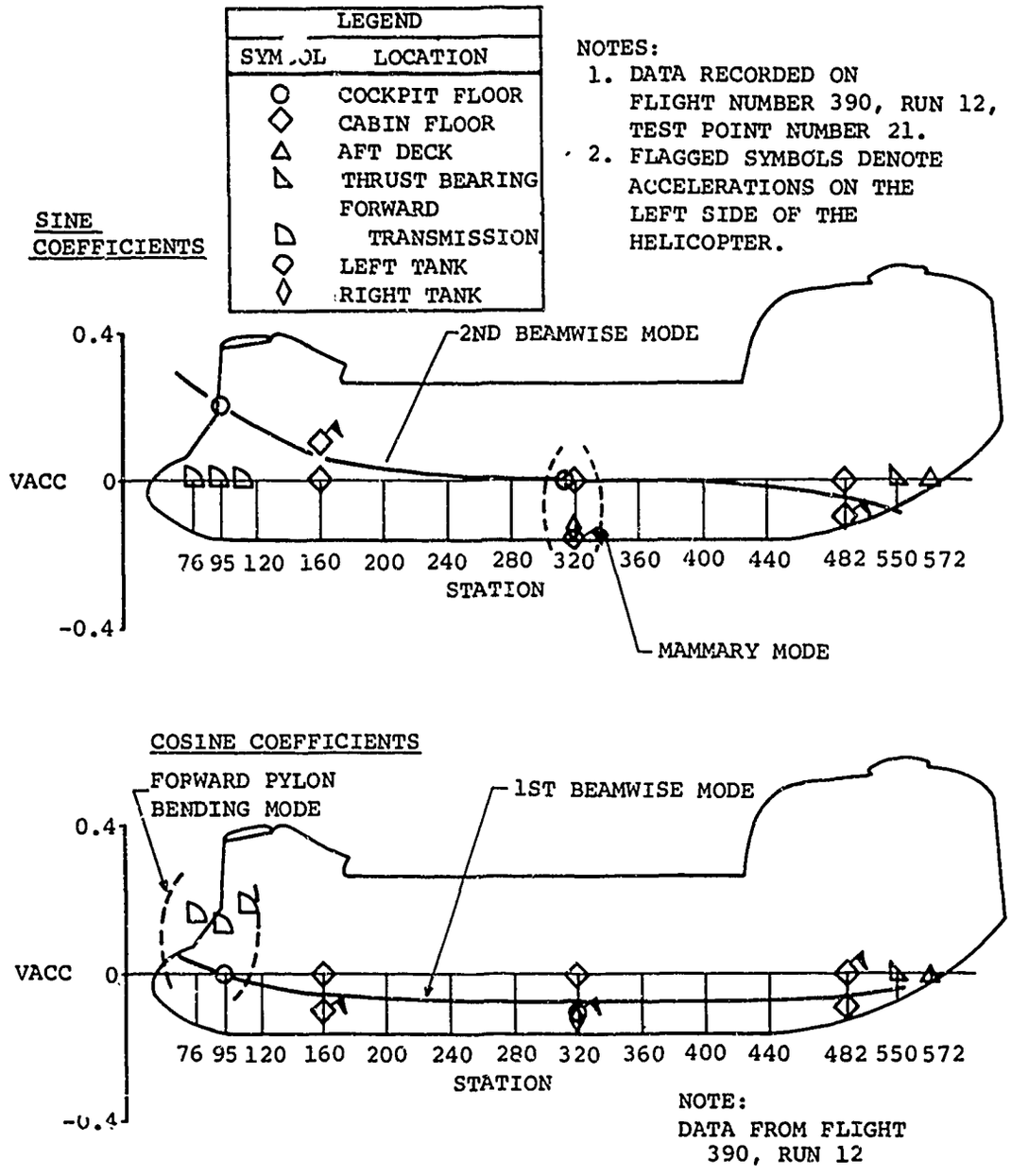

Figure 93. Vertical Third Harmonic Vibration Amplitude Distribution in Test Aircraft.

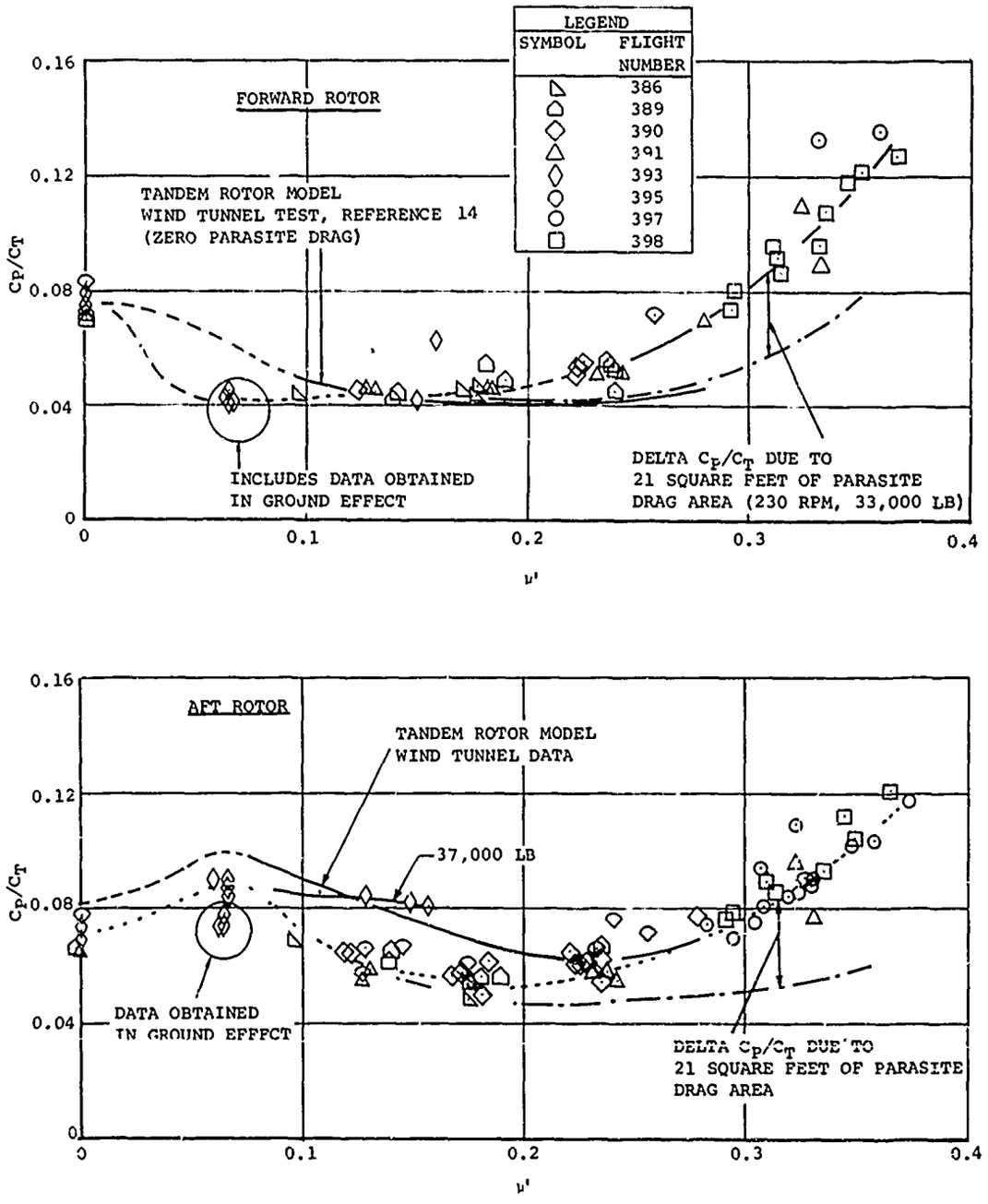

Figure 94. Nondimensional Rotor Performance of Test Aircraft.

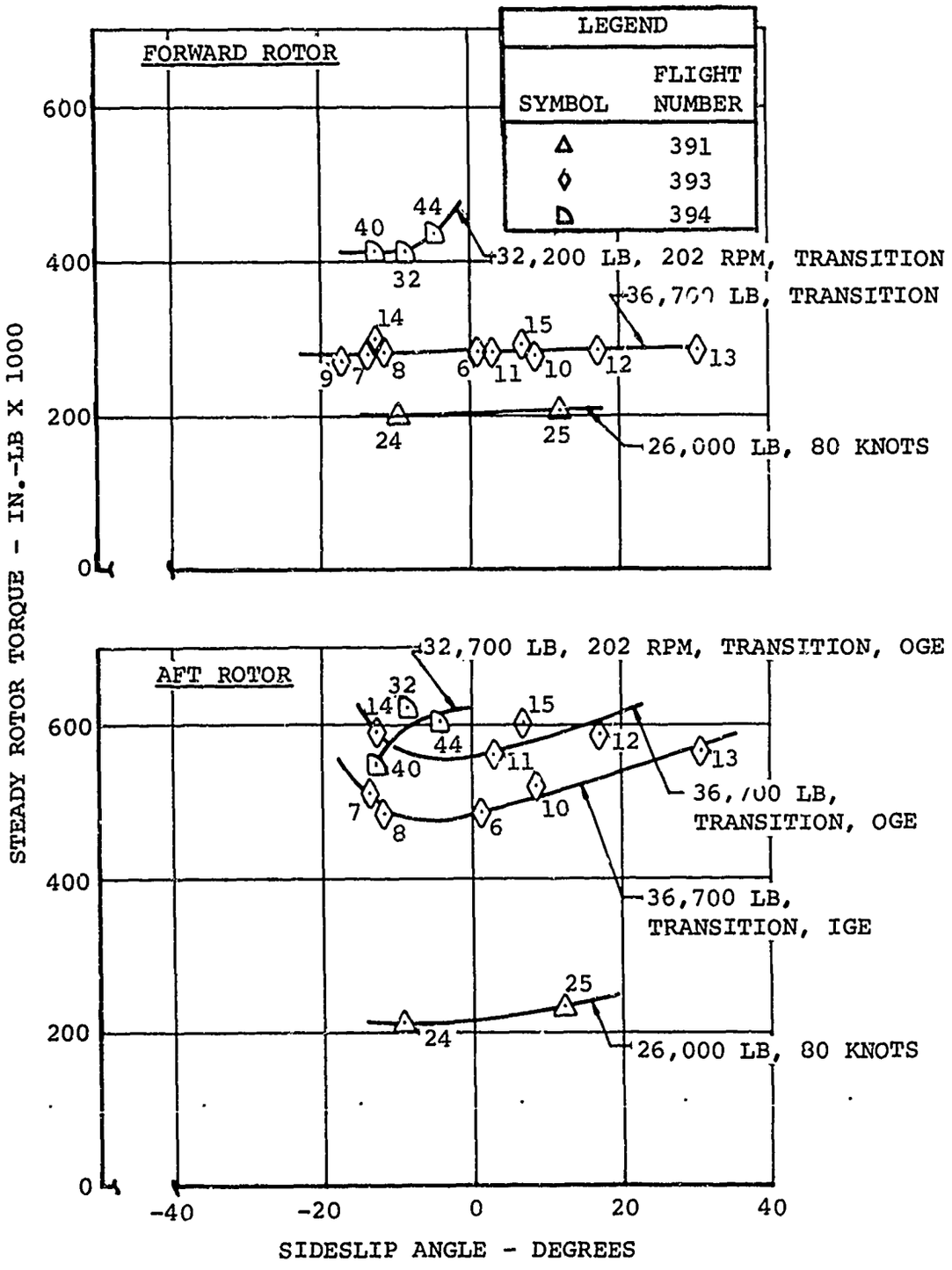

Figure 95. Effect of Sideslip on Performance in Transition and at 80 Knots.

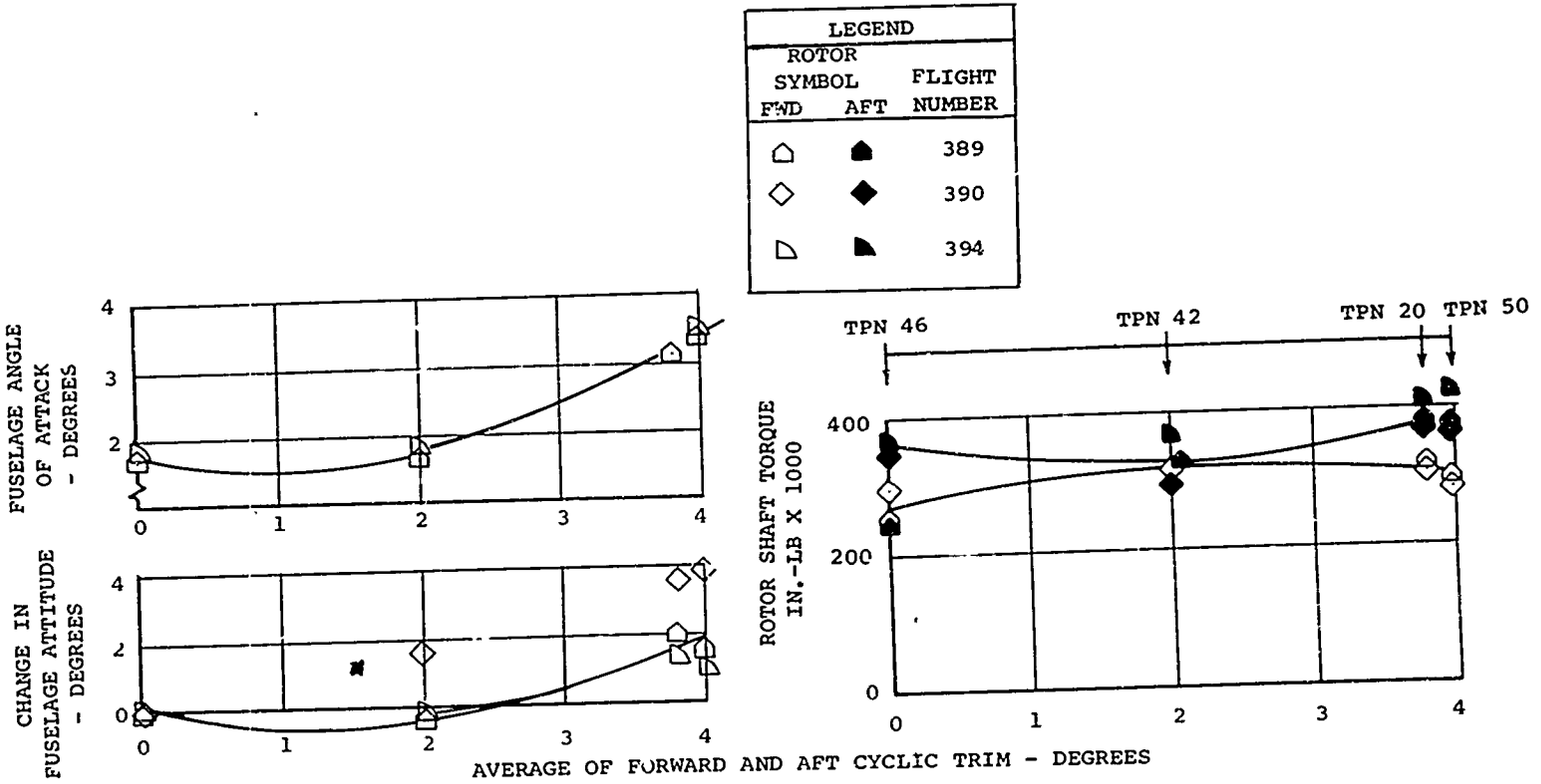

Figure 96. Effects of Longitudinal Cyclic Trim Setting on Trim and Performance at 100 Knots for a Gross Weight of 33,000 Pounds.

relatively poor results due to nose boom bending, gave consistent and repeatable results. Figure 96 shows about a 1.7-degree change in attitude (nose-up) resulting from an average change in cyclic trim of 4 degrees. It should be noted that the nonlinear effect of cyclic trim on fuselage attitude results from the geometry of the tandem rotor helicopter.

The fuselage attitude data shown in Figure 96 were prepared as the changes in attitude from zero trim settings. This should have eliminated preflight calibration errors and most of the drift; however, as shown in the figure, the data contain scatter of about ±2 degrees and are almost worthless. It is suggested that these data be used only for review of the maneuver data, since the scatter is about 50 percent of the usually expected 4-degree variations of fuselage attitude in level flight.

Similar poor results are also shown by the rotor collective (steady) pitch measurement . Typical data for level flight at 33,000 pounds gross weight are shown in Figure 97. Variations between flights of 1 to 1-1/2 degrees are shown. Within a given flight, the data are fairly consistent, with a similar spread shown between test points. For instance, note that for the aft rotor, test points 53 and 54 give essentially identical results for each flight. These data are believed to indicate a trend and could be of value on a statistical basis; however, use of these data for single-point analytical trim comparisons would be difficult and of questionable value.

BLADE FLAPPING

Blade lag and flap hinge angles were measured, and good quality data were obtained. Lag motions of the blades are generally of secondary interest, and therefore no lag motion data were prepared for this report. These data are, of course, available in the data report. Blade flap angle data are illustrated and are compared to the flap hinge airload moment data.

The rotor blade coning angle measurements, indicated by the azimuthal average (steady) flap angle, were normalized to 230 rpm and were divided by the run gross weight per rotor. As shown in Figure 98, these data are unusually consistent. There are some local variations in the data due to trim setting, and there is a rather gentle decrease with airspeed from zero to 80 knots followed by a gentle increase with airspeed above 80 knots. This trend is more pronounced for the forward rotor, which may be due to the previously mentioned inward shift of the forward

rotor lift when the airspeed is increased from hover. It appears that there are about 0.5×10^{-5} degrees per pound of scatter in this normalized coning data; this scatter is equivalent to about 0.2 degree at 33,000 pounds.

The first harmonic longitudinal blade flapping is generally of predominant interest, since this angle defines the rotor tip path plane inclination. These data were corrected for cyclic trim and normalized by the thrust coefficient-solidity ratio. It is expected from uniform downwash-linear aerodynamic rotor theory that the resulting normalized control axis flapping will vary linearly with advance ratio. As shown in Figures 99 and 100, these data show a linear variation with a slope, $\partial\beta_{ALC}/\partial\mu'$, of 260 C_{TW}/σ on the forward rotor and 290 C_{TW}/σ on the aft rotor. The theoretical variation with uniform downwash rigid blades but with nonlinear aerodynamics is shown to have a smaller initial slope than the test data; however, at higher advance ratios, this theory shows a nonlinear variation and gives a prediction almost identical to the test data. These data also show variations due to trim setting, etc., and may have about 1 degree of scatter.

It is interesting to compare the blade flap hinge angle measurements to the moment about the flap hinge calculated from an integration of the airload pressures. This data comparison for the first harmonic resultants is shown in Figure 101. The ratio of the phase angles of the moment and the response is shown to be nearly unity (one). This was unexpected, since a 90-degree phase shift was expected. It is believed that the lack of a phase shift is due to the inclusion of the flap damping as well as the flap excitation in the airload measurements. The increase in the phase angle ratio with airspeed may be indicative of the decrease in flap damping due to advance ratio effects. These data also contain blade bending effects which may be significant.

The first harmonic response-moment ratio data of Figure 101 show considerable differences between the two rotors. Aft rotor data show a large increase in the response-moment ratio as the airspeed is increased from zero to 60 knots, followed by an equally steep decrease at higher airspeeds. Since the blade first harmonic flapping is not unusually high in this speed range, as shown in Figure 100, these data indicate that the first harmonic flapping moment decreases. This effect may be indicative of an increased significance of the higher harmonics and may help to explain the high vibration of the tandem

rotor helicopter in this speed range. The forward rotor response-moment data are shown to be consistent and to systematically decrease with airspeed.

Similar second harmonic flap response-flap moment data are shown in Figure 102 to be considerably different from the first harmonic data. The response-moment ratio is shown to increase with airspeed to 60 knots and then decrease for both rotors, but with a larger increase on the forward rotor. The phase angle ratio is shown to vary significantly with airspeed for both rotors with a value of about 0.25 at low speed, shifting between 60 and 100 knots to a value of about 2.5 at higher speeds.

The third harmonic flap response-flap moment data are shown in Figure 103. Due to the proximity of the third harmonic to the first mode bending natural frequency, these data were expected to be quite irregular. However, the aft rotor data are unexpectedly consistent and vary systematically with airspeed. The forward rotor data show a very large response-moment ratio in transition and at high speed. The phase angle ratio is more irregular for the aft rotor data.

The preceding rather limited data presentations are considered to be for-instance plots of typical data. It is believed that these data support the conclusions presented and provide a starting point for further analysis. It has been shown that most of the data have the repeatability and consistency expected and that other data have excessive scatter. Further evaluations of the data will be made in the next section of this report, which also contains a summary critique of the measurements.

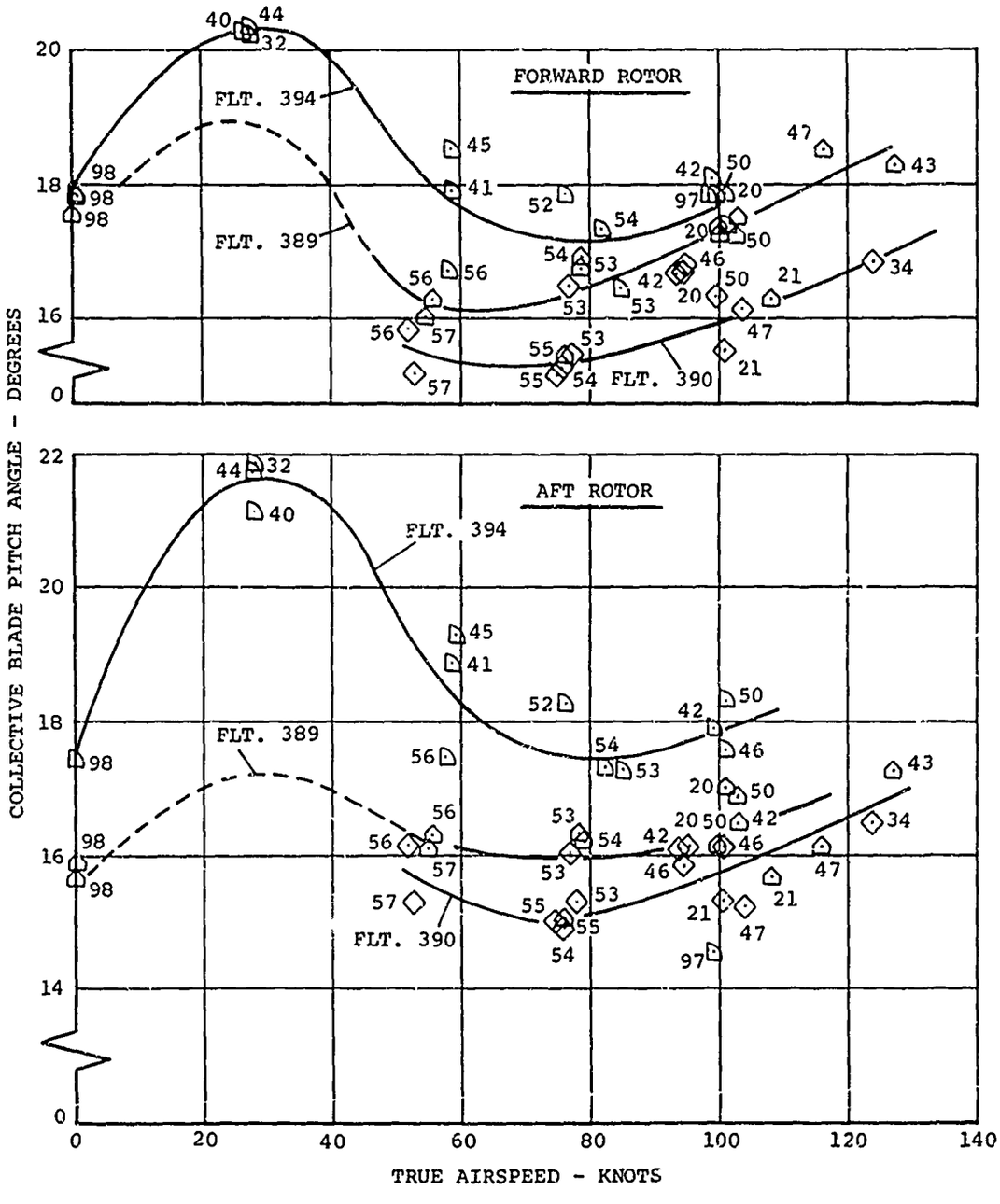

Figure 97. Collective Pitch Settings Required in Level Flight at a Gross Weight of 33,000 Pounds.

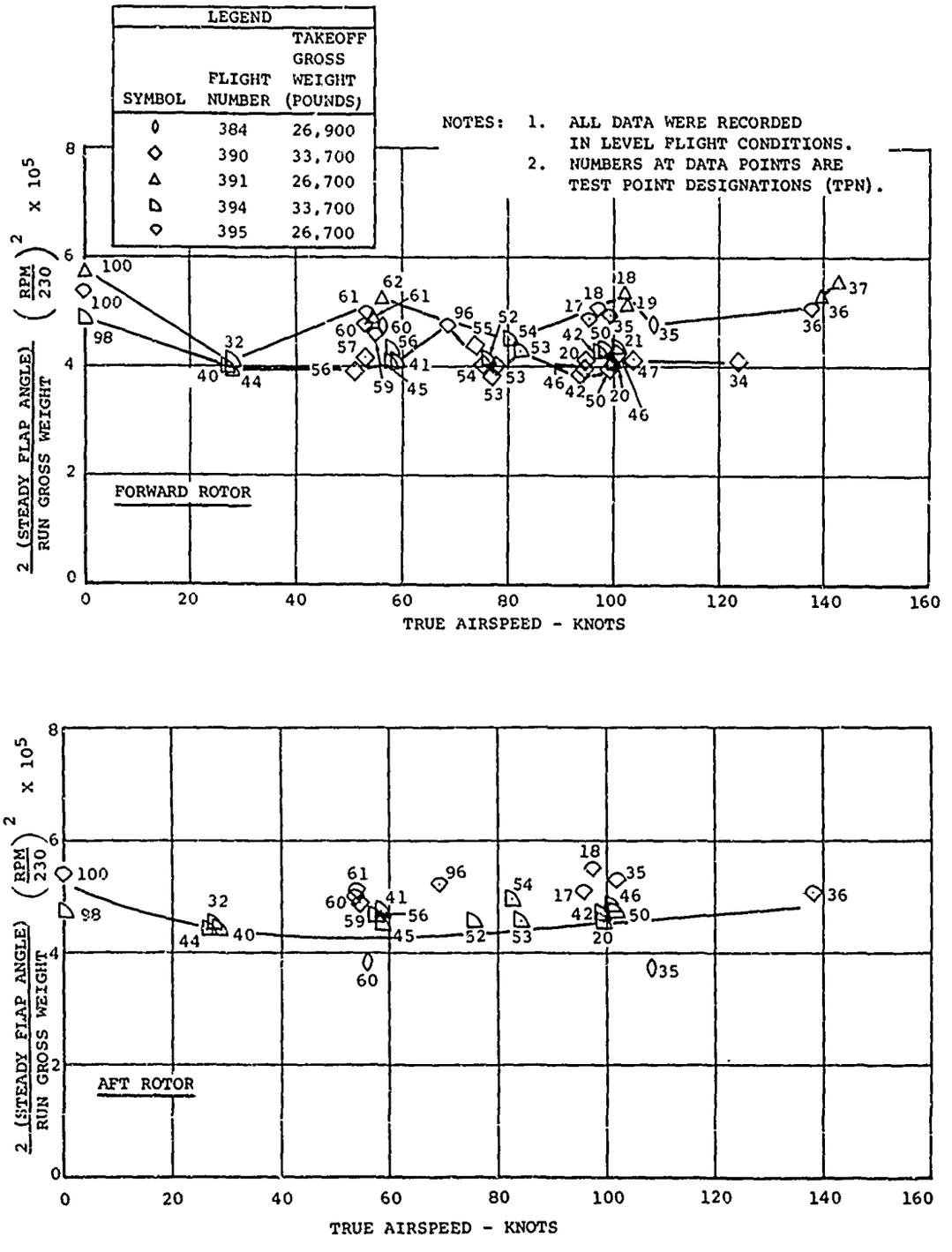

Figure 98. Variation of Normalized Blade Coning Angle with Airspeed.

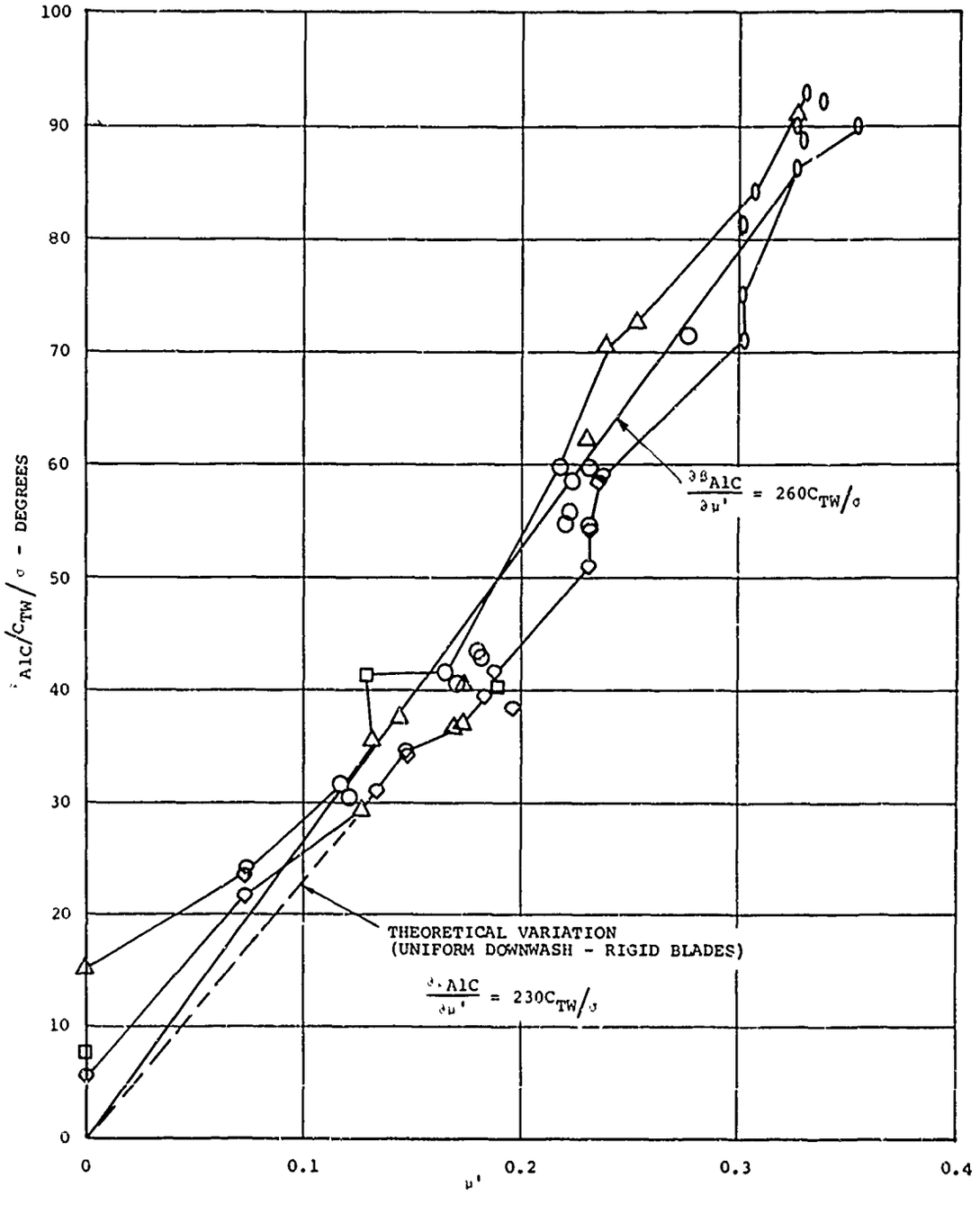

Figure 99. Normalized First Harmonic Longitudinal Blade Flapping with Respect to the Control Axis for the Forward Rotor.

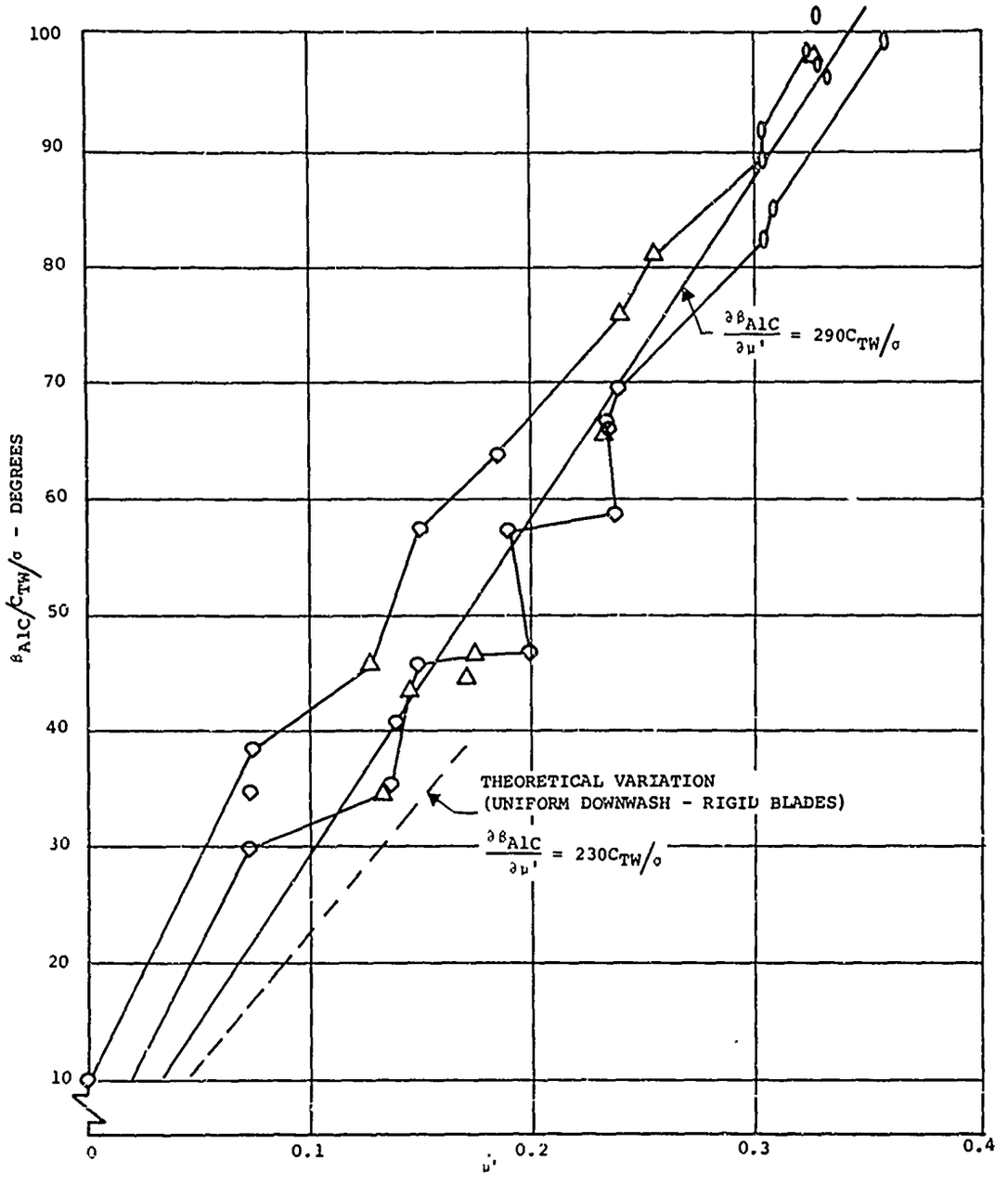

Figure 100. Normalized First Harmonic Longitudinal Blade Flapping with Respect to the Control Axis for the Aft Rotor.

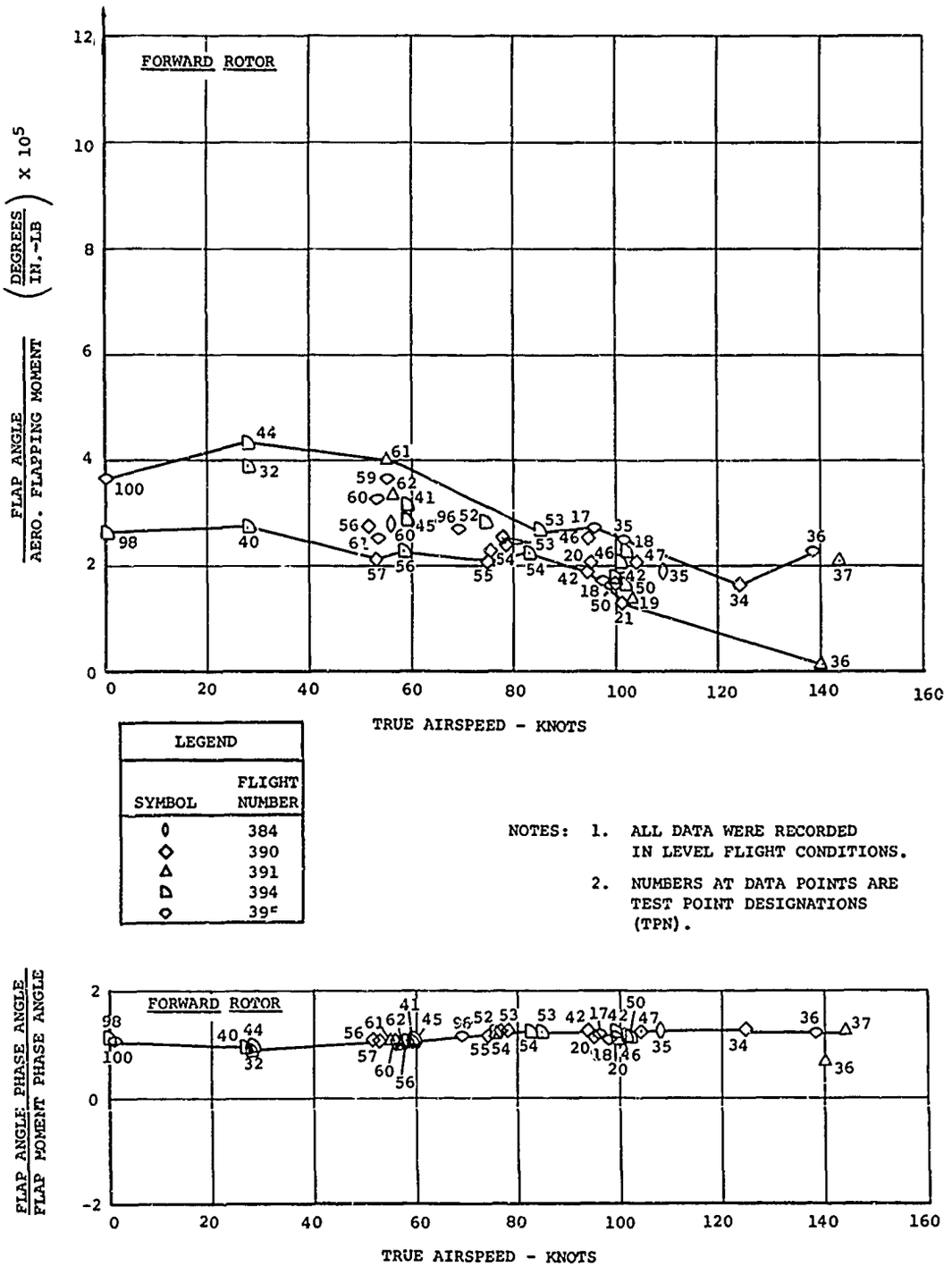

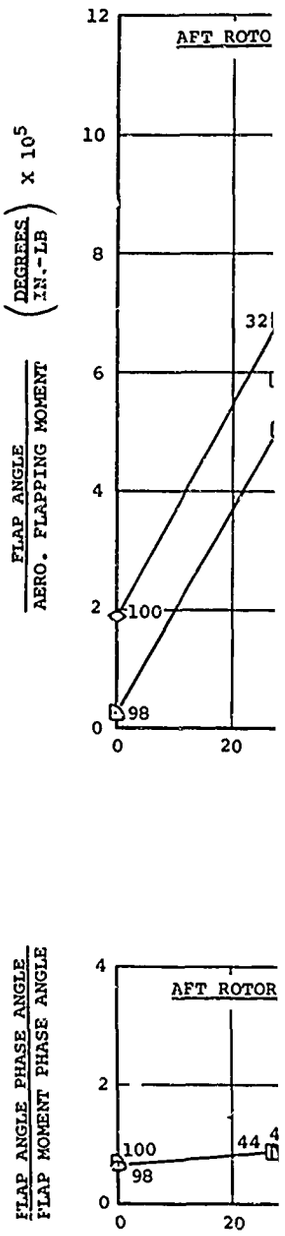

Figure 101. Comparison of Blade Flap Motion to First Harmonic Flapping Moment Airloads Data.

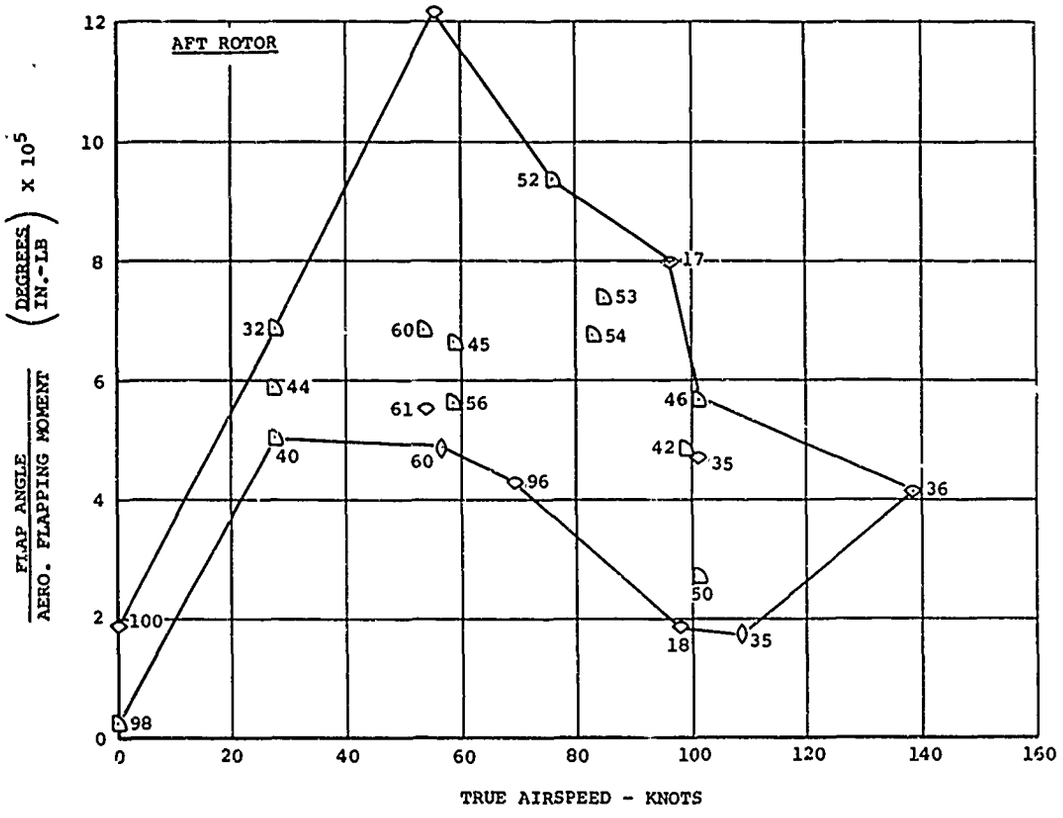
AFT ROTOR
FLAP ANGLE / AERO. FLAPPING MOMENT (DEGREES / IN.-LB) X 10^5
TRUE AIRSPEED - KNOTS

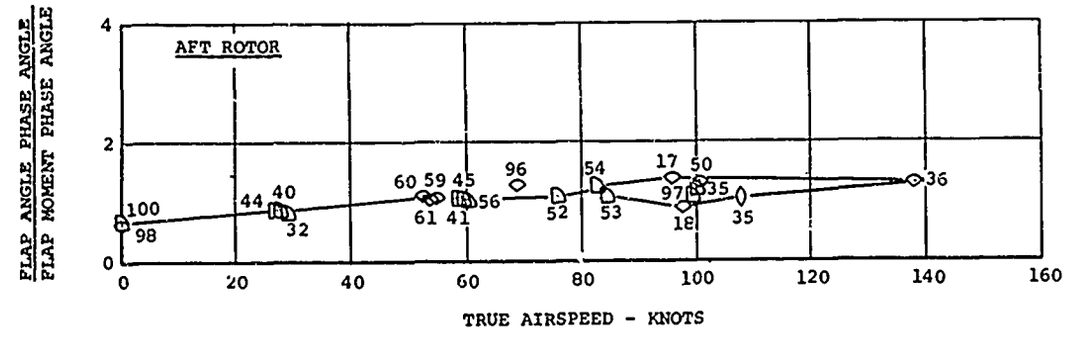
AFT ROTOR
FLAP ANGLE PHASE ANGLE / FLAP MOMENT PHASE ANGLE
TRUE AIRSPEED - KNOTS

Harmonic

B

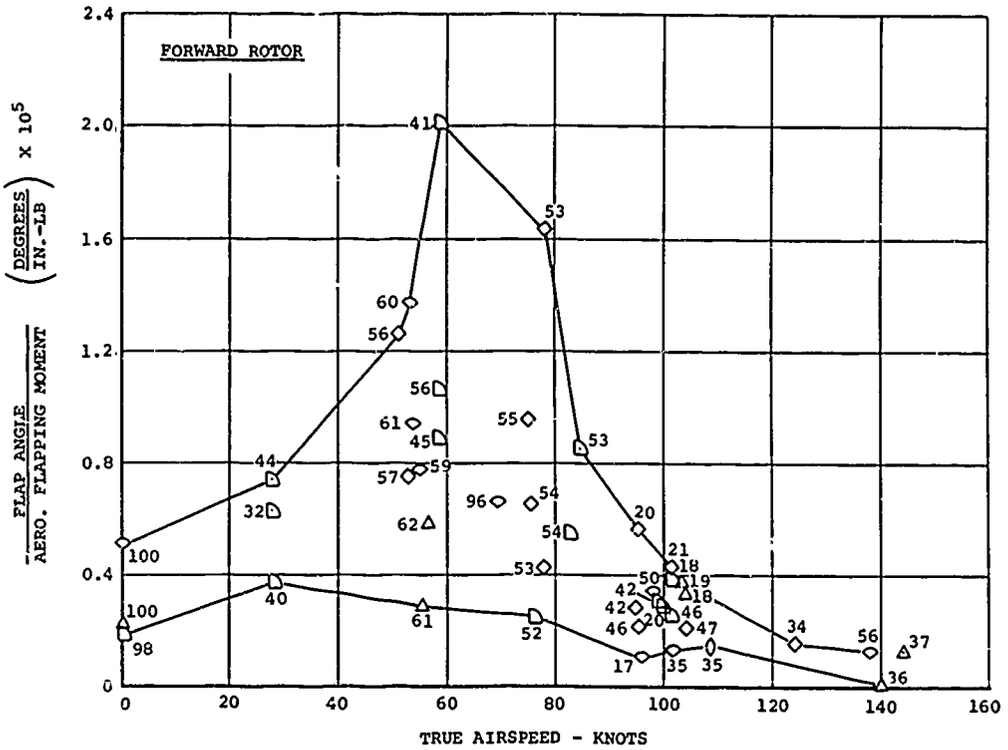

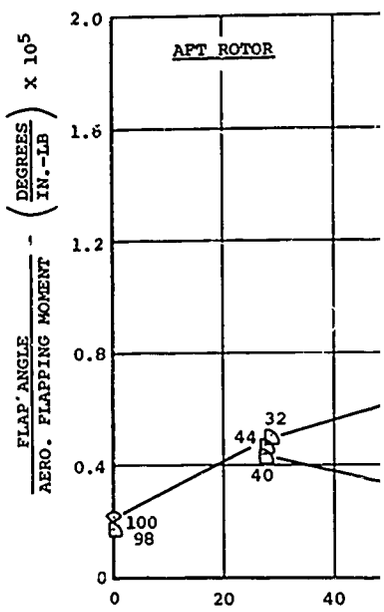

LEGEND	
SYMBOL	FLIGHT NUMBER
◊	384
◇	390
△	391
▷	394
○	395

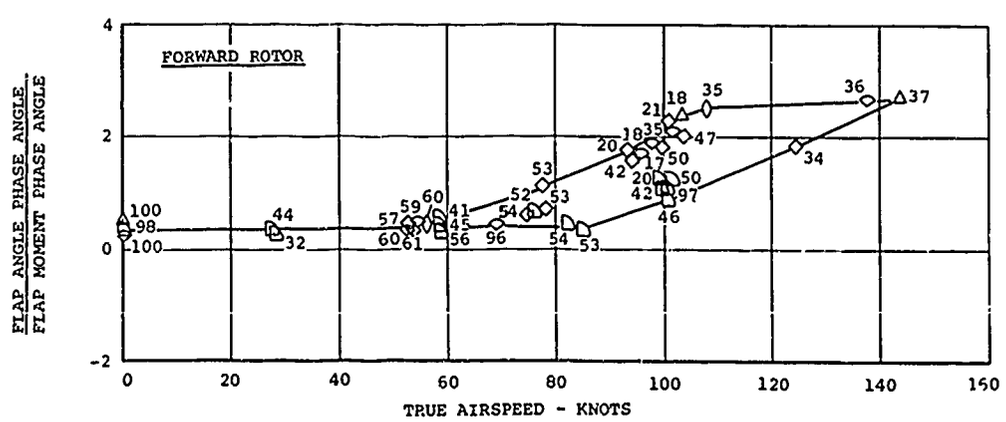

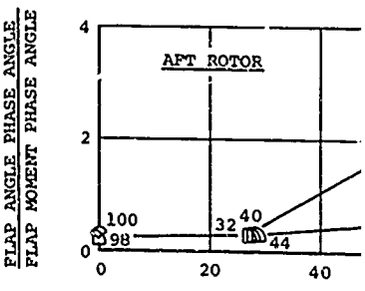

Figure 102. Comparison of Blade Flap Motion to Second Harmonic Flapping Moment Airloads Data.

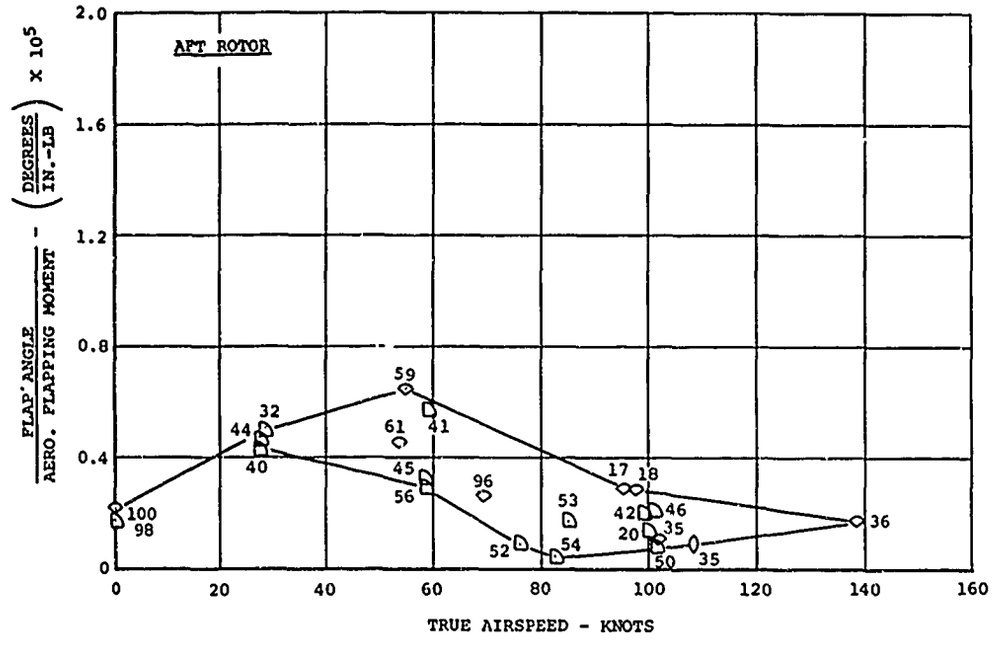

NOTES: 1. ALL DATA WERE RECORDED IN LEVEL FLIGHT CONDITIONS.

2. NUMBERS AT DATA POINTS ARE TEST POINT DESIGNATIONS (TPN).

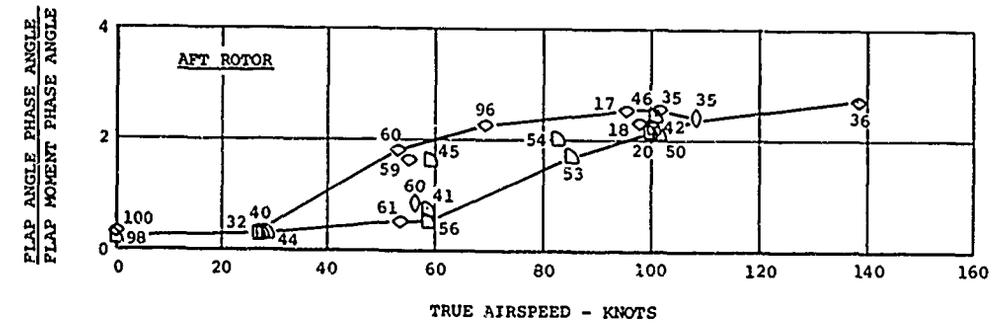

Second Harmonic

B

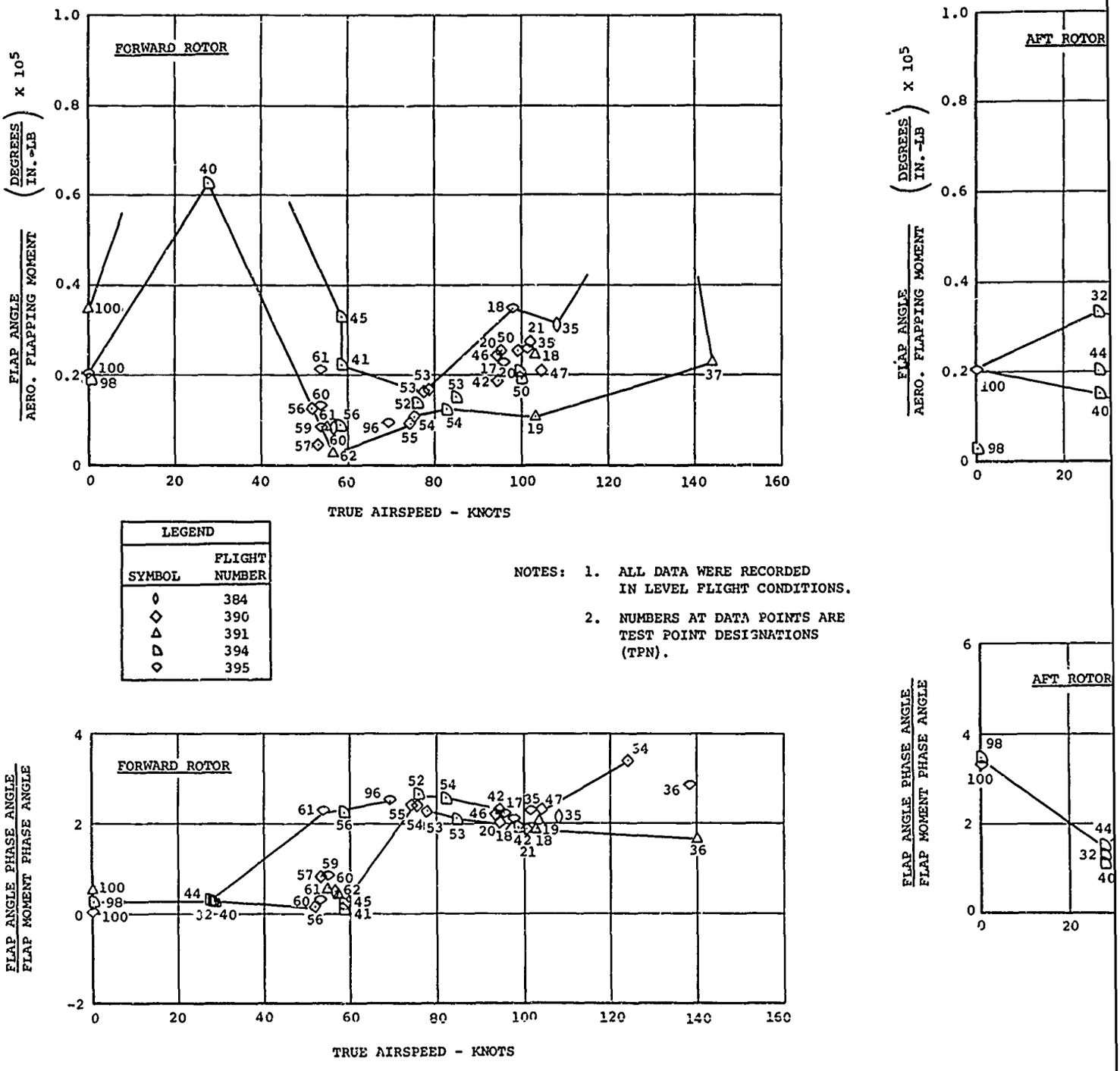

Figure 103. Comparison of Blade Flap Motion to Third Harmonic Flapping Moment Airloads Data.

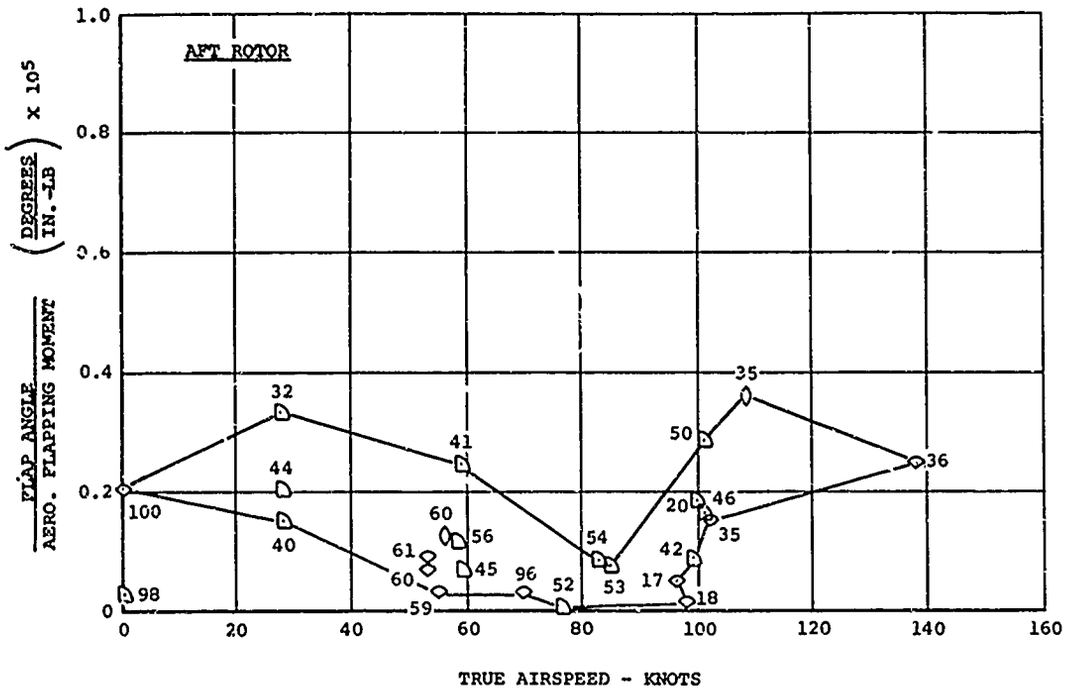

CORDED
CONDITIONS.

POINTS ARE
NATIONS

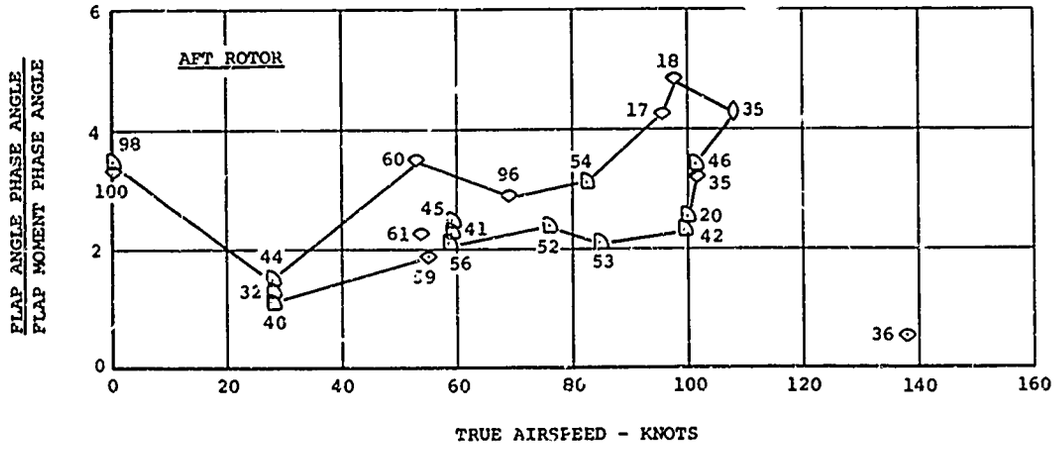

160

160

n to Third Harmonic

EVALUATION AND ANALYSIS OF RESULTS

The preceding data presentations gave some indication of the quality of the data, and further evaluations of the data are made in this section. Theoretical comparisons and comparisons with the experimental results from other programs are presented. A tabular summary of this data critique is presented, giving a quantitative evaluation whenever possible, and at least giving a subjective judgment of the quality of the results.

THEORETICAL COMPARISONS

In this section, comparisons with theoretical predictions are made with the blade airloads, collective pitch, and rotor torque data. Of these data, the airloads are considered to be most important and thus are emphasized.

A sampling of the azimuthal average airload pressures at the 85-percent radius is compared to the theoretical chordwise pressure distribution in Figure 104. The test data shown were selected for having been obtained within 10 knots of 70 knots and within 0.5 degree of 5 degrees Centigrade outside air temperature. The theoretical pressure distribution shown was obtained from reference 1 and is known to compare well with airfoil wind tunnel test data at small angles of attack, low Mach number, and full-scale Reynolds numbers. The azimuthal averaged rotor data generally meet these criteria except that the average Mach number (≈ 0.5 at $r/R = 0.85$) is rather high. However, the comparison shown in the figure is poor, with leading edge pressures higher than predicted and balanced by low pressures on the trailing 70 percent of the chord. It should be noted that, with this form of presentation, the low pressures at 37-, 65-, and 80-percent chord tend to make the other pressures appear too high. The data shown were integrated using straight lines (triangles and trapezoids) so that the low pressures made the lift per unit span (LS-L) low. Since even the low pressures were fairly repeatable between flights, it was decided to use the forced-fit integration method described previously to integrate the steady airloads pressure data. With this method, the low average pressures do not greatly affect the average lift or pitching moment data, and the signals contribute normally to the oscillating loads. These low average pressures could have resulted from the transducer mounting procedure which produced irregularities in the airfoil shape. The transducer mounting recesses could have caused systematic local low pressure regions. Another possible reason for the low value of the trailing edge pressures is the very low

electrical output of these transducers. Consistent measurement of the output that these transducers produced at an average pressure of 0.5 psid is unlikely. For these reasons, the forced-fit integration method was adopted, and it is believed that this method eliminated the effects of these average pressure errors from the airload data. In the general evaluation of the data, however, the pressure measurements are shown in Figure 104 to have about 0.5 psid error in the uncorrected azimuthal average value.

A comparison of the variations of two local-pressure-to-local-lift ratios with the advancing blade tip Mach number is shown in Figure 105. These data show consistent systematic data for many flights, with the pressure ratio increasing with advance ratio at the 2-percent chord and decreasing with advance ratio at the 37-percent chord. This variation is apparently a compressibility effect and is as predicted by the von Karman-Tsien transonic airfoil theory. This theory indicates that, prior to the formation of a shock, the larger differential-pressure values will get relatively larger with increased Mach number. These pressure ratios compare favorably with the incompressible theoretical pressure distribution values of reference 1 at the low Mach numbers associated with low advance ratios. This comparison is believed to indicate that the airload pressure data are consistent and believable.

The credibility of the airloads data is further supported by comparison with the predicted airloads from an aeroelastic nonuniform downwash rotor analysis, reference 12. Figure 106 shows a comparison of two blade stations for one test condition. The waveform of the airloads is shown to be predicted with reasonable accuracy; however, the predicted airloads tend to have greater irregularities than the test data for the aft rotor. Due to the limitations of the theory for predicting rotor-rotor interference, the average loadings at the blade stations are not predicted except at 85-percent radius of the aft rotor. This comparison is believed to indicate that the integrated airload pressures produce lift-per-unit-span data with adequate response and believable waveforms. The lack of comparison with the azimuthal average lift is due to failings of the theory and not the data.

A comparison of the azimuthally averaged airload lift measurements and a second rotor analysis is shown in Figure 107. This second theory, reference 6, has a more rigorous nonuniform downwash analysis but assumes rigid blades. As shown, the azimuthal average airload of the forward rotor is not predicted by

the theory. The loading over the inboard region is shown to be higher than predicted and is balanced by lower loading outboard on the blade. It is believed that this average rotor loading distribution is due to the upwash at the forward rotor caused by the aft rotor, which is neglected by the theory. Reference 13 shows that there is an upwash caused by a rotor which could be of sufficient magnitude to cause this effect.

The local velocity predictions of the reference 6 theory have been used to calculate normal force coefficients from the airload measurements. Figure 108 shows these airload coefficients plotted against the theoretical angle of attack. The azimuthal average coefficient is not predicted by the theory and has been suppressed. The resulting comparison is shown to be reasonably good. As compared to the essentially linear variation of the theoretical coefficients, the test data are shown to be concave upward and have significant bumps near 90 and 220 degrees azimuth. The concave upward shape is believed to be due to the rigid blade assumption of the theory. The bumps are believed due to tip vortex proximity effects which are more pronounced than predicted. Again, these differences are as expected and tend to support the measurements.

Comparison of the collective pitch data to the predictions of the uniform downwash-rigid blade theory confirms the conclusion reached previously that these data show excessive scatter. This comparison is shown in Figures 109 and 110 for the forward and aft rotors. Statistically, the theory appears to underestimate the collective pitch required by about 1 degree; however, the ± 1 degree of scatter shown does not give confidence in the data. These data should not be used for further analyses.

The rotor performance as indicated by the rotor torque measurements has been compared to a uniform downwash-rigid blade rotor analysis (reference 7), and the results are shown in Figure 111. This figure shows that the scatter in the data is about ± 8 percent for the forward rotor and ± 14 percent for the aft rotor. It should be noted that this comparison is based on calculations for the nominal test conditions and not the actual test conditions. Since the test points were generally within 2 knots of the requirement, and since the altitude was generally low but within 2000 feet of the requirement, this comparison is believed to be valid. However, some of the scatter shown is probably due to these differences. This comparison is believed to substantiate the measured torque values, which are probably nearly within the ± 3 percent estimated from the instrumentation

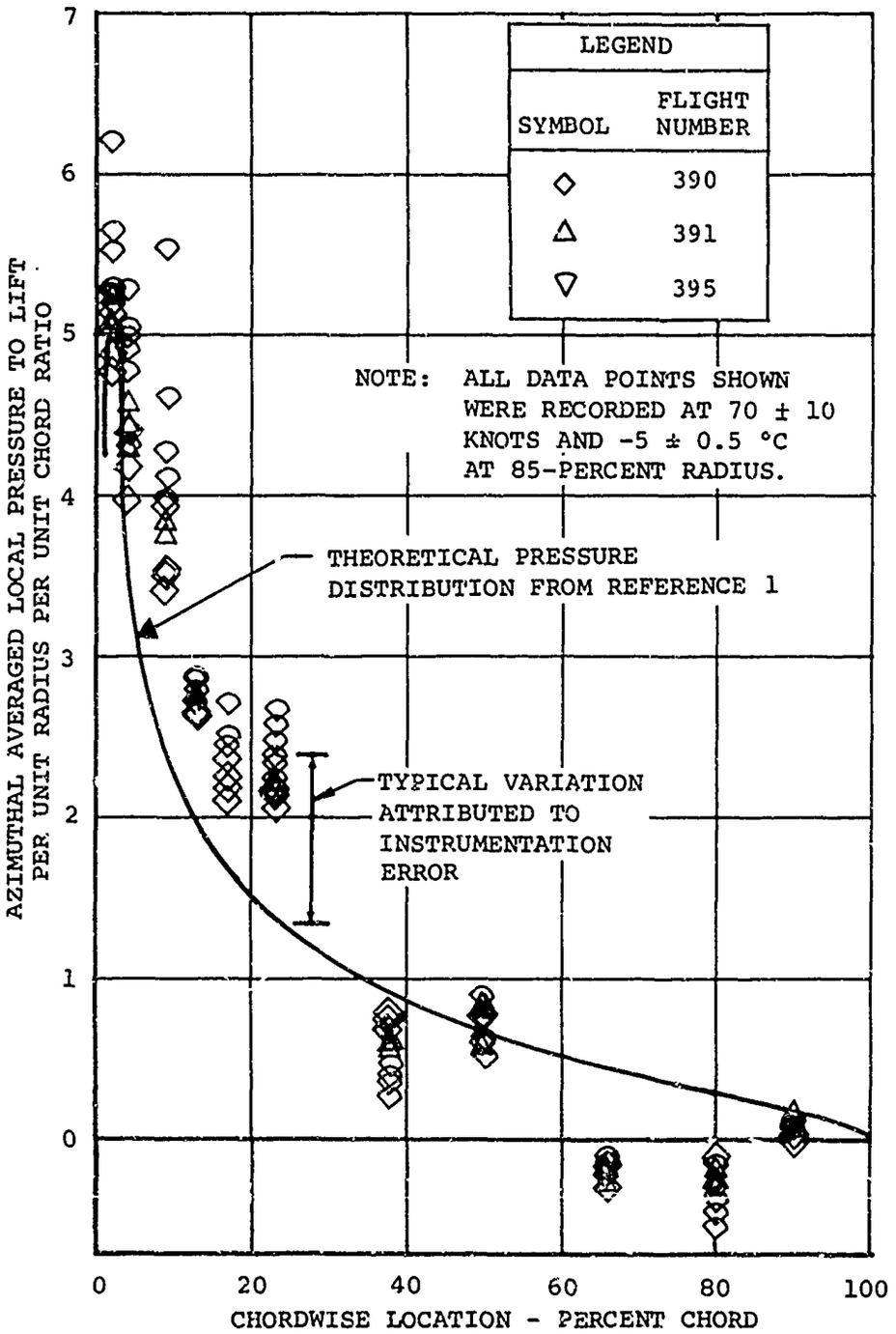

Figure 104. Comparison of Typical Azimuthal Averaged Airload Pressures with Theoretical Airfoil Pressure Distribution for Steady Motions.

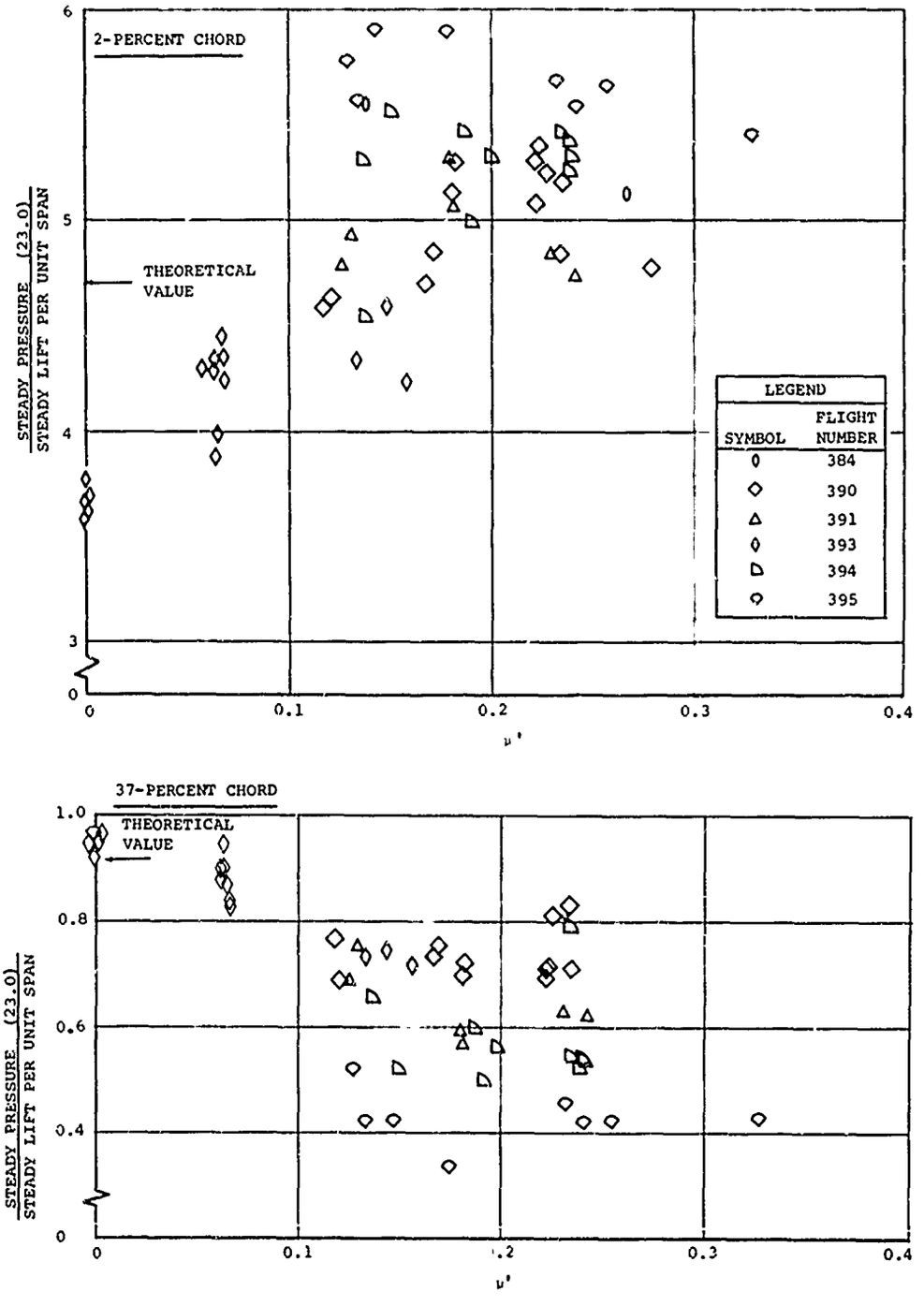

Figure 105. Effect of Advance Ratio on Typical Nondimensional Airload Pressures at 85-Percent Radius of the Forward Rotor.

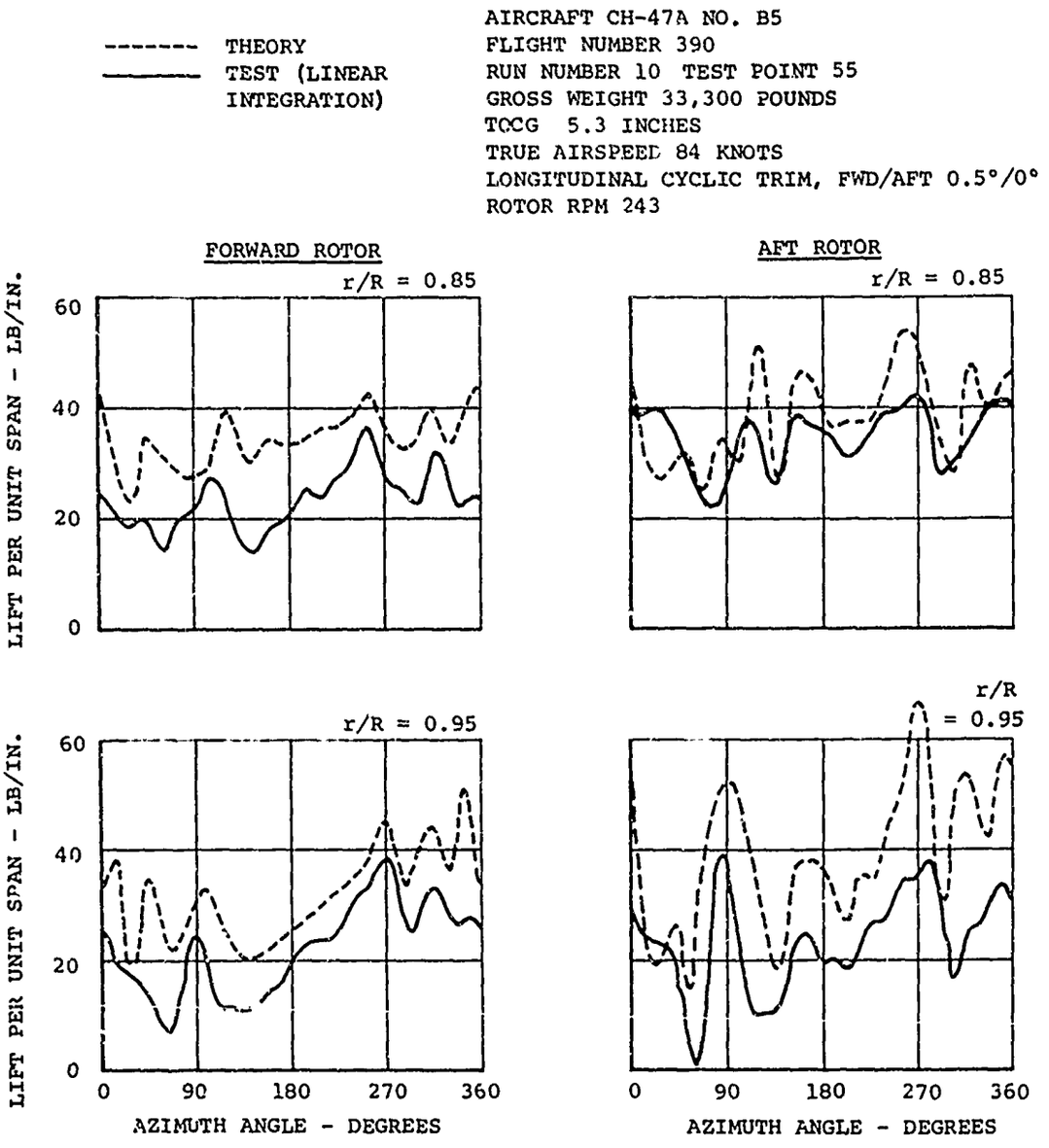

Figure 106. Initial Comparison of Lift-per-Unit-Span Data with Aeroelastic Nonuniform Downwash Rotor Analysis.

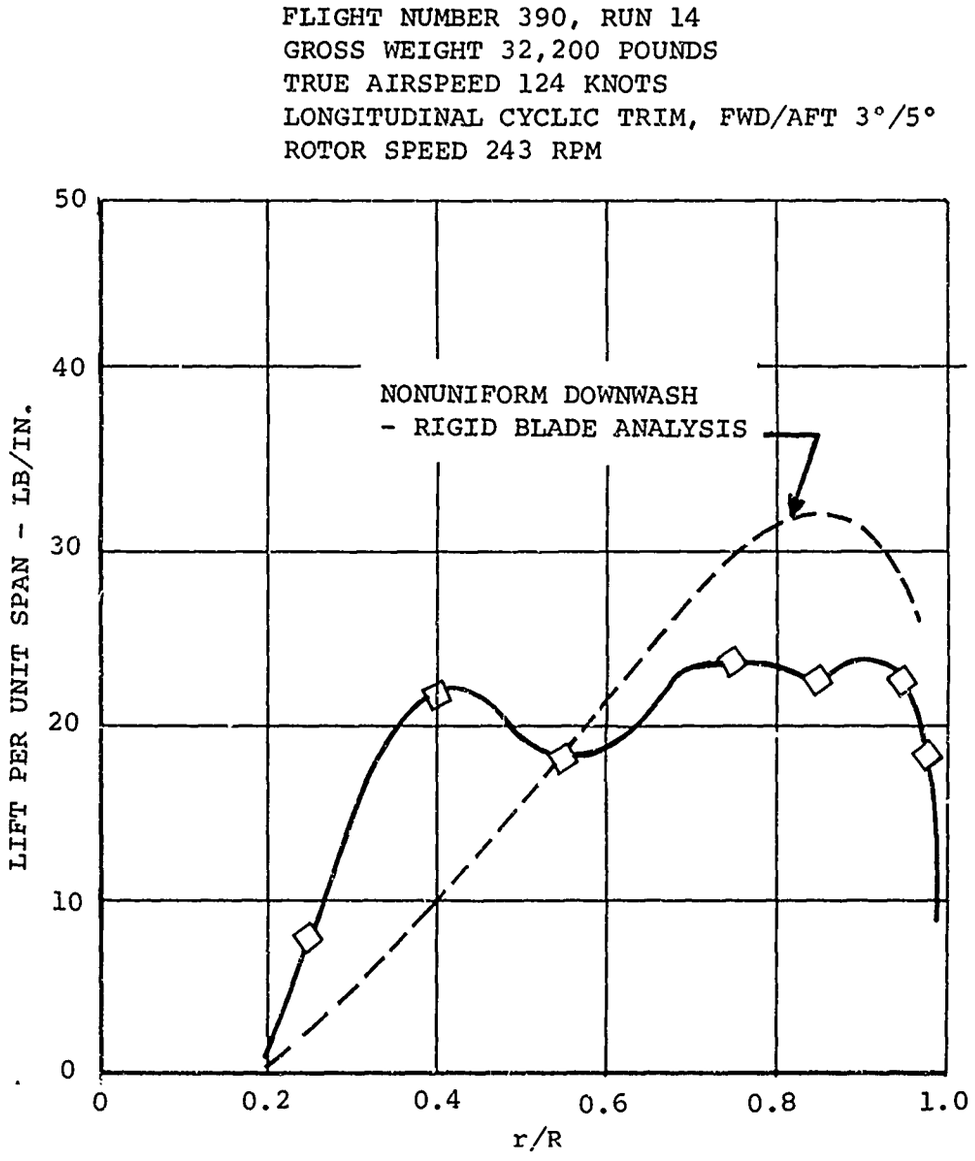

Figure 107. Comparison of Theoretical and Measured Average Loading of Forward Rotor.

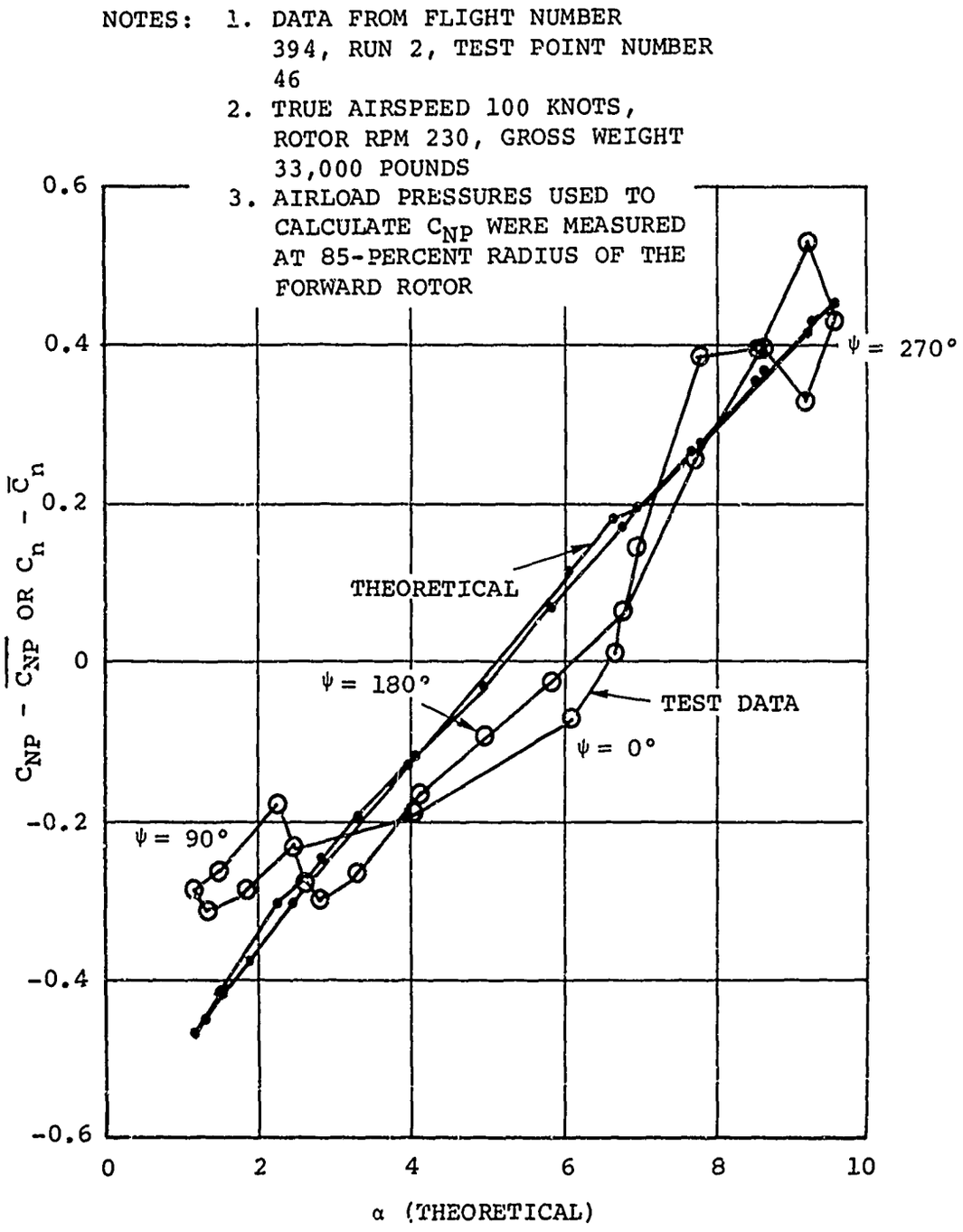

Figure 108. Initial Comparison of Normal Force Coefficient Data to Theoretical Prediction of Rigid Blade Nonuniform Downwash Analysis.

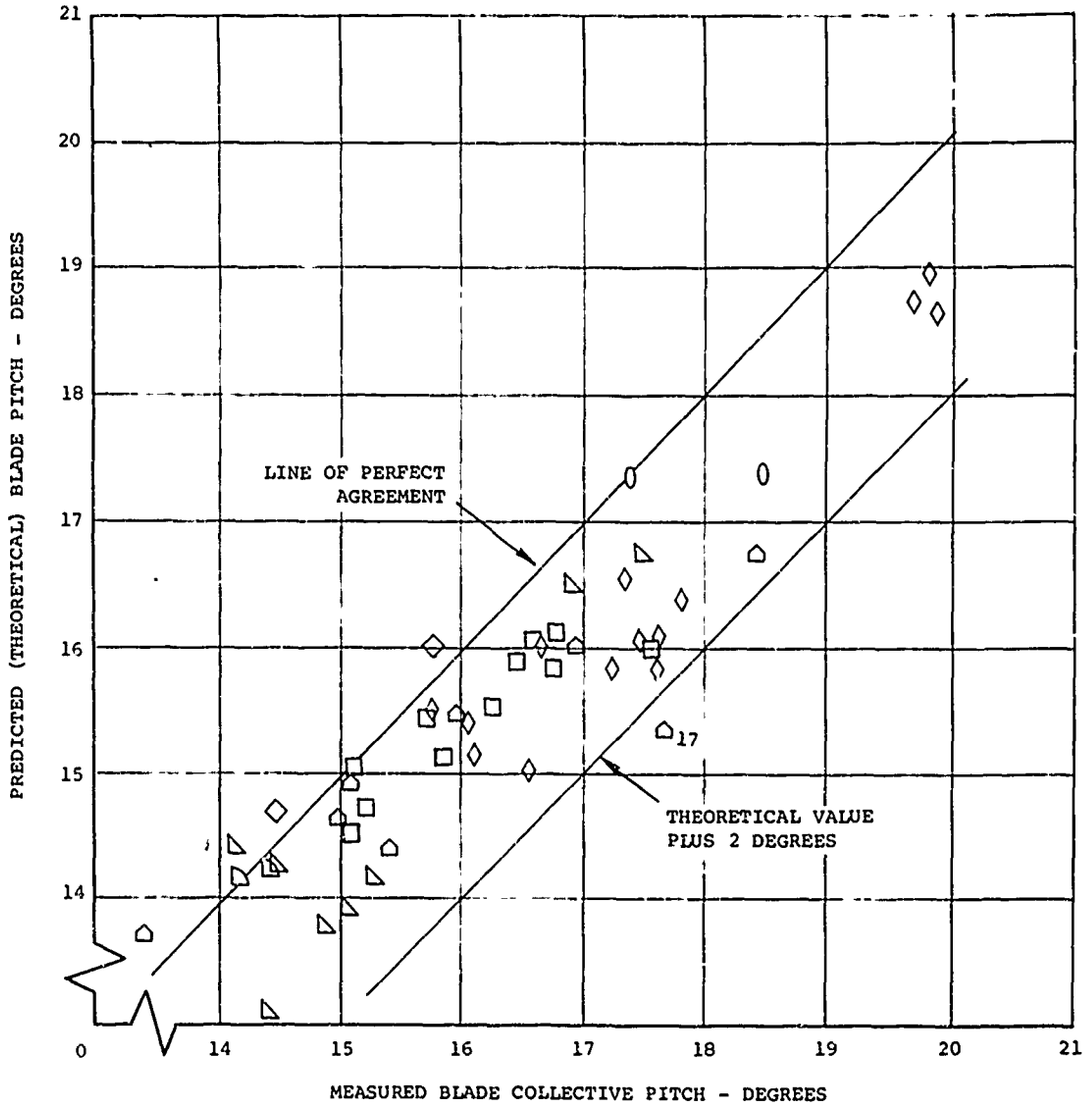

Figure 109. Comparison of Theoretical and Measured Collective Pitch Values for Forward Rotor.

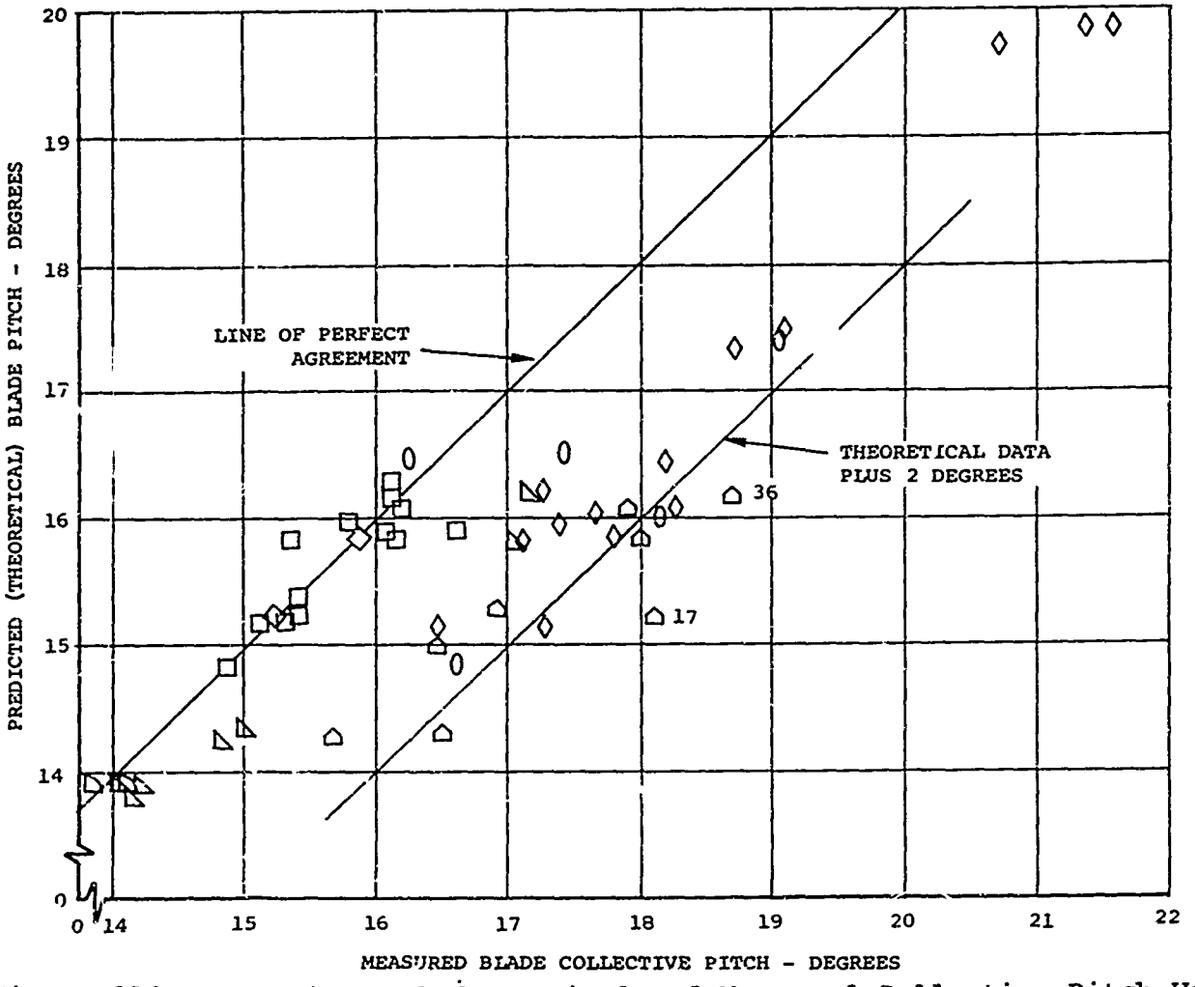

Figure 110. Comparison of Theoretical and Measured Collective Pitch Values for Aft Rotor.

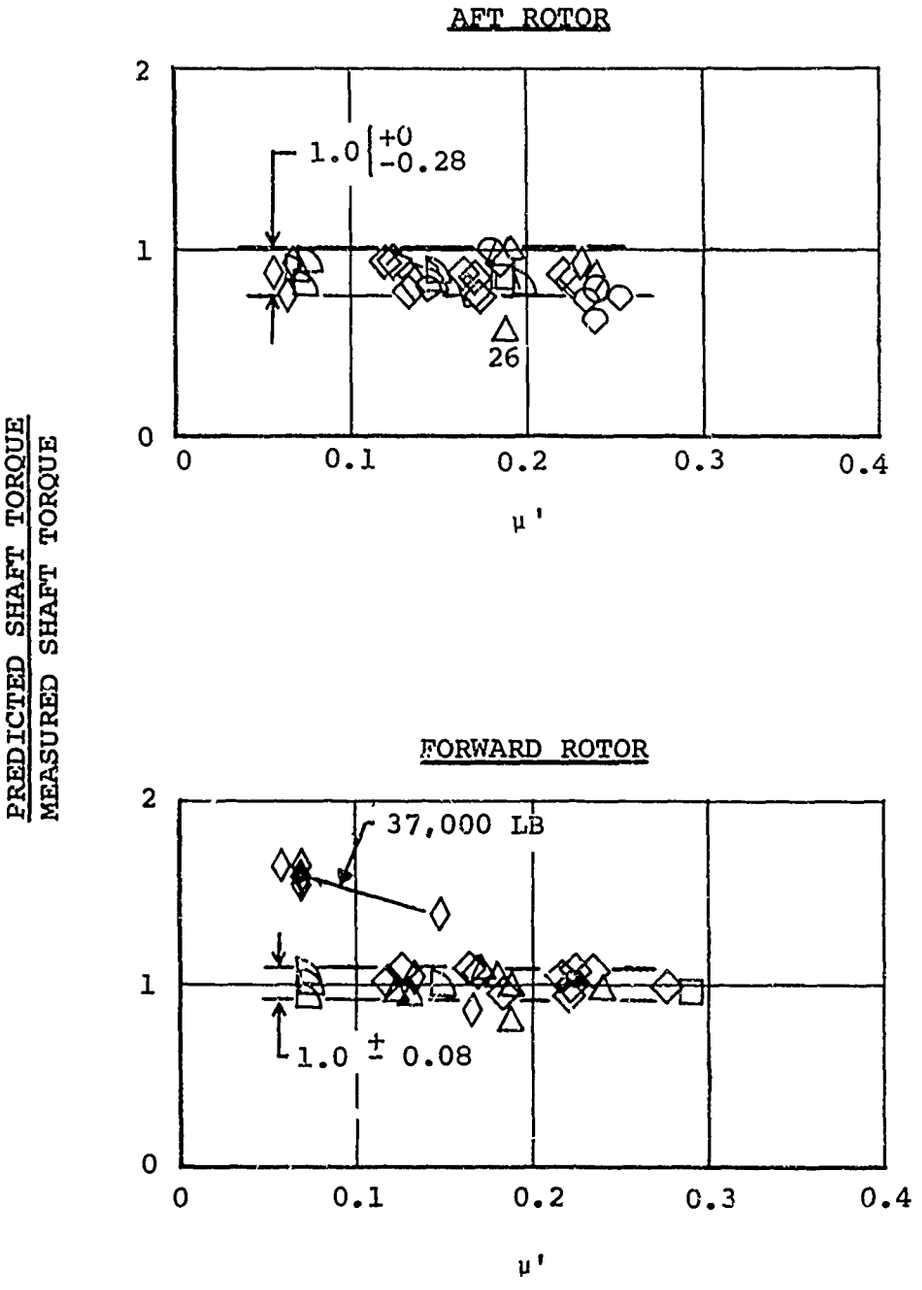

Figure 111. Effect of Advance Ratio on Prediction of Rotor Shaft Torque by Uniform Downwash-Rigid Blade Analysis.

design. It appears, however, that the theory predicts too large a torque for the forward rotor at high gross weight (37,000 pounds) and predicts too small a torque for the aft rotor throughout the speed range.

The theoretical comparisons made in this section are believed to be typical of what can be expected from the data of this program. It is believed that it is necessary to make a rather large sampling of any of these data to determine typical values before any detailed comparisons are performed. It is believed that the present data validation effort has eliminated the spurious readings due to instrumentation malfunctions; however, it is possible that some of the test points obtained are not consistent due to transient accelerations or nonlevel flight during data acquisition. Therefore, single test point comparisons should be avoided.

COMPARISON WITH DATA FROM OTHER PROGRAMS

There is now a considerable body of rotor airloads data acquired in flight and in wind tunnel tests, and many comparisons of these data are possible. Comparative tests at an airspeed of about 110 knots are available from the two-bladed single rotor flight test data of references 2 and 3, from the four-bladed single rotor flight test data of reference 27, and from wind tunnel data of reference 23, as well as from the presently reported tandem rotor airloads data. The parameters of the test conditions compared are given in Table V. The chordwise pressure distributions at about the 85-percent radius are shown for various azimuth angles in each of the four quadrants of the rotor disk in Figures 112 through 115. As expected, the two-bladed rotor has the largest chordwise pressure irregularities on the advancing blade. This rotor had a large lift per foot of blade, which is a reasonable measure of tip vortex strength, and also had the largest advancing blade tip Mach number. Further, the data shown were obtained at near 90-percent radius for the two-bladed rotor, and the blades of this rotor were of 15-percent thickness rather than the 11- to 12-percent thickness of the other rotors. Since the blades move into the proximity of the vortex trailed from the preceding blade on the advancing side of the disk, rather large angle-of-attack variations are imposed which, due to the relatively high Mach number, result in a significant disturbance of the chordwise pressure distribution. The two-bladed rotor data show definite signs of a compressibility shock at about 25 percent of the chord for azimuth positions of 60 to 120 degrees. The four-bladed rotor wind tunnel test

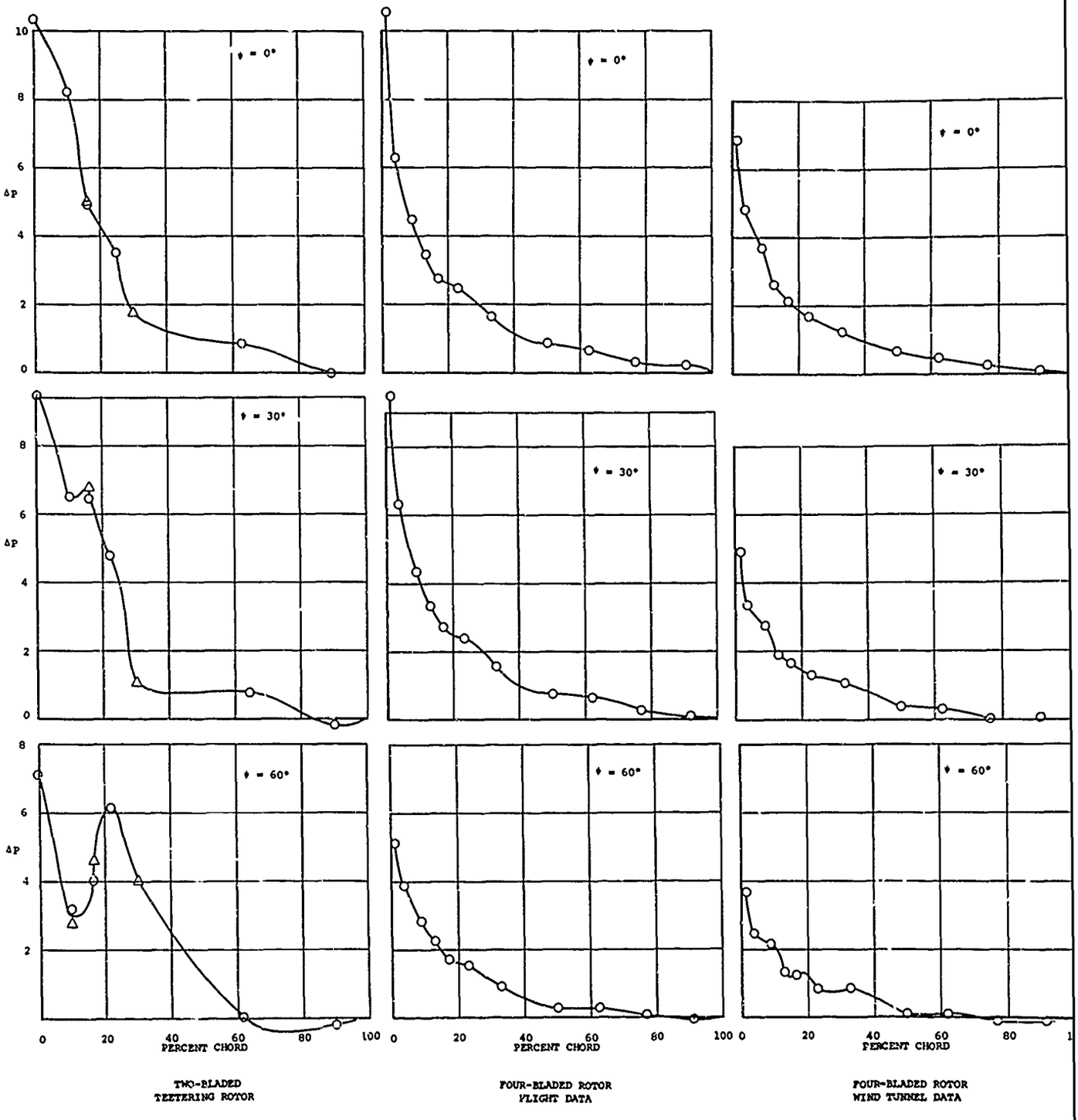

Figure 112. First Quadrant Chordwise Airload Distributions as Measured Near 110 Kn Airloads Measurement Programs.

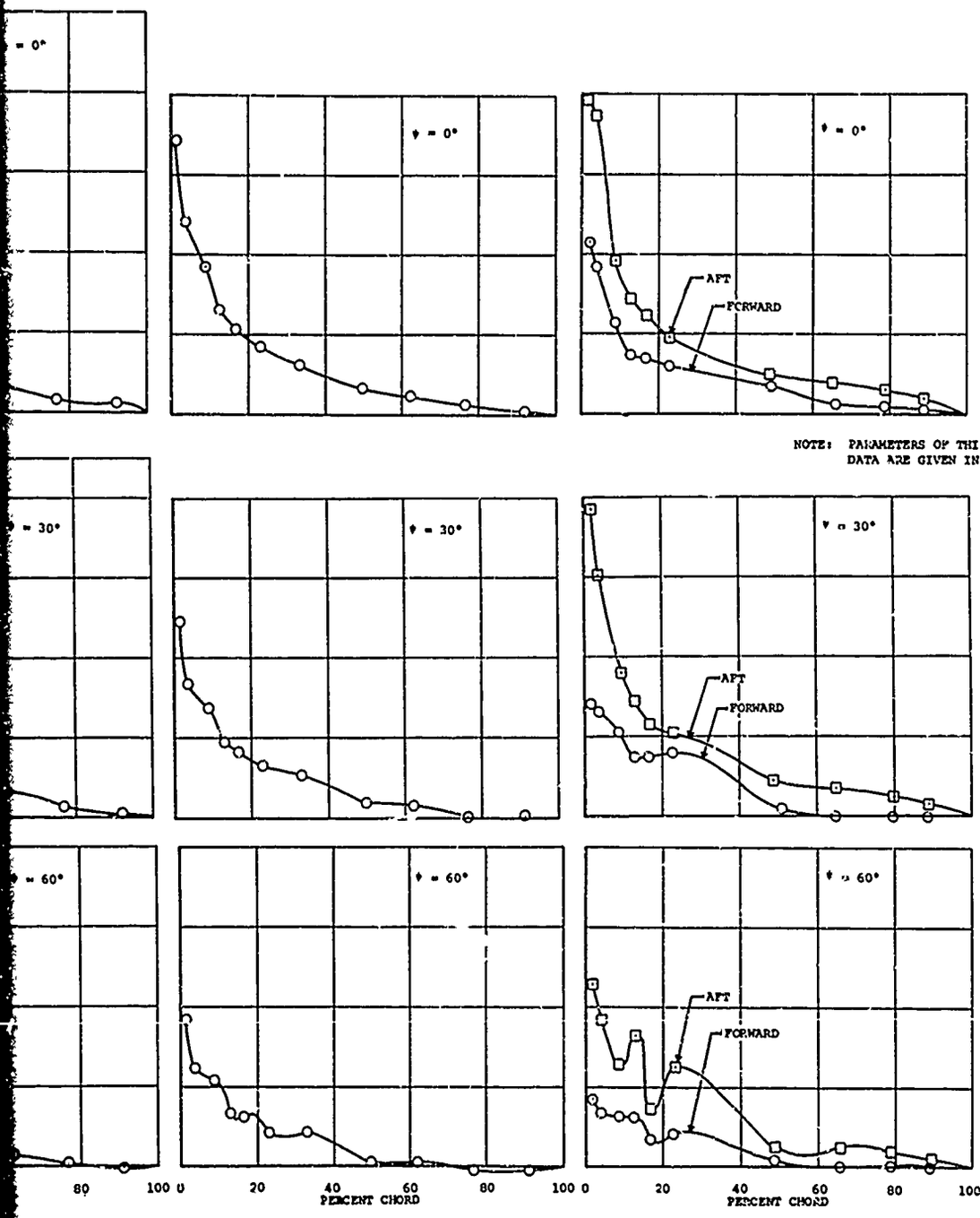

istributions as Measured Near 110 Knots in Four Similar Full-Scale

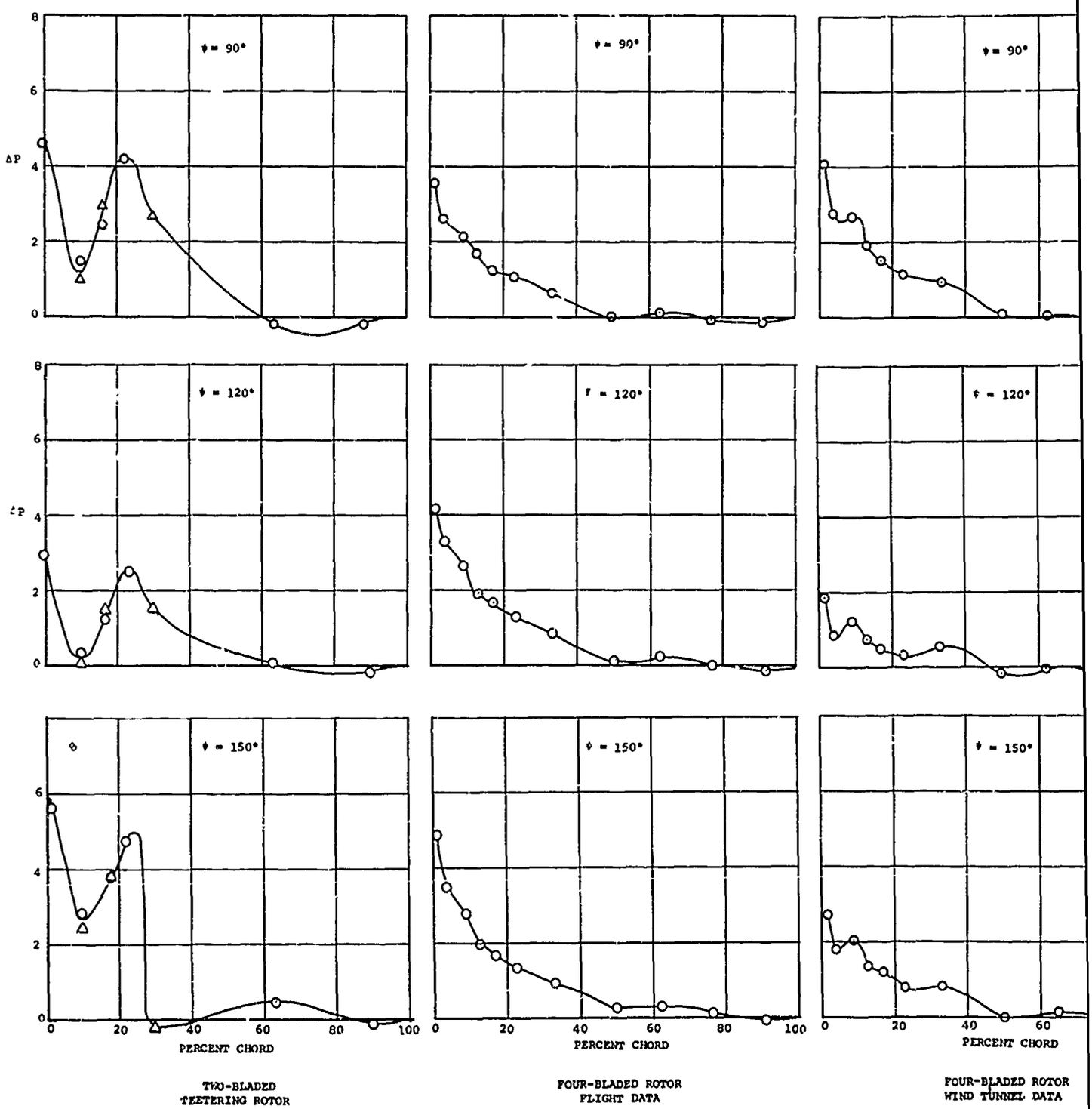

Figure 113. Second Quadrant Chordwise Airload Distributions as Measured Near 110 K Airloads Measurement Programs.

A

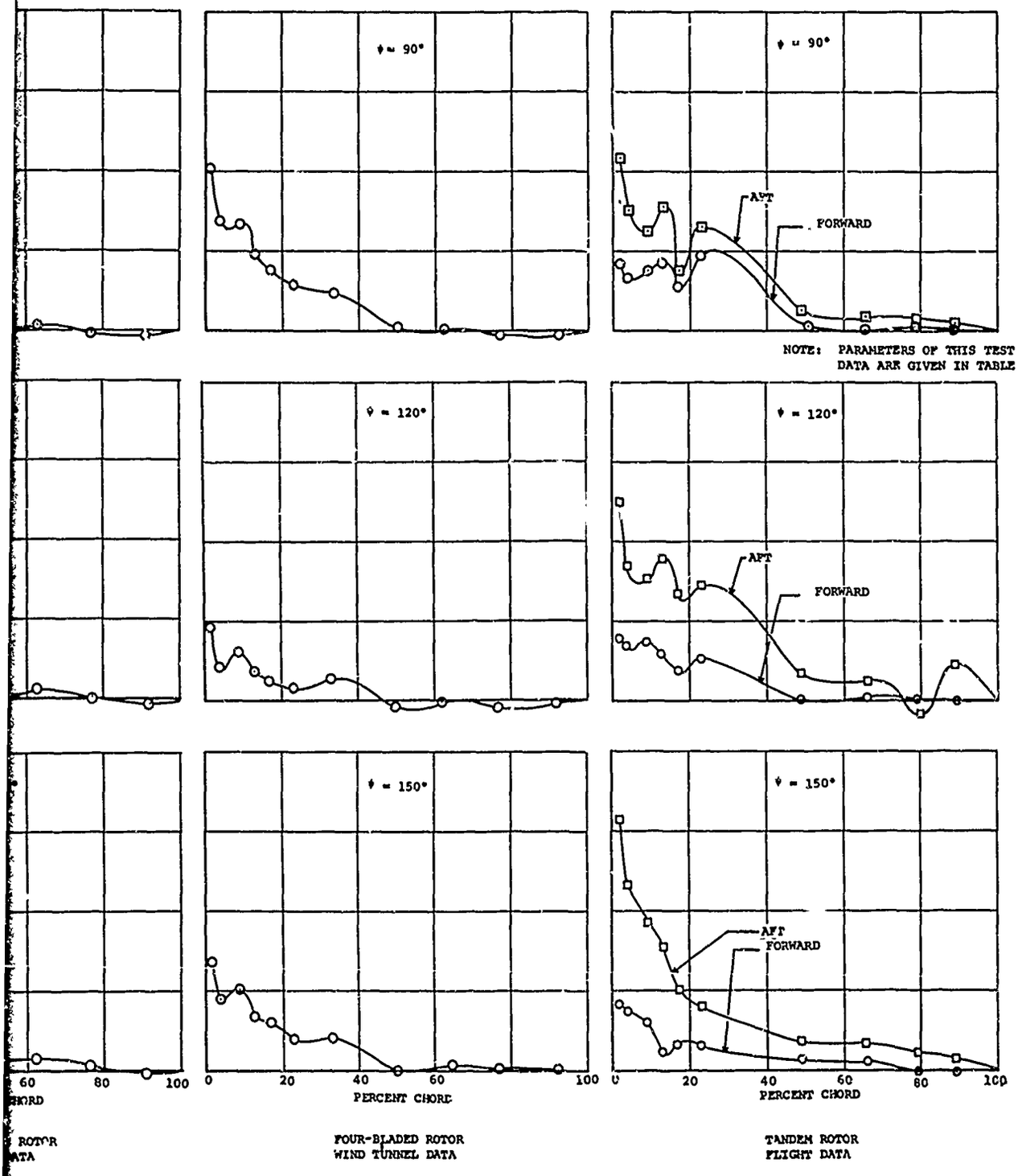

istributions as Measured Near 110 Knots in Four Similar Full-Scale

B

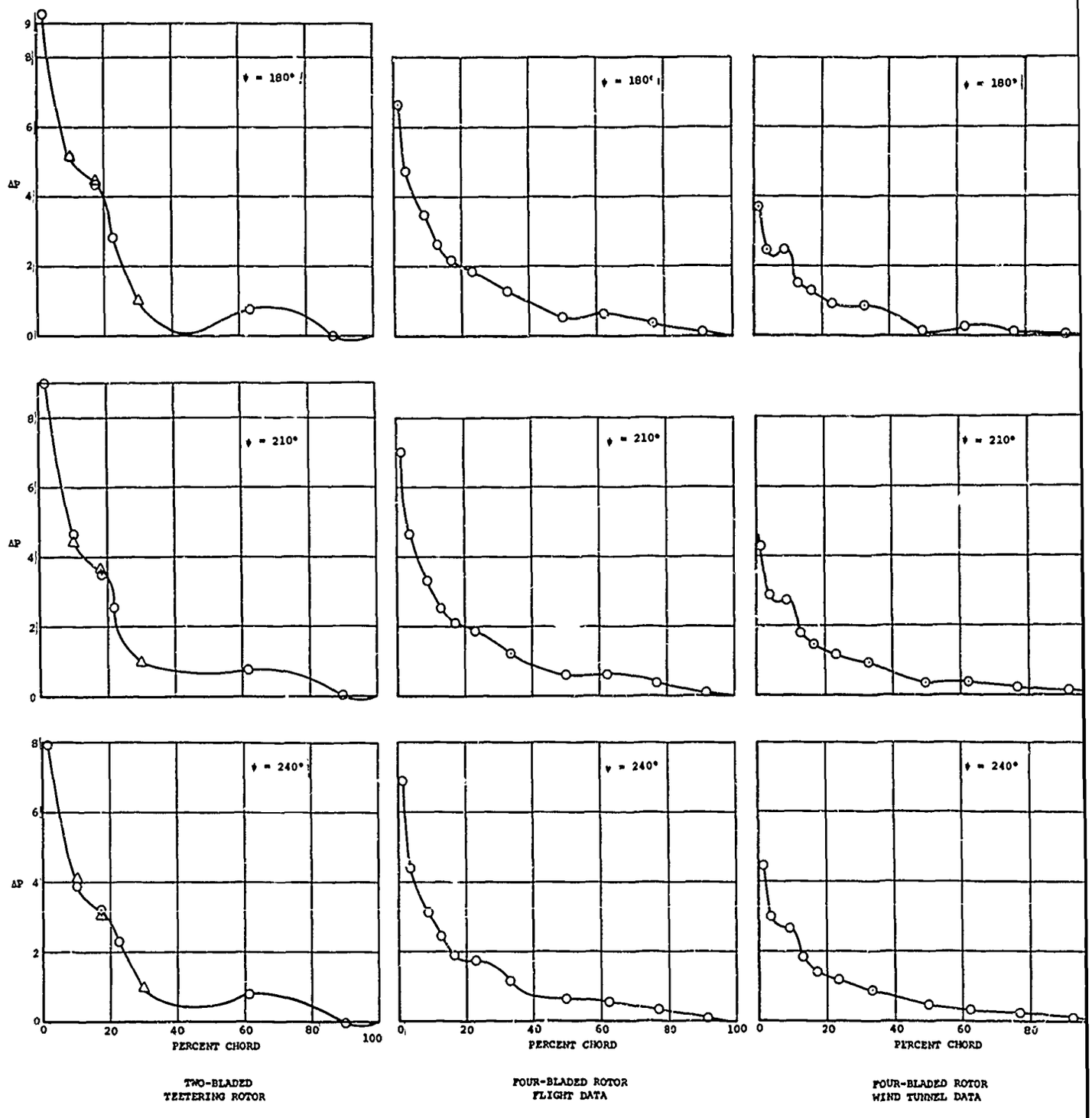

Figure 114. Third Quadrant Chordwise Airload Distributions as Measured Near 110 K Airloads Measurement Programs.

A

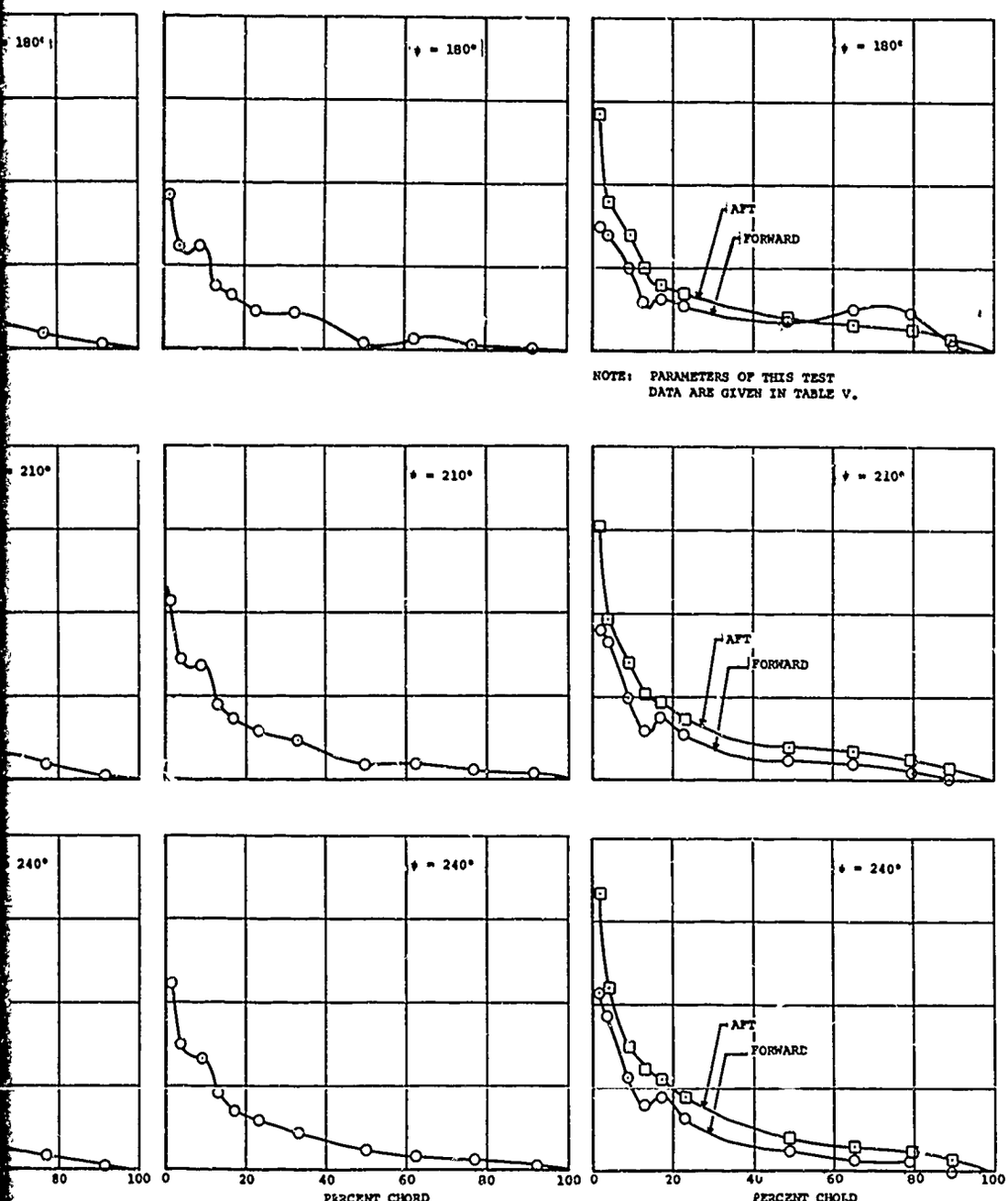

stributions as Measured Near 110 Knots in Four Similar Full-Scale

B

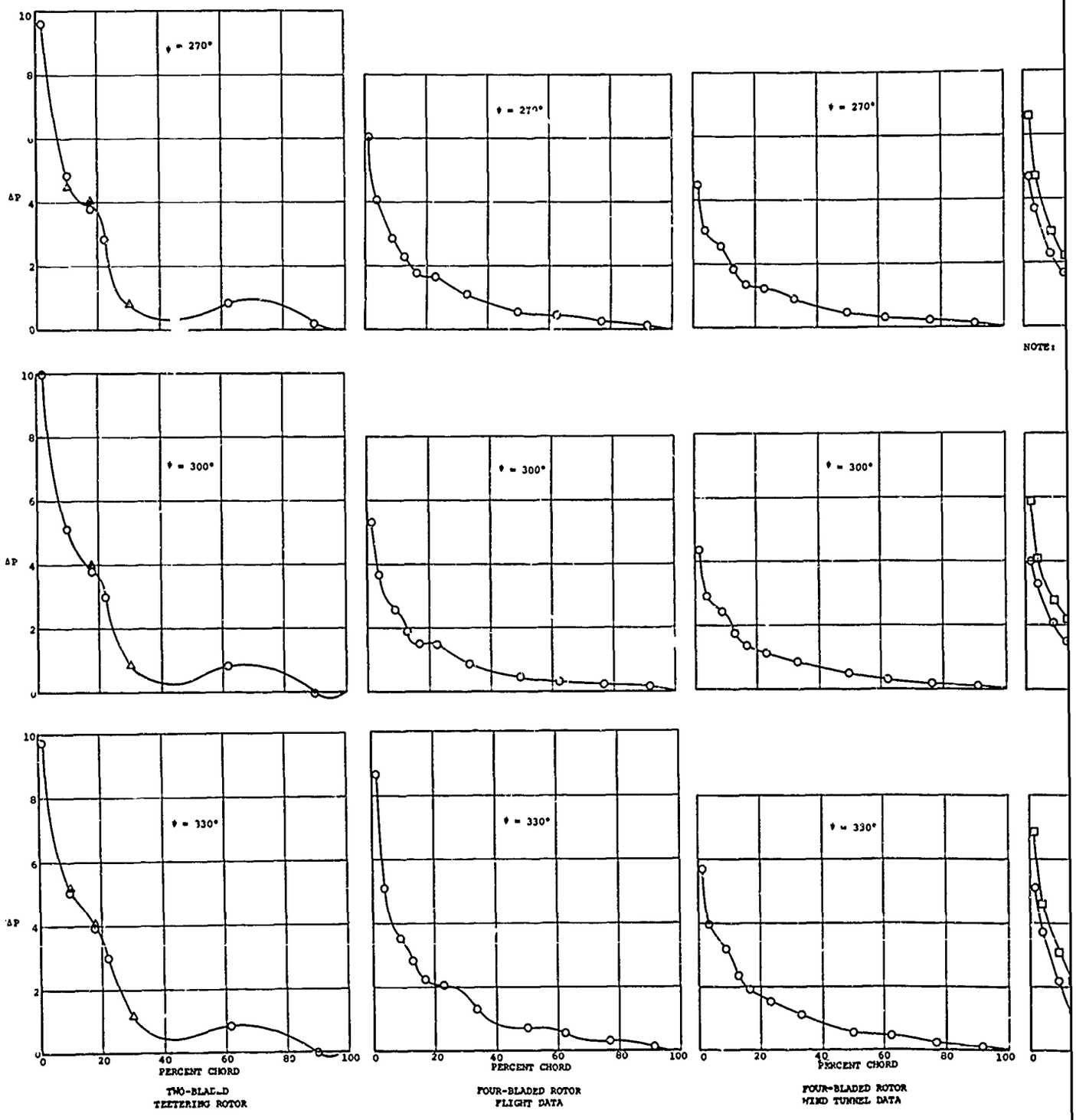

Figure 115. Fourth Quadrant Chordwise Airload Distributions as Measured Near 110 Airloads Measurement Programs.

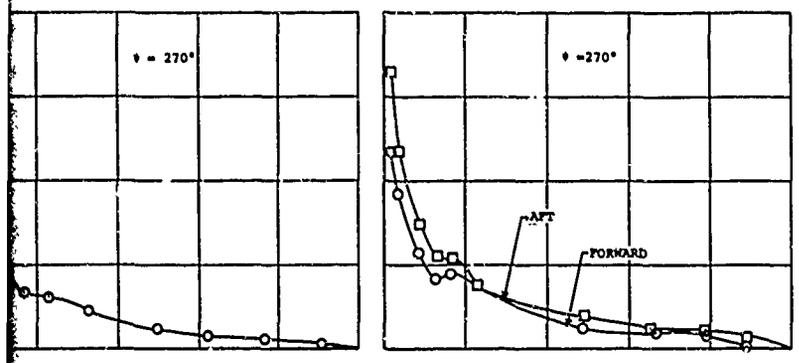

NOTE: PARAMETERS OF THIS TEST DATA ARE GIVEN IN TABLE V.

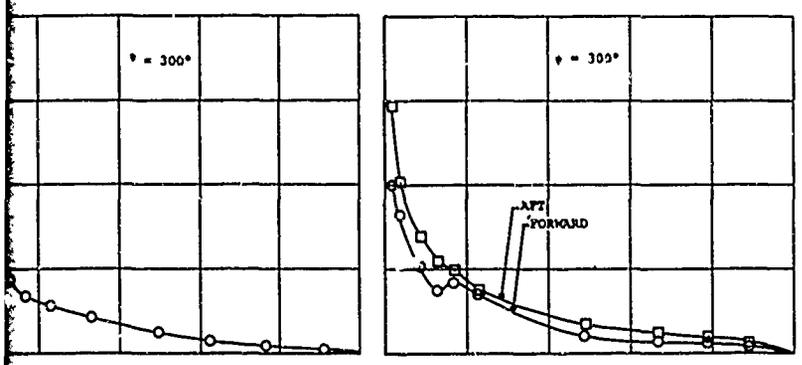

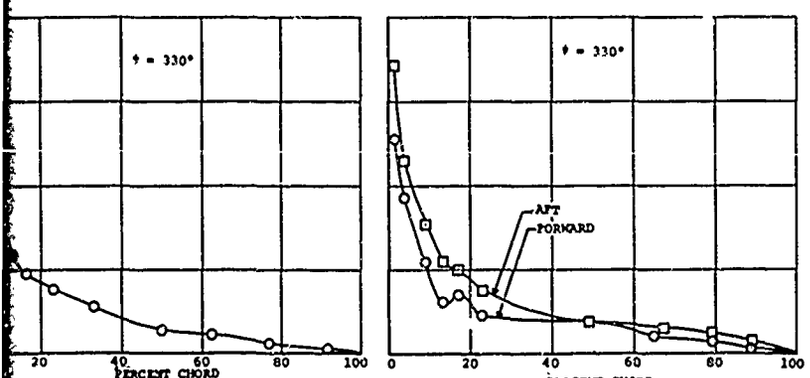

FOUR-BLADED ROTOR WIND TUNNEL DATA

TANDEM ROTOR FLIGHT DATA

ions as Measured Near 110 Knots in Four Similar Full-Scale

B

data have the lowest lift per length of blade as well as the lowest advancing tip Mach number, and therefore show almost no disturbance on the advancing blade. The tandem rotor data fall between these two tests and show some disturbance, particularly on the aft rotor. The tandem rotor data shown are for a lift loading and Mach number similar to the two-bladed rotor, but the tandem rotor blades have thinner (11-percent thickness) sections and are therefore less sensitive to compressibility effects.

TABLE V
PARAMETERS OF AIRLOADS TESTS COMPARED
IN FIGURES 112 THROUGH 115

Parameter	Rotor Configuration			
	Two-Bladed Teetering	Four-Bladed (Flight Data)	Four-Bladed (Wind Tunnel Data)	Tandem
μ	0.25	0.29	0.29	*0.27
C_T/σ (or C_{TW}/σ)	0.093	0.090	0.058	*0.076
M(1.0,90)	0.81	0.73	0.73	0.81
ΩR, fps	724	626	650	683
V, knots	105	108	110	108
Density Altitude, ft	1500	3700	2100	2950
θ_0 Fwd (or SLR)	Unknown	15.0	12.6	16.8
θ_0 Aft	NA	NA	NA	16.5
θ_{A1} Fwd (or SLR)	Unknown	3.3	6.0	3.4
θ_{A1} Aft	NA	NA	NA	5.3
β_{A1S} Fwd (or SLR)	Unknown	-0.1	-0.7	-2.1
β_{A1S} Aft	NA	NA	NA	0.2
Lift per rotor, lb	6120	11,500	8252	*12,950
Lift per foot of blade, lb/ft	139	103	74	*146
Reference	3	27	23	NA
Flight	NA	14	NA	384
Run	NA	NA	Table 8	4

* Average value for two tandem rotors.

The persistence of the advancing blade disturbance shown in Figures 112 and 113 is surprising. While it appears that this disturbance is triggered by the tip vortex proximity, the chordwise pressure distribution does not recover to the expected airfoil distribution until 150 to 180 degrees azimuth is reached. This initial disturbance is so great that the additional disturbance which the aft rotor of the tandem experiences at 120 degrees azimuth is hardly noticeable. Also significant is the fact that each of the rotors would be expected to have an additional vortex proximity disturbance at about 300 degrees azimuth. There is no evidence of any significant disturbance, which indicates either that local Mach numbers greater than about 0.6 are required for this disturbance to take place, or that rotor wake distortion is such that the vortex is moved away from the blade. It seems that compressibility effects are the most likely reason for this disturbance.

The typically airfoil-like pressure distributions shown on the retreating side of the rotor disk for the four rotor airloads tests in Figures 114 and 115 are believed to indicate that rotor airfoil sections normally perform as two-dimensional sections. On an azimuthal average basis, this two-dimensional characteristic is believed to occur even with large pressure irregularities on the advancing blade. The data used for Figure 112 were azimuthally averaged and are shown in Figure 116 to illustrate this tendency. Unfortunately, the uncorrected tandem rotor data show considerable variations in average chordwise pressure distribution. These variations were corrected to match the forced-fit pressure integration curve, equation (1), prior to the preparation of Figures 112 through 115. The comparison shown is believed to substantiate the need for this correction. It should be noted that in the reference 4 data report, the pressure data are presented without any corrections, but the integrated airloads data presented were prepared with the correction for these average pressure variations.

The relatively smooth airfoil-like performance of rotors on an azimuthally averaged basis does not apply to the harmonics of the azimuthal variations. Figure 117 shows the first three harmonic pressure amplitudes as a function of chordwise location for three test conditions of the H-34 rotor and one test point of the tandem data. It is shown that, even for the very smooth flight 14 data from reference 27, the harmonic loading distribution is somewhat irregular. The first harmonic loading was more irregular in descent in a flight condition described as rough. Of the single rotor data, the wind tunnel test results

are the most irregular, possibly due to the larger local Mach number of this test. Of all the data shown, the forward rotor of the tandem experienced the largest irregularities, again probably due to the significantly larger local Mach number. It is significant that the higher pressures which occur on the first 40 percent of the chord have increased variations with increased frequency, while the pressures on the remaining 60 percent of the chord decrease. This tendency is believed to be due to the impulsive nature of the pressure disturbance on the advancing blade, which disturbs all harmonics. Comparable harmonic rotor airloads data are available for the aft rotor of a tandem in reference 9. The comparison of some typical third harmonic flight data with these model data is made in Figure 118, and considerable differences on the outermost 20 percent of the blade are evident. This lack of correlation is probably due to the larger-than-scale stiffness of the model blades used for the tandem rotor model test. Other reference 9 tests on single lifting rotor models with blades of various stiffnesses showed this kind of change in blade loading with blade stiffness. The high inboard airload at 40-percent radius on the model at an advance ratio of 0.1 is not like the flight test data shown. This unexpected inboard loading may be due to transition which, as shown in Figure 57, tends to increase the inboard third harmonic loading. The flight data are at a somewhat higher advance ratio and are clear of transition effects.

Considerably more sophisticated comparisons of the various rotor airloads data available can and should be made. For example, Figure 119 shows a two-case comparison of normal force coefficients prepared from the chordwise integrated airloads data. The single lifting rotor coefficients are from reference 26 and are based on the airloads data of reference 27. Forward rotor data from this program for these two rather typical flight test points show good comparison of the azimuthal waveform. Since the tandem rotor data were obtained at a thrust coefficient and propulsive force similar to those of the single rotor data, the lower values of normal force coefficients shown for the tandem data are attributed to rotor-rotor interference. This kind of airload coefficient data preparation and comparison should be greatly expanded with the ultimate objective of preparing the airloads data as synthesized rotor airfoil coefficients.

EVALUATION OF DATA ACCURACY

It is believed that the most important task of this report is to evaluate the quality of the data obtained so that subsequent

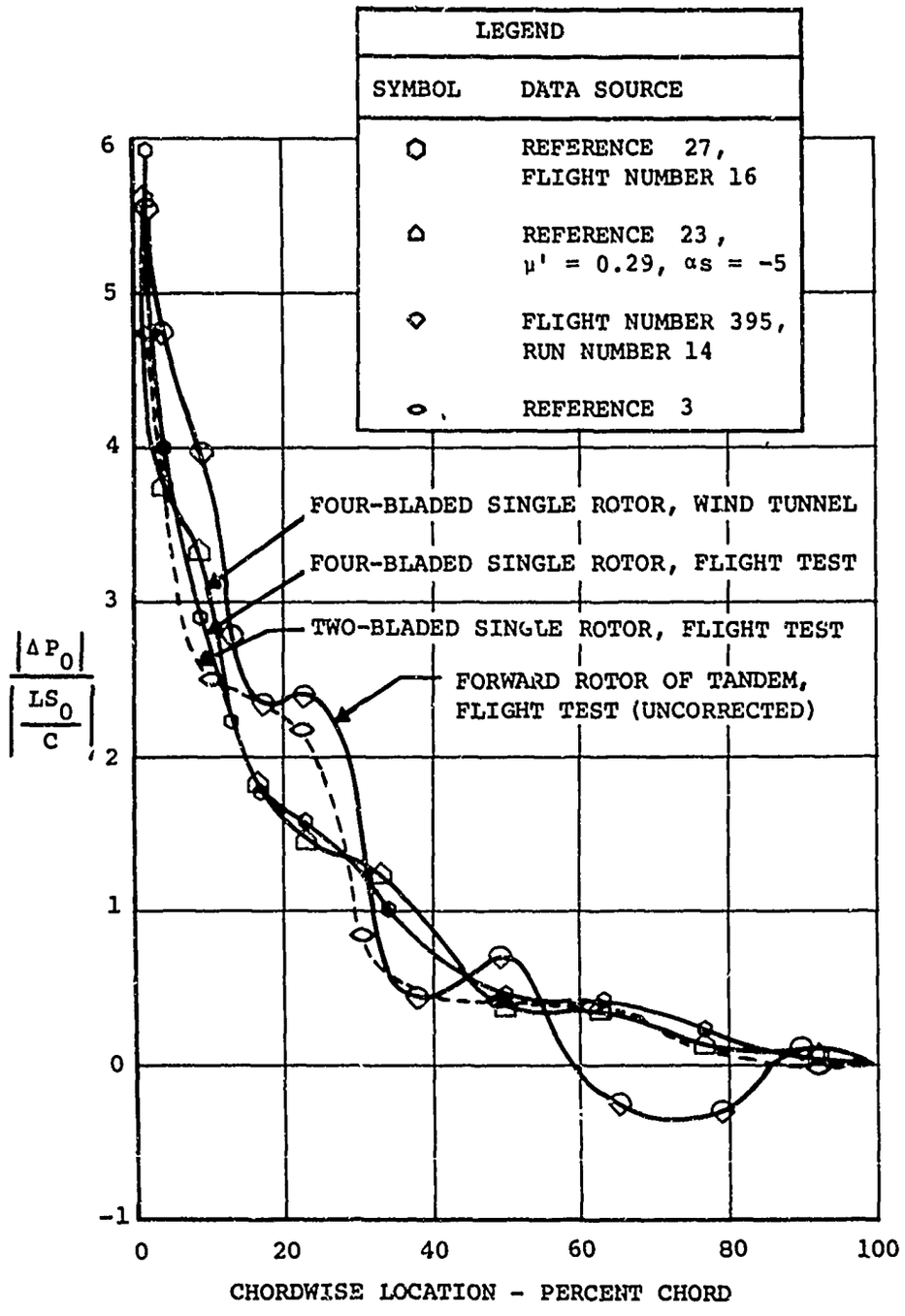

Figure 116. Comparison of Chordwise Distribution of Azimuthal Averaged Airload Pressure from Various Airloads Programs.

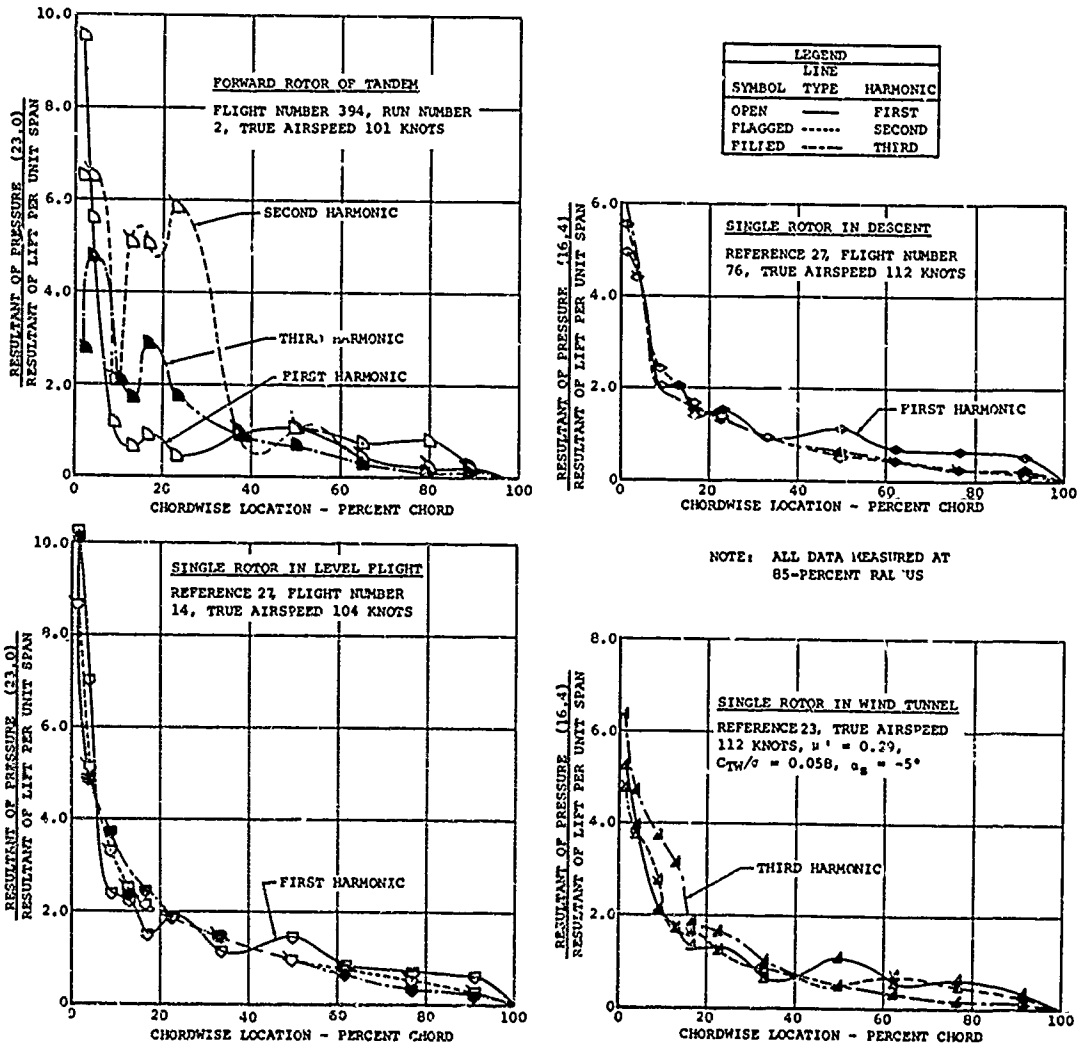

Figure 117. Comparison of Chordwise Loading Harmonics of Other Airloads Programs with Forward Rotor Data.

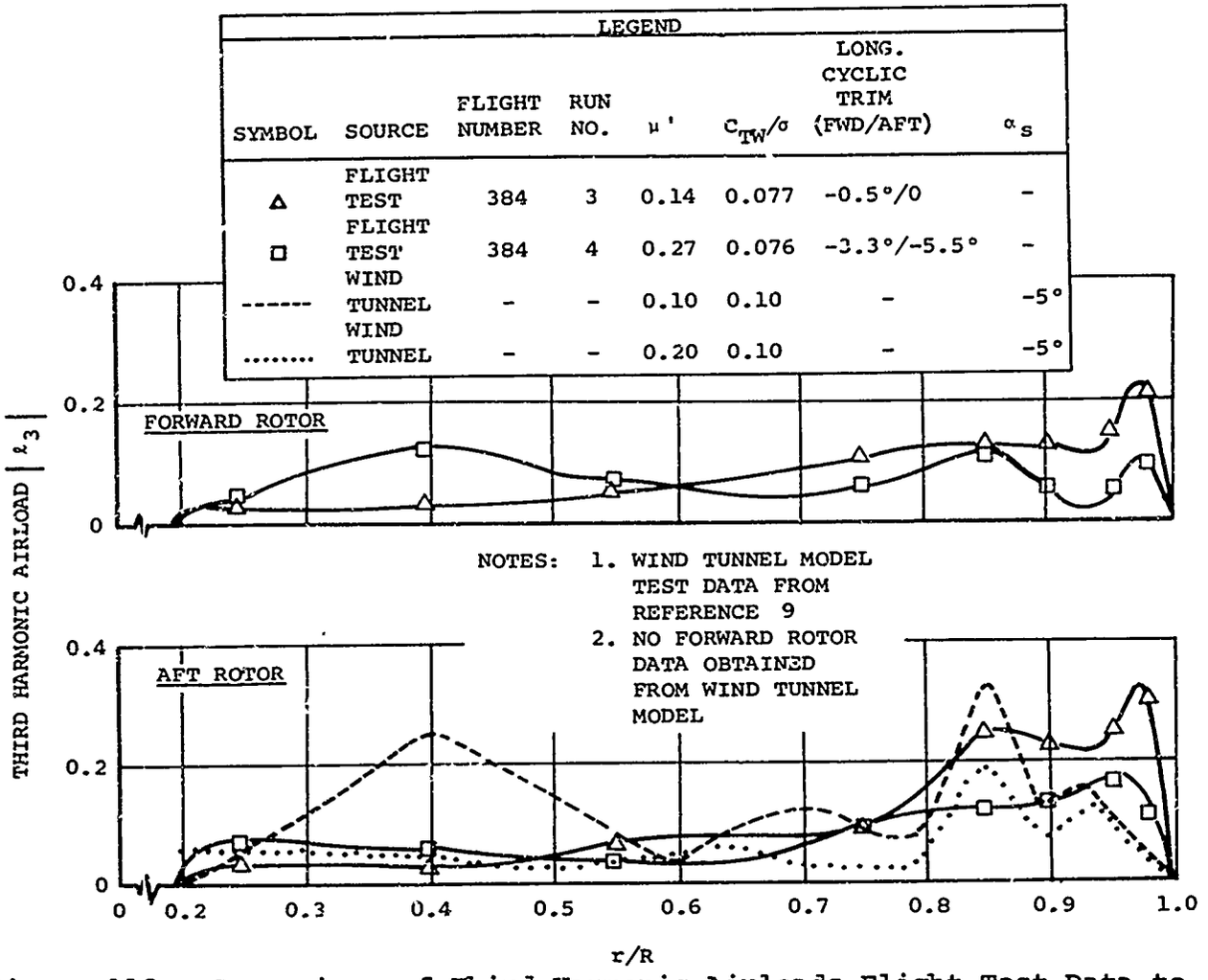

Figure 118. Comparison of Third Harmonic Airloads Flight Test Data to Airloads Measured on a Wind Tunnel Tandem Rotor Model.

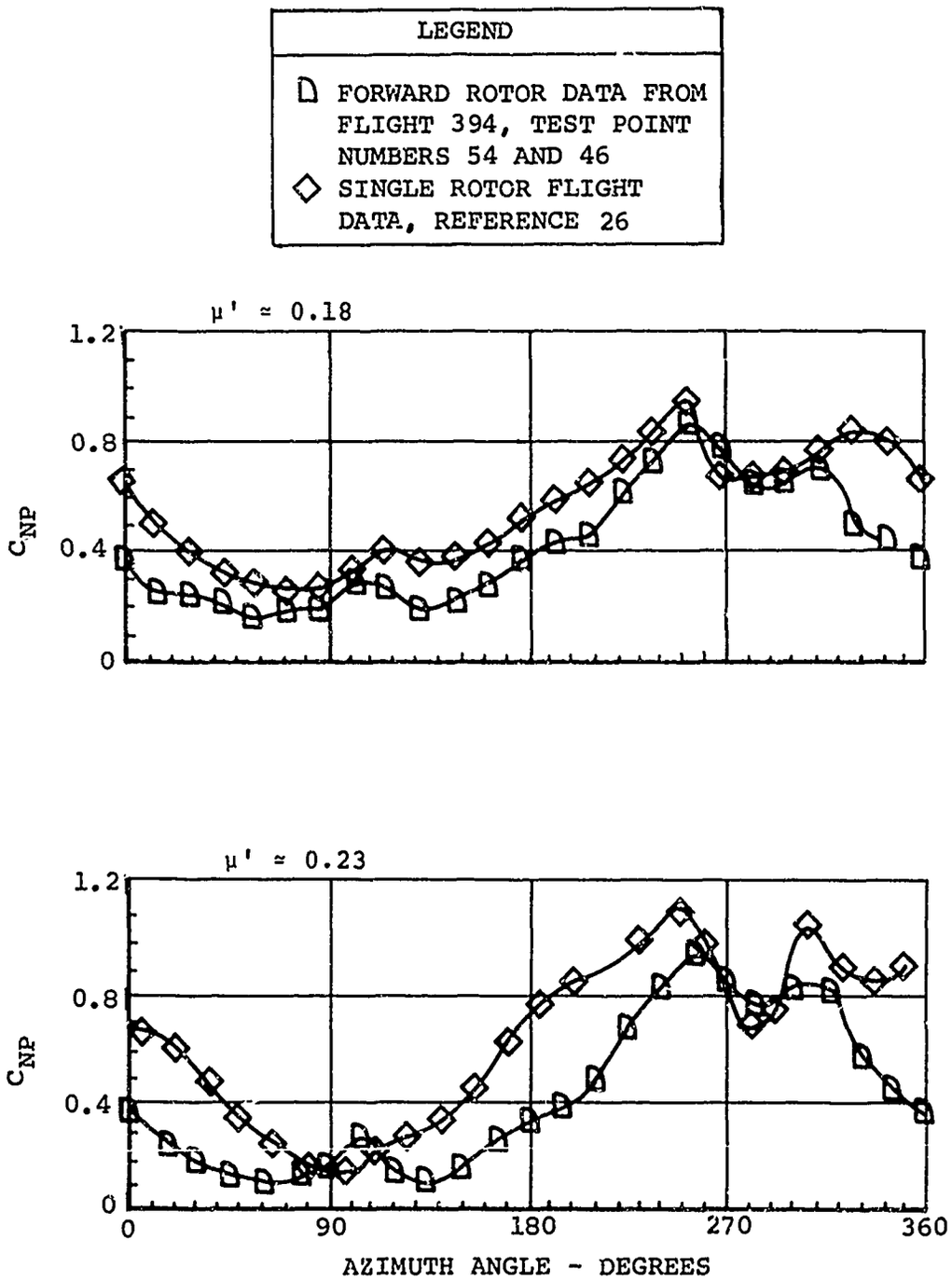

Figure 119. Comparison of Normal Force Coefficient Data as Measured at 85-Percent Radius on Single Rotor and on Forward Rotor of Tandem.

analysts can use these data with confidence. The use of these data is believed to be more important than the possible loss of image resulting from the exposure of the relatively few bad measurements; therefore, this evaluation will be candid. Generally, the data are believed to be of very good quality; however, even before this report was written, some attempts to use these data were almost abandoned due to the use of the inadequate fuselage attitude data of this program in an analysis. It must be acknowledged that some of the measurements are poor, and most of these have been deleted; however, due to extenuating circumstances or error, some inadequate measurements may remain.

The data unique to this program, the tandem rotor airloads data, have been emphasized in this evaluation. These data initially had excessive scatter in the steady measurements which resulted in low values of integrated lift per blade as shown in Figures 120 and 121. After detailed final editing, which uncovered about six additional bad transducer signals per flight, and the use of forced-fit integration, these data are shown to have about 10-percent scatter. Some of the scatter shown in Figures 120 and 121 is due to variations in trim setting which vary the fuselage download and the propulsive force distribution between the rotors. The trend of increasing lift with airspeed, which is especially noticeable on the forward rotor, is believed to be due to the fuselage download. The forward rotor lift data are also shown to be somewhat lower than expected except for hovering, even after final editing and forced-fit integration. This is believed to be due to the more uniform loading of the forward rotor which results from aft rotor interference. The more uniform loading causes one-half of the blade lift to be imposed on the inboard area of the blade, where it is measured by only one-third of the pressure transducers. This apparently results in a low measurement of blade lift, since the extrapolations required with the sparse array are more significant. Generally, these data are believed to be of very good quality and are much better than expected. Contractually, the program was required to provide only alternating airloads data, which are considerably easier to obtain. The acquisition of these good steady data has greatly increased the confidence in the alternating values as well as given significant information on the average rotor loading.

It is expected that the detailed analysis of rotor airloads data will principally involve the aerodynamic pitching moment data, since most contemporary rotor blade problems are due to torsional loadings. Blade stall and compressibility effects

are of this nature and are problems which require considerable further analysis. Figure 122 was prepared to indicate the consistency of the airloads data in predicting pitching moments. It is shown that the radially averaged aerodynamic center of the blade is measured repeatedly within 2 percent of the chord. A trend of slightly increasing pitching moment with airspeed is shown in these data. This trend is probably due to reversed flow and compressibility effects, both of which tend to cause a nose-up moment on the blade. These data are generally believed to be consistent and repeatable and are worthy of considerable analysis.

A summary of the evaluation of the data obtained as discussed in this and previous sections of this report is presented in Table VI. Where possible, quantitative data evaluations are presented which are generally obtained from repeated flights of the same data point. Test points 46 and 50, for instance, were repeated in two flights; test point 25 was repeated in flights 386, 391, and 395. These points were the predominant source of the scatter evaluation. The mean accuracy of the data was more a subjective evaluation, but an attempt was also made to put a quantitative measure on their accuracy. These data generally substantiated the pretest instrumentation system analysis, except for those signals which were poor. For example, the rotor shaft alternating lift instrumentation in-flight calibration system did not work, so these data were deleted. The steady rotor shaft lift data were of poor accuracy due to low sensitivity but were not deleted so that the shaft interaction matrix would be complete. However, the steady value of the steady lift data was set equal to one-half of the run gross weight. The fuselage attitude data were inadequate and were deleted; but as shown in the table, the accuracy was within the pretest specifications. This was due to an inadequate definition of the program requirements. The rotor blade collective pitch measurements are also poor due to excessive scatter; but they were not deleted, since the data are believed to be of value if considered statistically. All other data are believed to be of the expected accuracy. The rotor shaft shear data obtained are believed to be worthy of mention as being unique to this program and of excellent quality.

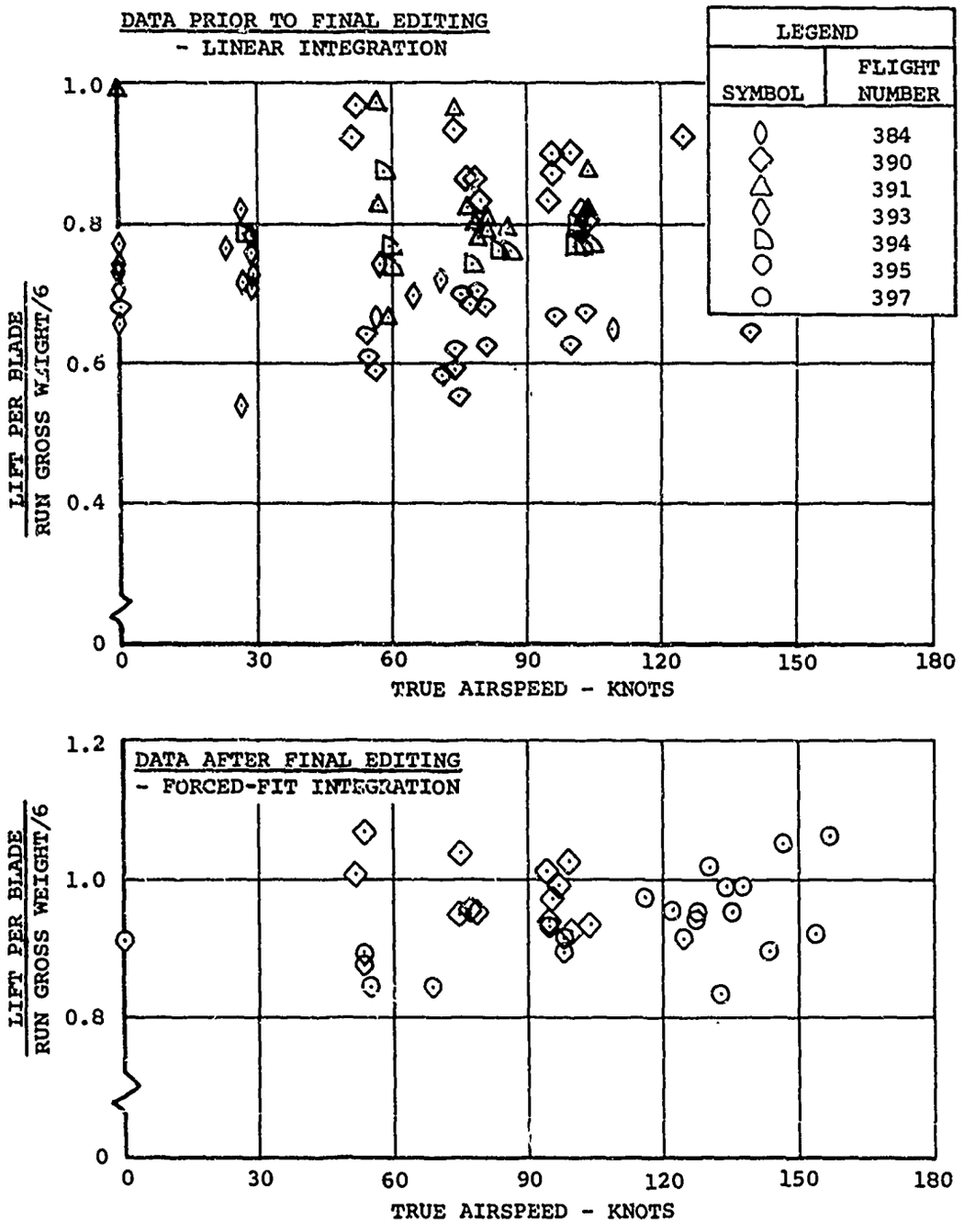

Figure 120. Comparison of Forward Rotor Lift Measurements Obtained from the Azimuthal Averaged Airloads to Run Gross Weight.

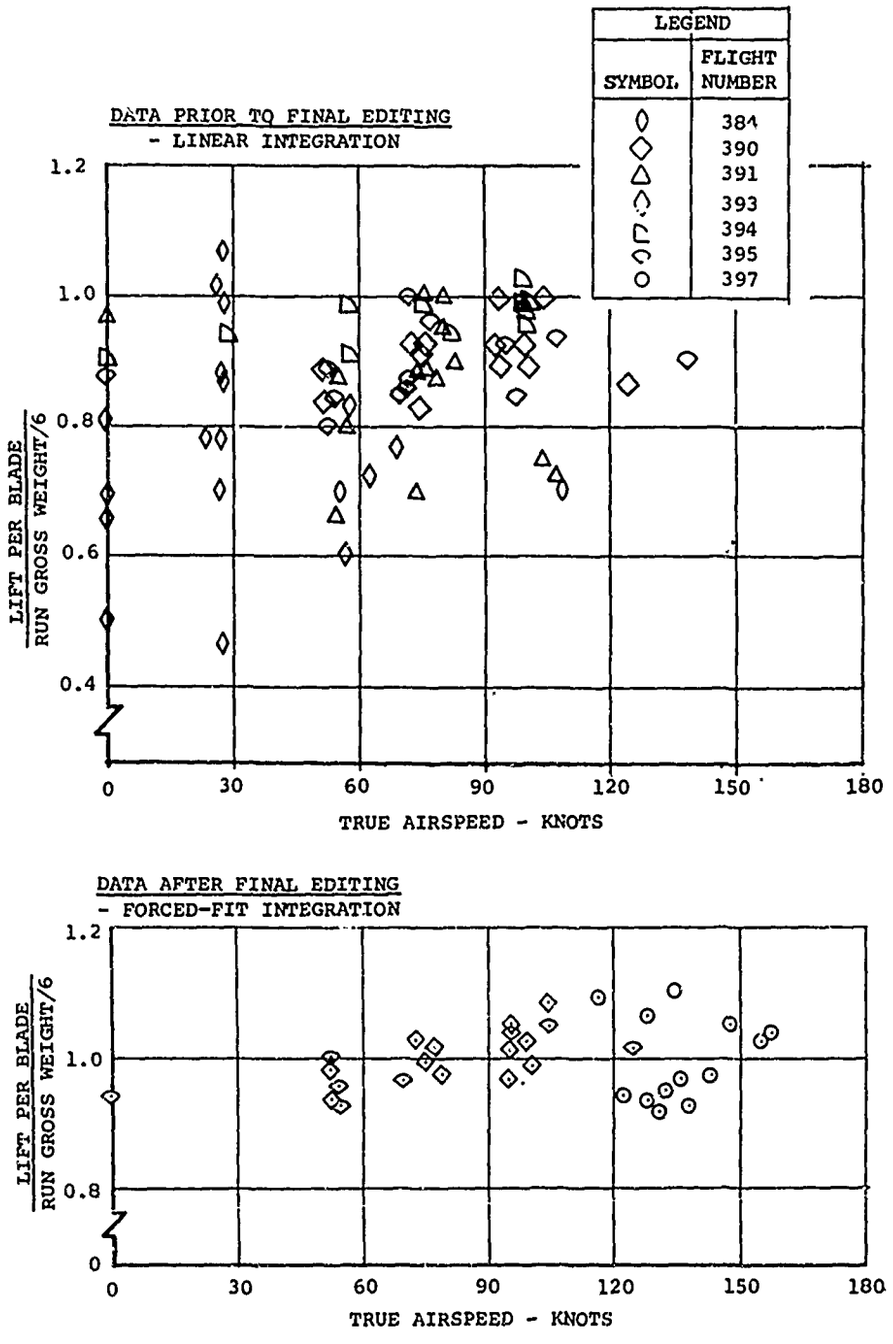

Figure 121. Comparison of Aft Rotor Lift Measurements Obtained from the Azimuthal Averaged Airloads to Run Gross Weight.

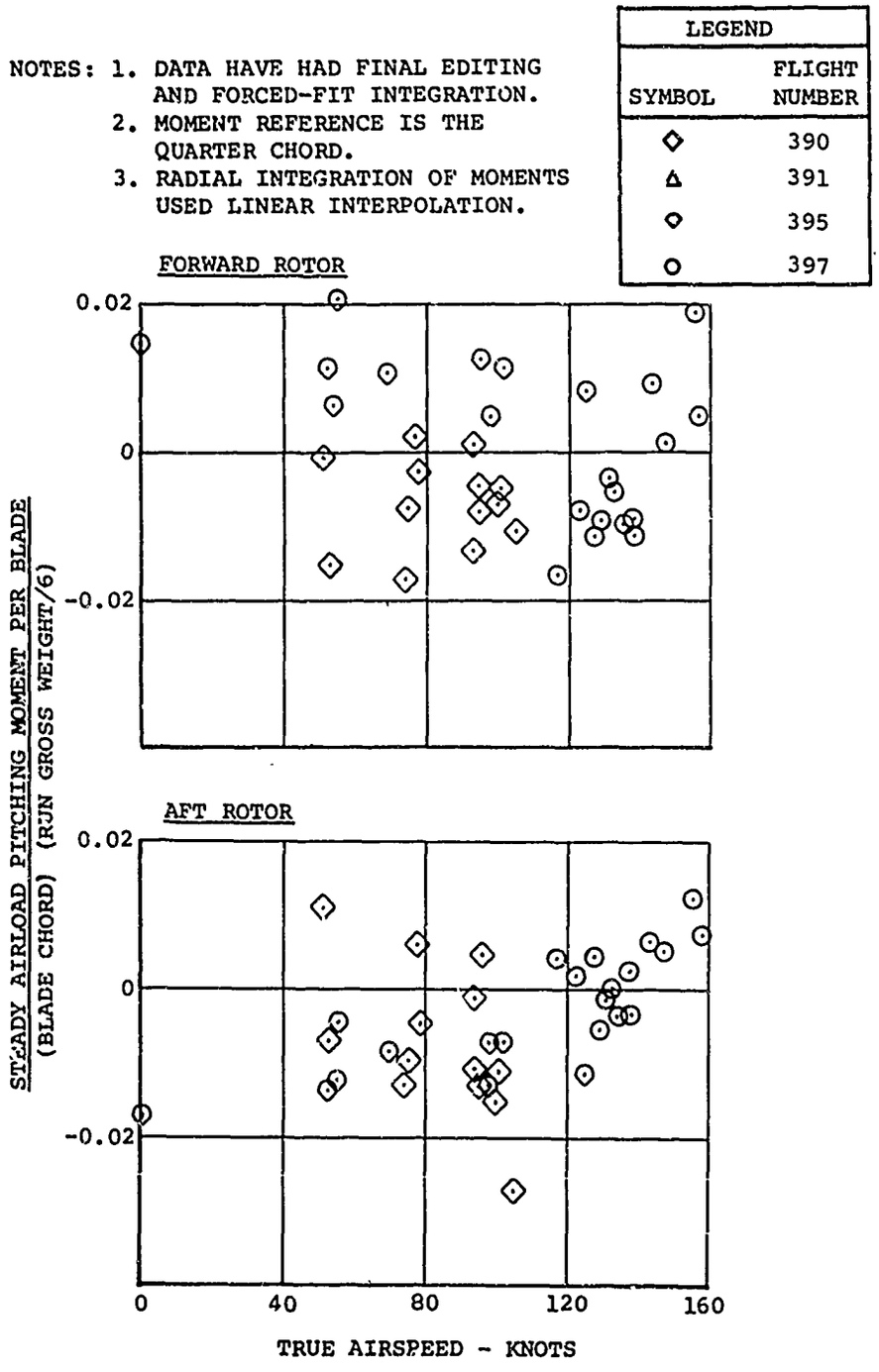

Figure 122. Azimuthal Averaged Rotor Blade Aerodynamic Pitching Moment Data.

TABLE VI

ESTIMATED DATA ACCURACY BASED ON COMPARISON

Parameter	Pretest Estimated Accuracy ***	Steady Values	
		Scatter	Accuracy Mean
Airloads Data			
Pressures	0.4 psid	0.5 psid	0.5 psid
Section lifts	DNE	2 lb/in.	1 lb/in.
Section moments	DNE	4 in.-lb/in.	2 in.-lb/
Blade lifts	DNE	0.05 RGW	*Low ≈ 150
Blade moments	DNE	0.0005 RGW x c	DCR
Blade Loads			
Flap bending	1000 in.-lb	400 in.-lb	200 in.-l
Chord bending	1000 in.-lb	DNE	DNE
Torsion	1000 in.-lb	DNE	DNE
Tension	2800 lb	1000 lb	500 lb
Shaft Loads			
Lift - steady	750 lb	**0.2 RGW	**0.2 RGW
Lift - alternating	345 lb		
Shear	135 lb		
Bending	1260 in.-lb		
Torque	3100 in.-lb	20,000 in.-lb	10,000 in
Control Loads			
Pitch links	240 lb	DNE	DCR
Accelerometers			
Hub motion	0.03 g at 3Ω		
Fuselage vibration	0.03 g at 3Ω	0.03 g	0.03 g

TABLE VI

ACCURACY BASED ON COMPARISON OF RESULTS

Test Results			
Steady Values		Oscillating Values	
catter	Accuracy of Mean	Scatter	Accuracy of Mean
psid	0.5 psid	0.1 psid	NEP
b/in.	1 lb/in.	0.5 lb/in.	0.3 lb/in.
n.-lb/in.	2 in.-lb/in.	1 in.-lb/in.	0.5 in.-lb/in.
5 RGW	*Low ≈ 150 lb	DNE	DNE
005 RGW x c	DCR	DNE	DNE
in.-lb	200 in.-lb	200 in.-lb	NEP
	DNE	500 in.-lb	NEP
	DNE	500 in.-lb	NEP
0 lb	500 lb	DNE	DNE
RGW	**0.2 RGW	DNE	DNE
		DD	DD
		0.05 RGW	0.02 RGW
		DCR	DCR
000 in.-lb	10,000 in.-lb	DNE	DNE
	DCR	50 lb	20 lb
		DNE	DNE
3 g	0.03 g	0.01 g	0.01 g

B

TABLE VI - CONTINU

Parameter	Pretest Estimated Accuracy ***	Steady Values	
		Scatter	Acc
Trim			
Airspeed	3 knots	2 knots	1 k
Density altitude	200 feet	200 feet	50
Fuselage attitude	2 degrees	2 degrees	1 d
Angle vanes	1 degree	1 degree	1 d
Blade pitch	0.25 degree	1 degree	0.5
Blade Hinge Angles			
Flap	0.25 degree	0.1 degree	0.0
Lag	0.25 degree	DNE	DNE

Notes: 1. Abbreviations

DCR Data consistent and repeatable
DD Data deleted (no value)
DNE Data not evaluated
NEP No evaluation possible
⊗ Value not significant

2. Stated accuracy for airloads data is based on forced-fit integration method.

*3. Forward rotor lift data are low due to the unexpected lift distribution.

**4. Steady rotor shaft lift data were deleted and set equal to 0.5 RGW due to the noted poor accuracy.

***5. Refer to Figure 15 of this report and for further explanation see Volume I.

A

TABLE VI - CONTINUED

Test Results			
Steady Values		Oscillating Values	
Scatter	Accuracy of Mean	Scatter	Accuracy of Mean
knots	1 knot		
00 feet	50 feet		
degrees	1 degree		
degree	1 degree		
degree	0.5 degree	0.1 degree	0.1 degree
.1 degree	0.05 degree	0.5 degree	0.2 degree
NE	DNE	DNE	DNE

on forced-fit

unexpected

nd set equal

urther explanation

B

CONCLUSIONS

AIRLOADS DATA

1. The radial distribution of the azimuthally averaged loadings on the forward and aft rotors of a tandem helicopter tends to be significantly different. The forward rotor has a more uniform loading distribution than an equivalent isolated rotor or the aft rotor. This effect is apparently due to the upwash caused by the aft rotor, which increases the inboard loading on the forward rotor.

2. Chordwise airload pressure distributions obtained in this program are similar to prior dynamic airloads measurements. These data simulate two-dimensional airfoil airloads, on an azimuthal average basis and locally, when significantly far from blade tip vortex interference effects.

3. Adversely trimmed flight configurations can cause blade tip vortex interference on the aft rotor of a tandem helicopter in the form of large, suddenly applied changes in the local blade airload pressures. At 85-percent radius, these pressure spikes are of the greatest magnitude near 13-percent chord. Chordwise airload pressure distributions during tip vortex interference have a characteristic sawtoothed shape. Tip vortex interference spiking is more pronounced at 85-percent radius than at 98-percent radius for the forward and aft rotors.

4. Sideslip causes significant changes in the aft rotor airloads. In transition, the changes in airload waveform with sideslip are reflected in sharply increased flapwise blade bending.

5. Harmonic content of rotor blade airloads tends to include significant amounts of all harmonics up to the eighth. First harmonic airloading has an amplitude of about one-third of the average lift per unit span of the blades. Second harmonics tend to be somewhat smaller than the first harmonic. Third to eighth harmonic amplitudes tend to average about one-tenth of the average lift per unit span. Ninth and tenth harmonics are significantly smaller than the lower harmonics. All harmonics are characterized by a higher loading near the blade tip.

This effect is probably due to the impulsive nature of tip vortex interference.

6. Third harmonic airloads tend to decrease with increased thrust coefficient and decrease with advance ratio until advance ratios greater than 0.27 are reached. Cyclic trim does not change the third harmonic airloads significantly, even for conditions for which spiking is known to be varied. Sideslip causes large changes in the third harmonic airloads for the aft rotor.

7. The occurrence of rotor-rotor interference pressure spiking on the aft rotor apparently occurs so rapidly that the lift-per-unit-span loadings are not affected.

8. Airload pitch axis-pitching moment per unit span of the forward rotor is characterized by a once-per-revolution oscillation with some eighth harmonic excitation. For the data shown, there is no evidence of any coupling with the 5/rev. first mode torsional deflection of the blade; however, the 12/rev. second torsional mode is in evidence. Aft rotor pitching moment is characteristically a 6/rev. oscillation, particularly for outboard blade stations. Pronounced nose-down pitching moments can occur on the advancing side of the rotor disk for conditions which produce negative lift in this region.

9. First, second, and third harmonic airloads data are substantiated by comparison of the harmonics of the flapping motion to the harmonics of the airload moment about the flapping hinge. This ratio of flapping response to flapping excitation varies with airspeed within a reasonable scatter band for both rotors and for all three harmonics.

10. Due to the azimuthal nonlinearity of the airload pressure data, the consideration of these data as harmonics gives peculiar results. For example, chordwise distributions of the harmonics of airload pressures indicate that even the first harmonic airloads do not produce airfoil-like pressure distributions. Aft of the quarter chord, the first harmonic pressure distribution is usually airfoil-like; but the first quarter of the airfoil, which is most sensitive to compressibility and vortex interference spikes, displays a rather unusual pressure distribution.

11. An azimuth-by-azimuth comparison of one test condition of the available full-scale rotor airloads data from this

program and three reference programs shows considerable similarity between these four sets of data. All data show intrarotor interference effects at 30 to 150 degrees, as evidenced by a disturbance in the chordwise pressure distribution. Most of these data also show a trace of a disturbance at 270 to 300 degrees. The aft rotor of the tandem shows about the same chordwise disturbances as the forward rotor.

12. Airload pressures, when converted to normal force coefficient form, show good agreement between tandem forward rotor and single rotor data. At 85-percent radius, the maximum normal force coefficient occurs at 250 degrees azimuth, and a rapid decrease in this coefficient occurs immediately following the peak.

13. Comparison of the tandem rotor airloads measured in flight to tandem rotor model data shows general similarity, but with detail variations which may be caused by difference in blade bending.

14. The waveform of some of the lift-per-unit-span data has been compared with theory. Agreement between the waveform predicted by an aeroelastic analysis and an arbitrarily selected single test case (84 knots, 33,000 pounds) is good for the forward rotor at the 85- and 95-percent radii. Waveform prediction is not as good for the aft rotor. This agreement in the prediction of the airload waveform of the forward rotor does not imply that the azimuth average airload values are predicted by theory. As noted previously, the azimuthal average airloads on the aft rotor are as predicted by theory, but the radial distribution of the azimuthal average airloading on the forward rotor is considerably different.

15. An initial attempt at reducing the recorded rotor airloads data to synthesized airfoil data has been made using a rigid blade-nonuniform downwash analysis. Significant variations between the theoretical and measured normal force coefficients were found. Some of these variations may be due to the lack of blade bending effect in the theory; however, sizable variations attributable to wake effects are shown. It should be noted that rather small variations tend to be amplified by the normal-force-coefficient theoretical-angle-of-attack plot, making the agreement with theory appear worse than it would appear if the same data were compared as lift per unit span against azimuth.

BLADE BENDING MOMENTS

1. Alternating flapwise blade bending data obtained in level flight are consistent and are less than predicted by theory. Above 60 knots, the effects of increased airspeed on alternating flapwise bending are shown to be small.

2. The harmonic content of blade flapwise bending is predominantly first, second, and eighth harmonic. The relatively low response of third harmonic bending was unexpected, due to the proximity of the first flapwise bending natural frequency of about 2.5/rev. The eighth harmonic response is due to the third flapwise bending mode. The second flapwise bending mode, which has a natural frequency of about 5/rev., apparently does not receive much excitation.

3. Chordwise blade bending is predominantly 4/rev. on the forward rotor and 5/rev. on the aft rotor. The first mode chordwise natural frequency is about 4.3/rev. and is nearly identical for both rotors. The differences in the bending response between the two rotors must be due to differences in the aerodynamic excitation.

4. Blade torsional moments are due principally to 1/rev. airloads excitation. Excitation of the first torsional mode (5/rev.) is generally negligible.

SHAFT AND CONTROL LOADS

1. First harmonic longitudinal shaft shear varies systematically with run gross weight, rotor advance ratio, and longitudinal cyclic trim setting. Rotor shaft shear is predominantly first harmonic (due to rotor propulsion or drag), but for the forward rotor, significant in-plane vibratory forces of the second and fourth harmonics are also present. First harmonic longitudinal shear varies linearly with cyclic trim.

2. Rotor blade control loads tend to increase with the square of velocity as expected, due predominantly to first and second harmonic loads. Control loads are shown to be high for the aft rotor in transition.

VIBRATION

1. Cockpit vibration of the test aircraft, which is predominantly 3/rev. vertical, reaches a maximum at 60 knots and then decreases with airspeed. At 130 knots, vibration is nearly as low as it is in hover. While in hover, wind from the left increases cockpit vibration by a factor of three.

2. Sideslip is shown to cause a significant change in vertical third harmonic cockpit vibration in transition and at speeds of 80 and 100 knots. Minimum vibration occurs at positive (nose-left) sideslip angles. Sideslip produces changes in the pattern of the rotor-rotor interference, which apparently causes this change in vibration.

3. Vertical vibration of the airframe at 3/rev. is shown to be in phase and distributed, as would be expected for a predominantly second mode beamwise bending; that is, both pylons move in the same direction. Vertical acceleration data also show a fuel tank-fuselage structure mode.

TRIM AND PERFORMANCE

Aircraft trim and performance data show the overall effects of airspeed and trim setting and reflect the consistency of the data acquisition. Coning of the rotors when normalized for run gross weight and rotor speed squared varies systematically with airspeed within a reasonably small scatter band. Longitudinal blade flapping data are systematic and vary linearly with rotor advance ratio when measured with respect to the control axis and when normalized by the rotor thrust coefficient. Performance data are generally consistent with previous measurements. Tandem rotor interference factors obtained from reference 14 NASA model tests do not appear to be applicable to the CH-47A configuration.

RECOMMENDATIONS

1. Rotor blade design for tandem helicopters should be reviewed. Reduced twist on the forward rotor and increased twist on the aft rotor should be considered; planform taper appears beneficial. Blade twist requirements to have zero load on the advancing blade tip should be evaluated for various gross weights and flight conditions. This design review should be guided by use of the measured airloads, since the available rotor theories are inadequate.

2. Future tandem helicopter configuration studies should evaluate the benefits in reduced blade loads which can result with less overlap and greater vertical rotor spacing than the CH-47A. Canted fuselage-rotor orientations should be considered to improve performance and reduce vibration. Efforts to reduce aft rotor loads in transition should strongly influence the design. The effect of vertical spacing and overlap on sideslip transition airloads should be established to ensure that future tandem helicopter designs do not have high loads at critical sideslip angles.

3. A method of predicting tandem rotor loadings in transition with sideslip should be developed using the airloads measurements from this program. Due to the analytical complication of this problem, an empirical approach is recommended.

4. Rotor blade airfoil section lift and moment performance in a rapidly changing angle-of-attack environment at high subsonic Mach numbers should be determined and compared to the available advancing blade airloads measurements. These data should be related to determine the rotor performance degradation and control loads due to advancing blade section loading irregularities. Limitations on advancing blade tip Mach number should be established.

5. Airloads measurements obtained in this program should be used to develop methods for predicting the onset and significance of blade stall. This development should be approached both from the aerodynamic and the dynamic loads viewpoints.

6. Reversed flow effects on rotor blade performance should be isolated. A large number of test points were obtained at advance ratios larger than 0.25 with pressure measurements obtained at 25-percent radius. These data should be analyzed to show reversed flow effects. While these data are directly applicable only to tandem rotors due to flow field effects, it is believed that analysis of these data can also be of value to help explain the performance of rotor blades in the reversed flow region of single rotors.

7. A systematic approach to the development of airfoil sections with beneficial time-dependent characteristics should be initiated. A detailed analysis of the existing rotor airloads data should provide guidance to this development. Wind-tunnel test programs, such as the program being performed under Contract DA 44-177-AMC-438(T), should be expanded. Airfoils which have reduced sensitivity to suddenly applied loads, as evidenced by a more stable center of pressure, are desired.

8. Rotor blade bending and airloads measurement should be compared to determine the structural damping of the blades.

9. Methods to predict rotor-rotor interference, trim, and blade motions need improvement; elastic blade effects should be included in such a study.

10. Considerably more effort should be expended to analyze the results of this program. Rotor shaft loads and airframe vibration data are shown to be especially worthy of such effort.

BIBLIOGRAPHY

1. Abbott, I.H., and Von Doenhoff, A.E., Theory of Wing Sections, Dover Publications, Incorporated, New York, New York, 1959.

2. Burpo, F.B., Measurement of Dynamic Airloads on a Full-Scale Semirigid Rotor, TRECOM Report 62-42, U.S. Army Aviation Material Laboratories, Fort Eustis, Virginia, December 1962.

3. Burpo, F.B., Summary Report - Development of a Subminiature Surface Mounted Pressure Transducer, Bell Helicopter Company Report 299-099-200 (Contract NOnr 2877(00)), January 1963.

4. Childs, R.C., and Grant, W.J., Tabular Test Data Summary of Measurements of Dynamic Airloads on a CH-47A Tandem Rotor Helicopter, Boeing Document D8-0387, to be issued.

5. Conner, Willey, and Twomey, A Flight and Wind Tunnel Investigation of the Effect of Angle-of-Attack Rate on Maximum Lift Coefficient, NASA CR-321, October 1965.

6. Davenport, F.J., "A Method for Computation of the Induced Velocity Field of a Rotor in Forward Flight, Suitable for Application to Tandem Rotor Configurations," Journal of the American Helicopter Society, Volume 9, Number 3, July 1964.

7. Davis, J.M., Tandem Helicopter Trim and Stability Analysis, IBM Program A-81, Boeing-Vertol Report A.I. III-264, March 1965.

8. Gabel, R., et al., AVID Program, Advanced Vibration Development, Boeing-Vertol Report 107M-D-09 (Contract NOw-62-0177f) , April 1965.

9. Ham, N.D., and Madden, P.A., An Experimental Investigation of Rotor Harmonic Airloads Including the Effects of Rotor-Rotor Interference and Blade Flexibility, USAAML Technical Report 65-13, U.S. Army Aviation Material Laboratories, Fort Eustis, Virginia, May 1965.

10. Ham, N.D., An Experimental Investigation of the Effect of a Nonrigid Wake on Rotor Blade Airloads in Transition Flight, Cornell Aeronautical Laboratory/TRECOM Symposium on Dynamic Load Problems Associated with Helicopters and

V/STOL Aircraft, Proceedings, Vol. I, June 1963.

11. Harris, Franklin D., Spanwise Flow Effects on Rotor Performance, presented at the USAAVLABS-CAL Symposium on the Aerodynamic Problems Associated with V/STOL Aircraft, June 1966.

12. Henderson, B.O., et al., Rotor Load Correlation Report, Boeing-Vertol Report DYMR-9, December 1965.

13. Heyson, Harry H., and Katzoff, S., Induced Velocities Near a Lifting Rotor With Nonuniform Disk Loading, NACA Report 1319, 1957.

14. Huston, R.J., Wind Tunnel Measurements of Performance, Blade Motions, and Blade Airloads for Tandem Rotor Configuration with and without Overlap, NASA TN D-1971, October 1963.

15. Mayo, A.P., Comparison of Measured Flapwise Structural Bending Moments on a Teetering Rotor Blade with Results Calculated from the Measured Pressure Distribution, NASA Memo 2-28-59L, March 1959.

16. Meyer, J.R., and Falabella, G., An Investigation of the Experimental Aerodynamic Loading on a Model Helicopter Rotor Blade, NACA TN2953.

17. Pruyn, R., and Alexander, W.T.,Jr., The USAAVLABS Tandem Rotor Airloads Measurement Program, paper presented at the Aerodynamic Testing Conference of the American Institute of Aeronautics and Astronautics, Boeing Document D8-0381, September 1966.

18. Pruyn, R.R., Lamb, H., and Grant, W.J., Results of Whirl Testing of Partially Instrumented Forward Rotor Blade, Boeing Document R-433, 20 May 1965.

19. Pruyn, R.R., Obbard, J., and Shakespeare, C., The Measurement and Analysis of Rotor Blade Airloads and the Resulting Dynamic Response of a Large Tandem Rotor Helicopter, paper presented at the Fourth International Aerospace Instrumentation Symposium, Boeing Document D8-0296, March 1966.

20. Pruyn, R.R., Preliminary Data Report of Dynamic Airloads Flight Test Results as Prepared for Cornell Aeronautical

Laboratories Correlation Studies, Boeing Document D8-0408, June 1966.

21. Rabbott, J.P., and Churchill, G.B., Experimental Investigation of the Aerodynamic Loading on a Helicopter Blade in Forward Flight, NACA RM L56107, October 1956.

22. Rabbott, J.P., Lizak, A.A., and Paglino, V.M., A Presentation of Measured and Calculated Full Scale Rotor Blade Aerodynamic and Structural Loads, USAAVLABS Technical Report 66-31, U.S. Army Aviation Material Laboratories, Fort Eustis, Virginia, July 1966.

23. Rabbott, J.P., Lizak, A.A., and Paglino, V.M., Tabulated Sikorsky CH-34 Blade Surface Pressures Measured at the NASA/Ames Full-Scale Wind Tunnel, Sikorsky Aircraft Division Report SER-58399 (Contract DA 44-177-AMC-53(T)), January 1966.

24. Rabbott, J.P., Static-Thrust Measurements of the Aerodynamic Loading on a Helicopter Rotor Blade, NACA TN3688, July 1956.

25. Reber, R.M., Flight Test Report - Dynamic Airloads Program, Boeing Document D8-0402, 27 May 1966.

26. Scheiman, J., and Ludi, L.H., Effect of Helicopter Rotor Blade Tip Vortex on Blade Airloads, NASA TN D-1637, May 1963.

27. Scheiman, J., A Tabulation of Helicopter Rotor Blade Differential Pressures, Stresses, and Motions as Measured in Flight, NASA TM X952, March 1964.

APPENDIX I

FLIGHT TEST ACCOMPLISHMENT SUMMARY

This appendix summarizes the appropriate data from the flight test report (reference 25) and from the data summary (reference 4) and provides a readily accessible index to the flight test data obtained in this program. Each useful data flight is represented by a table of the parameters of the test conditions as measured in flight. These tables include the measured aircraft attitude, the total rotor power coefficient, and a test point number (TPN) which is used to relate the test point to the test program requirements. The flight test requirements are presented in Table VII. Tables VIII through XVII summarize the test point accomplishments by flight. A summary of testing accomplished for the various nominal test weights is presented in Tables XVIII through XXII. The test point number was used to denote a test condition as defined in the Flight Test Point Requirements, Table VII. These test points were obtained in one or more of the various flights. The run numbers denote the flight test data recordings which were made on each flight and are numbered consecutively in the sequence in which they were obtained. The flights were also numbered consecutively. The flight and run numbers which are missing from the sequence denote nonproductive attempts to obtain data.

TABLE VII
FLIGHT TEST DATA POINT REQUIREMENTS

Test Point Number (TPN)	Condition	Trim Fwd/Aft (deg)	Gross Weight (pounds)	Airspeed True/Ind (knots)	Altitude (feet)	Rotor RPM	Side-slip (deg)
1	Hover, wind from left	0.5/0	38,500	0	10, IGE	230	0
2	Hover, wind from left forward quarter	0.5/0	38,500	0	10, IGE	230	0
3	Hover, wind from nose	0.5/0	38,500	0	10, IGE	230	0
4	Hover, wind from right forward quarter	0.5/0	38,500	0	10, IGE	230	0
5	Hover, wind from right	0.5/0	38,500	0	10, IGE	230	0
6	Level flight	0.5/0	38,500	30/25	10, IGE	230	0
7	Nose-left sideslip	0.5/0	38,500	30/25	10, IGE	230	+15
8	Nose-left sideslip	0.5/0	38,500	30/25	10, IGE	230	+7.5
9	Nose-right sideslip	0.5/0	38,500	30/25	10, IGE	230	-15
10	Nose-right sideslip	0.5/0	38,500	30/25	10, IGE	230	-7.5
11	Level flight	0.5/0	38,500	30/25	500	230	0
12	Level flight	0.5/0	38,500	30/25	500	230	+15
13	Level flight	0.5/0	38,500	30/25	500	230	+30
14	Level flight	0.5/0	38,500	30/25	500	230	-15
15	Level flight	0.5/0	38,500	30/25	500	230	-30
16	Deleted	-	-	-	-	-	-
17	Level flight	2.23/3.47	26,000	94/92	5000	215	0
18	Level flight	2.86/4.73	26,000	99/87	5000	230	0
19	Level flight	3.0/5.0	26,000	106/94	5000	243	0
20	Level flight	2.86/4.73	33,000	99/87	5000	230	0
21	Level flight	3.0/5.0	33,000	106/94	5000	243	0
22	Left turn, 30° bank	0.5/0	26,000	80/69	5000	230	-

TABLE VII - CONTINUED

Test Point Number (TPN)	Condition	Trim Fwd/Aft (deg)	Gross Weight (pounds)	Airspeed True/Ind (knots)	Altitude (feet)	Rotor RPM	Side-slip (deg)
23	Right turn, 30° bank	0.5/0	26,000	80/69	5000	230	-
24	Nose-right sideslip	0.5/0	26,000	80/69	5000	230	-10
25	Nose-left sideslip	0.5/0	26,000	80/69	5000	230	10
26	Descent, 1000 fpm	0.5/0	26,000	80/69	5000	230	0
27	Autorotation	0.5/0	26,000	80/69	5000	230	0
28	Abrupt roll, right	0.5/0	26,000	80/69	5000	230	0
29	Abrupt roll, left	0.5/0	26,000	80/69	5000	230	0
30	Symmetrical pullup	0.5/0	26,000	80/69	5000	230	0
31	Approach and flare	0.5/0	26,000	60/55	300	230	0
32	Level flight	0.5/0	33,000	30/23	5000	204	0
33	Deleted	-	-	-	-	-	-
34	Level flight	3.0/5.0	33,000	125/111	5000	243	0
35	Level flight	3.0/5.0	26,000	110/97	5000	215	0
36	Level flight	3.0/5.0	26,000	137/123	5000	230	0
37	Level flight	3.0/5.0	26,000	145/130	5000	243	0
38	Level flight	0.5/0	38,500	60/56	4000	230	0
39	Level flight	0.5/0	38,500	70/61	4000	243	0
40	Level flight	2/2	33,000	30/23	5000	204	0
41	Level flight	2/2	33,000	60/51	5000	215	0
42	Level flight	2/2	33,000	100/88	5000	230	0
43	Level flight	2/2	33,000	120/107	5000	243	0
44	Level flight	0/0	33,000	30/23	5000	204	0
45	Level flight	0/0	33,000	60/51	5000	215	0
46	Level flight	0/0	33,000	100/88	5000	230	0
47	Level flight	0/0	33,000	110/97	5000	243	0
48	Level flight, rough air	0.5/0	33,000	30/23	5000	204	0
49	Level flight, rough air	0.5/0	33,000	60/51	5000	215	0
50	Level flight, rough air	3.0/5.0	33,000	100/88	5000	230	0

TABLE VII - CONTINUED

Test Point Number (TPN)	Condition	Trim Fwd/Aft (deg)	Gross Weight (pounds)	Airspeed True/Ind (knots)	Altitude (feet)	Rotor RPM	Side-slip (deg)
51	Level flight, rough air	3.0/5.0	33,000	125/111	5000	243	0
52	Level flight, rough air	0.5/0	33,000	77/66	5000	222	0
53	Level flight, rough air	0.5/0	33,000	80/69	5000	230	0
54	Level flight, rough air	0.5/0	33,000	83/72	5000	238	0
55	Level flight	0.5/0	33,000	84/73	5000	243	0
56	Level flight	0.5/0	33,000	60/51	5000	230	0
57	Level flight	0.5/0	33,000	60/51	5000	243	0
58	Level flight	0.5/0	38,500	60/52	4000	243	0
59	Level flight	0.5/0	26,000	60/51	5000	204	0
60	Level flight	0.5/0	26,000	60/51	5000	215	0
61	Level flight	0.5/0	26,000	60/51	5000	230	0
62	Level flight	0.5/0	26,000	60/51	5000	243	0
70	Level flt. airspeed calib.	-	26,000	40	200-400	230	0
71	Level flt. airspeed calib.	-	26,000	40	200-400	230	0
72, 73	Level flt. airspeed calib.	-	26,000	80	200-400	230	0
74, 75	Level flt. airspeed calib.	-	26,000	120	200-400	230	0
76, 77	Level flt. airspeed calib.	-	26,000	40	200-400	230	+15
78, 79	Level flt. airspeed calib.	-	26,000	40	200-400	230	+30
80	Level flt. airspeed calib.	-	26,000	40	200-400	230	-15
81	Level flt. airspeed calib.	-	26,000	40	200-400	230	-15
82, 83	Level flt. airspeed calib.	-	26,000	40	200-400	230	-30
84, 85	Level flt. airspeed calib.	-	26,000	80	200-400	230	+10
86, 87	Level flt. airspeed calib.	-	26,000	80	200-400	230	-10
88	Level flt. yaw calib.	-	26,000	80	2000	230	0
89	Level flt. yaw calib.	-	26,000	80	2000	230	+10
90	Level flt. yaw calib.	-	26,000	80	2000	230	-10

TABLE VII - CONTINUED

Test Point Number (TPN)	Condition	Trim Fwd/Aft (deg)	Gross Weight (pounds)	Airspeed True/Ind (knots)	Altitude (feet)	Rotor RPM	Side-slip (deg)
91	Level flt. yaw calib.	-	26,000	40	2000	230	0
92	Level flt. yaw calib.	-	26,000	40	2000	230	+15
93	Level flt. yaw calib.	-	26,000	40	2000	230	+30
94	Level flt. yaw calib.	-	26,000	40	2000	230	-15
95	Level flt. yaw calib.	-	26,000	40	2000	230	-30
96	Level flight	0.5/0	26,000	75/65	5000	215	0
97	Level flight	2.9/4.7	33,000	100/93	1000	230	0
98	Hover, into wind	0.5/0	33,000	0	10, IGE	230	0
99	Approach and flare	0.5/0	33,000	60/55	300	230	0
100	Hover, into wind	0.5/0	26,000	0	10, IGE	230	0
101	Approach and flare	0.5/0	38,500	60/55	300	230	0
102	Level flt. airspeed calib.	0.5/0	21,000	140	200-400	230	0
201	Level flight	3/5	21,000	131/119	2000	238	0
202	Level flight	3/5	21,000	141/128	2000	238	0
203	Level flight	3/5	21,000	152/138	2000	238	0
204	Level flight	3/5	21,000	163/148	2000	238	0
205	Level flight	3/5	21,000	126/115	2000	230	0
206	Level flight	3/5	21,000	136/124	2000	230	0
207	Level flight	3/5	21,000	146/133	2000	230	0
208	Level flight	3/5	21,000	156/142	2000	230	0
209	Level flight	3/5	21,000	165/150	2000	230	0
210	Level flight	3/5	23,000	131/110	7500	238	0
211	Level flight	3/5	23,000	141/118	7500	238	0
212	Level flight	3/5	23,000	152/128	7500	238	0
213	Level flight	3/5	23,000	163/137	7500	238	0
214	Level flight	3/5	23,000	126/110	5000	230	0
215	Level flight	3/5	23,000	136/119	5000	230	0

TABLE VII - CONTINUED

Test Point Number (TPN)	Continued	Trim Fwd/Aft (deg)	Gross Weight (pounds)	Airspeed True/Ind (knots)	Altitude (feet)	Rotor RPM	Side-slip (deg)
216	Level flight	3/5	23,000	146/127	5000	230	0
217	Level flight	3/5	23,000	156/136	5000	230	0
218	Level flight	3/5	23,000	165/144	5000	230	0
219	Level flight	3/5	23,000	124/110	3500	225	0
220	Level flight	3/5	23,000	134/119	3500	225	0
221	Level flight	3/5	23,000	144/128	3500	225	0
222	Level flight	3/5	23,000	154/137	3500	225	0
223	Level flight	3/5	23,000	165/147	3500	225	0
224	Level flight	3/5	23,000	124/98	11,000	225	0
225	Level flight	3/5	23,000	134/106	11,000	225	0
226	Level flight	3/5	23,000	144/114	11,000	225	0
227	Level flight	3/5	23,000	154/122	11,000	225	0
228	Level flight	3/5	23,000	165/131	11,000	225	0

NOTE: All altitude values shown are density altitude except as noted. Tapeline altitudes (10 feet, IGE) are approximate wheel clearance to ground.

TABLE VIII
FLIGHT TEST POINTS OBTAINED DURING FLIGHT 384

Flight Parameter	Run Number	
	3	4
Run gross weight (pounds)	26,100	25,900
Run CG (inches forward of midpoint between rotors)	6.5	6.4
Calibrated true airspeed (knots)	56	108
Density altitude (feet)	2900	2950
Pressure altitude (feet)	5050	5050
Outside air temp. (°C)	-12.9	-12.4
Rotor rpm	221	221
Longitudinal cyclic trim (deg fwd/aft)	-0.6 0	-3.4 -5.3
Fuselage attitude (deg) - Pitch	3.6	1.9
- Roll	1.4	1.8
- Sideslip	3.8	3.2
Test point number	60	35
C_{TW}/σ	0.08	0.08
μ'	0.14	0.27
$C_p \times 10^4$	2.4	2.7
ρ (slugs/ft^3) x 10^3	2.18	2.18
Maneuver	level flight	level flight

TABLE IX
FLIGHT TEST POINTS OBTAINED DURING FLIGHT 386

Flight Parameter	Run Number				
	2	3	4	5	6
Run gross weight (pounds)	25,900	25,800	25,700	25,500	25,450
Run CG (inches forward of midpoint between rotors)	5.0	5.0	4.9	4.8	4.8
Calibrated true airspeed (knots)	71	74	74	74	77
Density altitude (feet)	4950	5100	5050	4800	4750
Pressure altitude (feet)	6000	6050	5950	5800	5750
Outside air temp. (°C)	-5.2	-4.8	-4.1	-4.7	-4.4
Rotor rpm	230	230	230	230	230
Longitudinal cyclic trim (deg fwd/aft)	-0.5 / 0	-0.5 / 0	-0.5 / 0	-0.5 / 0	-0.5 / 0
Fuselage attitude (deg) - Pitch	1.3	0.4	0.1	0.7	1.9
- Roll	-1.3	-3.1	2.1	26.4	-20.3
- Sideslip	0.6	-8.3	13.2	9.9	-10.4
Test point number	88	24	25	23	22
C_{TW}/σ	0.07	0.07	0.07	0.07	0.07
μ'	0.17	0.18	0.18	0.17	0.18
$C_p \times 10^4$	2.3	2.1	2.3	2.0	1.9
ρ(slugs/ft3)x10^3	2.06	2.05	2.05	2.07	2.07
Maneuver	level flight	side-slip	side-slip	right turn 30° bank	left turn 30° bank

TABLE IX - CONTINUED

Flight Parameter	Run Number			
	7	8	9	11
Run gross weight (pounds)	25,400	25,350	25,300	25,200
Run CG (inches forward of midpoint between rotors)	4.8	4.8	4.7	4.7
Calibrated true airspeed (knots)	71	77	40	74
Density altitude (feet)	3700	2800	2100	4300
Pressure altitude (feet)	4950	4200	3750	5350
Outside air temp. (°C)	-5.2	-4.9	-5.5	-3.9
Rotor rpm	230	230	230	230
Longitudinal cyclic trim (deg fwd/aft)	-0.5 0	-0.5 0	-0.5 0	-0.5 0
Fuselage attitude (deg) - Pitch	1.2	1.6	4.4	4.1
- Roll	-1.9	-1.7	-1.5	0.5
- Sideslip	-2.3	-4.1	3.8	-0.7
Test point number	26	27	91	27
C_{TW}/σ	0.07	0.07	0.07	0.07
μ	0.17	0.18	0.10	0.17
$C_p \times 10^4$	1.2	0.3	2.3	0
ρ(slugs/ft^3)x10^3	2.13	2.19	2.24	2.09
Maneuver	1000 fpm descent	auto-rotation	level flight	auto-rotation

TABLE X
FLIGHT TEST POINTS OBTAINED DURING FLIGHT 389

Flight Parameter	Run Number					
	1	5	6	7	9	10
Run gross weight (pounds)	33,300	32,500	32,100	32,074	32,050	32,000
Run CG (inches forward of midpoint between rotors)	5.3	5.1	5.0	5.0	5.0	5.0
Calibrated true airspeed (knots)	0	0	56	79	103	101
Density altitude (feet)	-950	-1000	3800	3400	3400	3450
Pressure altitude (feet)	200	100	6050	5950	5850	5850
Outside air temp. (°C)	5.1	5.4	-15.3	-17.2	-16.6	-16.1
Rotor rpm	229	229	233	231	232	229
Longitudinal cyclic trim (deg fwd/aft)	-0.7 -1.1	-0.7 -0.3	-0.8 -0.4	-0.9 -0.6	-2.2 -1.6	-2.6 -2.9
Fuselage attitude (deg) - Pitch	5.1	-	1.3	-2.7	-4.0	-2.0
- Roll	30.9	-	1.9	-1.0	0.7	0.8
- Sideslip	-41.0	-	6.6	0.5	2.6	4.0
Test point number	98	98	56	53	42	20
$C_{TW/\sigma}$	0.08	0.09	0.09	0.09	0.09	0.09
μ	0	0	0.14	0.19	0.24	0.24
$C_p \times 10^4$	3.3	3.2	2.8	2.8	3.0	3.2
ρ (slugs/ft3)x10^3	2.44	2.44	2.13	2.14	2.15	2.16
Maneuver	hover	hover	level flight	level flight rough air	level flight	level flight

TABLE X - CONTINUED

Flight Parameter	Run Number					
	11	12	13	14	16	18
Run gross weight (pounds)	32,000	31,900	31,850	31,800	31,750	31,750
Run CG (inches forward of midpoint between rotors)	4.9	4.9	4.9	4.9	4.9	4.9
Calibrated true airspeed (knots)	103	79	55	76	108	127
Density altitude (feet)	3350	3600	3550	3750	3900	3650
Pressure altitude (feet)	5850	6050	6200	6250	6250	6100
Outside air temp. (°C)	-16.6	-17.1	-18.4	-17.6	-16.2	-16.8
Rotor rpm	230	237	241	244	244	244
Longitudinal cyclic trim (deg fwd/aft)	-3.2 -3.3	-1.0 -0.6	-0.9 -0.6	-1.0 -0.7	-3.3 -3.7	-3.5 -3.8
Fuselage attitude (deg) - Pitch	-3.8	-2.9	-0.2	-2.3	-1.2	-1.1
- Roll	-0.2	-0.6	0.5	0.7	0.9	-0.6
- Sideslip	0.6	-1.7	1.6	3.1	0.7	-0.9
Test point number	50	54	57	55	21	43
C_{TW}/σ	0.09	0.08	0.08	0.08	0.08	0.08
μ'	0.24	0.18	0.14	0.18	0.24	0.27
$C_p \times 10^4$	3.2	2.9	2.7	-	-	-
$\rho(slugs/ft^3) \times 10^3$	2.16	2.14	2.14	2.14	2.12	2.14
Maneuver	level flight rough air	level flight rough air	level flight	level flight	level flight	level flight

TABLE XI
FLIGHT TEST POINTS OBTAINED DURING FLIGHT 390

Flight Parameter	Run Number						
	2	3	4	5	6	7	8
Run gross weight (pounds)	33,100	33,050	33,050	33,025	33,000	32,950	32,950
Run CG (inches forward of midpoint between rotors)	5.1	5.1	5.1	5.1	5.1	5.1	5.1
Calibrated true airspeed (knots)	52	95	94	95	100	77	78
Density altitude (feet)	2800	2900	3150	3150	3100	3100	3100
Pressure altitude (feet)	4300	4300	4550	4500	4450	4450	4450
Outside air temp. (°C)	-6.1	-5.3	-5.4	-5.4	-5.1	-5.5	-5.4
Rotor rpm	229	233	229	232	230	229	233
Longitudinal cyclic trim (deg fwd/aft)	-0.9 -0.7	-3.0 -4.3	-2.3 -2.4	-1.2 -0.8	-3.4 -4.8	-1.0 -0.8	-1.1 -0.7
Fuselage attitude (deg) - Pitch	2.8	2.2	0.8	-0.8	3.0	1.9	1.1
- Roll	5.2	1.0	0.2	1.2	0.5	0.2	0.1
- Sideslip	0.9	4.7	1.8	2.0	-0.1	0.1	2.0
Test point number	56	20	42	46	50	53	53
C_{TW}/σ	0.09	0.09	0.09	0.09	0.09	0.09	0.09
μ	0.12	0.22	0.22	0.22	0.24	0.18	0.18
$C_p \times 10^4$	2.9	3.1	3.0	2.9	3.0	3.0	-
ρ (slugs/ft^3) x 10^3	2.19	2.19	2.18	2.18	2.18	2.18	2.18
Maneuver	level flight	level flight	level flight	level flight	level flight rough air	level flight rough air	level flight

TABLE XI - CONTINUED

Flight Parameter	Run Number					
	9	10	11	12	13	14
Run gross weight (pounds)	32,850	32,750	32,700	32,700	32,650	32,600
Run CG (inches forward of midpoint between rotors)	5.1	5.0	5.0	5.0	5.0	5.0
Calibrated true air speed (knots)	76	75	53	101	104	124
Density altitude (feet)	3000	3000	2950	3200	3300	3150
Pressure altitude (feet)	4350	4400	4400	4550	4650	4550
Outside air temp. (°C)	-4.9	-5.2	-5.7	-5.2	-5.4	-5.4
Rotor rpm	238	244	244	244	242	243
Longitudinal cyclic trim (deg fwd/aft)	-1.0 -0.8	-1.1 -0.8	-0.9 -0.7	-3.6 -5.3	-1.3 -1.0	-3.3 -5.3
Fuselage attitude (deg) - Pitch	1.1	1.9	2.7	3.1	-0.6	1.3
- Roll	0.6	1.0	-0.6	1.2	0.7	-0.3
- Sideslip	1.3	1.6	1.5	1.3	1.7	1.1
Test point number	54	55	57	21	47	34
C_{TW}/σ	0.08	0.08	0.08	0.08	0.08	0.08
μ	0.17	0.17	0.12	0.23	0.23	0.28
$C_p \times 10^4$	2.5	2.4	2.6	2.6	2.7	3.4
ρ(slugs/ft^3)x10^3	2.18	2.18	2.18	2.17	2.16	2.17
Maneuver	level flight rough air	level flight	level flight	level flight	level flight	level flight

TABLE XII
FLIGHT TEST POINTS OBTAINED DURING FLIGHT 391

Flight Parameter	Run Number				
	1	2	6	7	11
Run gross weight (pounds)	26,300	26,100	26,050	25,900	25,700
Run CG (inches forward of midpoint between rotors)	5.2	5.1	5.1	5.0	5.0
Calibrated true airspeed (knots)	0	55	77	77	75
Density altitude (feet)	400	3700	4300	3900	4250
Pressure altitude (feet)	240	4800	5150	5100	5300
Outside air temp. (°C)	17.2	-3.8	-4.8	-5.2	-4.3
Rotor rpm	233	229	230	229	230
Longitudinal cyclic trim (deg fwd/aft)	-0.5 -0.6	-1.2 -0.6	-1.5 -0.6	-1.1 -0.9	-1.5 -0.8
Fuselage attitude (deg) - Pitch	6.9	2.5	1.2	1.4	1.9
- Roll	1.2	-1.2	2.6	-3.9	26.6
- Sideslip	40.5	3.6	12.3	-9.8	6.1
Test point number	100	61	25	24	23
C_{TW}/σ	0.06	0.07	0.07	0.07	0.07
μ	0	0.13	0.18	0.18	0.18
$C_p \times 10^4$	2.6	2.3	2.1	2.0	2.1
ρ (slugs/ft^3) x 10^3	2.36	2.13	2.12	2.14	2.10
Maneuver	hover	level flight	side-slip	side-slip	right turn 30° bank

TABLE XII - CONTINUED

Flight Parameter	Run Number			
	12	13	16	19
Run gross weight (pounds)	25,700	25,700	25,700	25,500
Run CG (inches forward of midpoint between rotors)	5.0	5.0	5.0	4.9
Calibrated true airspeed (knots)	77	78	84	103
Density altitude (feet)	4900	5050	5150	4100
Pressure altitude (feet)	5900	6050	6150	5050
Outside air temp. (°C)	-5.2	-5.3	-5.8	-2.7
Rotor rpm	231	229	232	233
Longitudinal cyclic trim (deg fwd/aft)	-0.2 -0.8	0 -0.8	0 -0.8	-1.2 -4.4
Fuselage attitude (deg) - Pitch	1.8	1.2	4.0	3.7
- Roll	10.9	-15.1	0.3	0
- Sideslip	-1.5	2.3	0.1	0.9
Test point number	28	29	30	18
C_{TW}/σ	0.07	0.07	0.07	0.07
μ	0.18	0.18	0.20	0.24
$C_p \times 10^4$	2.2	2.3	1.7	2.2
ρ (slugs/ft^3)x10^3	2.06	2.05	2.05	2.11
Maneuver	abrupt roll right	abrupt roll left	sym-metrical pullup	level flight

TABLE XII - CONTINUED

Flight Parameter	Run Number				
	22	23	24	25	26
Run gross weight (pounds)	25,400	25,300	25,300	25,200	25,200
Run CG (inches forward of midpoint between rotors)	4.9	4.8	4.8	4.8	4.8
Calibrated true airspeed (knots)	103	56	75	80	59
Density altitude (feet)	3750	3950	3050	3150	0
Pressure altitude (feet)	4700	5100	4200	4150	500
Outside air temp. (°C)	-2.0	-4.1	-2.9	-1.5	9.9
Rotor rpm	242	242	229	230	226
Longitudinal cyclic trim (deg fwd/aft)	-0.5 -5.2	0 -0.7	0 -0.8	0 -0.9	0 -0.5
Fuselage attitude (deg) - Pitch	3.7	4.1	3.5	2.3	10.7
- Roll	-0.6	-0.1	-0.3	-1.2	-2.9
- Sideslip	-3.0	1.0	0.6	2.3	3.4
Test point number	19	62	27	26	31
C_{TW}/σ	0.06	0.06	0.07	0.07	0.06
μ	0.23	0.13	0.18	0.19	0.14
$C_p \times 10^4$	2.0	1.9	0.7	1.3	1.1
ρ (slugs/ft^3) x 10^3	2.13	2.12	2.18	2.17	2.38
Maneuver	level flight	level flight	auto-rotation	descent 1000 fpm	approach and flare

TABLE XIII
FLIGHT TEST POINTS OBTAINED DURING FLIGHT 393

Flight Parameter	Run Number				
	1	2	3	4	5
Run gross weight (pounds)	36,873	36,823	36,823	36,773	36,773
Run CG (inches forward of midpoint between rotors)	3.6	3.6	3.6	3.6	3.6
Calibrated true airspeed (knots)	27	27	27	27	27
Density altitude (feet)	-1600	-1750	-1700	-1750	-1700
Pressure altitude (feet)	200	150	150	150	150
Outside air temp. (°C)	-0.4	-0.3	-0.3	-0.5	-0.3
Rotor rpm	230	231	229	231	231
Longitudinal cyclic trim (deg fwd/aft)	-0.5 0	-0.5 0	-0.5 0	-0.5 0	-0.5 0
Fuselage attitude (deg) - Pitch	-	-	-	-	-
- Roll	3.7	0.5	-1.1	0.3	0.8
- Sideslip	1.1	-11.8	-13.8	8.6	+17.3
Test point number	6	8	7	10	9
C_{TW}/σ	0.09	0.09	0.09	0.09	0.09
μ'	0.06	0.06	0.06	0.06	0.06
$C_p \times 10^4$	3.2	3.1	3.3	3.3	1.3
ρ (slugs/ft^3) x 10^3	2.49	2.50	2.50	2.50	2.50
Maneuver	level flight	side-slip	side-slip	side-slip	side-slip

TABLE XIII - CONTINUED

Flight Parameter	Run Number				
	6	7	8	9	10
Run gross weight (pounds)	36,573	36,473	36,423	36,373	36,323
Run CG (inches forward of midpoint between rotors)	3.5	3.5	3.4	3.4	3.4
Calibrated true airspeed (knots)	28	28	28	28	28
Density altitude (feet)	-550	-150	350	50	250
Pressure altitude (feet)	1350	1650	2150	2000	2150
Outside air temp. (°C)	-2.7	-3.0	-3.8	-4.8	-4.9
Rotor rpm	231	229	231	229	229
Longitudinal cyclic trim (deg fwd/aft)	-0.5 0	-0.5 0	-0.5 0	-0.5 0	-0.5 0
Fuselage attitude (deg) - Pitch	-	-	-	-	-
- Roll	-0.8	-0.2	0.4	1.7	-1.6
- Sideslip	2.8	6.8	17.1	30.6	-12.7
Test point number	11	15	12	13	14
C_{TW}/σ	0.09	0.09	0.09	0.09	0.09
μ	0.07	0.07	0.07	0.07	0.07
$C_p \times 10^4$	3.6	3.9	3.8	3.7	3.9
ρ(slugs/$_{ft}3$)x10^3	2.42	2.39	2.36	2.38	2.36
Maneuver	level flight	side-slip	side-slip	side-slip	side-slip

TABLE XIII - CONTINUED

Flight Parameter	Run Number				
	11	12	13	14	15
Run gross weight (pounds)	36,273	35,973	35,923	35,873	35,273
Run CG (inches forward of midpoint between rotors)	3.4	3.3	3.3	3.3	3.1
Calibrated true airspeed (knots)	25	63	69	59	57
Density altitude (feet)	350	3050	3300	3450	-1700
Pressure altitude (feet)	2250	5200	5500	5750	150
Outside air temp. (°C)	-5.1	-12.7	-13.8	-14.9	-0.5
Rotor rpm	231	231	241	240	231
Longitudinal cyclic trim (deg fwd/aft)	-0.5 0	-0.5 0	-0.5 0	-0.5 0	-0.5 0
Fuselage attitude (deg) - Pitch	-	-	-	-	-
- Roll	-2.4	-0.7	-0.9	0.3	0.2
- Sideslip	-19.0	5.7	-1.5	8.4	-
Test point number	15	38	39	58	101
C_{TW}/σ	0.09	0.10	0.09	0.09	0.08
μ	0.06	0.15	0.16	0.13	0.14
$C_p \times 10^4$	3.8	3.8	3.9	3.9	1.9
ρ (slugs/ft^3)x10^3	2.36	2.18	2.16	2.14	2.51
Maneuver	side-slip	level flight	level flight	level flight	approach and flare

TABLE XIII - CONTINUED

Flight Parameter	Run Number				
	17	18	19	20	21
Run gross weight (pounds)	35,123	35,073	35,023	34,998	34,973
Run CG (inches forward of midpoint between rotors)	3.0	3.0	3.0	3.0	3.0
Calibrated true airspeed (knots)	0	0	0	0	0
Density altitude (feet)	-1550	-1500	-1500	-1500	-1500
Pressure altitude (feet)	150	150	100	100	150
Outside air temp. (°C)	0.9	1.5	1.7	1.5	1.6
Rotor rpm	229	230	230	229	231
Longitudinal cyclic trim (deg fwd/aft)	-0.5 0	-0.5 0	-0.5 0	-0.5 0	-0.5 0
Fuselage attitude (deg) - Pitch	-	-	-	-	-
- Roll	-2.8	-1.5	-0.2	0.1	0.6
- Sideslip	-26.0	11.5	-	-	-
Test point number	1	2	3	4	5
C_{TW}/σ	0.08	0.08	0.08	0.08	0.08
μ	0	0	0	0	0
$C_p \times 10^4$	4.1	3.7	3.7	3.8	3.8
ρ (slugs/ft^3) x 10^3	2.48	2.48	2.48	2.48	2.48
Maneuver	hover	hover	hover	hover	hover

TABLE XIV
FLIGHT TEST POINTS OBTAINED DURING FLIGHT 394

Flight Parameter	Run Number					
	0	1	2	3	4	5
Run gross weight (pounds)	33,300	33,300	33,200	33,200	33,150	33,100
Run CG (inches forward of midpoint between rotors)	5.3	5.3	5.3	5.3	5.3	5.2
Calibrated true airspeed (knots)	0	58	101	85	99	100
Density altitude (feet)	-1100	2400	2920	2800	2750	2500
Pressure altitude (feet)	-250	4150	4720	4670	4680	4340
Outside air temp. (°C)	8.8	-7.4	-9.2	-9.7	-9.7	-8.2
Rotor rpm	231	231	231	231	230	229
Longitudinal cyclic trim (deg fwd/aft)	-0.5 -0.8	-0.8 -0.8	-1.3 -1.0	-1.0 -1.0	-2.5 -2.8	-3.0 -4.9
Fuselage attitude (deg) - Pitch	6.5	2.8	-0.8	1.3	1.3	3.3
- Roll	-1.3	-1.2	0.3	0.3	-0.6	-1.5
- Sideslip	5.5	-2.4	0.2	-2.3	-3.9	-3.5
Test point number	98	56	46	53	42	20
C_{TW}/σ	0.08	0.09	0.09	0.09	0.09	0.09
μ	0	0.14	0.24	0.20	0.24	0.24
$C_p \times 10^4$	-	-	-	-	-	-
ρ (slugs/ft^3) x 10^3	2.46	2.22	2.19	2.20	2.20	2.21
Maneuver	hover	level flight	level flight	level flight rough air	level flight	level flight

TABLE XIV - CONTINUED

Flight Parameter	Run Number				
	6	7	8	9	11
Run gross weight (pounds)	33,050	33,000	32,950	32,850	32,700
Run CG (inches forward of midpoint between rotors)	5.2	5.2	5.2	5.2	5.1
Calibrated true airspeed (knots)	101	76	59	59	28
Density altitude (feet)	2500	2585	2350	2525	2400
Pressure altitude (feet)	4420	4500	4490	4370	4310
Outside air temp. (°C)	-9.0	-9.5	-9.9	-9.4	-8.8
Rotor rpm	229	222	214	213	202
Longitudinal cyclic trim (deg fwd/aft)	-3.5 -5.8	-1.2 -1.0	-1.1 -0.9	-1.2 -0.9	-0.9 -0.8
Fuselage attitude (deg) - Pitch	3.4	1.2	2.0	4.2	4.4
- Roll	-1.7	-1.7	-0.1	-0.8	-1.7
- Sideslip	-4.0	-9.0	-5.2	-6.2	-8.9
Test point number	50	52	45	41	32
C_{TW}/σ	0.09	0.09	0.10	0.10	0.11
μ'	0.24	0.19	0.15	0.15	0.07
$C_p \times 10^4$	-	-	-	-	-
ρ(slugs/ft^3)x10^3	2.21	2.20	2.21	2.21	2.22
Maneuver	level flight rough air	level flight rough air	level flight	level flight	level flight

TABLE XIV - CONTINUED

Flight Parameter	Run Number				
	12	13	14	15	16
Run gross weight (pounds)	32,550	32,550	32,450	32,300	32,150
Run CG (inches forward of midpoint between rotors)	5.1	5.1	5.1	5.0	5.0
Calibrated true airspeed (knots)	28	28	82	99	59
Density altitude (feet)	2810	2505	3025	90	-1200
Pressure altitude (feet)	4730	4510	4930	1150	-300
Outside air temp. (°C)	-10.0	-10.0	-10.4	-5.0	8.6
Rotor rpm	202	202	235	231	231
Longitudinal cyclic trim (deg fwd/aft)	-0.5 -0.8	-2.0 -2.3	-1.0 -1.1	-1.1 -1.8	-2.6 -4.7
Fuselage attitude (deg) - Pitch	4.1	6.3	1.4	3.3	-
- Roll	-2.1	-2.1	-0.2	-	-1.0
- Sideslip	-4.8	-13.0	-3.9	-4.8	-15.2
Test point number	44	40	54	97	99
C_{TW}/σ	0.11	0.11	0.08	0.08	0.08
μ	0.07	0.08	0.19	0.23	0.14
$C_p \times 10^4$	-	-	-	-	-
ρ (slugs/ft^3) $\times 10^3$	2.20	2.21	2.18	2.46	2.46
Maneuver	level flight	level flight	level flight	level flight	approach and flare

TABLE XV
FLIGHT TEST POINTS OBTAINED DURING FLIGHT 395

Flight Parameter	Run Number					
	2	3	4	5	6	7
Run gross weight (pounds)	25,600	25,500	25,450	25,450	25,400	25,200
Run CG (inches forward of midpoint between rotors)	-0.2	-0.3	-0.3	-0.3	-0.3	-0.5
Calibrated true airspeed (knots)	0	54	98	138	55	53
Density altitude (feet)	-600	2650	2650	2700	2300	2300
Pressure altitude (feet)	-240	4000	3950	3950	3750	3800
Outside air temp. (°C)	12.6	-4.0	-3.7	-2.8	-4.3	-4.5
Rotor rpm	230	229	229	229	204	216
Longitudiral cyclic trim (deg fwd/art)	-0.7 -0.7	-1.1 -0.9	-3.3 -5.2	-3.9 -5.4	-1.3 -0.8	-1.2 -0.8
Fuselage attitude (deg) - Pitch	7.1	2.5	4.1	-0.8	3.2	2.6
- Roll	0	0	0.7	-1.1	-0.8	0.5
- Sideslip	39.4	-3.9	-0.7	-2.4	-4.0	-0.1
Test point number	100	61	18	36	59	60
C_{TW}/σ	0.06	0.07	0.07	0.07	0.09	0.08
μ	0	0.13	0.23	0.33	0.15	0.13
$C_p \times 10^4$	-	-	-	-	-	-
ρ(slugs/ft3)x10^3	2.42	2.21	2.21	2.20	2.22	2.22
Maneuver	hover	level flight	level flight	level flight	level flight	level flight

TABLE XV - CONTINUED

Flight Parameter	Run Number				
	9	10	11	12	13
Run gross weight (pounds)	25,200	25,200	25,150	25,150	25,150
Run CG (inches forward of midpoint between rotors)	-0.5	-0.5	-0.5	-0.5	-0.5
Calibrated true airspeed (knots)	96	102	76	74	79
Density altitude (feet)	2500	2550	2650	2500	2650
Pressure altitude (feet)	3900	3950	4200	4000	4100
Outside air temp. (°C)	-4.2	-4.6	-5.5	-5.2	-4.9
Rotor rpm	215	216	229	229	229
Longitudinal cyclic trim (deg fwd/aft)	-3.0 -3.7	-3.7 -5.6	-0.8 -1.1	-1.0 -1.0	-1.2 -0.8
Fuselage attitude (deg) - Pitch	2.2	2.1	1.4	-1.2	2.9
- Roll	-3.0	-0.6	-26.4	27.2	3.4
- Sideslip	-1.6	-2.6	-	-5.2	10.9
Test point number	17	35	22	23	25
C_{TW}/σ	0.08	0.08	0.07	0.07	0.07
μ	0.24	0.26	0.18	0.18	0.19
$C_p \times 10^4$	-	-	-	-	-
ρ(slugs/ft^3)x10^3	2.21	2.21	2.20	2.21	2.20
Maneuver	level flight	level flight	left turn 30° bank	right turn 30° bank	side-slip

TABLE XV - CONTINUED

Flight Parameter	Run Number 14	15	16	17	18	19
Run gross weight (pounds)	25,100	24,950	24,950	24,950	24,900	24,900
Run CG (inches forward of midpoint between rotors)	-0.5	-0.6	-0.6	-0.6	-0.6	-0.6
Calibrated true airspeed (knots)	72	77	78	76	72	73
Density altitude (feet)	2650	2750	2600	2300	2350	1600
Pressure altitude (feet)	4150	4050	4100	3850	3850	3100
Outside air temp. (°C)	-5.5	-5.0	-5.2	-5	-5.1	-3.3
Rotor rpm	229	229	229	229	229	-
Longitudinal cyclic trim (deg fwd/aft)	-0.9 -1.1	-1.1 -1.0	-0.9 -1.0	-0.8 -0.8	-1.0 -1.1	-1.1 -0.9
Fuselage attitude (deg) - Pitch	1.3	-1.1	0.8	-18.3	3.0	3.8
- Roll	-2.5	22.8	3.9	-13.2	0.2	-0.4
- Sideslip	-9.8	-9.4	-7.4	-	-2.4	-5.4
Test point number	24	28	29	30	26	27
C_{TW}/σ	0.07	0.07	0.07	0.07	0.07	-
μ'	0.17	0.18	0.19	0.18	0.17	-
$C_p \times 10^4$	-	-	-	-	-	-
ρ(slugs/ft^3)x10^3	2.20	2.19	2.21	2.22	2.22	2.26
Maneuver	side-slip	abrupt roll right	abrupt roll left	sym-metrical pullup	descent 1000 fpm	auto-rotation

TABLE XVI
FLIGHT TEST POINTS OBTAINED DURING FLIGHT 397

Flight Parameter	Run Number			
	1	2	3	4
Run gross weight (pounds)	23,600	23,550	23,500	23,200
Run CG (inches forward of midpoint between rotors)	3.5	3.5	3.4	3.3
Calibrated true airspeed (knots)	133	143	155	127
Density altitude (feet)	7500	7450	7500	8100
Pressure altitude (feet)	6750	6550	6600	8000
Outside air temp. (°C)	8.4	9.6	10.0	-0.3
Rotor rpm	235	235	235	225
Longitudinal cyclic trim (deg fwd/aft)	-3.6 -5.2	-3.7 -5.3	-3.9 -5.5	-3.8 -5.1
Fuselage attitude (deg) - Pitch	-1.3	-3.5	-5.4	-2.2
- Roll	1.4	0.3	-1.4	1.8
- Sideslip	3.8	2.7	0.4	2.8
Test point number	210	211	212	225
C_{TW}/σ	0.07	0.07	0.07	0.08
μ'	0.31	0.33	0.36	0.31
$C_p \times 10^4$	4.8	4.7	5.2	6.0
ρ (slugs/ft^3) x 10^3	1.90	1.90	1.90	1.86
Maneuver	level flight	level flight	level flight	level flight

TABLE XVI - CONTINUED

Flight Parameter	Run Number			
	5	6	7	8
Run gross weight (pounds)	23,100	23,100	22,900	22,850
Run CG (inches forward of midpoint between rotors)	3.3	3.3	3.2	3.2
Calibrated true airspeed (knots)	117	134	129	137
Density altitude (feet)	8150	8200	5250	4950
Pressure altitude (feet)	8050	8050	4650	4450
Outside air temp. (°C)	0	0.5	10.8	10.1
Rotor rpm	225	225	230	230
Longitudinal cyclic trim (deg fwd/aft)	-3.5 -5.2	-3.8 -4.9	-3.5 -5.4	-3.6 -5.3
Fuselage attitude (deg) - Pitch	-0.6	-1.9	-1.5	-7.4
- Roll	-1.3	-1.9	-1.5	-0.1
- Sideslip	1.7	2.4	-0.4	0.5
Test point number	224	226	214	215
C_{TW}/σ	0.08	0.08	0.07	0.07
μ	0.28	0.32	0.30	0.32
$C_p \times 10^4$	5.5	6.1	5.2	5.2
ρ (slugs/ft^3)x10^{-3}	1.86	1.86	2.04	2.05
Maneuver	level flight	level flight	level flight	level flight

TABLE XVI - CONTINUED

Flight Parameter	Run Number				
	9	10	11	12	13
Run gross weight (pounds)	22,850	22,800	22,700	22,600	22,600
Run CG (inches forward of midpoint between rotors)	3.2	3.1	3.1	3.0	3.0
Calibrated true airspeed (knots)	147	158	122	132	137
Density altitude (feet)	5050	5150	3450	3450	3600
Pressure altitude (feet)	4500	4450	2800	2700	2800
Outside air temp. (°C)	10.7	12.0	15.4	16.5	16.2
Rotor rpm	230	230	225	225	225
Longitudinal cyclic trim (deg fwd/aft)	-3.9 -5.4	-3.8 -5.5	-3.4 -5.3	-3.5 -5.3	-3.5 -5.3
Fuselage attitude (deg) - Pitch	0.5	-2.4	-2.7	-3.8	-6.1
- Roll	0.3	-1.2	-1.1	0.2	0.8
- Sideslip	2.9	0.5	-2.0	1.2	0.3
Test point number	216	217	219	220	221
C_{TW}/σ	0.07	0.07	0.06	0.06	0.06
μ	0.35	0.37	0.30	0.32	0.33
$C_p \times 10^4$	5.5	6.0	4.8	5.0	4.6
ρ (slugs/ft^3) x10^3	2.04	2.04	2.14	2.14	2.14
Maneuver	level flight	level flight	level flight	level flight	level flight

TABLE XVII
FLIGHT TEST POINTS OBTAINED DURING FLIGHT 398

Flight Parameter	Run Number						
	1	2	4	5	6	7	9
Run gross weight (pounds)	23,900	23,850	23,700	23,650	23,600	23,550	23,400
Run CG (inches forward of midpoint between rotors)	3.2	3.2	3.1	3.1	3.0	3.0	2.9
Calibrated true airspeed (knots)	129	138	126	133	147	122	148
Density altitude (feet)	3650	3600	1950	1950	2000	1850	1950
Pressure altitude (feet)	3700	3600	1900	1850	1950	1900	1950
Outside air temp. (°C)	7.4	7.8	11.7	12.1	11.9	11.0	11.2
Rotor rpm	225	225	235	235	235	230	230
Longitudinal cyclic trim	-3.3	-3.3	-3.1	-3.3	-3.4	-3.1	-3.4
(deg fwd/aft)	-5.2	-5.2	-5.2	-5.3	-5.3	-5.1	-5.4
Fuselage attitude (deg) - Pitch	-2.8	-6.1	-1.4	-3.8	-5.6	-1.8	-5.7
- Roll	3.5	1.0	-0.4	0.6	1.0	1.0	0.3
- Sideslip	4.0	2.4	1.9	1.3	3.9	1.7	2.5
Test point number	220	221	201	202	203	205	207
C_{TW}/σ	0.07	0.07	0.06	0.06	0.06	0.06	0.06
μ'	0.31	0.34	0.29	0.31	0.34	0.29	0.33
$C_p \times 10^4$	3.6	4.0	2.9	3.5	4.2	2.8	4.0
ρ(slugs/$_{ft^3}$)x10^3	2.14	2.14	2.24	2.24	2.24	2.25	2.24
Maneuver	level flight	level flight	level flight	level flight	level flight	level flight	level flight

NOTE: Runs 11 to 13 were airspeed calibrations.

TABLE XVIII

FLIGHT LOG OF TEST POINTS ACCOMPLISHED

Basic Program Summary of Records Obtained	Nominal Test Gross Weight (Pounds)		
	26,000	33,000	37,000
Total in Level Flight	34	41	3
(Level Flight Near Region of High Dynamic Loads (RHDL))	(2)	(23)	(1)
Maneuvers	33	0	0
Hovering and Transition	2	1	21
Total at Test Weight	69*	42	24
Total for Basic Program	135 Records		
Extended Program Summary of Records Obtained	Minimum Test Flying Weight ≈ 24,000 Pounds		
Total in High-Speed Level Flight for Extended Program	20 Records		
*32 of these records were not digitized due to noise or other failures.			

The contract requirement for the basic program was 62 records. The following tables show the points obtained and the repeated conditions by test point number (TPN) from Plan of Flight Test 5-26. One test point number (48) of the basic program was inadvertently missed, but was not considered of sufficient value to warrant a repeat of the flight. Several test point numbers of the extended program could not be obtained due to excessive vibration at high speed.

TABLE XIX

TEST POINTS ACCOMPLISHED AT 26,000 POUNDS GROSS WEIGHT

TPN	TAS	RRPM	Flight Number											Flight Condition
			379	380	381	382	383	384	385	386	387	391	395	
17	94	215							x				x	Level flight
18	99	230							x			x	x	Level flight
19	106	243										x		Level flight
22	80	230								x	x	x	x	30° bank turn - left
23	80	230								x	x	x	x	30° bank turn - right
24	80	230									x	x	x	Yaw - 10° left
25	80	230									x	x	x	Yaw - 10° right
26	80	230								x	x	x	x	PPD
27	80	230								x	x	x	x	Auto
28	80	230									x	x	x	Abrupt roll - right
29	80	230									x	x	x	Abrupt roll - left
30	80	230									x	x	x	Symmetrical pullup
31	60	230									x	x		Approach and flare
35	110	215						x	x				x	Level flight (near rhdl)
36	137	230									x	x	x	Level flight (near rhdl)
37	145	243										x		Level flight
59	60	204											x	Level flight
60	60	215						x	x		x		x	Level flight
61	60	230							x		x	x	x	Level flight
62	60	243										x		Level flight
70	40	230							x					Airspeed calibration
71	40	230							x					Airspeed calibration
72	80	230							x					Airspeed calibration
73	80	230							x					Airspeed calibration
74	120	230							x					Airspeed calibration
75	120	230							x					Airspeed calibration

TABLE XIX - CONTINUED

TPN	TAS	RRPM	Flight Number 379	380	381	382	383	384	385	386	387	391	395	Flight Condition
88	80	230								x				Yaw calibration 0
89	80	230								x				Yaw calibration +10
90	80	230								x				Yaw calibration -10
91	40	230								x				Yaw calibration 0
96	75	215											x	Level flight
100	0	230										x	x	Hover (wind-nose)
Flight Totals			*	*	*	*	*	2	11**	8**	13***	17	18	
			Total Records at Test Weight = 69 Records Near RHDL = 2											

*Instrumentation check flights at 26,000 pounds; no valid test data obtained.
**Noise.
***No strain gage data from rotors due to a strain gage module failure.

TABLE XX

TEST POINTS ACCOMPLISHED AT 33,000 POUNDS GROSS WEIGHT

TPN	TAS	RRPM	Flight Number				Flight Condition	RHDL
			388	389	390	394		
20	99	230		x	x	x	Level flight	Near
21	106	243		x	x		Level flight	-
32	30	204				x	Level flight	Near
34	125	243			x		Level flight	Near
40	30	204				x	Level flight	Near
41	60	215				x	Level flight	Near
42	100	230		x	x	x	Level flight	Near
43	120	243		x			Level flight	Near
44	30	204				x	Level flight	Near
45	60	215				x	Level flight	Near
46	100	230			x	x	Level flight	Near
47	110	243			x		Rough air	-
49	60	215				x	Rough air	Near
50	100	230		x	x	x	Rough air	Near
51	125	243			x		Rough air	Near
52	77	222				x	Rough air	Near
53	80	230		x	x	x	Rough air	-
54	83	238		x	x	x	Level flight	-
55	84	243		x	x		Level flight	-
56	60	230		x	x	x	Level flight	-
57	60	243		x	x		Level flight	-

TABLE XX - CONTINUED

TPN	TAS	RRPM	Flight Number 388	389	390	394	Flight Condition	RHDL
97	100	230				x	Level flight	-
98	0	230		x		x	Level flight	-
99	60	230				x	Approach and flare	-
Flight Totals			0*	11	13	17		
Total Records at Test Weight						= 41		
Records Near RAL						= 23		

*No data due to bad weather.

TABLE XXI

TEST POINTS ACCOMPLISHED AT 37,000 POUNDS GROSS WEIGHT

TPN	TAS	RRPM	Flight Number 392	Flight Number 393	Flight Condition
1	0	230	x	x	Wind from left
2	0	230	x	x	Wind from left fwd 1/4
3	0	230	x	x	Wind from nose
4	0	230	x	x	Wind from right fwd 1/4
5	0	230	x	x	Wind from right
6	30	230		x	Zero sideslip
7	30	230		x	+15° sideslip
8	30	230		x	+7.5° sideslip
9	30	230		x	-15° sideslip
10	30	230		x	-7.5° sideslip
11	30	230		x	Zero sideslip
12	30	230		x	+15° sideslip
13	30	230		x	+30° sideslip
14	30	230		x	-15° sideslip
15	30	230		x	-30° sideslip
38	60	230		x	Level flight (near rhdl)
39	70	243		x	Level flight (near rhdl)
58	60	243		x	Level flight (near rhdl)
101	60	230		x	Approach and flare
Flight Totals			5	19	

Total Records at Test Weight = 24 (One Record Near RHDL)

TABLE XXII

TEST POINTS ACCOMPLISHED IN EXTENDED PROGRAM

TPN	TAS	RRPM	Flight Number 397	Flight Number 398	Density Altitude (feet)
201	131	238		x	2000
202	141	238		x	2000
203	152	238		x	2000
205	126	230		x	2000
207	146	230		x	2000
210	131	238	x		7500
211	141	238	x		7500
212	152	238	x		7500
214	126	230	x		5000
215	136	230	x		5000
216	146	230	x		5000
217	156	230	x		5000
219	124	225	x		3500
220	134	225	x	x	3500
221	144	225	x	x	3500
224	124	225	x		11,000
225	134	225	x		11,000
226	144	225	x		11,000
Flight Totals			13	7	
Total Records at Test Weight = 20					
NOTE: All data obtained in straight level flight.					

APPENDIX II

INSTRUMENTATION DISCREPANCIES ENCOUNTERED IN USEFUL DATA FLIGHTS

GENERAL

The corrective actions shown in Table XXIII were required to obviate the errors or omissions which were encountered in all data flights.

TABLE XXIII

GENERAL INSTRUMENTATION DISCREPANCIES

Item	Data Codes Affected	Action
Forward rotor shaft strain gages - phase error	5247,5248,5249, 5250,5251,5252, 5453	Rerun with correct phase angle (293 degrees)
Forward rotor shaft shear gages - equivalent load error	5247 (0°-180°) 5248 (90°-270°)	Rerun with correct equivalent load values 0°-180°=8368 lb 90°-270°=9400 lb
Rotating accelerometers - useless steady terms	1044,1045,1046, 1047,1048,1049	Deleted steady terms
Aft blade torsion, station 89 - sign error	5279	—

SPECIFIC

Due to malfunctions, there were also instrumentation discrepancies which pertained only to specific flights. The corrective actions that were required are itemized in the following tables.

Flight 384

This flight had invalid data on run 0 and only forward rotor data on run 5; these runs were deleted.

TABLE XXIV

SPECIFIC INSTRUMENTATION DISCREPANCIES - FLIGHT 384

Data Code	Discrepancy	Action
1020	No Rcal	Delete entirely
1021	No Rcal	Delete entirely
1022	No Rcal	Delete entirely
4198	Harmonic values zero	Delete entirely
4200	VCO on band edge	Delete entirely
4218	Rcal on band edge	Delete entirely
4230	No Rcal	Delete entirely
4241	Rcal on band edge	Delete entirely
4254	VCO on band edge	Delete entirely
5153	No Rcal	Delete entirely
5253	Small Rcal	Delete entirely
5259	Small Rcal	Delete entirely
5267	Sign error (noted in steady term)	Reverse sign
5272	Sign error (noted in steady term)	Reverse sign
5273	Sign error (noted in steady term)	Reverse sign
5288	Sign error (noted in steady term)	Reverse sign

These discrepancies were in addition to the following data codes which were deleted in digitizing:

2001	2016	3005	4181	4207	4247	5247	7115	7198
2002	2017	3012	4198	4212	4271	5252	7134	7213
2003	3003	3013	4199	4228	4282	5254	7163	7214
2004	3004	3052	4203	4229	4284	5260	7167	

Flight 386

This flight had no bad runs.

TABLE XXV

SPECIFIC INSTRUMENTATION DISCREPANCIES - FLIGHT 386

Data Code	Discrepancy	Action
1020	No Rcal	Delete entirely
1021	No Rcal	Delete entirely
1022	No Rcal	Delete entirely
4189	Rcal on band edge	Delete entirely
4198	Zero harmonic values	Delete entirely
4202	No Rcal	Delete entirely
4207	Rcal on band edge	Delete entirely
4212	Rcal on band edge	Delete entirely
4226	Rcal on band edge	Delete entirely
4229	Rcal on band edge	Delete entirely
4230	No Rcal	Delete entirely
4263	Rcal on band edge	Delete entirely
4266	Inconsistent steady and harmonic values	Delete entirely
4271	Rcal on band edge	Delete entirely
4284	Inconsistent steady and harmonic values	Delete entirely
5252	Small Rcal	Delete entirely
5253	Small Rcal	Delete entirely
5259	Sign error of steady term	Reverse sign
5260	Inconsistent steady and harmonic values and small Rcal	Delete entirely
5265	X_o error	Correct X_o and reprocess
5269	X_o error	Correct X_o and reprocess
5270	X_o error	Correct X_o and reprocess
5272	Sign error in steady term and X_o error	Reverse sign and correct X_o
5273	Sign error in steady term	Reverse sign

TABLE XXV - CONTINUED

Data Code	Discrepancy	Action
5275	Sign error in steady term and X_o error	Reverse sign and correct X_o
5280	X_o error	Correct X_o
5284	X_o error	Correct X_o
5285	X_o error	Correct X_o
5287	X_o error	Correct X_o
5288	Sign error in steady term	Reverse sign
5290	Sign error in steady term and X_o error	Reverse sign and correct X_o
5295	No X_o	Input X_o
5296	No X_o	Input X_o

These discrepancies were in addition to the following data codes which were deleted in digitizing:

2001	2016	3005
2002	2017	3012
2003	3003	3013
2004	3004	

Flight 389

For this flight, run 8 contained invalid data and was deleted.

TABLE XXVI

SPECIFIC INSTRUMENTATION DISCREPANCIES - FLIGHT 389

Data Code	Discrepancy	Action
1020	Small Rcal	Delete entirely
1021	Small Rcal	Delete entirely
1022	Small Rcal	Delete entirely
2016	Small Rcal	Delete entirely
4198	Bias on band edge	Delete entirely
5265	X_o error	Correct X_o and reprocess
5269	X_o error	Correct X_o and reprocess
5270	X_o error	Correct X_o and reprocess
5272	Sign error in steady term and X_o error	Reverse sign and correct X_o
5275	Sign error in steady term and X_o error	Reverse sign and correct X_o
5280	Sign error in steady term	Reverse sign
5284	Sign error in steady term	Reverse sign
5285	No X_o	Input X_o
5287	X_o error	Correct X_o
5290	Sign error in steady term and X_o error	Reverse sign and correct X_o

These discrepancies were in addition to the following data codes which were deleted in digitizing:

2001	2017	3012
2002	3003	3013
2003	3004	4230
2004	3005	

Flight 390

All runs were valid.

TABLE XXVII

SPECIFIC INSTRUMENTATION DISCREPANCIES - FLIGHT 390

Data Code	Discrepancy	Action
1020	No Rcal	Delete entirely
1021	No Rcal	Delete entirely
1022	No Rcal	Delete entirely
4212	Harmonic values zero	Delete entirely
4214	Incorrect baseline values for in-flight calibration	Delete entirely
5247	Equivalent load wrong	Correct equivalent load
5248	Equivalent load wrong	Correct equivalent load
5253	Small Rcal	Delete entirely
5272	Sign error in steady term and X_o error	Reverse sign and correct X_o
5275	Sign error in steady term and X_o error	Reverse sign and correct X_o
5285	Bias on band edge	Delete entirely
5287	X_o error	Correct X_o
5288	Sign error in steady term	Reverse sign

These discrepancies were in addition to the following data codes which were deleted in digitizing:

2001	2016	3004	4179	4253	5252	5276	7167
2002	2017	3005	4185	4263	5260	5290	7213
2003	2027	3012	4199	4278	5267	5296	
2004	3003	3013	4230	4284	5273	7134	

Flight 391

Runs 8, 20, and 21 were invalid and were deleted.

TABLE XXVIII

SPECIFIC INSTRUMENTATION DISCREPANCIES - FLIGHT 391

Data Code	Discrepancy	Action
1020	Small Rcal	Delete entirely
1021	Small Rcal	Delete entirely
1022	Small Rcal	Delete entirely
4213	In-flight calibration	Delete entirely
4228	Inconsistent steady values	Delete steady value
4257	Rcal on band edge	Delete entirely
5247	Equivalent load wrong	Correct equivalent load
5248	Equivalent load wrong	Correct equivalent load
5253	Small Rcal	Delete entirely
5272	Bias on band edge	Delete entirely
5287	X_o error	Correct X_o
5288	Sign error in steady term	Reverse sign
5289	Sign error in steady term	Reverse sign
5290	Bias too close to band edge	Delete steady term

These discrepancies were in addition to the following data codes which were deleted in digitizing:

2001	2017	3005	4185	4230	4263	5260	5283
2002	2027	3012	4199	4252	4284	5263	5296
2003	2029	3013	4204	4253	5250	5267	7134
2004	3003	4179	4212	4254	5252	5273	7176
2016	3004	4184	4214	4258	5257	5275	7213

Flight 393

Runs 5, 101, and 201 were either invalid flight data or ground runs and were deleted.

TABLE XXIX

SPECIFIC INSTRUMENTATION DISCREPANCIES - FLIGHT 393

Data Code	Discrepancy	Action
1020	Small Rcal	Delete entirely
1021	Small Rcal	Delete entirely
1022	Small Rcal	Delete entirely
4177	No Rcal	Delete entirely
4178	Rcal on band edge	Delete entirely
4231	No Rcal	Delete entirely
4233	VCO and Rcal on band edge	Delete entirely
4234	No Rcal	Delete entirely
4235	Small Rcal	Delete entirely
4245	Small Rcal	Delete entirely
2024	Small Rcal	Delete entirely
2028	Small Rcal	Delete entirely
8207	Small Rcal	Delete entirely
5208	Small Rcal	Delete entirely
5253	Small Rcal	Delete entirely
5261	Small Rcal	Delete entirely
5269	Sign error in steady term	Reverse sign
5270	Sign error in steady term	Reverse sign
5271	No Rcal	Delete entirely
5272	Sign error in steady term and X_o error	Reverse sign and correct X_o
5287	No X_o	Input correct X_o
5288	Sign error in steady term	Reverse sign
5290	Sign error in steady term	Reverse sign

These discrepancies were in addition to the following data codes which were deleted in digitizing:

1044	1047	2002	2016	2025	2029	3003
1045	1048	2003	2017	2026	2034	3004
1046	2001	2004	2018	2027	2035	3005

3012	4184	4212	4226	4282	5263	5275	7134
3013	4189	4213	4229	4284	5264	5276	7167
3052	4191	4214	4230	5153	5266	5278	7198
4179	4192	4217	4237	5207	5267	5279	
4180	4194	4219	4239	8208	5268	5283	
4181	4198	4220	4253	5252	5273	5286	
4183	4199	4225	4267	5260	5274	5295	

Flight 394

Run 5 was an invalid flight record and runs 0, 101, and 102 were ground runs; these runs were deleted.

TABLE XXX

SPECIFIC INSTRUMENTATION DISCREPANCIES - FLIGHT 394

Data Code	Discrepancy	Action
4178	VCO on band edge	Delete entirely
4206	VCO on band edge	Delete entirely
4212	Values inconsistent by comparison	Delete entirely
4232	VCO on band edge	Delete entirely
4260	VCO on band edge	Delete entirely
4263	VCO on band edge	Delete entirely
5272	Sign error in steady term and X_o error	Reverse sign and correct X_o
5273	Sign error in steady term	Reverse sign
5275	Sign error in steady term and X_o error	Reverse sign and correct X_o
5281	Steady value inconsistent when compared to other test data	Delete steady term
5287	X_o error	Correct X_o
5288	Sign error in steady term	Reverse sign
5290	Sign error in steady term and X_o error	Reverse sign and correct X_o

These discrepancies were in addition to the following data codes which were deleted in digitizing:

1020	2017	4200	5266	7167
1021	3003	4213	5279	7213
1022	3004	4214	5285	
2001	3005	4230	7107	
2002	3012	4233	7134	
2003	3013	4284	7163	
2004	4198	5252	7164	
2016	4199	5260	7165	

Flight 395

Run 17 was edited incorrectly and runs 22 and 23 had malfunctions; these runs were deleted.

TABLE XXXI

SPECIFIC INSTRUMENTATION DISCREPANCIES - FLIGHT 395

Data Code	Discrepancy	Action
4178	VCO on band edge	Delete entirely
4206	VCO on band edge	Delete entirely
4209	VCO on band edge	Delete entirely
4212	Values inconsistent by comparison	Delete entirely
4232	VCO on band edge	Delete entirely
4260	VCO on band edge	Delete entirely
4263	VCO on band edge	Delete entirely
2028	No Rcal	Delete entirely
2029	No Rcal	Delete entirely
5272	Sign error in steady term and X_o error	Reverse sign and correct X_o
5273	Sign error in steady term	Reverse sign
5275	Sign error in steady term and X_o error	Reverse sign and correct X_o
5281	Small Rcal	Delete steady term
5287	X_o error	Correct X_o
5288	Sign error in steady term	Reverse sign
5290	Sign error in steady term and X_o error	Reverse sign and correct X_o

These discrepancies were in addition to the following data codes which were deleted in digitizing:

1020	2016	4198	4284	7134
1021	2017	4199	5252	7163
1022	3003	4200	5260	7164
2001	3004	4213	5266	7165
2002	3005	4214	5279	7167
2003	3012	4230	5285	7213
2004	3013	4233	7107	

Flight 397

Run 15 was invalid and was deleted.

TABLE XXXII

SPECIFIC INSTRUMENTATION DISCREPANCIES - FLIGHT 397

Data Code	Discrepancy	Action
4212	Values inconsistent by comparison	Delete entirely
4214	Rcal on band edge	Delete entirely
4229	Rcal on band edge	Delete entirely
4230	No Rcal	Delete entirely
4263	Rcal on band edge	Delete entirely
4284	Low Rcal	Delete entirely
5252	Data not consistent when compared to other test data	Delete entirely
5253	Steady not consistent when compared to other test data	Delete entirely
5260	Data not consistent when compared to other test data	Delete entirely
5266	Data not consistent when compared to other test data	Delete entirely
5272	Sign error in steady term and X_o error	Reverse sign and correct X_o
5273	Sign error in steady term	Reverse sign
5275	Sign error in steady term and X_o error	Reverse sign and correct X_o
5287	X_o error	Correct X_o
5288	Sign error in steady term	Reverse sign
5290	Sign error in steady term and X_o error	Reverse sign and correct X_o
7134	No Rcal	Delete entirely
7135	No Rcal	Delete entirely
7141	No Rcal	Delete entirely
7167	No Rcal	Delete entirely
7199	No Rcal	Delete entirely
7213	No Rcal	Delete entirely

These discrepancies were in addition to the following data codes which were deleted in digitizing:

1020	2002	2017	3012
1021	2003	3003	3013
1022	2004	3004	
2001	2016	3005	

Flight 398

Runs 3, 8, and 10 had bad in-flight calibration and were deleted.

TABLE XXXIII

SPECIFIC INSTRUMENTATION DISCREPANCIES - FLIGHT 398

Data Code	Discrepancy	Action
4207	Low Rcal	Delete entirely
4214	Rcal on band edge	Delete entirely
4229	Rcal on band edge	Delete entirely
4230	No Rcal	Delete entirely
4263	Rcal on band edge	Delete entirely
4284	No Rcal	Delete entirely
5252	Small Rcal	Delete entirely
5253	Small Rcal	Delete entirely
5260	No Rcal	Delete entirely
5266	No Rcal	Delete entirely
5272	Sign error in steady term and X_o error	Reverse sign and correct X_o
5273	Sign error in steady term	Reverse sign
5275	Sign error in steady term and X_o error	Reverse sign and correct X_o
5287	X_o error	Correct X_o
5288	Sign error in steady term	Reverse sign
5290	Sign error in steady term and X_o error	Reverse sign and correct X_o

These discrepancies were in addition to the following data codes which were deleted in digitizing:

1020	2002	2017	3012
1021	2003	3003	3013
1022	2004	3004	
2001	2016	3005	

UNCLASSIFIED
Security Classification

DOCUMENT CONTROL DATA - R&D

(Security classification of title, body of abstract and indexing annotation must be entered when the overall report is classified)

1 ORIGINATING ACTIVITY (Corporate author) Vertol Division The Boeing Company Morton, Pennsylvania	2a. REPORT SECURITY CLASSIFICATION Unclassified 2b GROUP NA

3 REPORT TITLE In-Flight Measurement of Rotor Blade Airloads, Bending Moments, and Motions, Together with Rotor Shaft Loads and Fuselage Vibration, on a Tandem Rotor Helicopter Volume IV Summary and Evaluation of Results

4. DESCRIPTIVE NOTES (Type of report and inclusive dates)
Final Technical Report

5. AUTHOR(S) (Last name, first name, initial)
Pruyn, Richard R.

6. REPORT DATE	7a. TOTAL NO. OF PAGES	7b. NO. OF REFS
November 1967	285	27

8a. CONTRACT OR GRANT NO.	9a. ORIGINATOR'S REPORT NUMBER(S)
DA 44-177-AMC-124(T) b. PROJECT NO. c. Task 1F125901A14604 d.	USAAVLABS Technical Report 67-9D 9b. OTHER REPORT NO(S) (Any other numbers that may be assigned this report) Boeing Document D8-0382-4

10. AVAILABILITY/LIMITATION NOTICE
This document has been approved for public release and sale; its distribution is unlimited.

11. SUPPLEMENTARY NOTES	12. SPONSORING MILITARY ACTIVITY
Volume IV of a 5-volume report	U.S. Army Aviation Materiel Laboratories, Fort Eustis, Virginia

13. ABSTRACT

This report describes and evaluates the results of an extensive program to measure the dynamic effects of flight on a tandem rotor helicopter. The flight test results are reviewed and then compared with theoretical predictions and with other flight test data. The airloads measurements from this program are similar to those of other flight test programs, with one major exception: single lifting-rotor helicopter data differ from the forward rotor data of a tandem. The aft rotor apparently produces an upwash which gives an increase in the airloads on the inboard region of the forward rotor. This effect results in an airload distribution that is similar to that which would be obtained with an increased blade twist of the forward rotor. For most longitudinal cyclic trim settings, the oscillations of the airloads of both tandem rotors tend to be similar to those of a single rotor, with intrarotor tip vortex intersections causing the predominant disturbances. Longitudinal cyclic trim settings can be obtained experimentally with the tandem helicopter which cause large airload pressure oscillations due to the intersection of forward rotor blade vortexes by the aft rotor blades. These pressure oscillations occur rapidly and do not appear to increase blade stresses, rotor shaft loads, or airframe vibration.

DD FORM 1 JAN 64 1473

UNCLASSIFIED
Security Classification

UNCLASSIFIED
Security Classification

14. KEY WORDS	LINK A		LINK B		LINK C	
	ROLE	WT	ROLE	WT	ROLE	WT
In-Flight Measurement of Airloads						
Tandem Rotor Helicopter						
Instrumentation						
Test Program						
In-Flight Calibration						
Data Acquisition						
Data Processing						
Experimental Results						
Evaluation and Analysis of Results						
Conclusions						
Recommendations						

INSTRUCTIONS

1. ORIGINATING ACTIVITY: Enter the name and address of the contractor, subcontractor, grantee, Department of Defense activity or other organization *(corporate author)* issuing the report.

2a. REPORT SECURITY CLASSIFICATION: Enter the overall security classification of the report. Indicate whether "Restricted Data" is included. Marking is to be in accordance with appropriate security regulations.

2b. GROUP: Automatic downgrading is specified in DoD Directive 5200.10 and Armed Forces Industrial Manual. Enter the group number. Also, when applicable, show that optional markings have been used for Group 3 and Group 4 as authorized.

3. REPORT TITLE: Enter the complete report title in all capital letters. Titles in all cases should be unclassified. If a meaningful title cannot be selected without classification, show title classification in all capitals in parenthesis immediately following the title.

4. DESCRIPTIVE NOTES: If appropriate, enter the type of report, e.g., interim, progress, summary, annual, or final. Give the inclusive dates when a specific reporting period is covered.

5. AUTHOR(S): Enter the name(s) of author(s) as shown on or in the report. Enter last name, first name, middle initial. If military, show rank and branch of service. The name of the principal author is an absolute minimum requirement.

6. REPORT DATE: Enter the date of the report as day, month, year, or month, year. If more than one date appears on the report, use date of publication.

7a. TOTAL NUMBER OF PAGES: The total page count should follow normal pagination procedures, i.e., enter the number of pages containing information.

7b. NUMBER OF REFERENCES: Enter the total number of references cited in the report.

8a. CONTRACT OR GRANT NUMBER: If appropriate, enter the applicable number of the contract or grant under which the report was written.

8b, 8c, & 8d. PROJECT NUMBER: Enter the appropriate military department identification, such as project number, subproject number, system numbers, task number, etc.

9a. ORIGINATOR'S REPORT NUMBER(S): Enter the official report number by which the document will be identified and controlled by the originating activity. This number must be unique to this report.

9b. OTHER REPORT NUMBER(S): If the report has been assigned any other report numbers *(either by the originator or by the sponsor)*, also enter this number(s).

10. AVAILABILITY/LIMITATION NOTICES: Enter any limitations on further dissemination of the report, other than those imposed by security classification, using standard statements such as:

(1) "Qualified requesters may obtain copies of this report from DDC."

(2) "Foreign announcement and dissemination of this report by DDC is not authorized."

(3) "U. S. Government agencies may obtain copies of this report directly from DDC. Other qualified DDC users shall request through _____."

(4) "U. S. military agencies may obtain copies of this report directly from DDC. Other qualified users shall request through _____."

(5) "All distribution of this report is controlled. Qualified DDC users shall request through _____."

If the report has been furnished to the Office of Technical Services, Department of Commerce, for sale to the public, indicate this fact and enter the price, if known.

11. SUPPLEMENTARY NOTES: Use for additional explanatory notes.

12. SPONSORING MILITARY ACTIVITY: Enter the name of the departmental project office or laboratory sponsoring *(paying for)* the research and development. Include address.

13. ABSTRACT: Enter an abstract giving a brief and factual summary of the document indicative of the report, even though it may also appear elsewhere in the body of the technical report. If additional space is required, a continuation sheet shall be attached.

It is highly desirable that the abstract of classified reports be unclassified. Each paragraph of the abstract shall end with an indication of the military security classification of the information in the paragraph, represented as *(TS)*, *(S)*, *(C)*, or *(U)*.

There is no limitation on the length of the abstract. However, the suggested length is from 150 to 225 words.

14. KEY WORDS. Key words are technically meaningful terms or short phrases that characterize a report and may be used as index entries for cataloging the report. Key words must be selected so that no security classification is required. Identifiers, such as equipment model designation, trade name, military project code name, geographic location, may be used as key words but will be followed by an indication of technical context. The assignment of links, rules, and weights is optional.

UNCLASSIFIED
Security Classification